

# GEODYNAMIC EVOLUTION OF THE SHYOK SUTURE ZONE, NW HIMALAYAS

## A THESIS

*Submitted in partial fulfilment of the  
requirements for the award of the degree  
of*  
DOCTOR OF PHILOSOPHY  
*in*  
EARTH SCIENCES

by

**SIVAPRABHA S.**



DEPARTMENT OF EARTH SCIENCES  
INDIAN INSTITUTE OF TECHNOLOGY ROORKEE  
ROORKEE - 247 667 (INDIA)  
DECEMBER, 2008

**©INDIAN INSTITUTE OF TECHNOLOGY ROORKEE, ROORKEE-2008  
ALL RIGHTS RESERVED**



# INDIAN INSTITUTE OF TECHNOLOGY ROORKEE ROORKEE

## CANDIDATE'S DECLARATION

I, hereby, certify that the work which is being presented in this thesis entitled "GEODYNAMIC EVOLUTION OF THE SHYOK SUTURE ZONE, NW HIMALAYAS" in partial fulfilment of the requirements for the award of the degree of Doctor of Philosophy, submitted in the Department of Earth Sciences of the Indian Institute of Technology Roorkee, Roorkee is an authentic record of my own work carried out during the period from January, 2004 to December, 2008 under the supervision of Dr. D. K. Mukhopadhyay, Professor, Department of Earth Sciences, Indian Institute of Technology Roorkee, Roorkee 247667, India and Dr. T. Ahmad, Professor, Department of Geology, Delhi University, Delhi 110007, India.

The matter presented in this thesis has not been submitted by me for the award of any other degree of this or any other Institute.

(SIVAPRABHA S.)

This is to certify that the above statement made by the candidate is correct to the best of our knowledge.

(T. Ahmad)  
Supervisor

(D. K. Mukhopadhyay)  
Supervisor

Date: 22 December, 2008.

---

The Ph.D. viva voce examination of **Mrs. Sivaprabha S.**, Research Scholar has been held on 03/06/2009

Signature of Supervisors

Signature of External Examiner

## *ACKNOWLEDGEMENT*

The present work was carried out under the supervision of Professor D. K. Mukhopadhyay and Professor T. Ahmad. Their constructive suggestions, criticism and help from choosing the area of study through fieldwork, geochemical analyses, interpretation to the preparation of the final draft of the thesis are gratefully acknowledged.

I convey my heartfelt gratitude to the Head of the Department of Earth Sciences, IIT Roorkee and the Head of the Department of Geology, Delhi University for providing all the available facilities for smooth progress of work. I am thankful to my research committee members, Professor D. C. Srivastava and Dr. J. Das, for their valuable suggestions from time to time.

My special thanks are due to Mr. J. G. Nair for his support during my tenure as JRF/SRF. The support offered to me by all other technical and non-technical staff in the Department is also duly acknowledged.

Thanks are also due to Dr. P. P. Khanna and Dr. H. K. Sachan, Wadia Institute of Himalayan Geology, Dehra Dun for their help during geochemical analysis, which is the most important part of the thesis. I am obliged to Professor S. Balakrishnan for permitting me to carry out isotope analysis in TIMS Laboratory in the Department of Earth Sciences, Pondicherry University and for his help in interpretation of the geochemical data.

I express my heartfelt gratitude to Dr. Dorjey and my friends and colleagues, Rakhi, Ranjan, Pradeep, Ajanta, Ritu, Mondal, Purushothaman, Saju, Vivek, Deepti, Anand, Manish and Nihar for their continuous support, encouragement and company at crucial times.

I am indebted to my parents, in-laws, grand parents and brothers for their prayers, sacrifices, endless support and constant encouragement with love, affection and inspiration throughout the life and especially during the tough time of my research work.

I believe my husband's support and encouragement during the highs and lows of my research work needs a special mention. He always gave me a shoulder to lean on whenever I was down with impatience and frustration.

Financial support from the University Grants Commission, Government of India in the form of a fellowship is gratefully acknowledged.

A final acknowledgment is extended to the Omnipotent for keeping me determined, patient and optimistic during this research work.



(SIVAPRABHA S.)

<b>TABLE OF CONTENT</b>	Page No.
CANDIDATE'S DECLARATION	
ACKNOWLEDGEMENT	i
CONTENTS	iii-v
LIST OF FIGURES	v-vii
LIST OF TABLES	vii-vii
ABSTRACT	viii
<b>CHAPTER 1: INTRODUCTION</b>	<b>1-25</b>
1.1 PREAMBLE	1
1.2 INDIA-ASIA CONVERGENCE IN NW HIMALAYAS	3
1.3 IGNEOUS ACTIVITIES DURING THE CONVERGENCE	12
1.4 TECTONIC DIVISIONS OF HIMALAYAS	17
1.4.1 The Sub-Himalaya Zone	18
1.4.2 The Lesser Himalaya Zone	18
1.4.3. The Higher Himalaya Crystalline Zone	19
1.4.4. The Higher/Tethys Himalaya Sedimentary Zone	20
1.5 THE TRANS-HIMALAYAS	20
1.6 AIM OF THE PRESENT STUDY	25
<b>CHAPTER 2: GEOLOGY OF THE AREA</b>	<b>27-50</b>
2.1 LADAKH BATHOLITH	29
2.2 THE KARAKORAM BATHOLITH	32
2.3 SHYOK SUTURE ZONE (SSZ)	33
2.3.1 Flysch and Molasse	34
2.3.2 Felsic Volcanics	35
2.3.3 Granites and Granitoids	36
2.3.4 Mafic volcanics and Metabasalts	37
2.3.5 Ultramafics and Ophiolite mélange volcanics	38
2.3.6 Metasediments and Metamorphics	39
2.4 INDUS-TSANGPO SUTURE ZONE (ITSZ)	40
2.5 COMPARISON BETWEEN ITSZ AND SSZ	42
2.6 PREVIOUS WORK DONE IN THE STUDY AREA	43
2.7 SCOPE OF THE PRESENT WORK	46
2.8 OBJECTIVES OF THE PRESENT STUDY	49
<b>CHAPTER 3: METHODOLOGY</b>	<b>51-64</b>
3.1 PETROGRAPHY	51
3.2 GEOCHEMICAL STUDY	51
3.2.1 Sample processing	51
3.2.2 Sample analysis	52
3.2.2.1 <i>X-Ray Fluorescence (XRF)</i>	52
3.2.2.2 <i>Inductively Coupled Plasma Mass Spectrometry (ICP-MS)</i>	56
3.3 ISOTOPE STUDY	60
3.3.1 Sample dissolutions	60
3.3.2 Ion exchange chromatography	61
3.3.3 Analytical technique	62
3.3.3.1 <i>Thermal Ionization Mass spectrometry (TIMS)</i>	62

<b>CHAPTER 4: FIELD DESCRIPTION AND PETROGRAPHY</b>	<b>65-82</b>
4.1 FELSIC VOLCANICS	65
4.2 GRANITES AND GRANITOIDS	66
4.3 MAFIC VOLCANICS AND METABASALTS	69
4.4 OPHIOLITE MÉLANGE	69
4.5 METASEDIMENTS AND METAMORPHICS	71
<b>CHAPTER 5: GEOCHEMISTRY</b>	<b>83-118</b>
5.1 MAJOR ELEMENTS CHARACTERISTICS	83
5.1.1 Distribution of major elements	83
5.1.2 Chemical classification of SSZ rocks	87
5.1.3 Bivariate variation diagrams	91
5.1.4 Triangular variation diagrams	94
5.2 TRACE ELEMENT CHARACTERISTICS	100
5.2.1 Distribution of trace elements	100
5.2.1.1 <i>Binary plots</i>	102
5.2.1.2 <i>Multi-element plots</i>	103
5.2.2 Rare Earth Element abundances	111
<b>CHAPTER 6: PETROGENETIC MODELLING</b>	<b>119-142</b>
6.1 MINERAL COMPOSITION AND MELT CHEMISTRY	120
6.2 PEROGENETIC MODEL OF SUBDUCTION ENVIRONMENT	122
6.2.1 Hundar igneous suite	123
6.2.2 Shyok volcanics	127
6.2.3 Khardung volcanics	130
6.2.4 Tsoltak volcanics	133
6.2.5 Nubra ophiolite volcanics	135
6.2.6 Karakoram plutonic complex	137
6.3 SUMMARY	139
<b>CHAPTER 7: ISOTOPE GEOCHEMISTRY</b>	<b>143-154</b>
7.1 Rb-Sr SYSTEMATICS	143
7.2 Sm-Nd SYSTEMATICS	144
7.2.1 Evolution of Sm-Nd and Rb-Sr systematics	144
7.2.2 Isotope studies in Shyok suture zone rocks	147
7.3 COMPARISON WITH ROCKS FROM OTHER TECTONIC SETTINGS	151
<b>CHAPTER 8: DISCUSSION AND CONCLUSIONS</b>	<b>155-170</b>
8.1 DISCUSSION	155
8.2 COMPARISON OF SHYOK AND INDUS SUTURE ZONE ROCK UNITS	157
8.3 CONCLUSIONS	167
<b>REFERENCES</b>	<b>171-197</b>

## APPENDICES

Appendix 1	Sample locations and field descriptions	1995
Appendix 2	Major element abundance data	207
Appendix 3	Trace elemental abundance data	211
Appendix 4	Rare Earth Element (REE) abundance data	213
Appendix 5	Isotope data	215

## LIST OF FIGURES

Figure 1.1	Palaeopositions of continents and oceans and geodynamic processes related to northward flight of India/closure of Tethys Ocean from Early Permian to present	6
Figure 1.2	Schematic cross sections across Tethys showing geodynamic evolution associated with northward drifting of the Indian continent and collision with Asian plate	10
Figure 1.3	Simplified tectonic map of central and southeast Asia showing different continental blocks after the accretion and development of various suture zones	12
Figure 1.4	Simplified geological map of the Himalayas showing different litho-tectonic zone, major fault surfaces, suture zones and Trans-Himalayan batholiths	23
Figure 1.5	Schematic cross section across Himalayan collision zone.	24
Figure 2.1	SRTM image showing the study area	28
Figure 2.2	Tectonic map of the NW Himalayas and Western Tibet overlain on a Landsat-7 image	29
Figure 2.3	Geological map of Trans-Himalayas showing different litho-tectonic units	30
Figure 2.4	Geological map of the Shyok Suture Zone	35
Figure 3.1	WD-XRF (Siemens SRS 3000) at W.I.H.G., Dehra Dun...	53
Figure 3.2	Flow diagram of the XRF and its working principle	54
Figure 3.3	Basic instrumental components that make up an ICP-MS	57
Figure 3.4	ICP-MS (Perkin Elmer, Elan DRC-e) at W.I.H.G., Dehra Dun	59
Figure 3.5	Thermal Ionization Mass spectrometry (TIMS, model: Triton-Thermo Finnigan) at Pondicherry University	63
Figure 4.1	Map showing the sample locations from different litho-tectonic units	73
Figure 4.2	Field photographs from different litho-tectonic units	78
Figure 4.3	Photomicrographs of samples from different litho-tectonic units	81
Figure 5.1	Schematic variation diagrams for major element oxides in case of calc-alkaline volcanic series	85
Figure 5.2	Total alkali versus silica (TAS) diagram of different litho-tectonic units	90
Figure 5.3	Total alkali versus silica (TAS) diagram of different litho-tectonic unit according to their chemical composition	90
Figure 5.4	Classification schemes based on least mobile incompatible trace element ratios	91

Figure 5.5	Harker diagrams of major element wt% against SiO <sub>2</sub> wt%.	95
Figure 5.6	AFM diagram discriminating the tholeiitic and calc-alkaline series	99
Figure 5.7	Basaltic andesites with silica range 51-56 Wt% are plotted within the island arc and active continental margin field of Al <sub>2</sub> O <sub>3</sub> - FeO-MgO	99
Figure 5.8	Trace elements binary plots and their ratio plots	105
Figure 5.9	Primitive Mantle normalized multi element spidergrams of trace elements	108
Figure 5.10	Chondrite normalized REE plots of different litho-tectonic unit	114
Figure 6.1	The melting curve-I of basalt and basaltic source with sediment input (curve-II)	126
Figure 6.2	REE pattern of the assumed source and samples from the Hundar area	126
Figure 6.3	The melting of a contaminated mantle source and the fractionation of olivine and pyroxene give the samples of the Shyok area	128
Figure 6.4	The mantle source, parent magma formed by the melting of the source and fractionation the mineral phases from the magma to generate the HST-22 of Shyok area	129
Figure 6.5	Chondrite normalized REE pattern of the basaltic andesites of the Shyok area and the melt leaving clinopyroxene and plagioclase in residue	129
Figure 6.6	Partial melting of the assumed source at shallow depth and the REE pattern of the sample from Khardung	131
Figure 6.7	Partial melting of the assumed source at higher depth and the REE pattern of the sample KST-4	132
Figure 6.8	Felsic magma formed from the melting of basaltic composition leaving a residue with garnet	132
Figure 6.9	Partial melting of the mantle derived source generate the REE pattern similar to the Tsoltak volcanics	134
Figure 6.10	Mantle derived source (sample NST-69) modeled for REE pattern of the basaltic andesite of Nubra volcanics	136
Figure 6.11	The REE pattern of Tsoltak and Nubra volcanics	136
Figure 6.12	The sediment input in the source for diorite in Karakoram area	138
Figure 6.13	The melting of mantle derived source and the REE pattern of basic volcanics from Nubra and Karakoram dyke	138
Figure 6.14	Source characteristics of different rock units from Shyok Suture Zone	140
Figure 6.15	Source characteristics of different rock units from Kohistan arc of Pakistan	141
Figure 7.1	The evolution of Sm-Nd isotope system	145
Figure 7.2	Sm-Nd isotopic plot of different litho-tectonic units.	150
Figure 7.3	Rb-Sr isotopic plot of different litho-tectonic units.	150
Figure 7.4	Sr-Nd isotopic plot of different litho-tectonic units of Shyok Suture Zone	151



Figure 7.5	Comparison of isotopic ratios of other similar tectonic setting and suture zone rocks from Pakistan	152
Figure 7.6	Isotopic ratios of Kohistan island arc rocks along with Shyok Suture Zone rocks (t=110Ma)	153
Figure 7.7	<sup>87</sup> Sr/ <sup>86</sup> Sr- SiO <sub>2</sub> plot of different litho-tectonic units	153
Figure 8.1	Zr/Nb vs. Zr/Y plot of Nidar and Zildat ophiolites of ITSZ	159
Figure 8.2	Zr/Nb vs. Zr/Y plot shows Nidar and Zildat ophiolites of ITSZ and also the volcanics from ITSZ and SSZ	159
Figure 8.3	Zr/Nb vs. Zr/Y plot shows comparison of Nidar ophiolites of ITSZ and Tsoltak, Nubra and Shyok volcanics of SSZ	160
Figure 8.4	La vs.Y plot for comparison between intermediate and volcanic rocks from SSZ and ITSZ	160
Figure 8.5	Chondrite normalized REE pattern of Nidar volcanics	161
Figure 8.6	Chondrite normalized REE pattern of Shyok volcanics.	161
Figure 8.7	Chondrite normalized REE pattern of Nubra mélange volcanics	162
Figure 8.8	Chondrite normalized REE pattern of Tsoltak mélange volcanics	162
Figure 8.9	Zr/Nb vs. Ce/Y plot of volcanics from ITSZ and SSZ.	163
Figure 8.10	Zr/Nb vs. Ce/Y plot of volcanics from ITSZ and SSZ of present study	164
Figure 8.11	Chondrite normalized REE pattern of Hundar igneous suite	166
Figure 8.12	Chondrite normalized REE pattern of Khardung volcanics	166
Figure 8.13	Tectonic set up of Shyok Suture Zone	169

#### LIST OF TABLES

Table 3.1	Major element analysis of standard and other samples using XRF to estimate analytical uncertainty	55
Table 3.2	Trace element analysis of standard using XRF to estimate analytical uncertainty	55
Table 3.3	Rare earth element analysis of standard and other samples using ICP-MS to estimate analytical uncertainty	59
Table 3.4	Sr and Nd isotopic compositions and elemental concentrations of Rb, Sr, Sm and Nd for rock standards BHVO-1 and BCR-2	63
Table 5.1	Colour as well as litho-tectonic index	88
Table 5.2	REE data showing relative enrichment of LREE and HREE	117
Table 6.1	Concentration of Sr and Zr in the mixed source (sediment +basalt). Concentration of Sr and Zr in the resulting melts after different degrees of partial melting	125
Table 6.2	Concentration of Ce and Ni in the mixed source (basalt + peridotite). Different degrees of partial melting of the source and concentration of Ce and Ni in the melt	128
Table 6.3	Major element data of mantle pyrolite from different ophiolites along with sample NST-69 from Tsoltak	135

## ABSTRACT

In the established framework of continent-continent collision between the Indian and the Eurasian plates two suture zones are usually recognized, viz., Indus-Tsangpo Suture Zone (ITSZ) and Shyok Suture Zone (SSZ). The present study aims at enhancing our knowledge regarding lateral, temporal, petrological and geochemical variations of the rock units of SSZ and its evolutionary history. Petrogenetic modelling using major and trace elements as well as isotopic compositions of different rock units in the SSZ and their relations are utilized to reconstruct the geodynamic evolution of the SSZ.

Geochemical study involves major, trace and REE analyses of selected samples from each litho-tectonic unit. The data from different litho-tectonic units of SSZ have been analyzed separately using various discrimination diagrams and indicate subduction zone magmatism and arc affinity of the rock samples. Major and trace element abundances of the samples from different litho-tectonic units, viz., Hundar, Khardung, Shyok, Tsoltak, Nubra and Karakoram, demonstrate magmatic trends expected for a suite of rocks varying from mafic to felsic composition. This is indicative of fractionation of olivine, pyroxene, feldspars and Fe-Ti oxide phases during the evolution of their magmas.  $Al_2O_3$ ,  $Fe_2O_3$ , CaO, MgO,  $TiO_2$  and  $P_2O_5$  show negative correlation with  $SiO_2$ . Scattering in  $Na_2O$  and  $K_2O$  variation diagrams may be due to post-crystallization processes or fluid activity in the area.

In chondrite normalized rare earth element (REE) pattern of samples from different litho-tectonic units show light REEs enrichment and fractionation of middle and heavy REEs. Multi-element spidergrams show enrichment of large ion lithophile elements and depletion of high field strength elements with negative Nb, P, Ti, Sr and Eu anomalies. Shyok volcanics exhibit slightly less enrichment compared to other units.

Two component mixing curve between an old crustal component and a depleted mantle component explains the isotopic characteristics of the SSZ rocks. Most of the samples from SSZ plot along this mixing hyperbola. Isotopic study of the rocks from SSZ indicates source multiplicity, either by mixing of crustal material due to subduction during melting or during the transport of magma to the surface. Sediment involvement at the source region and influx of aqueous fluid also played a major role in modifying the geochemical characteristics of the rock units.

Isotopic and geochemical characteristics suggest that Khardung volcanics and Hundar intrusives are formed by melting of some components of the Kohistan-Ladakh island arc by recycling of the arc. The evidence from geochemical and isotopic study indicate that an active continental margin (Andean-type subduction) was present between the Kohistan and Karakoram during Cretaceous time. Shyok volcanics may be the basement on which the more calc-alkaline arc system developed. The more matured arc and back-arc basins are well preserved in the northern part (Pakistan area). These are translated along the Karakoram Fault (KF) towards Lhasa in Tibet. Therefore, the rock units <sup>described</sup> exposed in the study <sup>area</sup> probably <sup>were</sup> formed in the <sup>represent</sup> fore arc <sup>part</sup> and the accretionary complex of an Andean-type arc setting.

# **Chapter 1**

## **INTRODUCTION**

**1.1 PREAMBLE**

The Himalayan mountain range extends for about 2500 km in length from Nanga Parbat in NW to Namcha Barwa in the E (Wadia, 1931). This mountain range represents the most recent and spectacular consequences of continent-continent collision within the paradigm of plate tectonics (Argand, 1924; Dewey and Bird, 1970; Powell and Conaghan, 1975; Molnar and Tapponnier, 1975; Frank *et al.*, 1977a; Thakur and Viridi, 1979; Allegre *et al.*, 1980). Collision of the northward moving Indian plate along the southern margin of the Eurasian plate resulted in the formation of this mighty mountain range. There had been protracted geodynamic processes during northward drift of India and the eventual collision. Imprints of these geodynamic processes are still preserved in this mountain belt.

The movement of lithospheric plates has resulted in repeated assembly and break-up of continents through geologic history. A supercontinent called Rodinia is considered to have formed about a billion years (~ 750 Ma, Pozzi *et al.*, 1972; 900 Ma, Zhong *et al.*, 2007; 1100-900 Ma, Li *et al.*, 2008) ago and thought to have composed of most of the continents. Rodinia was broken up into seven major continents around 600 million years ago (Pozzi *et al.*, 1972; Burg, 1983; Nance *et al.*, 1988; Hoffman, 1991). These continents later re-assembled into another supercontinent called Pangea and a vast ocean associated with this continent was called Panthalassic ocean. Palaeo-Tethys ocean was part of this vast ocean (Fig. 1.1a). Pangea came into existence about 300 million years ago (Sengör, 1984; Matte *et al.*, 1996; Li and Powell, 2001; Veevers, 2004; Cawood and Buchan, 2007). Pangea had eventually broken up into Laurasia and Gondwana and Palaeo-Tethys came into existence (Allègre, 1984; Dewey *et al.*, 1988; Gurnis, 1988). At about 280 Ma, a part of the ancient super continent Pangea, including South China, Indo-China, and

Northern Tibet started rifting away from Gondwana. Subsequently Iran, Turkey, Southern Tibet (Lhasa) and few other blocks together called as the Cimmerian continent also rifted away from the Gondwana (Fig. 1.1b). The ocean basin existed between Palaeo-Tethys and the Neo-Tethys is called Meso-Tethys (Metcalf, 1999; Otofujii, 2007). The terms 'Palaeo-Tethys', 'Meso-Tethys' and 'Neo-Tethys' were first used by Stille (1958) for the Tethys ocean in different geological times.

The northward progression of the different micro-continental blocks (mainly South China, Indo-China and Northern Tibet or Qiangtang) led to the subduction of the Palaeo-Tethys. Closure of the main Palaeo-Tethys ocean occurred in the late Permian to early Triassic (Metcalf, 1999). Northward drifting of the Cimmerian plates including Iran, Turkey and Southern Tibet (Lhasa) blocks caused the subduction of Meso-Tethys and opening of Neo-Tethys (Fig. 1.1c, Sinha-Roy, 1982; Valdiya, 1997). The closure of the Meso-Tethys ocean and the suturing of the Cimmerian continent occurred between middle Jurassic and early Cretaceous (Fig. 1.1d) (Sengör, 1984; Van der Voo *et al.*, 1999; Zanchi *et al.*, 2000; Scotese, 2001; Cawood and Buchan, 2007). Gondwana began to break up in the middle Jurassic (about 167 Ma) into different plates including India. India started its northward movement at about 140 Ma in the early Cretaceous (Fig. 1.1e) (Metcalf, 1999). In the upper Cretaceous (84 Ma), the Indian plate began its very rapid northward drift at an average speed of 16 cm/year (Molnar and Tapponnier, 1975). Intra-oceanic subduction in the Neo-Tethys formed an oceanic island arc called Dras arc (Fig. 1.1f). Detailed description of the Neo-Tethys subduction and arc formation is given in the following section. The collision of India with Eurasia had occurred in early to middle Eocene time (Fig. 1.1g) and the velocity of northward drift of India slowed down to about 5 cm/year (Molnar and Tapponnier, 1975; Patriat and Achache, 1984; Sengör, 1984;

Klootwijk *et al.*, 1992; Shi and Archbold, 1998; Roy, 1999; Scotese, 2001). Distribution of the continents at present time is given in Fig. 1.1h.

## 1.2 INDIA-ASIA CONVERGENCE IN NW HIMALAYAS

As discussed in the previous section, India-Asia collision and Himalayan orogeny are part of a long subduction and accretion history. Rifting and northward drift of continental blocks derived from the Gondwana led to the opening and subsequent closure of the ocean basins, Palaeo-Tethys, Meso-Tethys and Neo-Tethys. Schematic representation of these events and associated tectonics are given in a series of cross section in Fig. 1.2. The schematic cross sections in Fig. 1.2 are oriented approximately N-S direction across Tethys ocean.

Initial rifting and opening of the Palaeo-Tethys occurred in the early Silurian and subducts at the southern margin of Asia at the Tethys trench (Fig. 1.2a). Haines *et al.* (2003) have suggested that Lhasa and Qiangtang blocks were originally a part of the Cimmerian continent. Qiangtang block remained on the margin of Gondwana until the Permian (Metcalf 1998, 1999). Qiangtang and Lhasa blocks successively broke off from Gondwana and started northward drift resulting in the formation of Palaeo-Tethys, Meso-Tethys and Neo-Tethys oceans (Fig. 1.2b). Based on the difference in palaeolatitude, Otofuji *et al.* (2007) suggested that the Lhasa block was located south of the Qiangtang block during Jurassic at a distance more than of 2200 km (Fig. 1.2c). Palaeo-Tethys was closed in the late Permian ( $\sim 267$  Ma) due to the rapid northward drift of Qiangtang block (Li *et al.*, 2004). Subsequently, the Qiangtang block accreted to the Asian margin along Jinsha suture.

Rapid drifting of the Qiangtang block towards north resulted in the opening of Meso-Tethys in the early Permian (Golonka and Krobicki, 2001). When the Lhasa block

drifted rapidly northward, the Meso-Tethys entered a closing phase in late Triassic to early Cretaceous (Girardeau *et al.*, 1984; Dewey *et al.*, 1988) (Fig. 1.2d, 1.2e). Spatial gap between Qiangtang and Lhasa blocks had been reduced by 1200 km by Cretaceous time which indicates the closing of Meso-Tethys ocean. The accretion of the Lhasa block to the Asian continental margin (Fig. 1.2e) along the Bangong suture was completed in the middle Cretaceous after the closure of Meso-Tethys (Besse *et al.*, 1984; Sengör *et al.*, 1988; Zanchi *et al.*, 2000).

At the Asian and Indian margin, the Himalayan orogenic cycle began with the opening of the Neo-Tethys ocean during Permo-Triassic (~ 248 Ma, Stampfli and Borel, 2001) time with the separation of the Lhasa blocks from India (Ricou, 1994; O'Brein, 2001; Gradstein *et al.*, 2004). The northward movement of India led to the subduction of Neo-Tethys oceanic crust under the Lhasa block. The slab pull resulted in the breaking off of the oceanic crust. Intra-oceanic subduction within the Neo-Tethys and formation of the Kohistan –Ladakh arc started in the late Jurassic (Fig. 1.1f, 1.2d). Development of the Kohistan-Ladakh arc took place during the middle Cretaceous (Coward *et al.*, 1986; Hanson, 1989; Rolfo *et al.*, 1997; Rolland *et al.*, 2000). Accretion of the intra-oceanic arc to Lhasa block and obduction of the arc to the Indian continental margin started in late Cretaceous (Fig. 1.2f) (Petterson and Windley, 1985; Searle, 1991; Searle, *et al.*, 1999; Dunlap and Wysoczanski 2002; Petterson and Treloar, 2004). The marginal basin that existed between the arc and the continent also closed subsequently. Accretion of the Kohistan-Ladakh arc to the Lhasa block occurred subsequent to the consumption of the Neo-Tethys under the Lhasa block and the continuous subduction along the Shyok Suture Zone (SSZ, Fig. 1.2f). The Kohistan-Ladakh arc was obducted onto the Indian margin along another suture zone in the western part during India-Asia collision (Thahirkheli *et al.*, 1979, 1982). There are different opinion about the development of the Ladakh arc and

the time of its accretion with the continental margin (Rolland *et al.*, 2002). By early Tertiary, the accretion of the arc to the continental margin of India was completed and formed another suture zone called ITSZ (Fig. 1.2g) (Gansser, 1980; Thakur, 1981; Honegger *et al.*, 1982; O'Brien, 2001; Atchinson *et al.*, 2007). Fig. 1.3 is a simplified map of Southeast Asia showing main continental blocks (Lhasa, Qiangtang and India) and sutures (Jinsha, Bangong, Indus-Tsangpo and Shyok sutures) that formed due to the accretion of these continents.

Collision of the continental plates occurred subsequent to the consumption of the oceanic crust. The initial contact between India and Eurasia plates estimated to have occurred at about 65 Ma (Klootwijk *et al.*, 1992). Suturing then continued eastward and completed about 55 Ma. India's northward movement slowed down from a pre-collision velocity of 18-19.5 cm/year to about 4.5 cm/year after initial collision (Molnar and Tapponier, 1975; Patriat and Achahe, 1984). Atchinson *et al.* (2007) assume the collision to have taken place at a later date at 35 Ma. Geological evidence that constrain the timing of collision initiation and associated processes are summarized by Searle *et al.* (1998). The terminal collision of the two plates is inferred from (1) the ending of marine sedimentation in the Indus-Tsangpo Suture Zone (2) the beginning of continental molassic sedimentation along the suture zone, (3) the ending of Andean type calc-alkaline magmatism along the Trans-Himalayan (Ladakh-Kohistan-Gangdese) batholiths, and (4) the initiation of major collision related thrust system in the Himalayan ranges. The cessation of marine sedimentation in the Tethyan Himalayas at the northern margin of India occurred at 52 Ma (Rowley, 1996). The beginning of molassic sedimentation along the Tibetan part of suture zone was regarded as Eocene with initiation of deposition of Indus molasses along the Indian part of the suture zone (Indus suture) (Searle *et al.*, 1987).



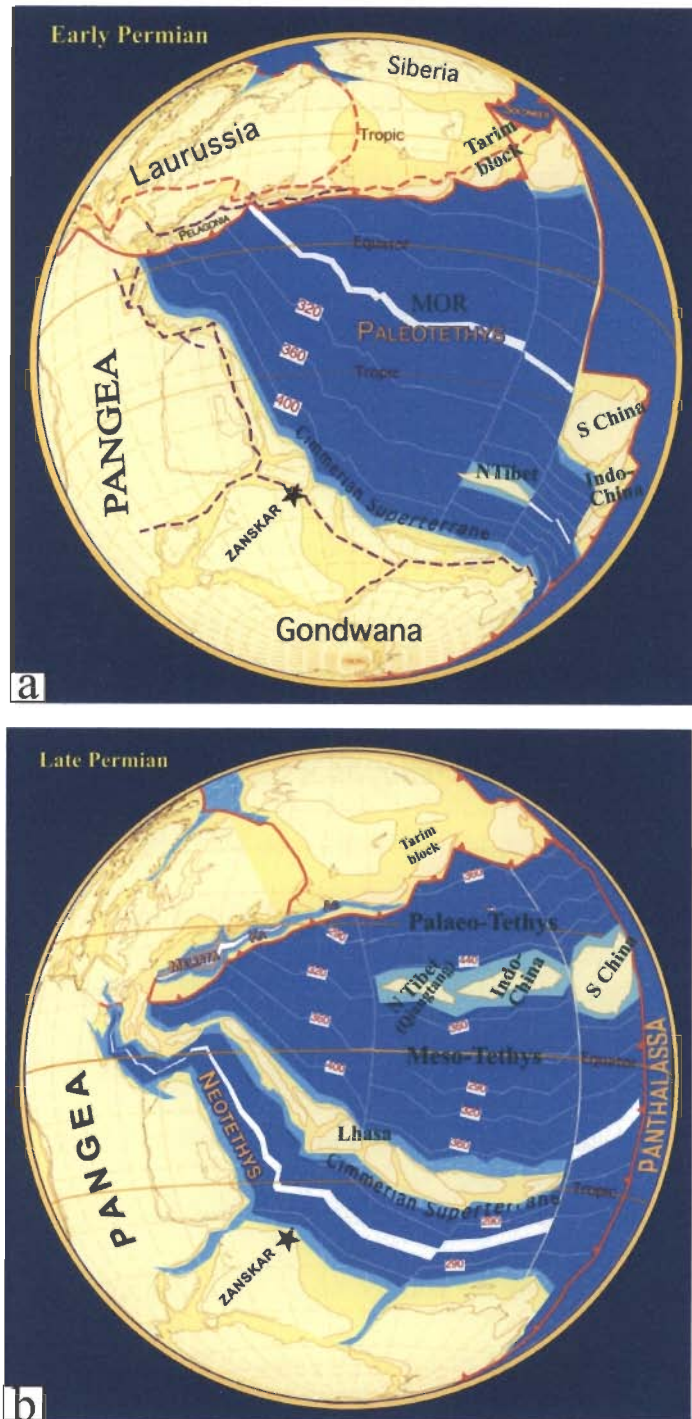


**Figure 1.1** Palaeopositions of continents and oceans (modified after Dezes, 1999; Scotese, 2001). (a) Supercontinent Pangea and Palaeo-Tethys ocean during early Permian. Northern Tibet, Indo-China and South China start moving towards north and Cimmerian continent (includes few other micro-continents) is rifting off from Gondwana (b) Opening of Neo-Tethys. Cimmerian continent, including Lhasa block move towards north. Palaeo-Tethys subducts below Laurasia due to the rapid northward drift of Northern Tibet, Indo-China and South China. Meso-Tethys is widening at south of Palaeo-Tethys.

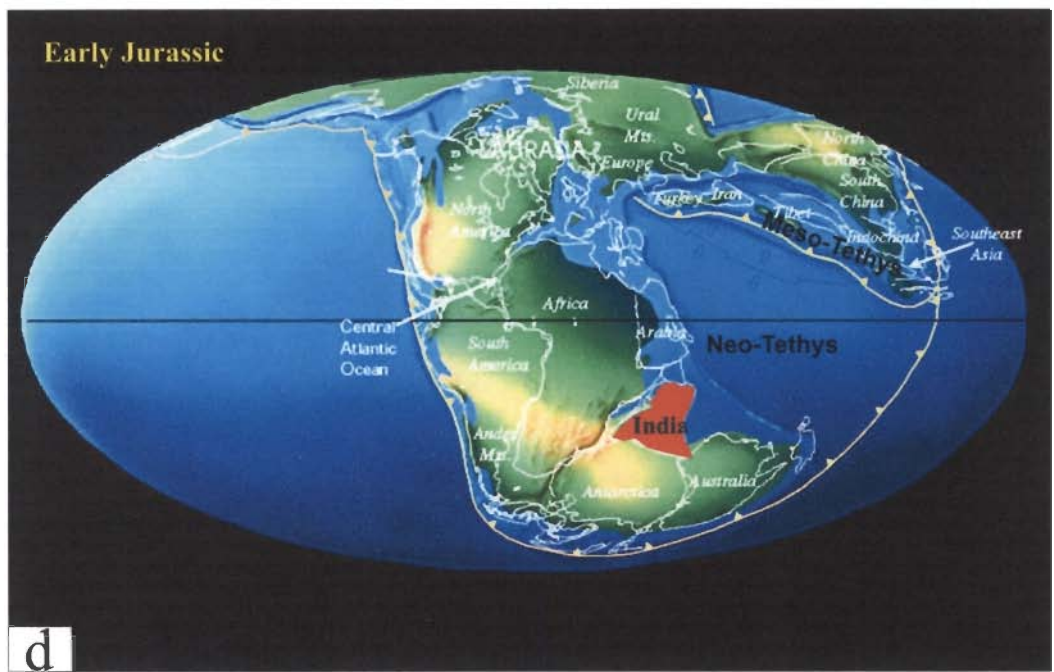
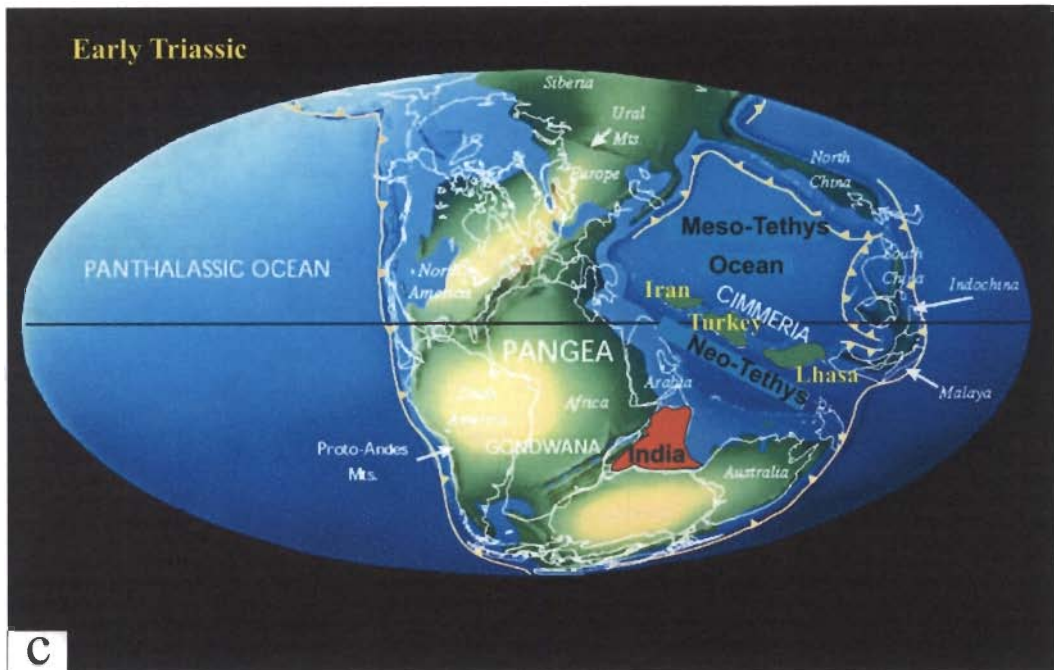


**Figure 1.1** Continued. (c) Palaeo-Tethys is closed and Northern Tibet, Indo-China and South China are accreted to the Asian margin. Different microcontinents of Cimmerian continent (including South Tibet or Lhasa) are drifting northward and closing Meso-Tethys (d) Closure of Meso-Tethys and Neo-Tethys ocean widening at early Jurassic. India is still attached to the Gondwana.

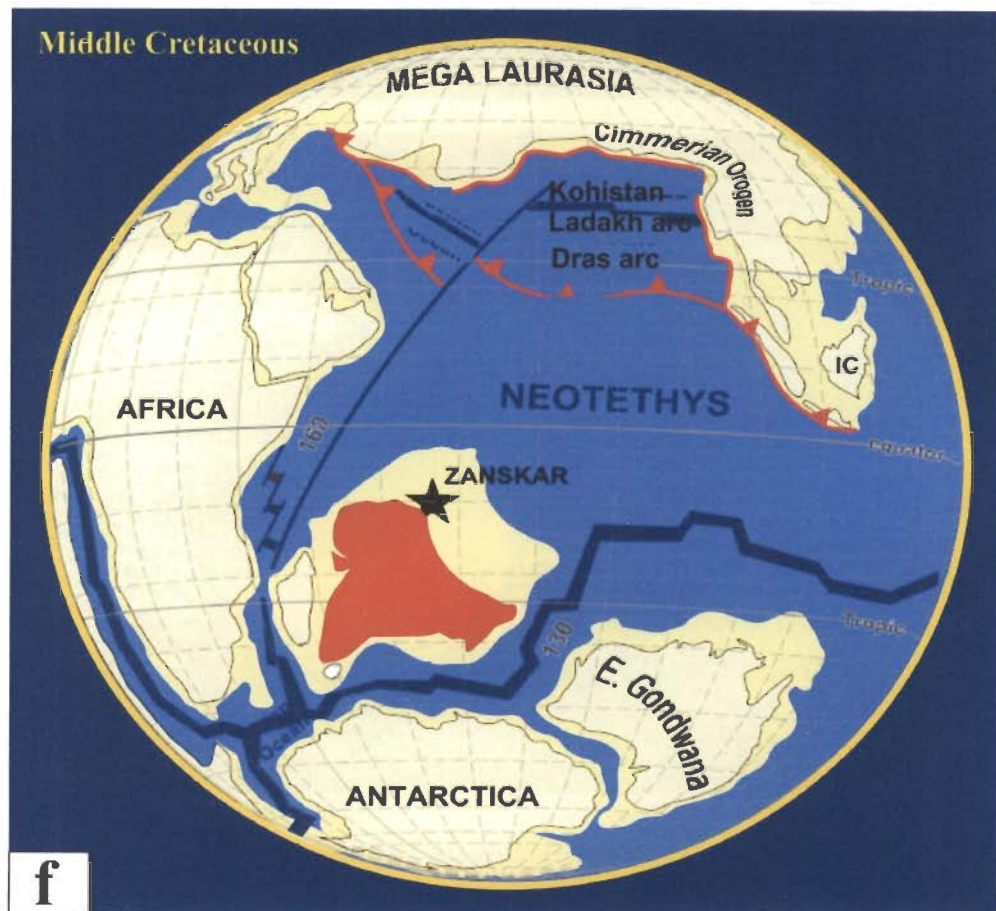
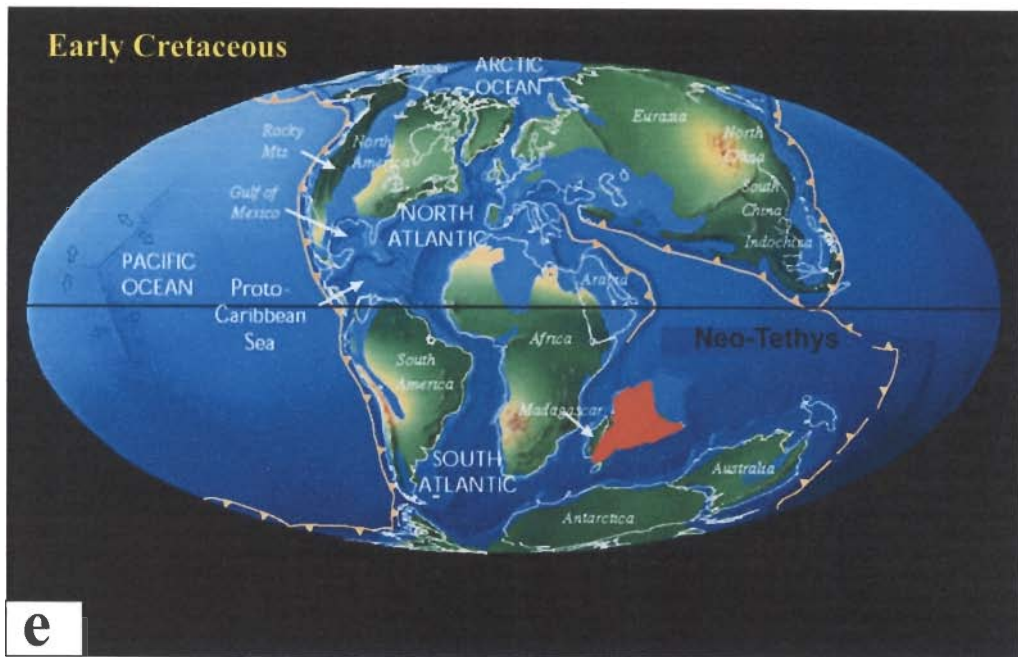


**Figure 1.1** Continued. (e) India breaks off from Gondwana and starts northward drifting. Gondwana is broken up into different continents (f) Intra-oceanic subduction within Neo-Tethys ocean results the development of Dras-Kohistan-Ladakh arc.

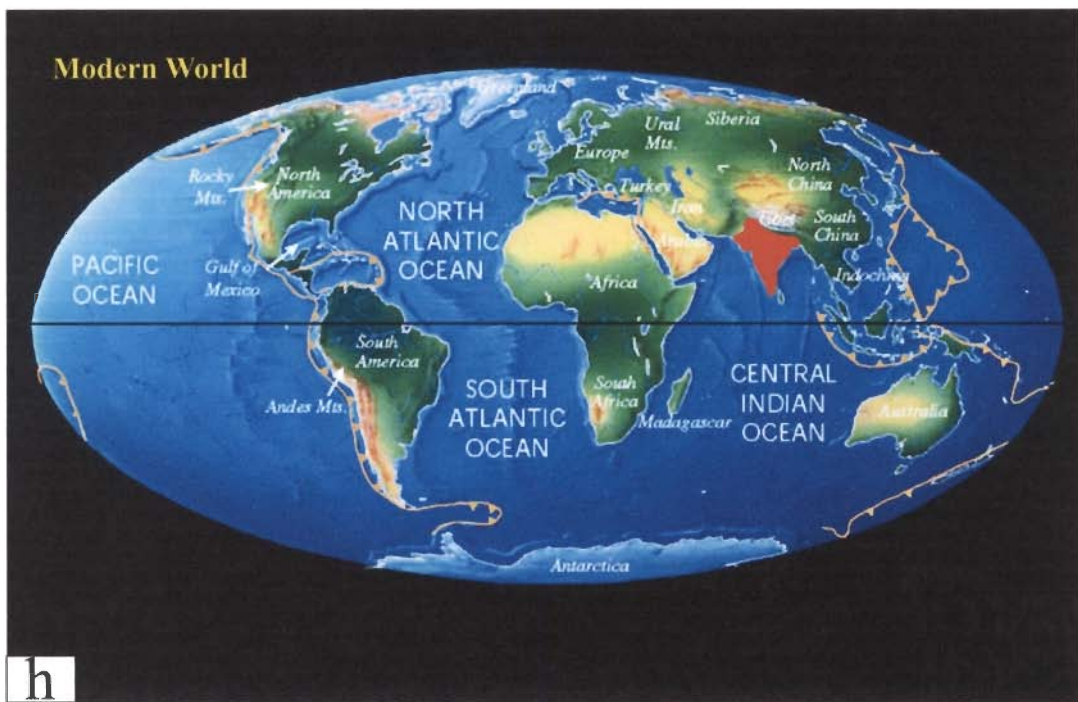
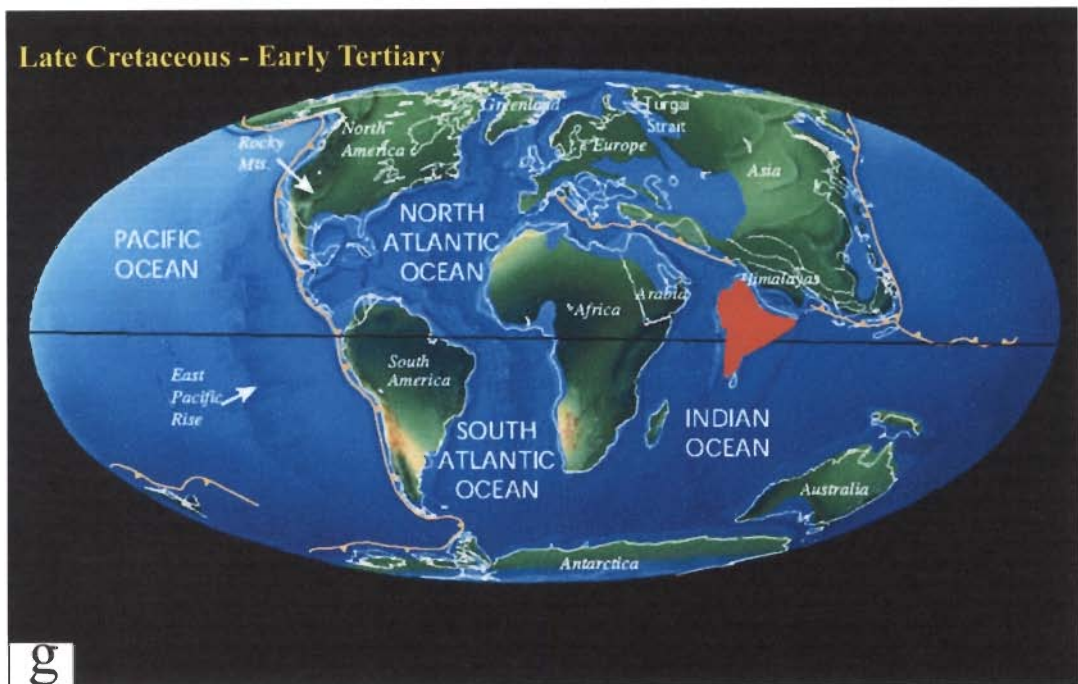


**Figure 1.1** Continued. (g) Closure of Neo-Tethys and accretion of the Dras-Kohistan-Ladakh arc to the Indian continental margin. Initial contact of Indian plate with Eurasian plate occurred at NW part of India SE part is still open. (h) Distribution of continents at present time. Continent-continent collision continues and results in the rising of Himalayas.

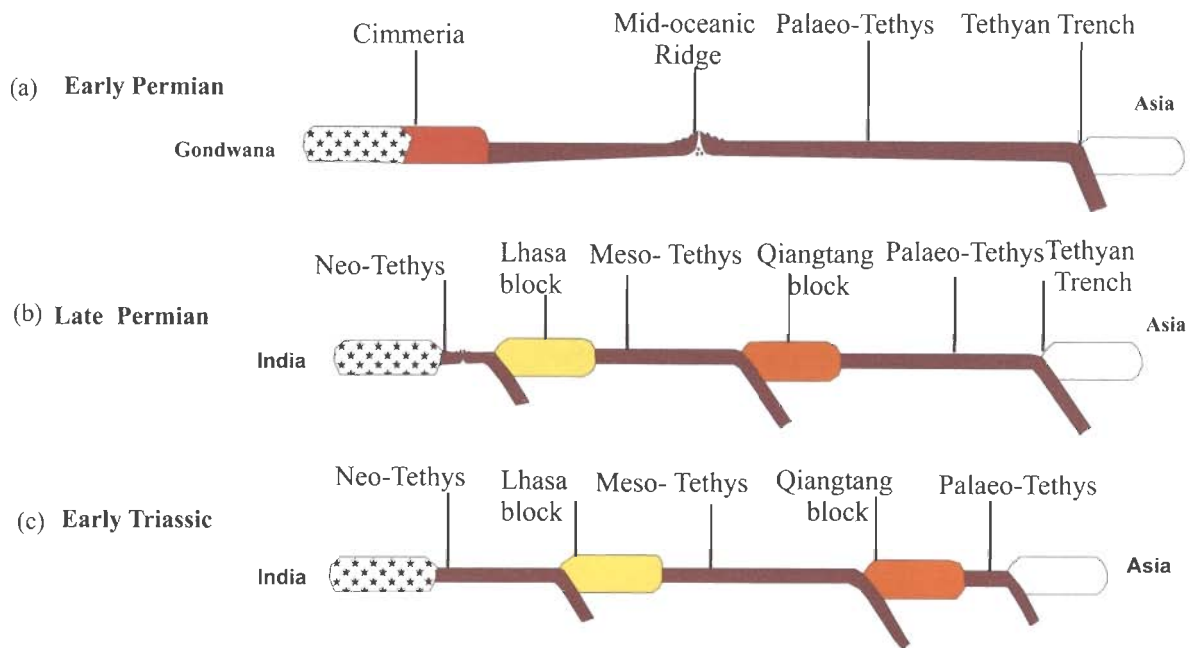


**Figure 1.2** Schematic cross sections across Tethys showing geodynamic evolution associated with northward drifting of the Indian continent and eventual collision with Asian plate (modified after O'Brien, 2001; with additional inputs from Girardeau *et al.*, 1984; Besse *et al.*, 1984; Petterson and Windley, 1985; Coward *et al.*, 1986; Dewey *et al.*, 1988; Sengör *et al.*, 1988; Hanson, 1989; Searle, *et al.*, 1991, 1999; Rolfo *et al.*, 1997; Metcalfe, 1999; Rolland *et al.*, 2000; Zanchi *et al.*, 2000; Golonka and Krobicki, 2001; Dunlap *et al.*, 2002; Li *et al.*, 2004; Petterson and Treloar, 2004; Otofujii *et al.*, 2007). (a) Palaeo-Tethys ocean between Asia and Gondwana at early Permian. The main Cimmerian continent is still attached to Gondwana (b) Qiangtang block (NTibet) has already broken off and moved away. Subduction of Palaeo-Tethys oceanic crust at the southern margin of Asia has also been initiated (cf., Fig. 1.1a). Rifting of Cimmeria (Lhasa block) opens up Neo-Tethys and initiates the subduction of Meso-Tethys at the southern margin of Qiangtang block. Subduction at the Asian margin continues (cf., Fig 1.1b). (c) Northward drifting of Qiangtang and Lhasa blocks continues and subductions taking place at three places. The Palaeo-, Meso- and Neo-Tethys oceans are now well defined (cf. Fig. 1.1c).

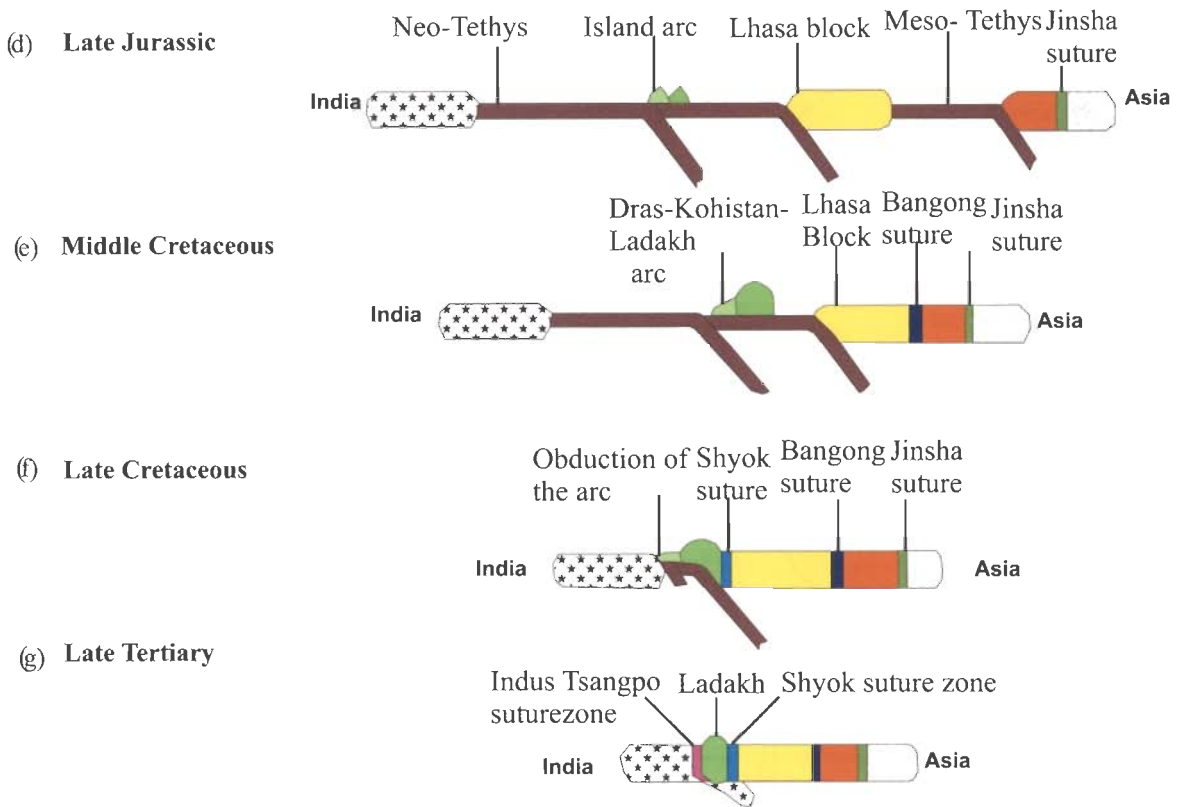


**Figure 1.2** Continued. (d) Palaeo-Tethys is closed and Qiangtang block is accreted to Asian margin at Jinsha suture. An intra-oceanic subduction within Neo-Tethys initiated with an embryonic island arc (cf., Fig. 1.1d). (e) Closure of Meso-Tethys and accretion of the Lhasa block to the Asian margin along Bangong suture take place in the middle Cretaceous (cf., Fig. 1.1f). Dras-Kohistan-Ladakh island arcs well developed. (f) Obduction of the island arc to the Indian continental margin and accretion of the arc to the Lhasa block along Shyok suture zone (cf., Fig. 1.1g). (g) Closure of Neo-Tethys, formation of Indus Tsangpo suture zone and initiation of Himalayan orogeny *sensu-stricto*.

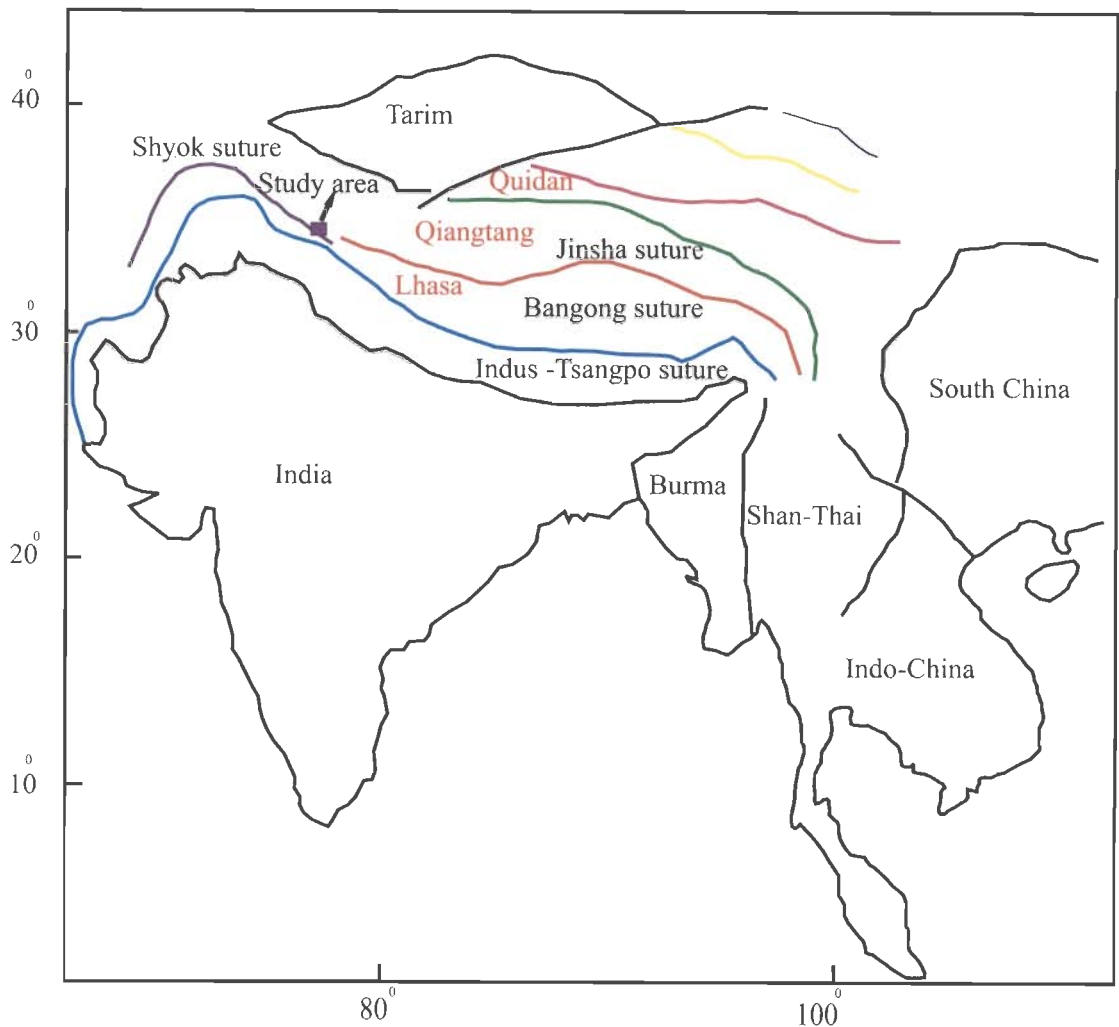


**Figure 1.3** Simplified tectonic map of central and southeast Asia showing Qiangtang, Lhasa, India, South China and Indo-China continental blocks after the accretion and various suture zones (after Yin and Harrison, 2000; Relumaz and Tapponier, 2003).

### 1.3 IGNEOUS ACTIVITIES DURING THE CONVERGENCE

Numerous volcanic activities have occurred during the opening and subsequent closure of Tethys ocean. The igneous activity associated with the opening of the ocean basin, subduction of the oceanic crust and magmatism in connection with the arc formation and its accretion are important to understand the sequential geodynamic processes that eventually led to the continent- continent collision. These volcanic activities involve the generation of new oceanic crust at mid-oceanic ridges, magmatism associated with the movement of the plates and subduction of the lithospheric plates with

both intra-oceanic (ocean-ocean) and continental-ocean (Andean type) types of subduction. Closure of the ocean and accretion of plate boundaries also give characteristic volcanic signatures.

New oceanic crust is created along mid-oceanic ridges (MOR) with basaltic volcanism having distinct geochemical characteristics of the newly formed oceanic crust. These basalts are usually tholeiitic with low alkali and low incompatible element composition and are variously termed as ocean floor basalts (OFB), abyssal basalts and mid-oceanic ridge basalts (MORB).

Movement of oceanic plate or continental plate over a mantle plume or a hot spot in the mantle may result in oceanic island volcanism or intra-plate volcanism. When a hot spot occurs within the interior of an oceanic plate, it results a single linear chain of islands and sea mounts. In contrast, if a continental plate comes over a hot spot the upwelling of the mantle plume rupture the continental lithosphere (intra-continental rifting) and initiates the formation of a new ocean basin. Both tholeiitic and alkali basalts are characteristics of oceanic island. These have distinct element and isotopic chemistry compared to MORB (Wilson, 1989). Basalts associated with continental fragmentation and formation of new ocean basin is called continental tholeiitic flood basalts (CFB). They are similar to MORB in terms of mineralogy and major element chemistry but the trace element characteristics are more or less similar to oceanic island tholeiite (Wilson, 1989; Philpotts, 1991).

Island arcs represent the arcuate chain of volcanic islands formed due to the subduction of one oceanic/continental plate beneath another oceanic plate. Region of partial melting for magma generation in an island arc scenario is variable. Fluids derived through dehydration reactions during metamorphism in a subduction zone can lead to calc-alkaline or alkaline series magmatism in an island arc. Partial melting of mantle



wedge (part of upper mantle) under dry condition may also produce basalts of low K-tholeiitic composition. In ocean-continent collision zone or active continental margin, the volcanic activity is similar to the intra oceanic subduction. Passage through the continental crust introduces crustal contamination to the magma and calc-alkaline series become richer in SiO<sub>2</sub> content. Crustal contamination may also lead to enrichment of LILE (Large Ion Lithophile Elements).

Although most of the oceanic crust is destroyed at the subduction zone, part of the oceanic crust may be preserved through obduction on to the continental margin. This obducted oceanic crust along with the pelagic sediments at the margin of lithospheric plate is called ophiolite suite. The suture zones are marked by the presence of ophiolites which represent the obducted oceanic crust and provide evidence for ocean closure. Ophiolite suite includes serpentinized ultramafics, gabbros pillow basalts, and pelagic sediments. Presence of ophiolite suite marks the site of oceanic subduction and suture zone.

Different volcanic activities during the break-up of Gondwana and also during the northward flight of Indian continent can be recognized in the Himalayas and adjoining areas. These volcanic rocks record rapidly changing tectonic environment that prevailed during the break up and collision. Rocks reported from early Carboniferous sequence of Indo-China and late Devonian to early Carboniferous MORB-like volcanic rocks preserved in South China may have been associated with the opening of Palaeo-Tethys (Li *et al.*, 2004). Late Permian alkali basalts of Shan-Thai block (Fig. 1.3) have been considered to be related to the subduction of Palaeo-Tethys ocean along the Tethyan trench (Li *et al.*, 1999). Ductile deformation and high temperature metamorphism in the late Permian to middle Triassic occurred in Indo-China, South China and Northern Tibet blocks supposedly indicate accretion of these blocks to the southern margin of the

Laurasia and closing of Palaeo-Tethys ocean (Carter *et al.*, 2001; Li *et al.*, 2004; Otofujii *et al.*, 2007).

Granitoids of Permian to middle Triassic age and intermediate to felsic volcanic succession along the southern part of Qiangtang block have been considered to be associated with the subduction of Meso-Tethys (Wang *et al.*, 2000; Sun *et al.*, 1994, 1997). Late Triassic molassic successions and emplacement of ophiolite in late Jurassic to early Cretaceous within the Bangong–Nujiang suture indicate age of accretion of Lhasa block to the Asian margin and the suturing (Dewey *et al.*, 1988; Metcalfe, 1998).

Late Triassic volcanoclastic sediments with abundant basalt fragments mostly restricted to the southeastern part of the Lhasa block indicate the rifting of Lhasa block from India. Early Permian basalts in the Himalayas, such as Panjal Traps in Zaskar, Abor Volcanics in Arunachal Pradesh and Bhote-Kosi basalts of South Tibet are also considered to have formed in a rift basin (Liu and Einsele, 1994; Garzanti *et al.*, 1999). In the western Himalayas (Pakistan and India), the eruption of tholeiitic type Panjal Trap covers more than 1000 km<sup>2</sup> area (Honegger *et al.*, 1982; Sengör, 1984; Sengör *et al.*, 1988; Vannay and Spring, 1993). Abor Volcanics consist of porphyritic basalts with rare association of felsic volcanics and tuffs (Talukdar and Majumdar, 1983) that are described to be similar to continental flood basalts and oceanic island tholeiites (Gautham *et al.*, 1995). These tholeiitic volcanic rocks are indicative of intense crustal thinning and rifting in an intra-continental extensional environment due to drifting of the Lhasa block from India and eventually resulted in the opening of Neo-Tethys (Pierce and Mei, 1988; Gaetani and Garzanti, 1991; Garzanti, *et al.*, 1999; Yin and Harrison, 2000). Extrusion of the continental type tholeiitic lavas were followed by more alkaline volcanism in Triassic to Jurassic within the Gondwana continental margin and is represented by the Lamayuru unit in NW Himalayas (Rolland *et al.*, 2002). Yunam granite, in the SE Zaskar-Upper

Lahul region of Himalayas is also considered to be associated with thinned lithosphere context related to the Permo-Mesozoic rifting of Neo-Tethys (Spring *et al.*, 1993).

Subduction of the Neo-Tethys ocean initiated in the upper Jurassic, represented by the emplacement of tholeiitic Dras arc, was followed by the formation of a more calc-alkaline magmatism as Trans-Himalayan batholiths (Kohistan-Ladakh) during the middle Cretaceous. The dehydration of the subducting slab (Neo-Tethys oceanic crust) at higher depth induced aqueous fluid into the overlying mantle wedge and generated the calc-alkaline magmatism in the area. The intra-oceanic subduction of the Neo-Tethys ocean to the south of the Lhasa block thus led to the formation of a huge arc sequence as the Kohistan-Ladakh arc (Fig. 1.2d,e) (Coward *et al.*, 1986; Hanson, 1989; Rolfo *et al.*, 1997; Rolland *et al.*, 2000). Subduction related alkaline magmatism continued until the accretion of the arc to the Asian margin in early Tertiary (Honegger *et al.*, 1982; Reynolds *et al.*, 1983; Scharer *et al.*, 1984; Beck *et al.*, 1995; Debon and Khan, 1996; Corfield *et al.*, 2001; Pedersen *et al.*, 2001). Calc-alkaline magmatism in the Ladakh area ceased at the time of collision (Scharer *et al.*, 1984; Beck *et al.*, 1995; Ernst, 1999). Closure of the Neo-Tethys left the Ladakh arc sandwiched between the ITSZ and SSZ (Fig. 1.2g).

The magmatic dykes that crosscut the SSZ is dated at 70–80 Ma (Pettersson and Windley, 1985; Weinberg *et al.*, 2000) and represent first phase of magmatic activity in the Shyok area. Major phase of calc-alkaline magmatism is dated at 55-60 Ma in Ladakh area. This age constrains the initial India-Asia contact to be in the early Tertiary. Further to the east, the 40 Ma age of calc-alkaline magmatism in the Gangdese batholith indicates that the time of final closure of the Neo-Tethys and terminal continental collision in the eastern Himalayas had occurred at least 10–12 Ma after the initial collision in the western Himalayas (Scharer, 1984; Coulon *et al.*, 1986; Debon *et al.*, 1986; Radhakrishna, 1987).

Collision shut off the magmatism in the Ladakh area (Scharer *et al.*, 1984; Beck, *et al.*, 1995). Post collision tectonics triggered metamorphism, partial melting and emplacement of leucogranite plutons in the crust (LeFort *et al.*, 1987; Srimal *et al.*, 1987; Crawford and Windley, 1990; Zeitler and Chamberlain, 1991; Scaillet *et al.* 1996; Hodges, 2000; Mukhopadhyay 2001, 2003; Guillot *et al.*, 2002, 2007; Dasgupta *et al.*, 2004).

#### **1.4 TECTONIC DIVISIONS OF HIMALAYAS**

The ITSZ, (Figs 1.2. and 1.3) marks the site of terminal collision between the Indian plate and the Tibetan plate. The ITSZ thus separates the southern Himalayan belt from the Trans Himalaya Zone, which occurs towards north and is an integral part of the Eurasian plate. South of the ITSZ, the continued post-collision convergence between these two plates led to south-directed thrusting events that gave rise to the Himalayan mountain belt. Considerable amount of shortening has been accommodated along foreland propagating intra-continental boundary thrusts, *viz.*, the Main Central Thrust (MCT), Main Boundary Thrust (MBT) and Main Frontal Thrust (MFT) (Figs.1.4 and 1.5, Heim and Gansser, 1939; Gansser, 1964; Valdiya, 1980 and others). The Himalayan belt is therefore bound by the ITSZ to the north and the MFT towards south separates it from the Indo-Gangetic plain. Four major litho-tectonic zones have been traditionally recognized in between these two limits (Fig. 1.4). From south to north the Himalayan belt is subdivided into Sub-Himalaya Zone (SHZ), Lesser Himalaya Zone (LHZ), Higher Himalaya Crystalline Zone (HHCZ or Central Crystallines) and Higher Himalaya Sedimentary Zone (HHSZ or Tethys Sedimentary Zone). The Main Boundary Thrust (MBT) separates the Sub-Himalaya Zone (SHZ) from the Lesser Himalayas. The Lesser Himalayas and the Higher Himalayas are separated by Main Central Thrust (MCT). A system of low angle normal fault, the South Tibetan Detachment System (STDS or Trans

Himadri Fault, Burg, 1983; Burg and Chen, 1984; Burchfiel and Royden, 1985; Valdiya, 1989; Burchfiel *et al.*, 1992), makes the boundary between the Higher Himalaya Crystalline Zone and the Higher Himalaya Sedimentary Zone. Towards NW, the Trans-Himalayan plutons occurring beyond the ITSZ are referred to as the Kohistan-Ladakh and Karakoram batholiths. These plutons, along with the Gangdese magmatic belt occurring further east, are the manifestations of pre-collision subduction of the Indian Plate (Coward *et al.*, 1982; Honegger *et al.*, 1982; Dietrich *et al.*, 1983; Khan *et al.*, 1989).

#### **1.4.1 The Sub-Himalaya Zone**

The Sub-Himalaya Zone (SHZ), consisting of the Cenozoic sedimentary rock sequences, represents the 'Himalayan Foreland Basin'. It is limited in the south by the Indo-Gangetic alluvial plain along MFT and in the north by the MBT. The Sub-Himalayan zone forms the topographic front of the Himalayas. The Tertiary rock sequences of this zone are divided into lower Sirmur and upper Siwalik system by Medlicott (1864). The SHZ is essentially composed of Miocene to Pleistocene molassic sediments derived from the erosion of the rising Himalayas except near the base that were deposited at the closing stages of the Neo-Tethys (Medlicott, 1864; Pilgrim, 1910, 1913; Parkash *et al.*, 1980; Thakur, 1993). The Palaeogene Foreland Basin sediments are subdivided into Subathu, Dagshai and Kasauli formations (Bhatia and Bhargava, 2006). The SHZ is now actively overriding the Indo-Gangetic alluvial plain along the Main Frontal Thrust (MFT) (Nakata *et al.*, 1990; Gahlaut and Chander, 1992).

#### **1.4.2 The Lesser Himalaya Zone**

The Lesser Himalaya Zone is limited to the south by the MBT and to the north by the MCT (Heim and Gansser 1939; Gansser, 1964; Le Fort, 1975; Thakur, 1993). This

zone is characterized by unfossiliferous arenaceous and carbonate sedimentary rocks and very low-grade metamorphic rocks of upper Proterozoic to lower Palaeozoic age (Rashid and Sharma, 2005). They were deposited at the passive Indian continental margin. Metavolcanics and intrusive diabasic rocks are present within some quartzite sequences (Bhat and LeFort, 1992). Amphibolite facies metamorphic assemblages have been described from the structurally highest portions in some of the areas. Granites and felsic volcanics are also found to be intercalated with the sedimentary rocks (Frank *et al.*, 1977). In recent years, some workers distinguish an upper Lesser Himalaya crystalline zone and a lower Lesser Himalaya sedimentary zone (e.g., Vannay and Grasemann, 1998). The Lesser Himalayas often appears in tectonic windows (e.g., Kishtwar or Larji-Kulu-Rampur windows) within the Higher Himalayan crystalline sequence (Gansser, 1964; Tewari *et al.*, 1978; Valdiya, 1980; Vannay and Grasemann, 1998).

### **1.4.3 The Higher Himalaya Crystalline Zone**

The Higher Himalaya Crystalline Zone (HHCZ) represents the leading edge of the Precambrian Indian crust, reactivated and remobilized during the Tertiary Himalayan orogeny. The highly deformed and metamorphosed rocks in the Himalayas occur in the HHCZ. The metamorphism increases from chlorite/biotite zones to sillimanite-K-feldspar zones and migmatites at successively higher structural levels giving rise to now-famous inverted metamorphism (eg., Pilgrim and West 1928; Ray, 1947; Lefort, 1975; Sinha-Roy, 1982; Barnicoat *et al.*, 1989). At highest structural levels small leucogranite plutons intrude into the high-grade metamorphic rocks of HHCZ (Le Fort, 1975; Scaillet, *et al.*, 1995, 1996). Most of the Higher Himalayan leucogranites crystallized during the early Miocene (Scharer, 1984; Deniel *et al.*, 1987; Harrison *et al.*, 1995). The HHCZ is thought to be the frontal part of the Indian craton, thrust back onto itself along a gently dipping

detachment (Seeber *et al.*, 1981; Ni and Barazangi 1984, 1985). The HHCZ is bound to the north by the South Tibetan Detachment System (STDS), which is a system of low-dipping normal faults and south by MCT. In the NW Himalayas, the STDS is represented by Zaskar Shear Zone (ZSZ) (Searle, 1986; Herren, 1987; Patel and Jain, 1997; Dezes *et al.*, 1999). The STDS was a thrust but reactivated as a normal fault during Tertiary extension (Burchfiel and Royden, 1985; Burchfiel *et al.*, 1992; Ahmad *et al.*, 2000).

#### **1.4.4 The Higher /Tethyan Himalaya Sedimentary Zone**

The Tethys Himalaya or the Higher Himalaya Sedimentary Zone (HHSZ) is the northern most litho-tectonic zone. It is made up of a very thick and almost continuous sequence of Proterozoic to Cretaceous/Palaeocene sedimentary rocks (Hayden, 1904; Bhargava and Bassi, 1999). These rocks were deposited on the leading edge of the Indian passive margin prior to and during northward flight of the Indian plate. Detailed stratigraphic and sedimentological analyses of the HHCZ rocks may have important bearing on the geological history of the northern continental margin of the Indian continent from its evolution to eventual collision with Eurasia. Structurally, the Tethys Sedimentary Zone is a complex zone with south vergent recumbent folds, north vergent back folds and back thrusts and other extensional structures (Searle, 1983; Burg and Chen, 1984; Herren, 1987; Patel *et al.*, 1993, Steck 1993; Grasemann *et al.*, 1999). The contact of the HHSZ with the underlying HHCZ is separated by STDS (Burchfiel *et al.*, 1992).

#### **1.5 THE TRANS-HIMALAYAS**

The area north of the Higher Himalaya Sedimentary Zone and north of the ITSZ is occupied by the so-called Trans-Himalaya Zone, which includes a belt of magmatic

rocks containing the Kohistan, Ladakh, Karakoram and Mansarovar batholiths in the northwest, and Kailash, Gangdese and Mishmi plutons towards east (Gansser, 1964, 1981; Sorkhabi *et al.*, 1999).

The Trans-Himalayan batholiths constitute an important segment of the Trans-Himalayas that occurs as linear belts from Pakistan in the west (Kohistan Batholith) to India in the east as the Ladakh Batholith and further southeast in the Tibet as Kailash Tonalite and the Gangdese pluton (Auden, 1935; Wadia, 1937; Desio, 1977; Frank *et al.*, 1977; Honegger *et al.*, 1982; Scharer *et al.*, 1984; Debon *et al.*, 1986; Thakur, 1993). Further east, the batholith is called Lohit Batholith in the Mishmi Hills of NE India (Thakur and Jain, 1975; Sharma *et al.*, 1991). The Trans-Himalayan plutons are manifestation of subduction of the Indian plate (Coward *et al.*, 1982; Honegger *et al.*, 1982; Dietrich *et al.*, 1983; Khan *et al.*, 1989; Rolland *et al.*, 2000). These batholiths represent calc-alkaline plutonic complex with compositions varying from norite, gabbro, granodiorite to granite (Honegger *et al.*, 1982). These plutonic complexes may have developed in a transitional environment between the Kohistan-Dras island arc and the continental margin of Eurasia (Raz and Honneger 1989; Rolland *et al.*, 2000; Dunlap and Wysoczanski, 2002) and originated by the partial melting of subducting Neo-Tethyan oceanic slab beneath the southern margin of Eurasia. The Ladakh batholith in NW Himalayas in India is a linear belt emplaced into unmetamorphosed pile of mafic volcanics (Dras volcanics). The bulk composition of the batholith varies from quartz diorite to granodiorite, dominantly tonolite.

Karakoram batholith is linear in shape and is parallel to the Ladakh batholith, which is elongated in NW-SE direction. The rocks in the Karakoram batholith vary from granite to granodiorite in composition. The granites in this batholith are considered as younger than Ladakh batholith (Desio *et al.*, 1964; Casnedi *et al.*, 1978; Srimal, 1986).



The batholith was assigned an age of upper Cretaceous to early Tertiary and also younger ages ranging from Oligocene to Miocene (Gansser, 1964; Desio, 1976). Karakoram batholith was emplaced into the rocks which show moderate metamorphism (Rai, 1983).

The Trans-Himalaya Zone also includes a conspicuous feature, the SSZ which marks an ancient subduction zone (Frank *et al.*, 1977b). Although there is a general agreement in the literature regarding the status of ITSZ, the status of the SSZ *vis-à-vis* the evolution of the Trans-Himalaya Zone is still debated. It is now generally agreed that the ITSZ represents the northern limit of the Himalayas and marks the site of Tertiary collision between the Indian and Eurasian plates (Dewey and Bird, 1970; Powell and Conaghan, 1973; Le Fort, 1975; Frank *et al.*, 1977; Klootwijk *et al.*, 1979; Brookfield and Reynolds, 1981 and others). Some workers consider the SSZ to represent a pre-Cretaceous Andean-type subduction zone, i.e., SSZ is older than the ITSZ (Figs. 1.2f, g; Frank *et al.*, 1977a; Gansser, 1977; Sharma and Gupta, 1978; Ahmad *et al.*, 1996, 1998, 2005, 2008). Other workers hold a contrasting view and consider the SSZ to represent a late Tertiary subduction, i.e., the ITSZ is older than SSZ (Brookfield and Reynolds, 1981). Collision of Himalayan micro-continent (a fragment of India, Sinha-Roy, 1981) and Tibet is considered to have occurred in middle Eocene along ITSZ and the large part of micro-continent along with the unconsumed part of Neo-Tethys underthrust the Tibet along a second subduction zone (Sinha-Roy, 1976; 1981, 1982) which may be younger to the ITSZ. Also, the SSZ is considered to be a back arc basin in the west and more mature back arc or a forearc setting towards east (Thakur, 1981; Rolland *et al.*, 2000, 2002; Dunlap and Wysoczanski, 2002; Robertson and Collins, 2002). Some workers believe that the SSZ is a continuation of either Bangong suture or Shiquanhe suture but displaced by the Karakoram Fault (Searle *et al.*, 1991; Matte, *et al.*, 1996; Weinberg *et al.*, 2001; Kapp *et al.*, 2003; Laccasin *et al.*, 2004; Phillips *et al.*, 2004).

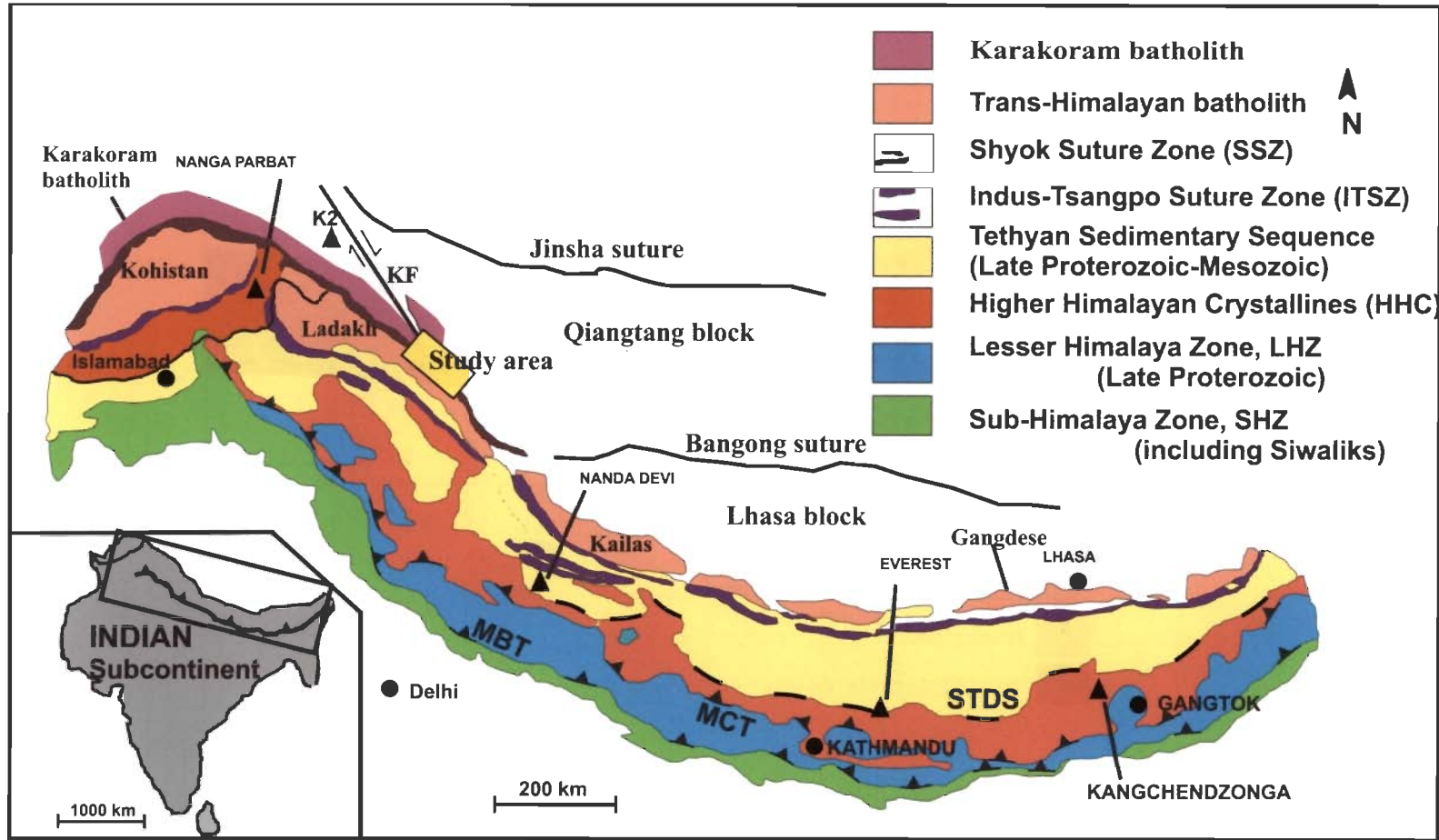


**Figure 1.4** Simplified geological map of the Himalayas showing different litho-tectonic zone, major fault surfaces, suture zones, Trans-Himalayan batholiths and the study area (modified after Gansser, 1981).

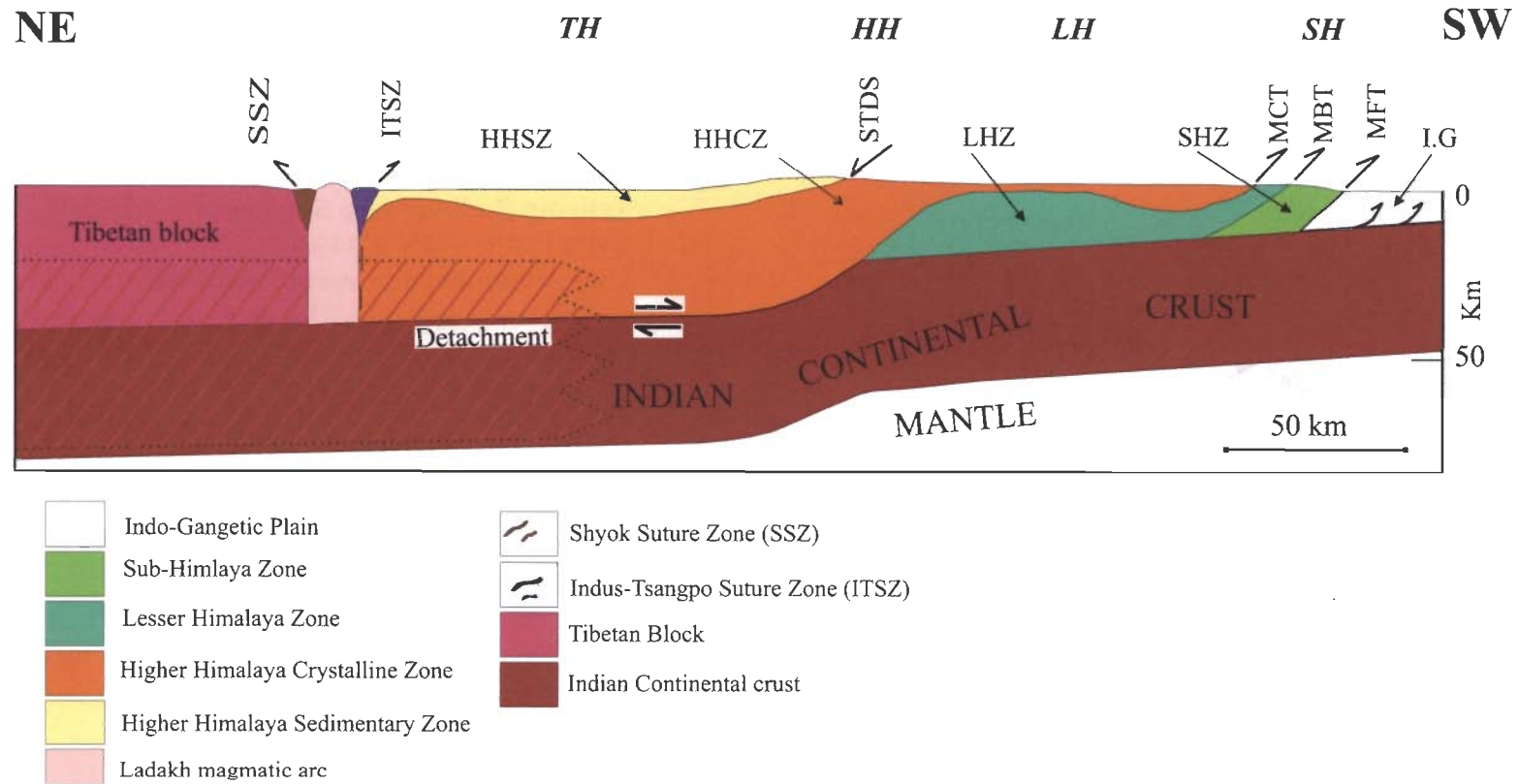


**Figure 1.5** Schematic cross section across Himalayan collision zone showing different litho-tectonic units and suture zones (compiled by Mukhopadhyay, 2003 from Seeber *et al.*, 1981; Hirn *et al.*, 1984; Ni and Barazangi 1984).

## 1.6 AIM OF THE PRESENT STUDY

From the above description, it is clear that there is little agreement among different workers regarding the status of the SSZ within the overall geodynamic framework of India-Asia collision. Specifically, the following questions need to be answered in order to understand the geodynamic significance of the SSZ:

- (a) Is the SSZ a distinct suture zone in addition to the ITSZ?
- (b) Is the SSZ developed in an intra-oceanic or an Andean-type setting?
- (c) Whether any magmatic arc originally existed north of Ladakh-Kohistan arc?
- (d) If SSZ is a distinct suture zone, how it has evolved tectonically?

A clear understanding on the petrogenesis of different rock units in the SSZ and their relations are important in order to reconstruct the geodynamic evolutionary history of the suture zone. Therefore, the present study aims to understand the geochemical nature and the petrogenesis of different rock units in the SSZ and their relation.

## **Chapter 2**

# **GEOLOGY OF THE AREA**

An accretionary prism consisting of sedimentary and volcanic rocks derived from both the plates form in an orogenic domain represented by subduction of an oceanic plate beneath a continental or another oceanic plate. When an oceanic crust is consumed along a subduction zone, the accretionary prism may be obducted on the continent but in front of the arc. The obducted accretionary prism marks a suture zone made up of ophiolitic *mélange*, intercalated with slices of metamorphosed rocks and sediments (Ernst, 1963, 1970; Shams, 1972; Gansser, 1974; Frank, *et al.*, 1977a; Maekawa, *et al.*, 1993). In the India–Asia convergence zone, the Indus-Tsangpo Suture Zone (ITSZ) and the Shyok Suture Zone (SSZ) are represented by ophiolites (relicts of subducted oceanic crust) and a palaeo-accretionary prism that records the subduction and closure of the Neo-Tethys ocean. In addition, the rocks of the Ladakh and Karakoram batholiths are also considered to record, the overall geodynamic processes related to opening and closure of the Neo-Tethys sea. Therefore, the various litho-tectonic units of the Trans-Himalayas from south to the north are, ITSZ, Ladakh batholith, SSZ and Karakoram batholith. As explained in the previous chapter, there are different opinions regarding the development and evolution of the SSZ. Considering different arguments from available literature, the present study aims to identify different lithological units in SSZ and understand their geochemical characteristics including the isotopic characteristics and the petrogenesis of different units in detail.

The study area falls within the longitude of 77°25' to 78°25' and latitude of 34° to 34°45' (Fig. 2.1). The study area covers Hundar, Khardung, Tsoltak and Nubra-Shyok valley of Trans-Himalayas.

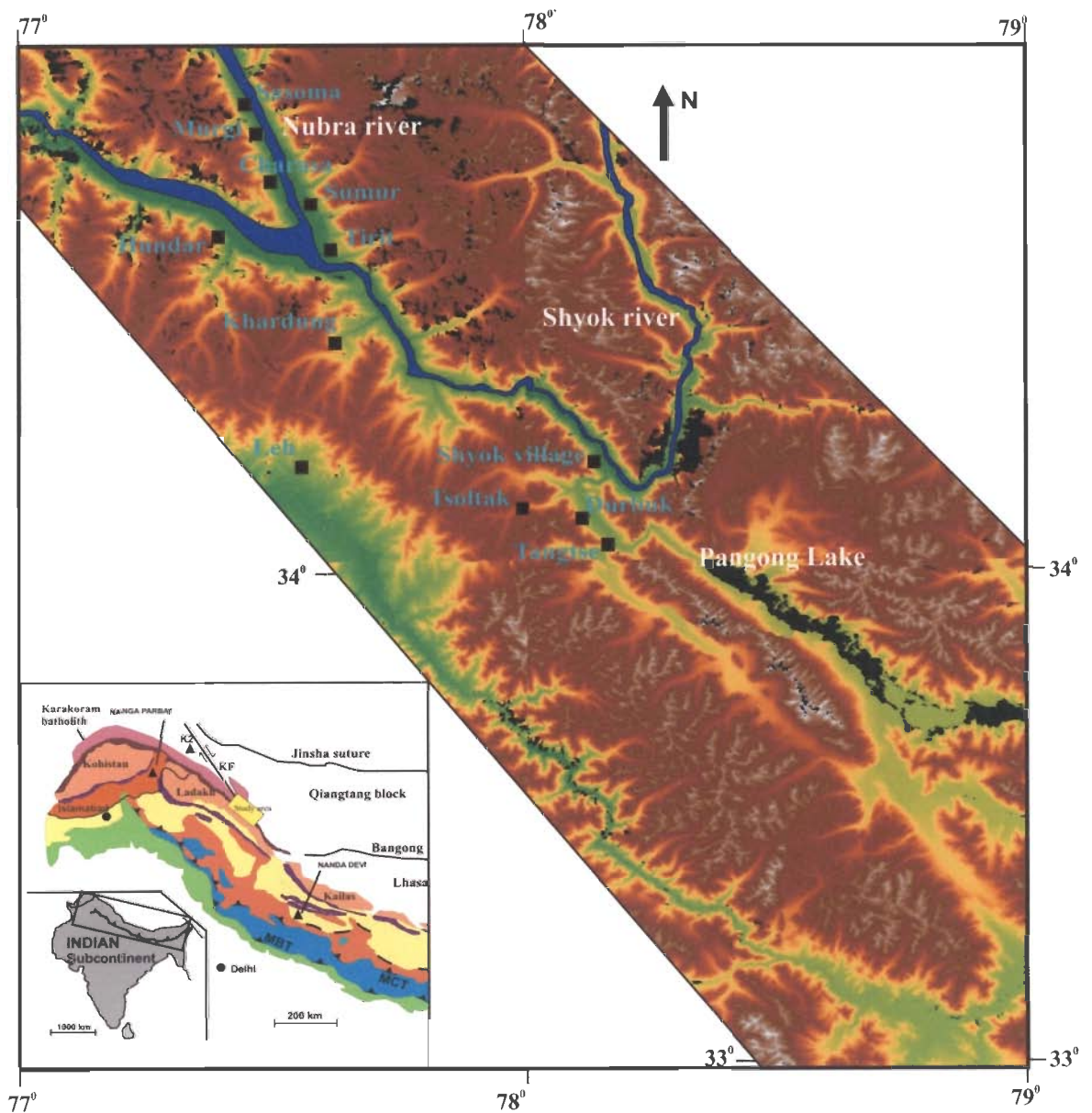


**Figure 2.1** SRTM (Shuttle Radar Topographic Mission) image of the study area (image from [glcf.umiacs.umd.edu](http://glcf.umiacs.umd.edu)). Inset shows different tectonic units of Himalayas including the study area, (*cf.*, Fig. 1.4).

There are many suture zones and thrusts formed due to the accretion and collision of the continental plates. Fig. 2.2 shows the tectonic units of NW Himalayas including various suture zones (eg., ITSZ, SSZ, BNS) and major thrusts and faults (eg., MBT, MMT, KF) in India and Tibet on a landsat image. Location of SSZ and present study area are also shown in the image.

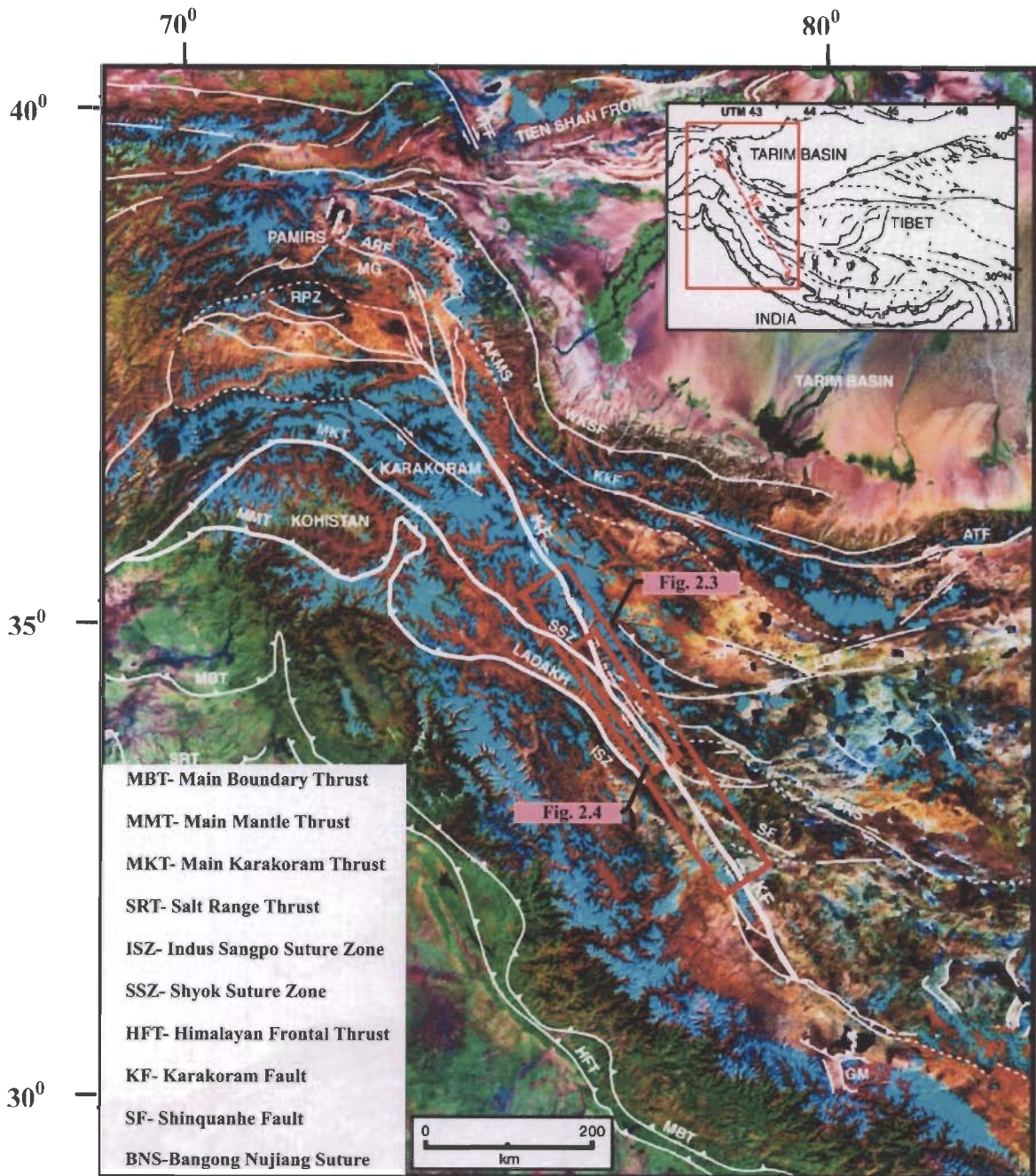


**Figure 2.2** Tectonic map of the NW Himalayas and western Tibet overlain on a Landsat-7 image (modified after Phillips *et al.*, 2004).

## 2.1 LADAKH BATHOLITH

A conspicuous feature in the geology of the Ladakh Himalayas is the presence of a huge plutonic mass, the Ladakh batholith. Major part of the Ladakh mountain range is occupied by plutonic rocks, which are variously known as Ladakh-Deosai granitic belt (Desio, 1979), Ladakh granite (Tewari, 1964), Ladakh intrusives (Frank *et al.*, 1977b), Ladakh-Desoai batholith (Brookfield and Reynolds, 1981), Ladakh batholith (Rai, 1982).



Similar batholiths occurring in a longitudinally continuous belt are known as Kohistan batholith in Pakistan and Gangdes pluton in Tibet. The Ladakh batholith extends for about 600 km approximately in the WNW-ESE direction and is about 30-35 km wide (Weinberg and Dunlap, 2000). This batholith represents the calc-alkaline plutonism related to the subduction of the Neo-Thethys oceanic crust during late Cretaceous to lower Eocene time (Thakur 1993; Ahmad *et al.*, 1998). Fig. 2.3 shows geological map of Trans-Himalayas including Trans-Himalayan batholiths (Ladakh and Karakoram) and suture zones (Indus-Tsangpo and Shyok).

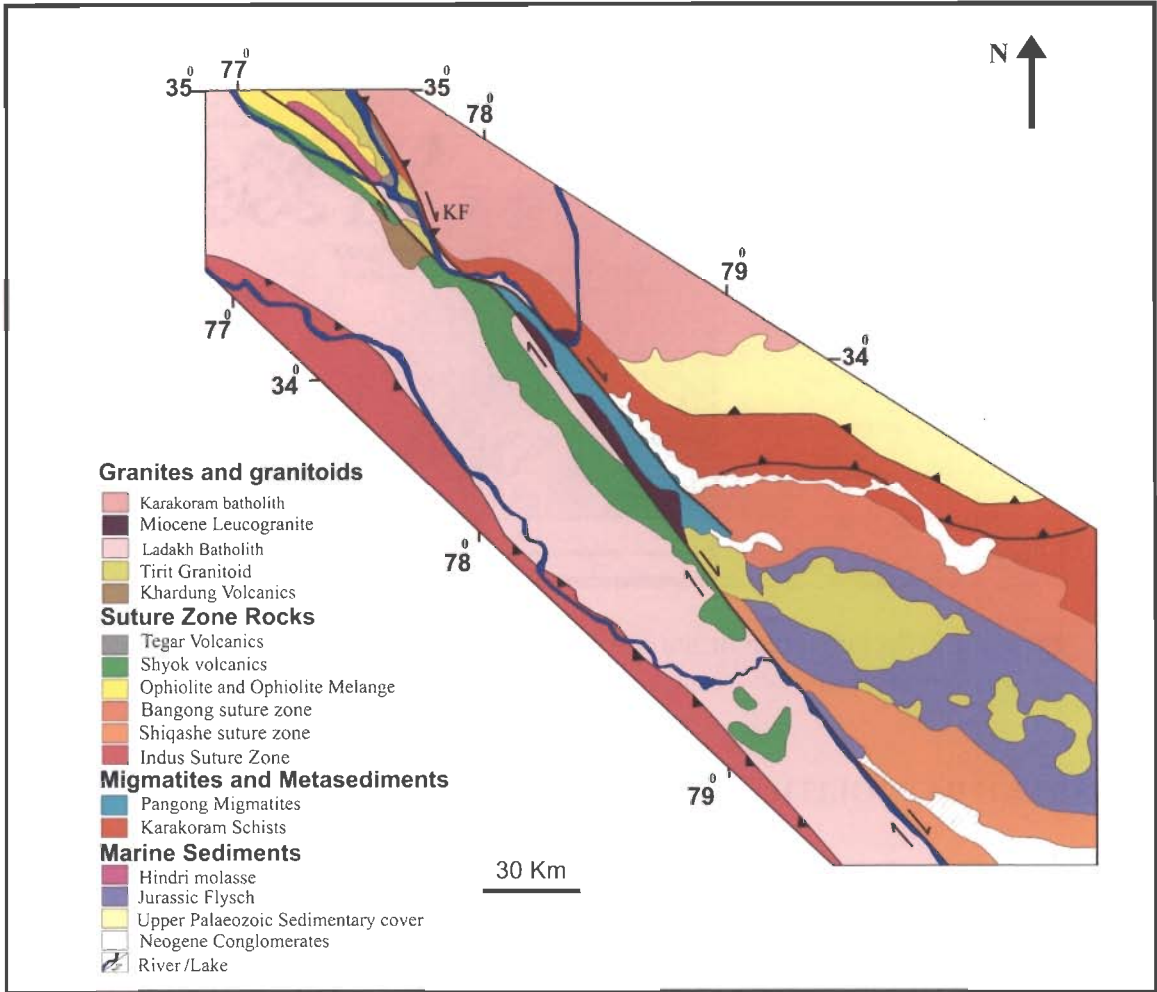


**Figure 2.3** Geological map of Trans-Himalayas showing different litho-tectonic units and suture zone rocks (modified after Dunlap and Wysoczanski, 2002).

The Ladakh batholith is a complex granitoid mass that intruded into a thick pile of unmetamorphosed mafic and ultramafic volcanics known as Dras volcanics. Enclaves in the form of large blocks of few meters and xenoliths varying in size from a few cm to few meters have been reported from different parts of the Ladakh batholith. These xenoliths and enclaves vary in composition from olivine-norite/gabbro through diorite to granodiorite (Honegger *et al.*, 1982, 1989; Sharma, 1990; Ahmad *et al.*, 1998). Honegger *et al.* (1982) suggested that some of the mafic enclaves within the Ladakh batholith are to be cumulate separated during the evolution of the batholith, but this possibility has not been investigated in detail to assess the significance of these enclaves in the genesis of Ladakh granitoids. Based on geochemical studies, Ahmad *et al.* (1998) suggested that the majority of the enclaves may represent remnant of the earliest phase of intra-oceanic arc magmatism, later intruded by granitoid plutonism (Ladakh batholith). The Ladakh batholith is also considered to have developed in a transitional environment between the intra-oceanic Dras-Kohistan island arc in the west and continental margin of Eurasia towards east (Raz and Honegger, 1989; Rolland *et al.*, 2000; Dunlap and Wysoczanski, 2002).

The Ladakh batholith consists dominantly of quartz diorite, granodiorite, monzodiorite, monzonite and granite but contains gabbro, norite, and anorthosite at some places. The bulk chemical composition of this batholith ranges from gabbroic to granitic (Honegger *et al.*, 1982; Sharma and Choubey, 1983). Though various types of igneous rocks have been described, the predominant rock type is hornblende and biotite bearing granitoid. Ladakh plutons are considered as I-type granitoids and the early phase of emplacement is considered to have occurred at  $102 \pm 4$  Ma (Scharér *et al.*, 1984; Petterson *et al.*, 1993) with a dominant second phase around 60 Ma (Honegger *et al.*, 1982; Blattner *et al.*, 1983; Scharér *et al.*, 1984). The granitoid occurs as coarse to

medium grained granular rock composed of plagioclase, hornblende, K-feldspar, quartz and biotite as the essential constituents, and zircon, sphene, apatite and magnetite as the major accessory phases (Rai, 1983; Sharma and Choubey, 1983).

## 2.2 THE KARAKORAM BATHOLITH

The Karakoram batholith (Karakoram axial granitic belt of Desio, 1979) occurs north of SSZ (Figs. 2.3, 2.4). It extends for about 700 km in the NW-SE direction, i.e., it is oriented in the same direction as the Ladakh batholith. SSZ is separated from Karakoram batholith by Main Karakoram Thrust (MKT). A dextral strike-slip fault of regional significance, the so-called Karakoram Fault (KF, Figs. 2.2, 2.3), offsets the Karakoram batholith on either side by a maximum of 150 km (Srimal, 1986; Searle *et al.*, 1998; Weinberg and Dunlap, 2000). The Karakoram mountain belt is not considered as a part of the Himalayan Range, as it lies as an independent unit between the Himalayan and Kun Lun range. The chemistry of Karakoram and Trans-Himalaya batholiths are very similar (Le Fort *et al.*, 1982; Debon *et al.*, 1986). The rocks of the Karakoram batholith are considered to have emplaced into a suite of low to medium grade of metamorphic rocks (Rai, 1982). The isotopic age of the Karakoram batholith varies from Jurassic to Miocene (Reynolds *et al.*, 1983; Le Fort, 1982; Debon *et al.*, 1986). The batholith has a multiphase intrusive history and composed of older granodiorite-tonolite phase of 120-85 Ma and a younger phase mainly composed of two-mica garnet leucogranite and biotite bearing monzogranite of 20-25 Ma (Searle, 1991; Weinberg and Searle, 1998; Weinberg and Dunlap, 2000). These younger granites are known as Baltoro granite in Pakistan (Searle *et al.*, 1992). Petrogenetic processes also indicate that the magmatism evolved from pre-collisional, subduction-related to post-collisional types (Debon *et al.*, 1986; Searle *et al.*, 1988).

The granites of this batholith are coarse grained and show hypidiomorphic granular and porphyritic textures. At some localities these rocks show cataclastic and mylonitic textures, and gneissose structures (Thakur, 1993). Quartz, K-feldspar and plagioclase are the major mineral constituents; with biotite, muscovite, and hornblende as minor mafic components. Garnet, apatite and zircon occur as accessories. Srimal and Basu (1987) identified two major sources of magma as Jurassic to early Cretaceous I-type magmatism by the result of subduction of the Neo-Tethys oceanic crust and a later S-type as a result of crustal anatexis due to intra continental thrusting. These S-type granites are considered as younger to the Ladakh batholith on the basis of radiometric ages by Desio *et al.* (1964).

### **2.3 SHYOK SUTURE ZONE (SSZ)**

The northern boundary of the Ladakh batholith is demarcated by another suture zone called SSZ which is sandwiched between Ladakh and Karakoram batholiths. It was first described by Gansser (1964) and later by many workers (Thahirkheli *et al.*, 1979; Brookfield and Reynolds, 1981, 1990; Rai 1982; Thakur and Misra, 1984; Srimal, 1986; Chandra *et al.*, 1999; Ahmad *et al.*; 1998, 2005, 2008; Rolland *et al.*, 2002).

It is difficult to describe the geology of a suture zone on the basis of stratigraphy. The SSZ constitutes a large-scale tectonic *mélange* in which most of the rocks are in tectonic contact with each other. Further, same rocks types occur at different localities and within particular litho-tectonic unit of different compositions also may occur. These make lateral correlations of rocks in terms of standard stratigraphic procedure nearly impossible. Consequently, different authors working in different or even the same area adopt different scheme of rock nomenclature. In this work, the rocks are described as litho-tectonic units in terms of specific rock types occurring in different geographic

locations, viz., Saltoro flysch and molasses, Nubra ophiolitic mélangé, Khardung felsic volcanics, Shyok volcanics, Tsoltak volcanics, Hundar igneous suite or Hundar intrusives, Pangong metamorphic complex and Karakoram plutonic complex.

Dominant rock types in the SSZ are mafic volcanics, felsic volcanics, intrusives and flyschoidal sediments. At some places rocks of ultramafic and mafic in compositions are present as ophiolite lenses. Metabasalts and medium to high grade metapelites of staurolite and garnet-mica schist are also present within the suture zone. Unlike ITSZ, true ophiolite sequence is not well developed. Serpentinised ultramafic rocks occur at places are not as part of ophiolite sequence but as isolated lensoid bodies. Andesitic dykes, cut through almost all the rock units in the SSZ. Detailed geological map showing different litho-tectonic units are given as Fig. 2.4.

### **2.3.1 Flysch and Molasse**

Discontinuous flyschoidal sediments and molasses are exposed along the southern slope of the Saltoro Hills (Fig. 2.4, Rai, 1982) (Saltoro Formation, Upadhyay *et al.*, 1999), which are of Cretaceous to Eocene in age (Srikantia *et al.*, 1982; Rai, 1983). The lithology and faunal assemblage of these sediments indicate submarine origin and hence classified as flysch.

The flysch composed of grayish, greenish grey and reddish brown argillaceous and calcareous shale, chert, grey limestone and quartzite bands. Saltoro molasse is dominantly shale, sandstone, gritstone and conglomerate. Conglomerate contains clasts of tonalite, granite, limestone, basalt, andesite and rhyolite. There are small granitoid intrusions also associated with the flysch. The whole molassic sequence is traversed by mafic to felsic dyke network. These dykes trend approximately NW-SE and NE-SW and cut each other.

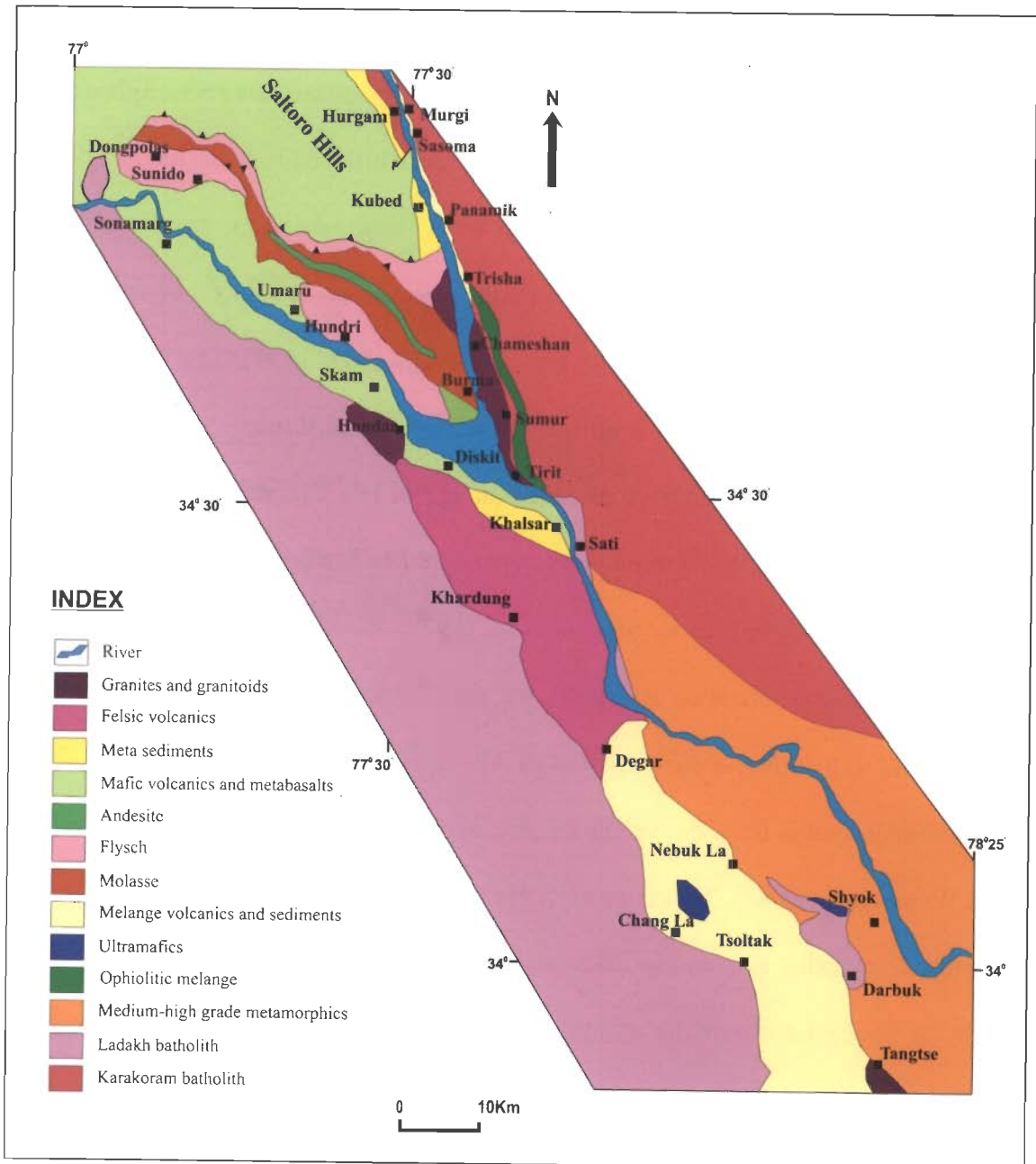


**Figure 2.4** Geological map of the Shyok Suture Zone shows different lithological units (modified after Rai, 1983, 1986).

### 2.3.2 Felsic Volcanics

Felsic volcanics occur as a linear, discontinuous and irregular belt along the northern margin of Ladakh batholith, best developed around Khardung village, are called Khardung volcanics (Weinberg *et al.*, 2000; Dunlap and Wysoczanski, 2002). These volcanics include five major types of felsic volcanics which can be distinguished by their

colour in the field and are rhyolitic to dacitic in composition. The end of the main volcanic sequence is considered to be marked by thick tuffaceous rock. Spherical lapilli are also found to be associated with the top most tuffaceous bed (Rai, 1979). These tuffaceous rocks are conformably overlain by a thick lahar unit consist of unsorted, rounded boulders and pebbles derived from the felsic volcanics. Two intermittent red and pink felsic flows are associated with the lahar (Rai, 1983, 1999). The tuffaceous bed is not a mapable unit and hence it is not shown in the geological map.

Thakur *et al.* (1981) have assigned an age of late Cretaceous for these volcanics based on fossil record. K-Ar whole rock age of 38 Ma has been assigned for these felsic volcanics of Khardung area by Sharma *et al.* (1978). As these volcanics have undergone extensive post-crystallization alteration, the significance of K-Ar ages is not clear. K-Ar age of 49.2 to 51.2 Ma is also reported by Thanh *et al.* (2005). U-Pb SHRIMP dating on single zircon grains from the volcanics give age between 64.7 Ma and 60.5 Ma (Dunlap and Wysoczanski, 2002). Thakur *et al.* (1981), Srimal (1986) and Rai (1999) have treated the felsic volcanics as a continuation of the volcano-sedimentary succession, associated with the Chang La ultramafic unit (Reuber, 1987) that are exposed near Chang La and Tsoltak area. These felsic volcanics are also found to be associated with mafic volcanics and a small sedimentary unit. The volcanic rocks associated with the ultramafic unit and mélangé are shown as mélangé volcanics in Fig. 2.4 and described as Tsoltak volcanics.

### **2.3.3 Granites and Granitoids**

Two types of granites are observed in Hundar area, micaceous felsic granite and pink granite. The granites are associated with diorite and gabbro. Micaceous granite is found to be intruded into all other rock units. Along the Hundar river section (detailed description of lithology is given in chapter 4), granite and diorite do not occur as

independent masses but as a complex magmatic sequence suggests mixing of granite and diorite magmas. Granite, diorite and the mixed rocks in the Hundar area are described as Hundar igneous suite or Hundar intrusives in the following chapters. These rocks have been dated by Thanh *et al.* (2005) using K-Ar dating of biotite and yield an age of 64 to 66 Ma. This indicates that the magmatic intrusion in Hundar area took place before the collision event between Indian and Asian continents. Therefore, these rocks could be older than the main episode of Ladakh batholith emplacement which is considered as 55 Ma.

Granites are also exposed at Tangtse area (Fig. 2.4). These granites are biotite-hornblende bearing granodiorites and garnet bearing leucogranites. Migmatitic gneiss and thin band of mylonitised granite are also exposed in the Tangtse area. Mafic bodies are embedded within the granitoids at some places. Leucogranite and mafic dykes are deformed along the Karakoram Fault. Leucogranite and biotite granite of Tangtse yield age of  $10.2 \pm 0.29$  Ma and  $10.77 \pm 0.3$  Ma respectively (Patra *et al.*, 2003). The granitoids and leucogranites exposed near Tirit area is considered as the extension of Tangtse unit but the older age (68 Ma) indicates these are different and Tirit granitoid could be a part of the Ladakh batholith.

#### **2.3.4 Maficvolcanics and Metabasalts**

The metabasalts occur along the Shyok valley and north of Hundar village have assemblages of chlorite + epidote + calcite  $\pm$  quartz which indicate greenschist facies metamorphism. These metabasalts are also associated with the mafic volcanics (basalt) and mafic dykes. Mafic volcanics, along the Shyok valley are called Shyok volcanics (Thakur, 1981), and are tholeiitic in nature suggesting chemical affinity between primitive N-MORB to E-MORB. Many workers correlate these volcanics with Chalt



volcanics (Pakistan), which is early Cretaceous tholeiitic basalts (e.g., Searle, 1991; Treloar *et al.*, 1996). The Shyok mafic volcanics have composition comparable to that of Dras volcanics of ITSZ (Thakur, 1993; Rolland, 2002). There are andesites associated with these mafic volcanics. These andesites are calc-alkaline having resemblance with transitional basalt between E-MORB and OIB (Chandra *et al.*, 1999). The Shyok volcanics are difficult to date because of the thermal over printing during the intrusion of Ladakh batholith and the activation of Karakoram Fault (KF). Sedimentary and metavolcanics of this unit give an age of 124 Ma by  $^{40}\text{Ar}/^{39}\text{Ar}$  method (Dunlap and Wysoczansky, 2002). This age indicates early Cretaceous primitive magmatism in the Shyok area.

The mafic volcanics are also found to be associated with the *mélange* unit along the Nubra valley. This volcanic unit exposed along Tirit-Panamik-Sasoma section is called Nubra ophiolitic volcanics by Ahmad *et al.* (2005). A mafic volcanic unit is also found to be associated with the ultramafic unit near Chang La area. This mafic volcanic unit is referred to as Tsoltak volcanics in the following sections. This volcanic unit is associated with a sedimentary unit which is not a mapable unit. Weinberg *et al.* (2000) and Dunlap and Wysoczanski (2002) considered these volcanics as a part of the mafic volcanics of Shyok area (Shyok formation according to Thakur *et al.*, 1981). The volcanic unit associated with the *mélange* is shown as *mélange* volcanics in Fig. 2.4.

### **2.3.5 Ultramafics and Ophiolite *mélange* volcanics**

Along the Nubra valley, the *mélange* unit occurs as a thin, irregular and narrow strip of heterogenous serpentinite components and mafic volcanics in chaotic condition. The *mélange* unit along Nubra valley is variously called as Nubra ophiolite *mélange* and Shyok ophiolite *mélange* by different authors (Rai, 1983; Ahmad *et al.*, 2005). This

mélange contains lenses of intensely deformed metapellites, metatuffs, metabasites and serpentinitised ultramafics. The mélange unit is better exposed in the eastern part of Nubra valley and near Chang La and Pangong complex (Fig. 2.4, Rolland *et al.*, 2000). The relation of mélange unit in Nubra valley and Chang La is not very clear. However, three units are identified as part of the ophiolite mélange in Chang La area. The ultramafic unit, called Chang La Ultramafics (Fig. 2.4, Reuber, 1987), is best seen in the Chang La-Nebok La area along with volcano-sedimentary unit and sedimentary unit.

The ultramafic unit of Chang La consists of thick band of harzburgite, dunite and gabbros with trace and REE pattern typical of N-MORB compositions (Rolland *et al.*, 2000). Rocks are altered to serpenites and again to talc and zeolites. The volcanics associated with the ophiolite mélange are already explained as mélange volcanics (Nubra ophiolite volcanics and Tsoltak volcanics) along with other mafic and felsic volcanics of the suture zone. Jurassic *Ammonoid* specimens are reported from the sedimentary unit of the mélange near Tsoltak village (Fig. 2.4, Tsoltak Formation, Ehiro *et al.*, 2007).

### **2.3.6 Metasediments and Metamorphics**

Metasediments and migmatites are exposed along the Diskit-Khalsar areas and west of Kubed and Hurgam villages. Narrow belt of medium to high grade metamorphic rocks bound at the north by Karakoram batholith and south by Ladakh batholith near Pangong is called Pangong Metamorphic Complex (Fig. 2.4). These metamorphics are supposedly exhumed through transpressive deformation along the Karakoram Fault (Weinberg and Searle, 1998). The metamorphic rocks are mostly pelitic, psammitic and calcareous in nature. The metamorphics of this area is classified into low grained and medium-high grade rocks. Low grade rocks are mostly phyllites and fine grained schists. In medium-high grade zone of metamorphic rocks, there is increase in grain size.

Metamorphic grade progressively increases from biotite to sillimanite zone of amphibolite facies (Choudhuri, 1983).

#### **2.4 INDUS-TSANGPO SUTURE ZONE (ITSZ)**

In Ladakh, ITSZ bound to the south by south-dipping Indus Suture Thrust (Main Mantle Thrust) separating it from the Tethys Himalayas and towards north by the Trans-Himalayan batholiths (Thakur and Misra, 1984). The suture represents a major tectonic crustal lineament from Hindu Kush to Mishmi Hills of Assam for about 2500 km, along which the Indian plate subducted below the Eurasian plate during the late Mesozoic. It follows the Indus river in the west and the Tsangpo river in the eastern Tibet, hence takes the name Indus-Tsangpo suture.

ITSZ is made up of ophiolites, intercalated flyschs and oceanic sediments represent the remnants of the Neo-Tethys ocean (Le Fort, 1975; Gansser, 1980). These oceanic remnants occur in two main tectonic settings. One is southward obducted ophiolite mélangé lying on the Tethyan Sedimentary Zone (TSZ) of the northern continental margin of the Indian plate and discontinuous steeply dipping tectonic lenses within the ITSZ. In Ladakh, ITSZ is delineated to the southeast by Nidar ophiolite and associated Zildat ophiolite mélangé and to the northwest by the Sapi-Shergol mélangé (Honegger *et al.*, 1989). ITSZ consists of several ophiolite lenses and mélanges, *viz.*, Zildat ophiolitic mélangé, Shergol ophiolitic mélangé, Spongtang ophiolite, Nidar ophiolite and Karzong ophiolite along with Dras volcanics, Nindam Formation, Indus Formation and Kargil/Liyan Formation in eastern and western Ladakh (Gansser, 1977; Thakur, 1981; Shrama and Gupta, 1983; Thakur and Bagati, 1983; Thakur and Misra, 1984; Ahmad *et al.*, 2008). Earlier, all the ophiolitic mélangé belts along the ITSZ were classified as Shergol mélangé (Thakur, 1981). Ophiolite mélanges all along the ITSZ

appears to have formed due to the accumulation of the *mélange* material in the subduction zone where they suffered metamorphism and retrograded partially to green schist grade and subsequently obducted to its present position (Ahmad *et al.*, 1996).

Shergol ophiolitic *mélange* consists of a chaotic assemblage of discontinuous bands and lenses of cherty and jasperoid shales, volcanics, bedded sandstone and conglomerate together with serpentinite, peridotite, blueschist, *Orbitolina* bearing limestone, magnesite and phyllite. In Shergol ophiolitic *mélange* two main ophiolitic horizons are separated by Nindam Formation which consists of bedded sandstone, siltstone and shales together with bedded tuffs, volcanoclastics and minor lava flows (Thakur and Misra, 1984; Ahmad *et al.*, 1996, 2005; Clift, *et al.*, 2000; Mahéo *et al.*, 2004, 2005).

The Nidar ophiolite exhibits a complete cross section from upper mantle ultramafic rocks to crustal rocks. It consists of pillow lavas, radiolarites and gabbros. Mafic dykes are cross cut across the gabbros. The Nidar ophiolite is thrust over the Zildat ophiolite *mélange* (Thakur and Viridi, 1979; de Sigoyer, 1997). Zildat ophiolitic *mélange* consists of mafic metavolcanics, green hornblende schists of volcanic origin, lenses of serpentinite, limestone, and glaucophane schist, calcareous jasperoids, shale and cherty limestone (Ahmad *et al.*, 1996).

The Karzog ophiolite consists of chromite, serpentinite and highly deformed and altered gabbros. Mahéo *et al.* (2004) considered this as a relic of transition zone between the crust and mantle. The Spongtang ophiolite is thrust over the Spongtang *mélange* (Reuber *et al.*, 1987; Corfield *et al.*, 1999). Recent studies on this ophiolite at the eastern part (eg., Corfield *et al.*, 2001; Pedersen *et al.*, 2001) of ITSZ suggest MORB affinity and consider this as an indicative of intra-oceanic subduction zone.

Dras volcanics are identified as relicts of upper Cretaceous to upper Jurassic volcanic island arc (Dras arc) which consists of tholeiitic basalt, felsic volcanics, volcanoclasts, pillow lavas and ultramafic rocks associated with radiolarian cherts together with limestone and serpentinite lenses. The older unit of Dras volcanics is considered to be emplaced at 105 to 95 Ma ago (Dietrich *et al.*, 1983; Reuber, 1989).

Indus Formation is a very thick sedimentary belt approximately 5 km thick lying south of the Ladakh plutonic complex. It consists of thickly interbedded conglomerate, sandstone, siltstone and shale together with calcareous shale and limestone. Kargil/Liyan Formation exposed at Kargil and extends along the Indus valley towards overlying Ladakh plutonic complex. This formation comprises of conglomerate, boulder bed and alternation of sandstone and shale with thin coal seams. Nindam Formation consists of alternating sand stone silt stone and shale (Tewari 1964; Bhandari *et al.*, 1978; Frank *et al.*, 1977b; Mathur, 1983). Nindam Formation corresponds to a fore-arc area filled with thick volcano-sedimentary deposits and interpreted as an accretionary prism related to the Dras arc (Cannat and Mascle, 1990; Clift *et al.*, 2000).

## **2.5 COMPARISON BETWEEN ITSZ AND SSZ**

Contrasting views have been expressed by different workers for the evolution of SSZ. Comparable lithologies and formations are reported from both ITSZ and SSZ. Kargil molasse from Indus valley corresponds to the Saltoro molasse in Nubra valley of SSZ. Ophiolite mélanges are reported from both the suture zones. Dras volcanics of Indus suture is synchronous with the Shyok volcanics of Shyok suture; eruption of both took place in submarine condition. Flysch and sediments of Indus suture (Lamayuru) is comparable to the Karakoram metasediments of Shyok suture. Though there is a belt of ophiolite mélange along the Nubra valley true ophiolite sequence is not well developed in

Shyok, whereas in Indus valley there are many ophiolite complexes. If the SSZ is a part of Indus suture, true ophiolite lenses could be expected in this suture zone also. The ophiolite and ultramafics are reported only from Chang La area in Shyok suture. The ITSZ is established as an intra-oceanic suture. The existence and spatial distribution of different volcanics (both felsic and mafic) and ophiolite in these two suture zones are not correlative in all aspects. Geochemical comparison of rocks from the two suture zones is given in chapter 8.

## **2.6 PREVIOUS WORK DONE IN THE STUDY AREA**

Prior to the collision between India and Asia, the Tethys sea existed between the two continents, disappeared but its presence for millions of years ago is recorded by scraps of oceanic crust preserved in suture zones and are correlative of ophiolitic rocks in Ladakh area (Corfield *et al.*, 2001; Mahéo *et al.*, 2004; Ahmad *et al.*, 2005). The closure of the Neo-Tethys and collision of the Dras-Kohistan island arc with the approaching margins of the Indian and Eurasian plates was not accommodated by a single but by two subduction zones in the Ladakh area, intra-oceanic and an ocean–continent subduction. These subduction zones now represent as ITSZ and SSZ respectively.

The ITSZ marks the zone of intra-oceanic subduction and consists of deep water sediments and highly disrupted ophiolitic sequences (Sinha and Misra, 1992). The remnants of a Mesozoic to Tertiary ocean (Neo-Tethys ocean), and a magmatic arc associated with the subduction zone are recognized in the ITSZ (Gansser, 1980; Le Fort, 1975; Thakur *et al.*, 1981; Honegger *et al.*, 1982). The subduction zone along which the oceanic crust undergone subduction is traced for ~3000 km (Hodges, 2000). Blueschist and eclogite facies of metamorphism in western Himalayas at Tso Morari gives an evidence of the subduction to a depth of ~ 100 km (Honegger *et al.*, 1989; Searle, 2001).

Pudsey *et al.* (1985) and Pudsey (1986) have studied the Karakoram-Kohistan suture (equivalent to Shyok suture) in northern Pakistan and interpreted it as mélangé zone derived from Kohistan- Ladakh arc in a small back-arc basin. Hence, this suture is believed to have formed in late Cretaceous during the closure of the back-arc basin between Kohistan island arc and Tibetan block. The lateral asymmetry found between western Kohistan- Ladakh arc in a marine back-arc environment and eastern Ladakh (Nubra-Shyok area) as evolved arc in a sub-continental environment suggests subduction oblique to the Asian margin (Rolland *et al.*, 2000; Robertson and Collins, 2002). The ophiolites in the western Tibetan Plateau (Lhasa) are also interpreted to have formed in a marginal basin setting (Qiu *et al.*, 2007). Similar stratigraphic successions of comparable age have been identified from Karakoram area of SSZ and the Lhasa block (Xu *et al.*, 1985; Rolland *et al.*, 2002).

As there are difference in the ophiolites from south and north of the Ladakh batholith, the nature of tectonic processes and their chronology appear to be different in the western and eastern Himalayan segments. The younger granite ages (40 Ma) indicate that continental collision occurred in the eastern Himalayas at least 10–12 Ma after the initial collision in the western Himalayas (Radhakrishna, 1987). In the western Himalayas, subduction (in an island-arc setting) and the collision are marked mainly by the occurrence of the Dras arc volcanics, trench deposits, ophiolitic blocks, calc-alkaline plutons and blueschist facies rocks (Srikantia and Razdhan, 1981; Radhakrishna *et al.*, 1984; Rai, 1989). In the eastern Himalayas, the lack of island-arc volcanism, the dominance of calc-alkaline plutonism and the epicontinental deposits are in favors of subduction in an Andean type tectonic setting (Searle *et al.*, 1998; Rolland and Pêcher 2001; Rolland *et al.*, 2000; Dunlap and Wysoczanski, 2002).

The mafic dykes cutting the SSZ rocks in Pakistan are dated 75 Ma by Ar-Ar method (Pettersson and Windley, 1985) that indicates an older age. Le Fort *et al.* (1983) recorded the U-Pb age of 95 Ma for the rocks from Hunza valley in Pakistan. K-Ar dating of biotite from Karakoram gives an age of 77 Ma and Ar-Ar age between 130 and 150 Ma (Pudsey, 1986; Reynolds *et al.*, 1983). Searle *et al.* (1989) also reported K-Ar age of Jurassic time from the SSZ. These ages indicate that the SSZ was developed much before the development of the ITSZ. Jurassic *Ammonoides* are also reported by Ehiro *et al.* (2007) from Tsoltak area of SSZ. However, there is a general agreement on the existence of another suture and its development in Jurassic-Cretaceous time (Searle *et al.*, 1989, 1991; Matte *et al.*, 1996; Sinha and Upadhyay, 1997; Weinberg *et al.*, 2000; Dunlap and Wysoczanski, 2002).

However, the geometry and mechanism of collision and suturing are not very simple in the NW Himalayas. Geology of the study area is well documented by many workers (eg., Sharma, 1978, Sharma *et al.*, 1978; Thakur *et al.*, 1981; Rai, 1982, 1983, 1986, Srimal and Basu 1987; Ahmad *et al.*, 1998, 2003, 2005 and others). Different lithotectonic units are identified and their structural, lithological, geochemical and geochronological aspects were studied. Lithological characteristics of Khardung volcanics have been studied and reported (Rai, 1979, 1983; Weinberg *et al.*, 2000). Isotopic age of this felsic volcanics is identified by K-Ar and Ar-Ar methods (Sharma *et al.*, 1978; Dunlap and Wysoczanski, 2002). Shyok volcanics are correlated to the Chalt volcanics and Dras volcanics from Pakistan (Searle, 1991; Treloar *et al.*, 1996). Hundar igneous suite is considered as part of the Shyok volcanics (Thakur *et al.*, 1981; Srimal *et al.*, 1986; Matte *et al.*, 1996). Therefore, the geochemical and geochronological characteristics of this unit are not studied separately. Tsoltak volcanics are considered as part of the Shyok volcanics based on the lithology (Dunlap and Wysoczanski, 2002). Geochemistry and



lithological characteristics of Nubra volcanics are well studied by Ahmad *et al.*, 2005, 2008. However, the correlation of the ophiolitic mélangé units in the study area is not attempted.

## 2.7 SCOPE OF THE PRESENT WORK

It is considered that the first stage the arc collided with the northern margin of India during the Palaeocene along the ITSZ. The final collision of the island arc-accreted northern margin of India with the Eurasian plate took place along the SSZ during the early Oligocene (Sharma, 1987; Sharma, 1990; O'Brien, 2001). There is another opinion about the development of SSZ as the final accretion of the arc to the continental margin of Eurasia took place after the obduction of the arc to the Indian margin along ITSZ, hence the SSZ is considered as a palaeosuture (Gansser, 1977; Frank *et al.*, 1977; Sharma and Kumar, 1978; Gupta and Sharma, 1978; Ahmad *et al.*, 2005, 2008). Some authors suggest that Shyok suture is younger to ITSZ (Thahirkheli *et al.*, 1979; Brookfield and Reynolds, 1981). The volcanics within the Shyok ophiolites are assigned an age older than the Indus ophiolites (Gansser, 1977; Coward *et al.*, 1986). There are different opinions about the development of the SSZ.

The rocks of the SSZ are interpreted to represent the tectonised remainder of a marginal (back-arc) basin (Thakur *et al.*, 1981; Rai 1982; Rolland *et al.*, 2000). Geochemical data by Rolland *et al.* (2000) show a northwest–southeast evolution, from back-arc to arc in the Ladakh area. Opening of this back-arc basin is considered to have occurred on the northwestern side of the Ladakh arc. This back-arc was progressively closing eastward. The arc is considered as more mature in the west, resembling the southern Tibetan continental arc, and is characterized by more continental sedimentation. It reflects an asymmetrical geometry along the Asian margin and Kohistan–Ladakh arc.

Dunlap and Wysoczanski (2002) suggest that back-arc basin was larger than what has been described by Rolland *et al.* (2000). In contrast with the interpretation of Rolland *et al.* (2000), they suggest the region between the Shyok and the Asian continental margin of the western Tibet was a wide Jurassic basin rather than a narrow back-arc basin terminating towards east. Many workers consider that Bangong-Nujiang suture zone is the continuation of SSZ in western Tibet (eg., Searle, 1996; Searle *et al.*, 1998; Weinberg and Dunlap, 2001; Phillips *et al.*, 2004). If SSZ has a continuation towards Tibet, the notion of a narrowing back-arc basin towards the east in Ladakh area by Rolland *et al.* (2000) may be discarded (Dunlap and Wysoczanski, 2002). Existence of the back-arc basin and its evolution along the Shyok suture are yet to be clarified.

The tholeiitic volcanics of the ITSZ and the SSZ are considered as same stratigraphic unit into which granitoids of the Ladakh plutonic complex intruded (Rai, 1982). Hence, the Shyok suture is considered as an extension of ITSZ. Based on the trace element modelling on the rocks from Dras and Nidar ophiolites of ITSZ and volcanics from Nubra, Hundar and Khardung area of the SSZ, Ahmad *et al.* (2003, 2005), suggest that the Indus ophiolites show an intra-oceanic signature where as the SSZ indicates an Andean type (ocean-continent subduction) setting. Mahéo (2002, 2004), also suggest that the ophiolites in the south of Ladakh batholith (Indus ophiolite) are clearly distinct from the ophiolites in the north (Shyok ophiolites) of the batholith. However, there are different perceptions about the development of Ladakh- Kohistan arc and the SSZ.

As the rock units of SSZ do not show any stratigraphic continuity, their interrelations are not very clear. The relation between Nubra ophiolite volcanics and the Tsoltak volcanics (both are considered as part of the ophiolite mélange) need to be clarified. Mafic volcanics of Tsoltak and the Shyok volcanics are considered as the same (Ehiro *et al.*, 2007) and different by other workers (Rai, 1983, 1989; Dunlap and

Wysoczanski 2002). Relationship between these two mafic volcanic units needs to be cleared.

Khardung volcanics and Hundar intrusives are considered as part of Shyok volcanics by many workers (Rai, 1982; Thakur and Misra, 1984). These are also treated as different units by many other workers (Rolland *et al.*, 2000; Dunlap and Wysoczanski, 2002). The Khardung volcanics considered to be a second volcanic eruption phase of Ladakh batholith (Sharma *et al.*, 1978; Rai, 1982; Rolland *et al.*, 2000). Khardung volcanics are also considered to be older than the Ladakh batholith (Bhandari *et al.*, 1978; Thakur *et al.*, 1981; Srimal and Basu, 1987; Dunlap and Wysoczanski, 2002). The geochemical nature and the petrogenesis of different rock units and the relation to subduction and magmatism needs to be better understood in this area.

Petrogenetic relationships between the Dras volcanics from Kohistan area and Shyok volcanics from Ladakh area (both are intermediate–mafic volcanics) and between different compositional groups will give a better understanding of the SSZ and the arc magmatism. Thus, the sequence of eruption and intrusion of various magmatic bodies and their relationship to subduction and finally to collision need to be understood in more detail.

Petrogenetic modelling is not clearly established to explain the generation of different magma series whether it is formed from partial melting of subducting oceanic crust or overlying mantle wedge. Their geochemical nature and petrogenesis are not much understood as different magma series are derived by partial melting of a single source or from diverse sources and what were the nature of their sources. These problems also need to be addressed.

A clear understanding of the petrogenesis of different rock units and their relations are important in order to reconstruct the geodynamic evolutionary history of SSZ. As

there are controversial opinions about the relationship between ITSZ and SSZ, comparing the geochemical and isotope characteristics of these two suture zones will resolve the question whether they are related or not.

## **2.8 OBJECTIVES OF THE PRESENT STUDY**

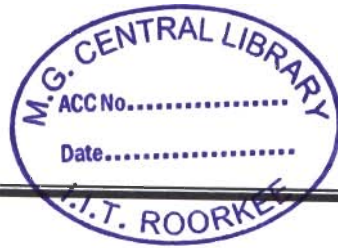
In the established framework of continent-continent collision of the Indian and the Eurasian plates, the present study aims at enhancing the existing knowledge of lateral, temporal, petrological and geochemical variations in the rock units of SSZ and its evolutionary history. As explained in the sections 2.6 and 2.7, uncertainties still persist regarding the status of different litho-tectonic units in SSZ.

Geochemistry and petrogenesis of Hundar igneous suite and its relationship with other rock units and their relative emplacement are not well established. Shyok volcanics have been correlated with many other mafic volcanics but their relation with mafic units in the study area is not well defined. Ophiolites and ophiolite volcanics are described from the study area by many workers but their comparison in geochemical aspects has not been done. Felsic volcanics from Khardung are well studied in isotopic aspects but its relation with other litho-tectonic units of the study area needs to be deciphered. Understanding the interrelations between litho-tectonic units and their petrogenesis should help in evaluating the geodynamic evolution of the SSZ. Main objectives of the present study include: (a) Geochemistry, petrogenesis and isotopic correlation of different litho-tectonic units and their source rock characterization. (b) Geochemical and petrogenetic similarities between Nubra and Tsoltak ophiolite volcanics. (c) Geochemistry of Shyok volcanics in comparison with other mafic volcanics in the area. (d) Based on the above studies a geodynamic evolution model of the SSZ is to be evolved.

G14889

## **Chapter 3**

# **METHODOLOGY**



Methodology adopted for the present study can be divided into three main parts, viz., (1) petrographic study (2) geochemical study, and (3) isotope study. Brief descriptions of procedures followed are given below. Geochemical study involves the major, trace and REE analyses of whole rock samples with appropriate analytical techniques. Isotopic study involves the determination of Sm-Nd and Rb-Sr isotope ratios in the whole rock samples using the Thermal Ionization Mass Spectrometer (TIMS).

### **3.1 PETROGRAPHY**

Petrographic study includes mineralogical, textural and micro-structural observations in thin sections made from the samples under petrological microscope. Based on this study, samples were chosen for detailed geochemical and isotopic investigations. Detailed petrographic descriptions of the samples along with representative photomicrographs are given in chapter 4.

### **3.2 GEOCHEMICAL STUDY**

The main purpose of this work is source characterization and geochemical modelling. Therefore, the quality of the geochemical data is of paramount importance. All possible care have been taken throughout the analytical process, from the choice of samples through sample processing to actual analysis to minimize uncertainty in the data.

#### **3.2.1 Sample processing**

For geochemical analysis powdered samples are required. Approximately 2-3 kilograms of unaltered samples are processed to get representative samples. The samples

are washed with distilled water to remove dust and other impurities. After drying, the samples are broken into small chips. About one kilogram of fresh sample chips are then crushed to -80 mesh size (ASTM) using steel mortar. Through coning-and-quartering several times, 250 gm of powdered sample is obtained. This sample is then ground to -200 mesh size (ASTM) in an automated agate ball mill. Appropriate precautions, such as thorough cleaning of ball mill and mesh, are taken to avoid cross contamination of samples.

### **3.2.2 Sample analysis**

Major and trace elements are analyzed by XRF and REEs are analyzed by ICP-MS using the instrumentation facilities at Wadia Institute of Himalayan Geology, Dehra Dun. Brief description of sample preparation and analytical techniques are given in following section.

#### ***3.2.2.1 X-Ray Fluorescence (XRF)***

***Sample preparation:*** Powdered rock samples are usually either pressed into disc-shaped pellets or fused with lithium metaborate into glass beads for XRF analysis. Pressed powder pellets are used for the present study. 5 grams of -200 mesh size of powder is taken in an agate mortar, 1-2 drops of polyvinyl alcohol is added to the sample and mixed thoroughly with a pestle. It is transferred into a steel cylinder and pressed with a hydraulic ram in order to get a disc-shaped pellet, which is used for analyses.

***XRF technique:*** Analysis of major and trace elements of the bulk rock samples were carried out using Siemens SRS 3000 (Fig. 3.1) WD-XRF instrument at Wadia Institute of Himalayan Geology, Dehra Dun. XRF spectrometry is a widely used analytical technique in the determination of the major and trace element concentration in rock samples.



This method is based on the excitation of an atom by X-ray. An inner shell electron is excited and ejected by an incident X-ray (Fig. 3.2). In order to fill up the vacancy created by the ejected electron, an electron moves from a higher energy level to inner shell. The energy difference of the electrons between the two shells appears as secondary X-ray. Each element has its own characteristic X-ray wave length. A typical XRF spectroscopy arrangement (Fig. 3.2) includes a source of primary radiation and detectors for the secondary X-rays (X- ray fluorescence). The X-ray spectrum produced during the above process gives a number of characteristic peaks. The intensity of the secondary X-ray is processed. The intensity of the peaks used to determine the concentrations of the elements present, by reference to the calibration standards.



**Figure 3.1** WD-XRF (Siemens SRS 3000) at Wadia Institute of Himalayan Geology, Dehra Dun.

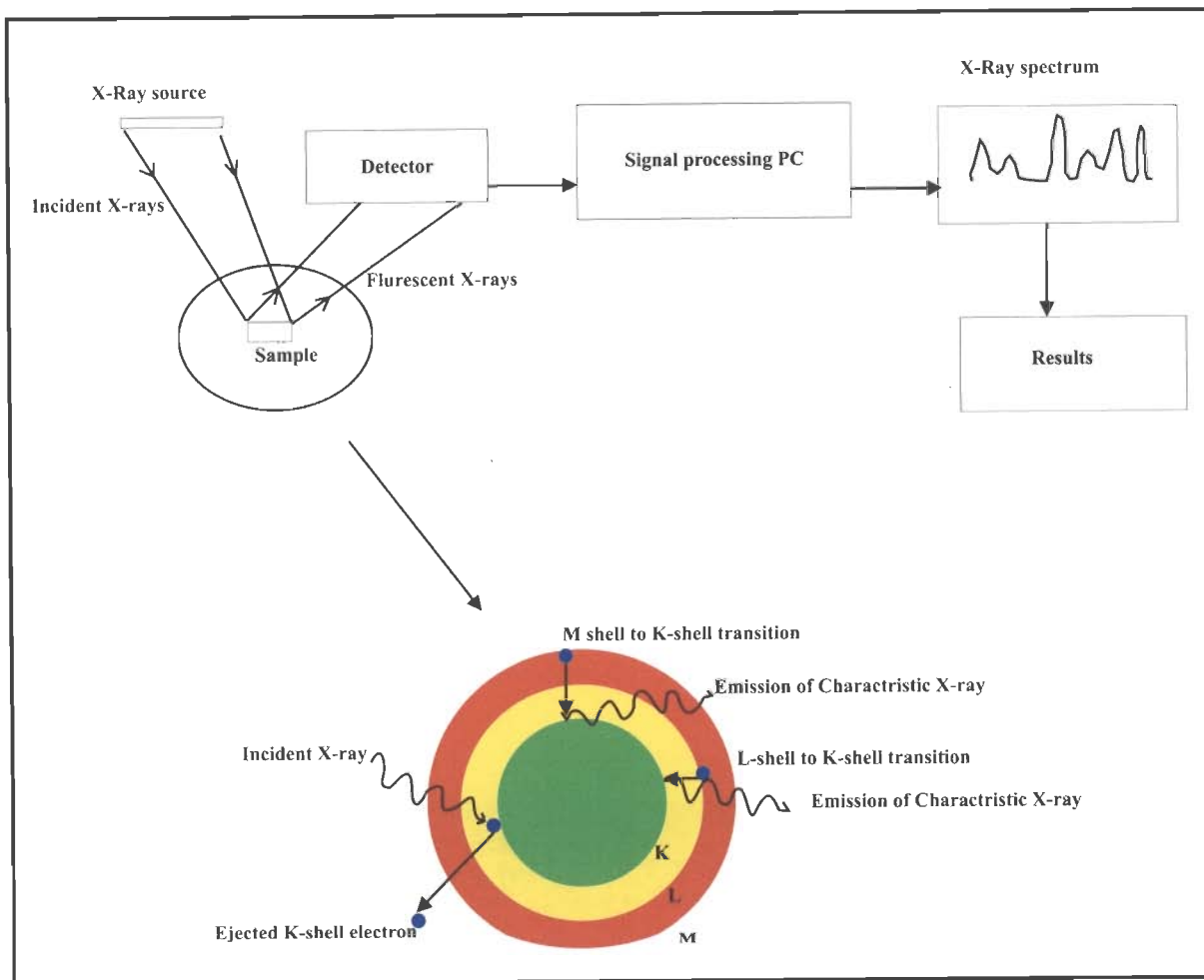


**Figure 3.2** Flow diagram of the XRF and its working principle. Incident X-ray excites an electron from inner shell. As an electron falls from higher shell to the lower shell (eg. L shell to K or M to L) emits characteristic X-rays.

**Estimation of uncertainty:** Precision and accuracy of the instruments used in the present study is given by Saini *et al.* (1998). The analytical accuracy is better than 5% for major elements and 12% for the trace elements. Precision in terms of maximum observed standard deviation on repeated measurement is better than 2% for major and trace elements.

Analytical data of major and trace elements for the standard (DGH) by Saini *et al.* (1998) and NST-31 in the present study are given Tables 3.1, 3.2. Average wt% of total analysis and standard deviation among repetitive determinations are also given.

**Table 3.1** Major element analyses of standard and other samples using XRF to estimate analytical uncertainty. Sample DGH is the standard and NST-31 is the sample in the present study.

Major oxides	DGH (Std) Avg. wt %	SD	CV	DGH (Analyzed)	NST 31A	NST 31B
SiO <sub>2</sub>	73.83	0.43	0.582	71.58	52.42	53.76
Al <sub>2</sub> O <sub>3</sub>	15.58	0.177	1.136	14.47	14.82	14.99
TiO <sub>2</sub>	0.14	0.003	1.944	.13	1.0	0.91
Fe <sub>2</sub> O <sub>3</sub>	1.77	0.022	1.212	1.09	9.52	9.4
MnO	0.03	0.0008	2.233	0.02	0.14	0.18
MgO	0.31	0.007	2.324	0.28	7.99	7.66
CaO	0.64	0.077	1.067	0.58	6.51	6.94
Na <sub>2</sub> O	3.69	0.096	2.598	3.55	2.0	1.64
K <sub>2</sub> O	4.62	0.021	0.507	4.08	3.48	3.36
P <sub>2</sub> O <sub>5</sub>	0.27	0.075	1.694	0.09	0.57	0.44

**Table 3.2** Trace element analyses of standard sample using XRF to estimate analytical uncertainty. Sample DGH is the standard.

Element	DGH(Std) Avg. ppm	SD	DGH (Analyzed)
Ba	146	3.0	142
Cr	142	2.10	139
Cu	6.3	0.45	5.9
Ga	17.7	0.48	16.8
Nb	14	0.23	12.0
Ni	5.5	0.54	5.00
Pb	37	0.92	34.6
Rb	332	1.69	329
Sr	52	0.38	50.0
Th	10.2	0.95	9.18
U	2.7	0.9	2.00
Y	11	0.58	9.80
Zn	51	0.54	49.8
Zr	66	0.87	65.5

Avg wt% or ppm: average of 32 determinations, SD: standard deviation among repetitive determinations, CV: coefficient of variance.

### 3.2.2.2 Inductively coupled plasma mass spectrometry (ICP-MS)

**Sample preparation:** The standard B-solution is used for ICP-MS analyses. Proper matching standard references were used for calibration. These standard references helped in checking the precision of measurement. The following procedure was adopted for the preparation of B-solution (Saini *et al.*, 1992; Balram *et al.*, 1995)

1. Weigh 0.04 g. of sample (powdered) into a Teflon crucible.
2. Add ~25 ml of 2:1 HF + HNO<sub>3</sub> mixture
3. Put the crucible on a hot plate at about 80°-120° C
4. Heat the mixture until it is dry
5. Repeat the steps 2-3
6. Keep the crucibles covered with lid on the hot plate at ~120° C till the solution becomes clear or transparent; if not repeat the step 2-3
7. Take the lid out and let the solution dry almost completely on the hot plate.
8. After adding 2-3 ml of perchloric acid (HClO<sub>4</sub>) place the lid on and let it dry.
9. Repeat the step three times.
10. After ~ 30 minutes take the lid off and let the solution dry almost completely.
11. Add ~ 10 ml of 10% HNO<sub>3</sub> and leave it for 5-10 minutes on the hotplate.
12. Make up the volume to 100 ml with ultra clean distilled water and store in a reagent grade bottle.

**Determination of loss on ignition (LOI):** Weigh in an empty silica crucible and add about 5 gm of sample while the crucible is still on the balance. Keep the crucible in a muffle furnace and increase temperature gradually to about 900°C and keep it at that temperature for about 20-30 minutes. After cooling, transfer the crucible in to a desiccator. Weigh the crucible after 6-8 hrs. The LOI% is given by:

$$\frac{(W_a - W_b) * 100}{W_s}$$

Where, W<sub>a</sub>= weight of the crucible with sample before putting in the furnace.

W<sub>b</sub>= weight of the crucible with sample after heating in the furnace and cooling.

W<sub>s</sub>= original weight of the sample before heating.

**ICP-MS technique:** Rare earth elements (REE) are analyzed by ICP-MS (Perkin Elmer, Elan DRC-e, Fig. 3.4) at Wadia Institute of Himalayan Geology, Dehra Dun. This method is capable of measuring most of the elements with low detection limit and good precision (precision and accuracy estimation are given in the following section). This is a flame technique with a flame temperature in the range of 6000-10000 K. The inductively coupled plasma is a stream of argon atoms, heated by inductive heating of a radio frequency coil and ignited by a high frequency Tesla spark.

The main components of an ICP-MS is the nebulizer, spray chamber, plasma torch, interface, and detector (Fig. 3.3), but can differ significantly in the design of the mass spectrometer and in particular the mass separation device.

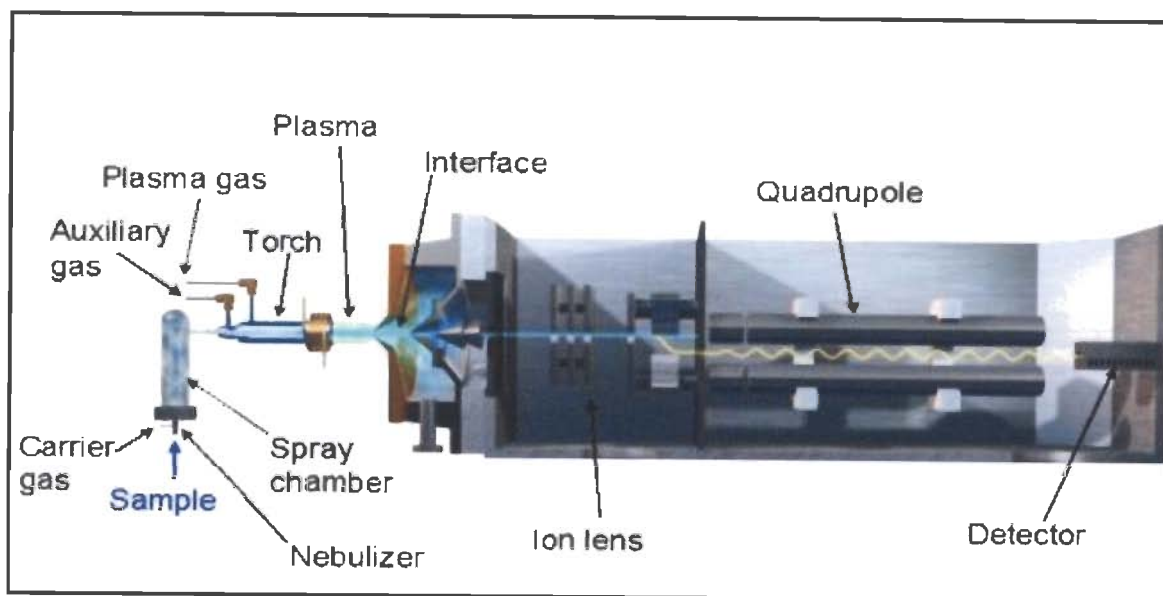


**Figure 3.3** shows basic instrumental components that make up an ICP-MS (source: chem.agilent.com).

The sample in a liquid form is pumped into a nebulizer, where it is converted into a fine aerosol with carrier argon gas. The fine aerosol then emerges from the exit tube of the spray chamber and is transported into the plasma torch via a sample injector. Argon (plasma gas) gas is introduced through a series of concentric quartz tubes. In ICP-MS, the

plasma is used to generate positively charged ions (rather than photons in the case of ICP-AES). The ions produced in the plasma are directed into the mass spectrometer via the interface region, which is maintained in a vacuum. This interface region consists of two metallic cones called the sampler and a skimmer cone. Each cone features a small orifice to allow the ions through to the ion optics, where they are guided into the mass separation device. The different masses are separated in the ion beam by a simple mass spectrometer known as a quadrupole. Quadrupole is equivalent to the magnetic separator in a mass spectrometer. Instead of the magnetic field radiofrequency deflects the path of the charged ions in ICP-MS. This mass analyzer separates the ions based on their mass/charge ratio. The trajectory of the ions injected is deflected by radio frequencies so that the ions of a specific mass cross the device and are counted by the detector. In the final process, an ion detector converts the ions into an electrical signal. They are compared with calibration signals and their intensities are converted in to concentrations.

***Estimation of uncertainties:*** The REEs of standard sample (MBH) analyzed for the present study is compared with the reported result of the sample accuracy is found to be within the error limit. The standard (Jb-1a) is analyzed by Rao and Rai (2006) by the same instrument and compared the result with the reported values of this sample. These results show that the accuracy is better than 2% and the error is within the permissible limit.

REE analytical data for standard, MBH in the present study and recommended standard values along with standard Jb-1a analyzed by Rao and Rai (2006) by same instrument at Wadia Institute of Himalayan Geology is also given in the Table 3.3

**Table 3.3** Rare earth element analyses of standards of present study (MBH) and standard (Jb-1a) analyzed by Rao and Rai (2006) using ICP-MS to estimate analytical uncertainty.

	<b>MBH (Reported values)</b>	<b>MBH (Analyzed values)</b>	<b>Jb-1a (Analyzed value)</b>	<b>Jb-1a (Reported values)</b>
		(Present study)	(Rao and Rai, 2006)	
<b>La</b>	33.82	36.00	36.17	38.10
<b>Ce</b>	72.51	73.60	63.6	66.10
<b>Pr</b>	9.84	-	7.09	7.3
<b>Nd</b>	38.95	39.40	26.06	25.5
<b>Sm</b>	9.06	9.69	5.26	5.07
<b>Eu</b>	2.81	2.77	1.62	1.47
<b>Gd</b>	10.23	9.28	5.29	4.54
<b>Tb</b>	1.62	-	0.72	0.69
<b>Dy</b>	9.23	9.35	3.99	4.19
<b>Ho</b>	1.96	-	0.79	0.64
<b>Er</b>	5.02	5.23	2.13	2.18
<b>Tm</b>	0.76	-	0.31	0.31
<b>Yb</b>	4.85	5.02	2.1	2.1
<b>Lu</b>	0.72	0.67	0.32	0.32



**Figure 3.4** ICP-MS (Perkin Elmer, Elan DRC-e) at Wadia Institute of Himalayan Geology, Dehra Dun.

### 3.3 ISOTOPE STUDY

Rb-Sr and Sm-Nd isotopic ratios have been determined using the mass spectrometer facility at Pondicherry University for the purpose of petrogenetic modelling. Care has been taken to minimize contamination during chemical procedures for sample dissolution and column separation.

#### 3.3.1 Sample dissolutions

Isotopic compositions of samples are determined from B-solution. The procedure for acid digestion to prepare B-solution has been described in section 3.3.2.2. However there are a few differences, *viz.*, (1) about 0.1 gm of sample is taken instead of 0.04 gm, (2) HF, HNO<sub>3</sub> and HCl are mixed in volumetric proportions of 2, 1 and 1, respectively, (3) perchloric acid is not used, (4) samples are weighed to the accuracy of 5 decimal places in a highly accurate balance, and (5) ultra-high pure acids are used.

Sample dissolution is carried out in a tightly capped teflon vessels on a hotplate at 70°C for 12 hrs. Then the lid is taken off and solution is allowed to evaporate and the residue is re-dissolved in 1 ml HNO<sub>3</sub> to remove traces of HF and dried. The last step is repeated three times. 1 ml HCl is added and dried again. The residue is then dissolved in 1 ml of 1N HCl to get a clear solution and ultra clean distilled water is added to make up the volume of the solution to half of the volume of the beaker. The solution is poured into two teflon beakers approximately in 3 to 2 ratio for isotopic concentration (IC) and isotopic dilution (ID), respectively. Weights of the beakers are measured before pouring the solution into them. The beakers (both IC and ID) are weighed with solution to determine the weight of the solution. Standard isotope spike solution is added to the solution marked for ID analysis. Weight of sample fraction used for isotopic dilution (ID) is calculated by



$$\text{Weight of sample in ID} = \frac{\text{Sample weight} * \text{Solution weight(ID)}}{\text{Total solution weight}}$$

A spike is a solution that contains a known concentration of a particular element in which natural isotopic composition is altered by enrichment of one or more of its naturally occurring isotope. Isotopic dilution method is based on the estimation of a known quantity of spike of that element contributed from the spike and the unknown amount of element that exists as two or more naturally occurring isotopes.

### **3.3.2 Ion exchange chromatography**

Digested samples, after appropriate spiking (isotopic dilution), are passed through the resin-filled columns (ion exchange chromatography) in order to separate the element of interest whose isotope ratios are to be determined. Ion exchange chromatography refers to any exchange method involving the distribution of components between a fixed (stationary) and moving (mobile) phase. The later is also called eluent. Ion exchange chromatography involves reversible exchange of ions between a solid phase (the resin) and a mobile phase (a solution) (Bilchert, 1993). The resin is packed in suitable glass tube and the sample solution is loaded on the top of the column. The sample is then eluted by washing its ionic components through the column using a suitable solvent at a controlled rate. Ions are separated from one another due to differences in their affinity towards the ion exchange resin.

The cation resin Bio-Rad AG-IX8 of 200-400 mesh size is used in Rb-Sr column and HDEHP coated Teflon powder is used in the Sm-Nd column for present study. The IC and the ID fractions were passed through Bio-Rad AG50-WX8 cation-exchange resin filled HCl columns. Rb and Sr were collected with 2N HCl and REE as a group was collected with 6N HCl. Rb and Sr fractions thus separated were purified further by passing through a set of secondary Bio-Rad (PP) columns that were also filled with Bio-

Rad AG50-WX8 cation-exchange resin. The collected Rb and Sr solutions were dried. The REE eluted as a group from the HCl column was dried and dissolved in 200  $\mu$ l of 0.18 N HCl. The IC and ID REE fractions were passed through different HDEHP columns. Nd was collected with 0.3N HCl and Sm was collected with 0.4N HCl. A drop of  $\sim 0.5$  ml of  $H_3PO_4$  was added to the collected Nd and Sm and dried.  $H_3PO_4$  ensures visibility of Nd and Sm while picking up for loading onto the filament.

### **3.3.3 Analytical technique**

Isotopic ratios of Rb-Sr and Sm-Nd are determined at National Facility for Geochronology and Geosciences at Pondicherry University, Pondicherry by using Thermal Ionization Mass spectrometry (Triton-Thermo Finnigan, Fig. 3.5).

#### ***3.3.3.1 Thermal Ionization Mass spectrometry (TIMS)***

Thermal Ionization Mass Spectrometry (TIMS) is a highly sensitive analytical technique to measure isotope ratios. The sample solution is placed on a filament of rhenium (or tantalum or tungsten), dried and heated to a high temperature (1200-1800°C) in vacuum and the elements are ionized. An applied accelerating voltage pulls the ions into a flight tube embedded in a magnetic field. By varying current flowing through a coil surrounding the flight tube, the magnetic field can be varied. The instrument is designed to separate ions on the basis of their masses based on their motion in the magnetic field. Mass analysis of several of isotopes an element is obtained by varying either the magnetic field or accelerating the voltage in such a way that the separated ion beams are focused in to the collector in succession. Ions are separated according to mass to charge ratio by passing through an electromagnet.

**Error estimation:** Sr and Nd isotope compositions and elemental concentrations of Rb, Sr, Sm and Nd for the rock standards BHVO-1 and BCR-2 were verified to establish the accuracy and precision of the isotopic measurements (Anand, 2007). Some of the analytical data for the above standards are given in Table 3.4.



**Figure 3.5** Thermal Ionization Mass spectrometry (TIMS, model: Triton-Thermo Finnigan) at National Facility for Geochronology and Geosciences, Pondicherry University, Pondicherry.

**Table 3.4** Sr and Nd isotopic compositions and elemental concentrations of Rb, Sr, Sm and Nd determined for rock standards BHVO-1 and BCR-2 (Anand, 2007). The recommended values (Mahoney *et al.*, 2003) are also given in the table.

Standard		$^{87}\text{Sr}/^{86}\text{Sr}$	$^{143}\text{Nd}/^{144}\text{Nd}$	Rb ( $\mu\text{g/g}$ )	Sr ( $\mu\text{g/g}$ )	Sm ( $\mu\text{g/g}$ )	Nd ( $\mu\text{g/g}$ )
BHVO-1	Recommended	$0.703482 \pm 13$	$0.512973 \pm 6$	$11 \pm 2$	$403 \pm 25$	$6.2 \pm 0.3$	$25 \pm 2$
	Replicate 1	$0.703472 \pm 5$	$0.512981 \pm 3$	10.3	418	6.2	24.9
	Replicate 2	$0.703494 \pm 7$	$0.512958 \pm 4$	9.3	417	6.3	25.2
BCR-2	Recommended	$0.705024 \pm 5$	$0.512639 \pm 6$	$48 \pm 2$	$346 \pm 14$	$6.7 \pm 0.3$	$28 \pm 2$
	Replicate 1	$0.705033 \pm 4$	$0.512626 \pm 4$	45.0	358	6.6	28.8
	Replicate 2	$0.705028 \pm 9$	$0.512628 \pm 4$	45.3	353	6.5	28.6
	Replicate 3	$0.705020 \pm 5$	$0.512621 \pm 4$	46.9	354	6.5	28.6

## **Chapter 4**

# **FIELD DESCRIPTION AND PETROGRAPHY**

Field work was carried out for about 35 days spread over in two field seasons. During fieldwork existing geological maps were thoroughly checked and modified as necessary, different lithological units were closely examined, and representative samples were collected from different lithological units. The fieldwork was carried out in and around of Shyok Suture Zone (SSZ) (Fig. 2.4). The areas where detailed outcrop-scale work was carried out include Khardung, Hundar, Nubra valley along Tirit-Panamik sector, near Hurgam-Murgi (Karakoram Plutonic Complex), Shyok valley along Diskit-Khalsar, Tangtse area, and Chang La-Tsoltak area (all these villages are on Fig. 2.4). Sample locations are given in Figs. 4.1 (a-h). In this chapter, both field relations of different rock units (Figs. 4.2a-4.2l) and petrographic descriptions (Figs. 4.3a-4.3l) are given. Description of individual rock samples that collected and used for geochemical analyses are given in appendix-1

#### **4.1 FELSIC VOLCANICS**

Felsic volcanic rocks occur as a linear and somewhat irregular body adjoining Ladakh batholith. These rocks are felsic pyroclastic volcanic flows. As these rocks are usually studied in exposures around Khardung village, they are often referred to as Khardung volcanics (Weinberg *et al.*, 2000; Dunlap and Wysoczanski, 2002). Majority of rocks are felsic but intermediate to mafic rocks are also present. In addition, volcanoclastics and sediments are present. Mafic dykes also traverse through the Khardung volcanics. Samples of so called Khardung volcanics are collected from in and around Khardung village. They are fine grained, massive and usually show flow banding. In handspecimen, it is difficult to separate different rock types. Rai (1983, 1999)

recognize five different types of volcanic rocks on the basis of colour in handspecimen, viz., pink, red, dark green, greenish grey and white coloured volcanics. Examples of different coloured felsic volcanic rocks (dacite to rhyolite) are shown in Fig. 4.2a-c. Aplitic dykes are found along Shyok valley and Diskit-Khalsar area.

Overall the Khardung volcanics are very fine grained (almost glassy) and individual grains are not identifiable in thin sections in majority of samples. Phenocrysts of spherulitic feldspars (Fig. 4.3a), anhedral quartz, twinned plagioclase and K-feldspar are present in varying proportions in different thin sections. Spene is also recognized in some thin sections. Red and dark greenish coloured volcanics contain feldspar phenocryst within very fine grained ground mass. White coloured volcanic rocks contain fine grained quartz and feldspar.

#### **4.2 GRANITES AND GRANITOIDS**

Granite and granitoid rocks occur as irregular or linear bodies near Hundar, Chumur–Tirit and Tagtse areas. The granites in Chumur–Tirit area is also called Tirit granite (or older granite), which gives U/Pb age of 68 Ma (Dunlap and Wysoczanski, 2002). Granites near Hundar area are referred to here as Hundar granite, which gives K-Ar age of 57-65 Ma (Thanh *et al.*, 2005). In the present study, only the granites occurring near Hundar village has been studied.

Two types of granites are observed in Hundar area, micaceous light-coloured granite and pink-coloured granite. Diorite, gabbro and volcanoclastic rocks, such as volcanic sand stone with basalt fragments and tuff, are present along with the granites. Pink granites intruded into diorite and gabbro. The micaceous granites are intruded into all the rock units including the pink granite, volcanic sandstone and tuff, and are in turn intruded by andesitic dykes. Micaceous granite is shown as Fig. 4.2d. Apart from separate

units, granite and diorite occur as a hybrid rock, which appears as mixture of granite and diorite rocks. These hybrid rocks with composition varying gradually from granite to diorite are observed in this area indicate magma mixing. At some places, dioritic patches are present within pink granite which suggests the diorite patches may represent magma mingling (Fig. 4.2e). Randomly oriented, long, and needle-shaped amphibole grains have been noted in diorite at a few localities. Gabbro shows gradational change in grain size from centre to periphery. The volcanoclastic unit consists of volcanic sand stone with basalt fragments and tuff. The volcanic sandstone shows layering in many outcrops. Geological sketch map showing distribution of different rock types and sample locations along a tributary (Hundar river) section, SW of Hundar village is shown in Fig. 4.1a.

Light-coloured granites have brown-green biotite grains, in addition to quartz and feldspars. Quartz and alkali feldspar show flame-shaped myrmekitic intergrowth. Commonly present undulose extinction in quartz grains suggests post-crystallization deformation. Sub-hedral plagioclase feldspar in pink granite is generally coarser than K-feldspar. Fine prismatic zircon grains are present as inclusions in quartz. Diorite samples from Hundar area have clinopyroxene, hornblende and plagioclase as major phases. Pyroxenes and amphiboles are altered and show signs of chloritization at the grain margins. In addition to plagioclase and pyroxene, biotite, and elongated hornblends are present in the gabbro. Feldspar grains in gabbro are zoned. Andesitic dykes have euhedral plagioclase phenocrysts within a ground mass consisting of volcanic glass and fine cryptocrystalline grains. Calcite grains with polysynthetic twinning are also found in the andesitic dyke and may suggest fluid activity.

Northwest of Hurgam village near Murgi, the Karakoram granitoid (batholith) is exposed along Gonbo-Kobed–Charasa road. Karakoram Fault (KF) passes along this batholith. Two traverses were taken to study and collect samples of Karakoram batholith.

Three types of granites are exposed in this area. Porphyritic granites are deformed into augen gneiss and mylonite near the Karakoram Fault (Fig. 4.2f). The second type of granite consists of hornblende and biotite without any porphyritic texture (Fig.4.2g). Third one is fine grained and very light-coloured leucogranite. The first two types are supposedly I-type granites and the leucogranite may be the S-type (Srimal, 1986). Granites are embedded with mafic xenolith of different sizes and shapes. Mafic dykes intrude the granites and show effects of deformation where the granites have undergone mylonitization. Along the Karakoram Fault these dykes are deformed and foliated. Foliation surfaces are subparallel to the Karakoram Fault. Volcano-sedimentary unit is exposed SW of the Karakoram Fault which consists of conglomerates and volcanogenic sandstone. This unit is also intruded by the leucogranite. The second traverse is taken north of Tangtse area, where the porphyritic granites deformed into augen gneisses and mylonites. Younger leucogranites are also observed in the area. Garnet bearing granites observed in this area was absent in the first traverse.

Granitic rocks from Karakoram Fault zone show highly deformed fabric under the microscope. Porphyritic granite is deformed into augen gneiss and is slightly mylonitised (Fig. 4.3b). In mylonite sample, the quartz grains are ribbon-shaped and the feldspar grains are fractured. Pyroxene (augite), amphibole (hornblende) and recrystallized quartz grains are present in diorite dykes. The feldspar grains show wavy extinction, which may be related to the deformation during faulting. Mafic dykes are very fine grained and show well developed foliation. Feldspars are found to be porphyroclasts, but are fractured due to deformation. Leucogranite from Tangtse area contain garnet and biotite along with quartz and plagioclase. Mylonitic foliation is also found in these granites. Cleavages in the mica are deformed in sample NST-46 and mica fish trails are also present (Figs. 4.3c, 4.3d). Amphibole and biotite bearing granite has sphene as accessory phase.



### 4.3 MAFIC VOLCANICS AND METABASALTS

Basaltic rocks occurring in the Shyok valley are collectively called “Shyok volcanics” by many workers (Thakur, 1981; Rai, 1982, 1999). Samples of Shyok volcanics are collected from north of Hundar village and along a traverse between Diskit and Khalsar. In the Diskit–Khalsar section, this unit includes greenschist facies metabasalt. Good exposures of metabasalts are found at the north of Hundar village. Sub-vertical andesitic dykes traverse through the metabasalts.

Mafic volcanics consist of plagioclase and pyroxenes as major phases. Chlorite, actinolite and plagioclase are found in metabasalts (Fig. 4.3e). Epidote is not uncommon. Plagioclases are randomly distributed in the basalt and show lamellar twinning. In some plagioclase grains twin lamellae are deformed due to shearing and showing wavy extinction. Muscovite also shows the sign of deformation in the form of bending of cleavages. Chlorite and quartz show wavy extinction indicate tectonic activity in the area. Andesitic dykes are fine grained with phenocrysts of plagioclase exhibit spherulitic texture.

### 4.4 OPHIOLITE MÉLANGE

Ophiolite mélange unit along the Nubra valley (called Nubra ophiolite mélange) consists of ultramafics, mafic volcanics and sedimentary rock units. The mafic volcanic rocks in the mélange along the Nubra valley are called Nubra ophiolitic volcanics (Ahmad *et al.*, 2005). The mafic volcanic rocks considered for the present study are referred to as Nubra volcanics. Nubra volcanics are exposed along the Tirit-Panamik section. These volcanic rocks of mafic composition are metamorphosed at some places. Tuffaceous rocks and volcanogenic sandstone are intercalated with this unit.

Chang La–Tsoltak section, which is considered as part of the Nubra ophiolite mélange sequence of Tirit-Panamik section, where it is best exposed is also sampled. In Chang La area, three different units have been found. These units are best exposed along the way to Durbuk from Tsoltak. Ultramafic unit includes herzbergite, dunite, pyroxenite and gabbro. Dunite found to be altered into serpentinite and talc. This ultramafic unit is followed by a sedimentary unit and volcanic unit from south to north. Sedimentary unit consists of thick pile of sandstone with minor limestone beds, carbonaceous shale and mudstone. Thick horizon of mudstone is followed by a horizon of conglomerate. Dolerite dykes are intruded into the carbonaceous shale and minor limestone unit. Volcanic unit, which is referred to as Tsoltak volcanics in previous chapter, consists of basalt, basaltic-andesite, and felsic volcanics with small tuffaceous horizon. Some basalts have secondary filling of zeolite (natrolite) in the vesicles. There is a small mafic volcanic unit with very big plagioclase grains (2-3 cm) which may be a giant plagioclase basaltic unit (Fig. 4.2h).

Giant plagioclase basalts (GPB) are generally the most differentiated lavas within a given formation (Hooper *et al.*, 1988; Sen, 2001). This suggests that the last erupting giant crystals may survive within the magma chamber until much of the magma erupts out of the chamber. GPB lavas are considered to mark the boundary between formations. These volcanics can also give the indication of age of the formation. The GPB erupted over conglomerate bed can possibly represents a hiatus between different eruptive activities (Hooper *et al.*, 1988; Khadri *et al.*, 1988; Subbarao *et al.*, 1988; Sen, 2001).

The mafic volcanics of the Tsoltak area are considered as part of the Shyok volcanics or continuation of the same by many workers (Rai, 1983, 1999; Wienberg *et al.*, 2000) but, mafic volcanic unit in the Tsoltak area are not metamorphosed and also contain plagioclase phenocrysts. GPB are absent in the Shyok volcanics. Hence, in the

present study these volcanics are considered as a separate volcanic unit. Comparison is given in the following chapters.

Nubra volcanics under microscope indicate that they are made up of clinopyroxene (augite) and plagioclase. Pyroxenes are surrounded by plagioclase laths and form subophitic texture. Plagioclase also occurs as phenocrysts. Basalt exhibits interlocking texture. Very fine grained basaltic rock with flow texture of plagioclase is also found in the Nubra volcanics.

In the so called GPB (NST-72), large plagioclase laths are embedded within the matrix composed of glass and small plagioclase and clinopyroxene grains (Fig. 4.3f). Some of the very big plagioclase laths in basalt show pericline twinning (Fig. 4.3g). Plagioclase in the matrix also shows albite type twinning. Some opaque minerals are also present. Gabbro in Tsoltak area contains clinopyroxene and amphiboles along with small amount of plagioclase and biotite. Some amphiboles show twinning same as in the case of Carlsbad twinning in plagioclase (Fig. 4.3h). Olivine are altered to serpentines.

#### **4.5 METASEDIMENTS AND METAMORPHICS**

Metamorphic rocks exposed at Tangtse and Pangong areas are called Pangong Metamorphic Complex which is made up of thickly-bedded marble, metapelites, quartzite, migmatite, and gneisses. The metamorphism varies from chlorite to kyanite zones. Carbonaceous schist and metapellites are exposed north of Muglib village (SE of Durbuk). Staurolite schist, garnet- muscovite schist, and marble are present well exposed near a lake on the way to Pangong. Kyanite schist is not exposed in the area but found further northeast of the Durbuk (Fig. 4.2i).

The rocks exposed in the Tangtse area include calc-silicates and metapelites intruded by leucogranites and mafic dykes. Calc-silicate rocks with alternate gray

calcareous and white siliceous bands show evidence of multiple folding (Fig. 4.2j). Patches of small granite gneiss are present within these calc-silicate rocks. Biotite bearing granitoid is intercalated with the metasediments and biotite is concentrated at some parts of the sediment layer. Mafic bodies are found as embedded within the granitoids and are also cut by the aplitic dykes (Figs. 4.2k, 4.2l). Metamorphic grade increases towards north. Metasediments and migmatites are exposed along the Diskit- Khalsar area and west of Kubed and Hurgam villages are not considered for the present study.

The low grade rocks of Pangong area are mostly fine grained schists in which biotite, garnet and plagioclase occur as porphyroblast. The mineral assemblages observed in the metamorphic rock is, Biotite+Chlorite+ Garnet+Quartz+Plagioclase  
In the high grade zone, there is a general increase in grain size. The shape of the garnet becomes sub-idioblastic (Fig. 4.3i). Sometimes the garnet shows poikiloblastic texture. The following mineral assemblages have been observed in the metamorphic rocks.

Biotite+Muscovite+ Garnet+Staurolite+Plagioclase

Biotite+Muscovite+ Garnet+Staurolite+ Kyanite+Plagioclase

Garnet, staurolite and kyanite are present as porphyroblasts and the foliation traced by the muscovite and biotite swerves around them (Fig. 4.3j). It indicates that these porphyroblasts are pre-kinematic with respect to foliation. At some places, muscovite replaces staurolite which suggests retrogression (Figs. 4.3k, 4.3l).

Amphibolite in the Pangong metamorphic complex consists of hornblende, pyroxene and garnet. Garnet grains have lots of inclusions. Amphibole controls the main foliation and plagioclase form a domain in the spaced foliation along with quartz. The main mineral assemblage observed in the amphibolite metamorphic rock is Garnet+Hornblende+Plagioclase+Quartz. Geochemical studies have not been carried out on any of these metamorphic rocks.

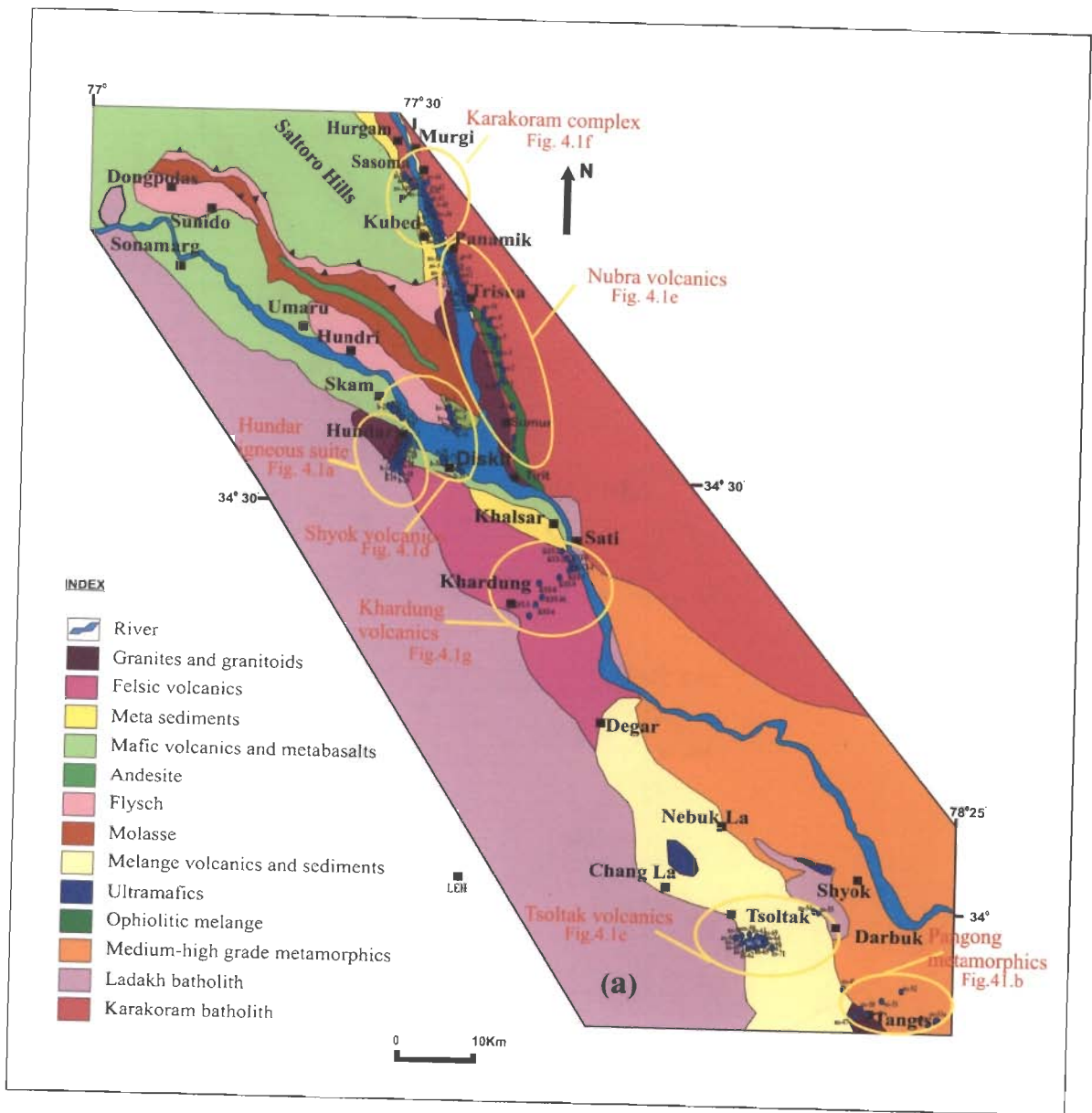


**Figure 4.1** (a) Geological map of the SSZ showing sample locations in different lithotectonic units. (b) to (h) give enlarged views of different sectors.

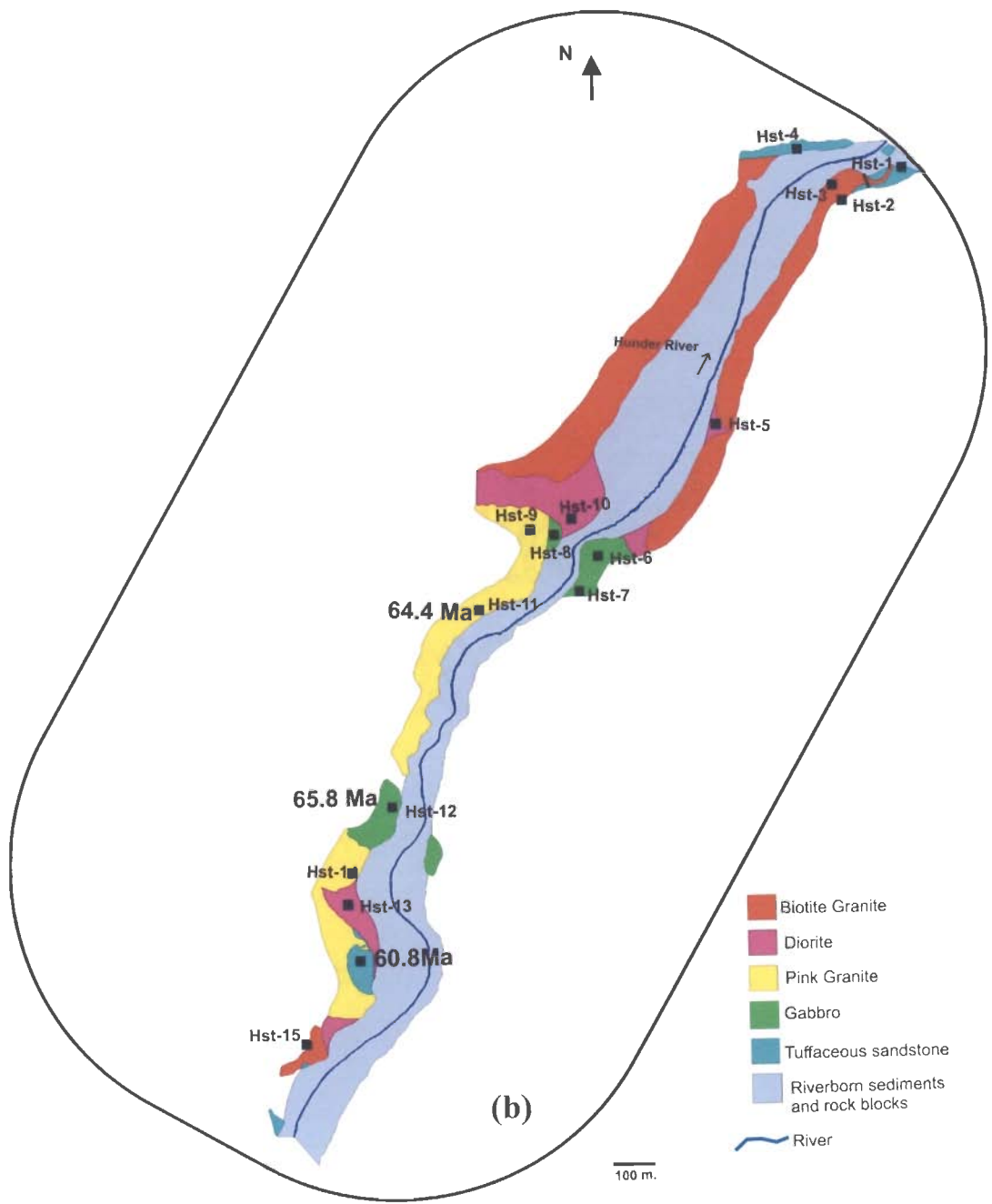


**Figure 4.1** Continued. (b) Geological traverse map shows sample locations along the Hundar river section. Age data are after Thanh *et al.* (2005).

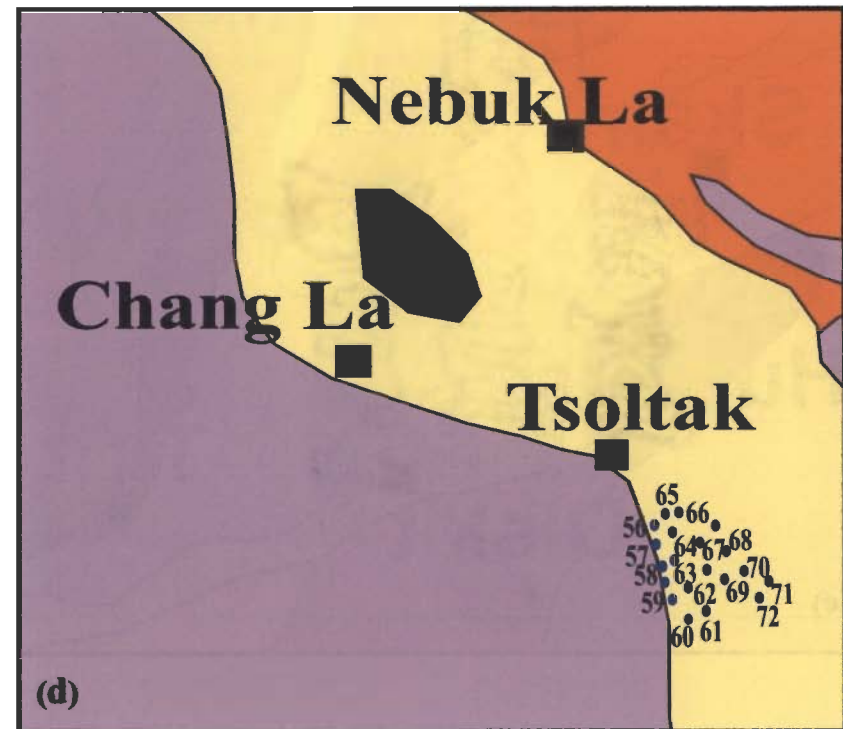
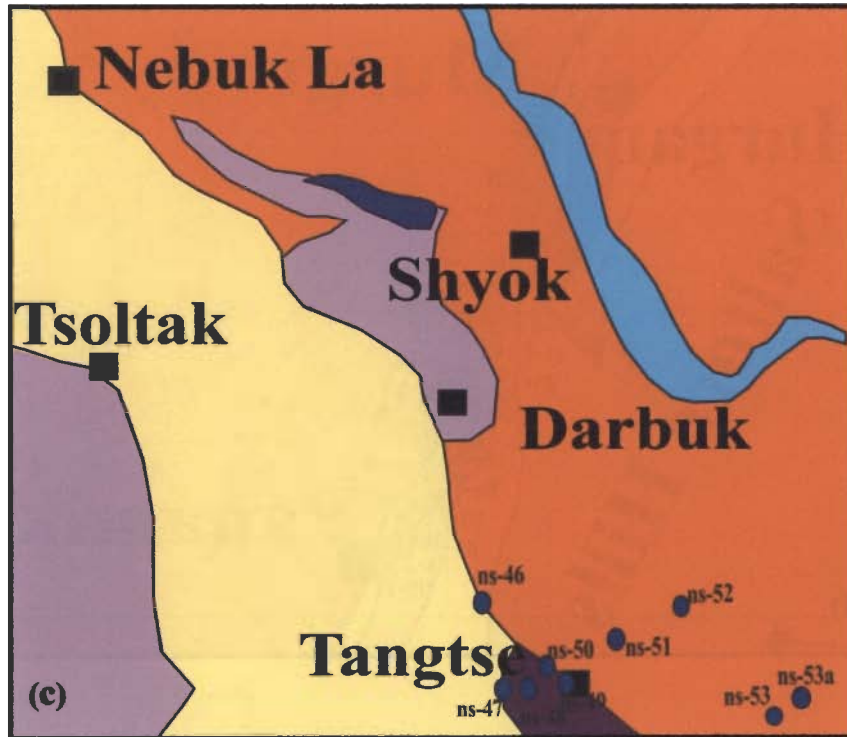


**Figure 4.1** Continued. (c) Pangong Metamorphic Complex (sample with prefix NST are shown as 'ns') (d) Tsoltak volcanics (all samples have prefix NST). For legend see Fig. 4.1a.

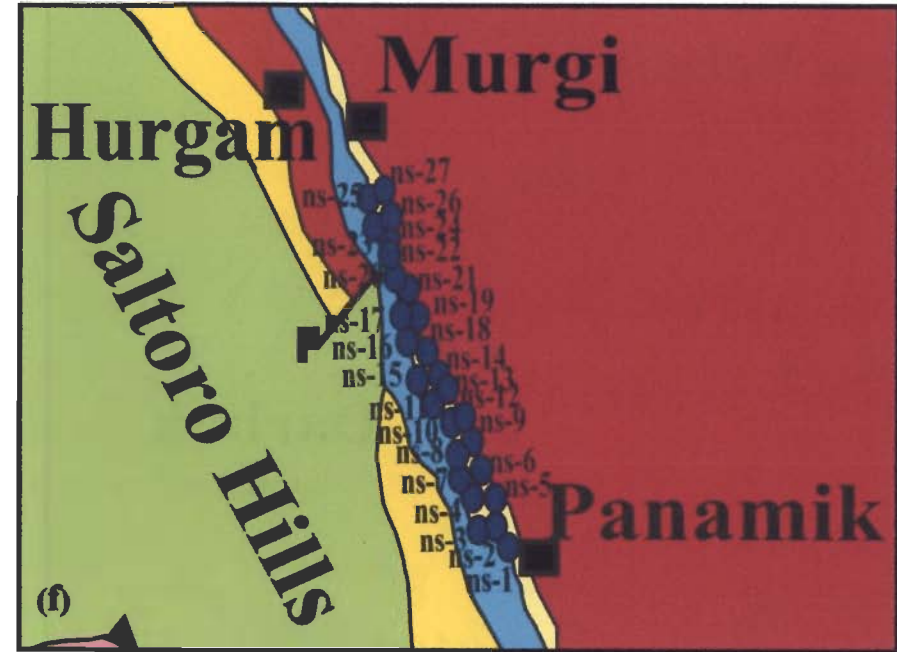


**Figure 4.1** Continued. (e) Shyok volcanics (sample with prefix HST are shown as 'h' and 'hv'). (f) Nubra volcanics (samples with prefix NST are shown as 'ns'). For legend see Fig. 4.1a.



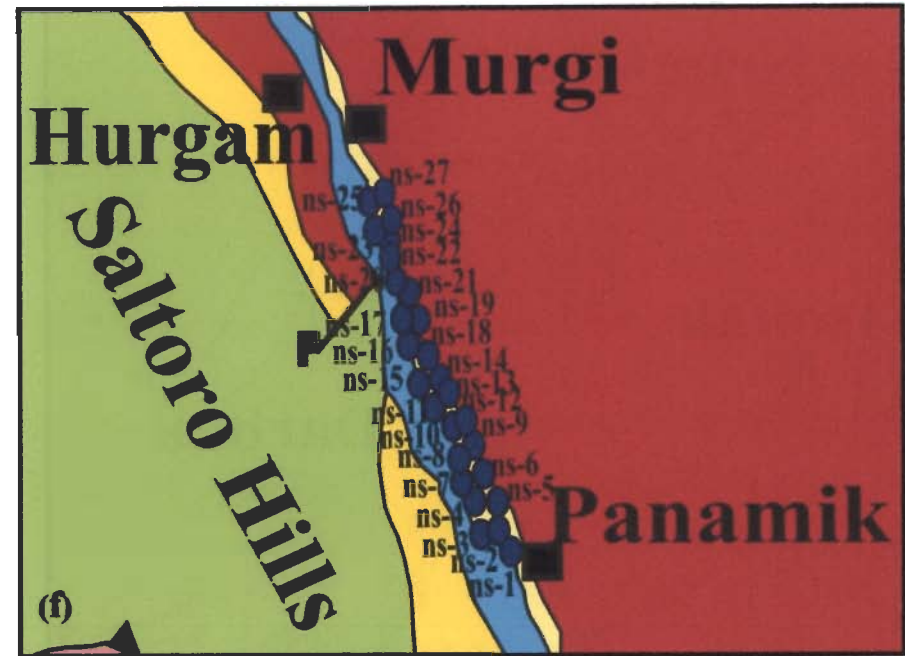
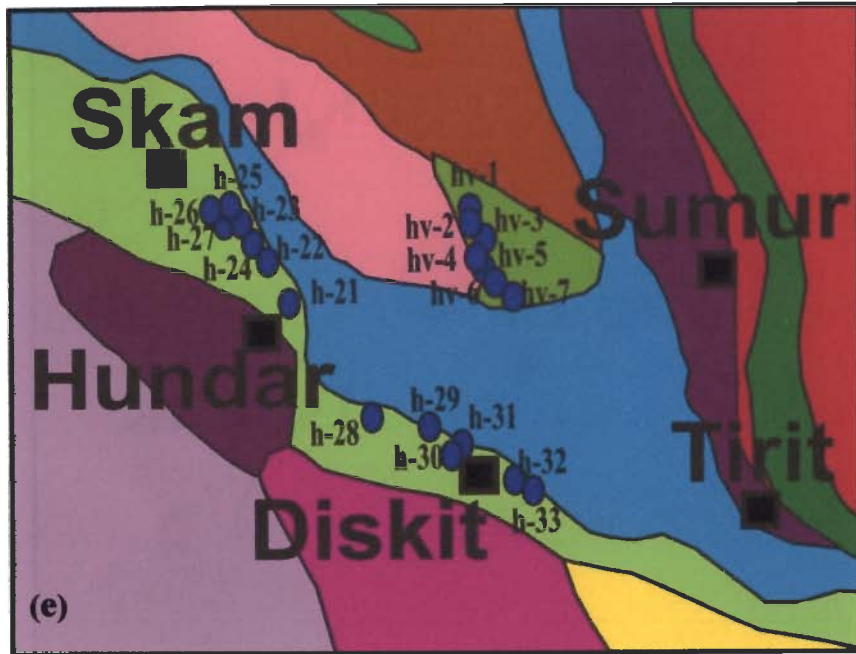


**Figure 4.1** Continued. (e) Shyok volcanics (sample with prefix HST are shown as 'h' and 'hv'). (f) Nubra volcanics (samples with prefix NST are shown as 'ns'). For legend see Fig. 4.1a.

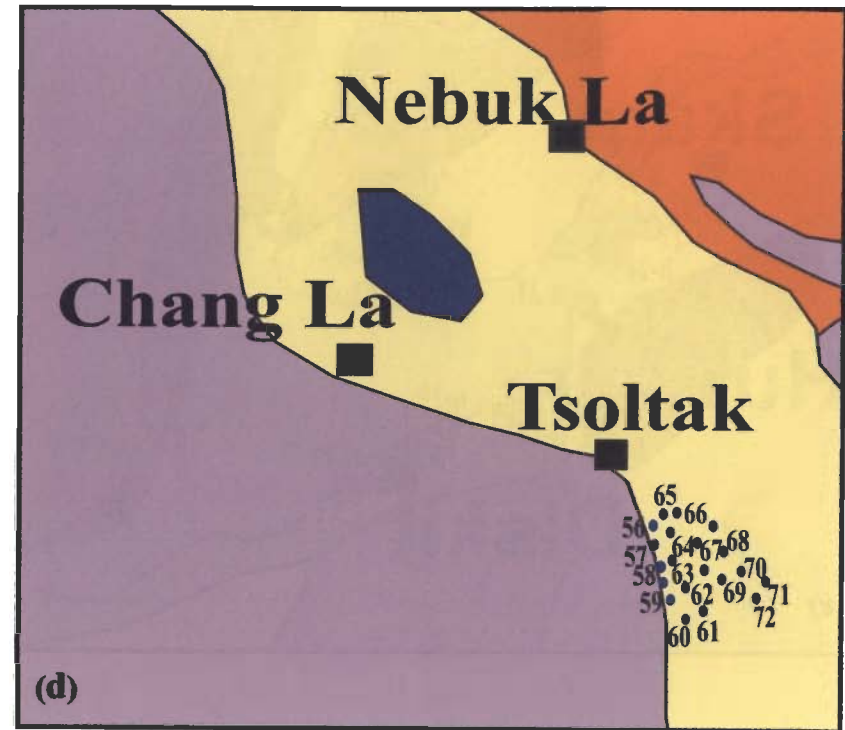
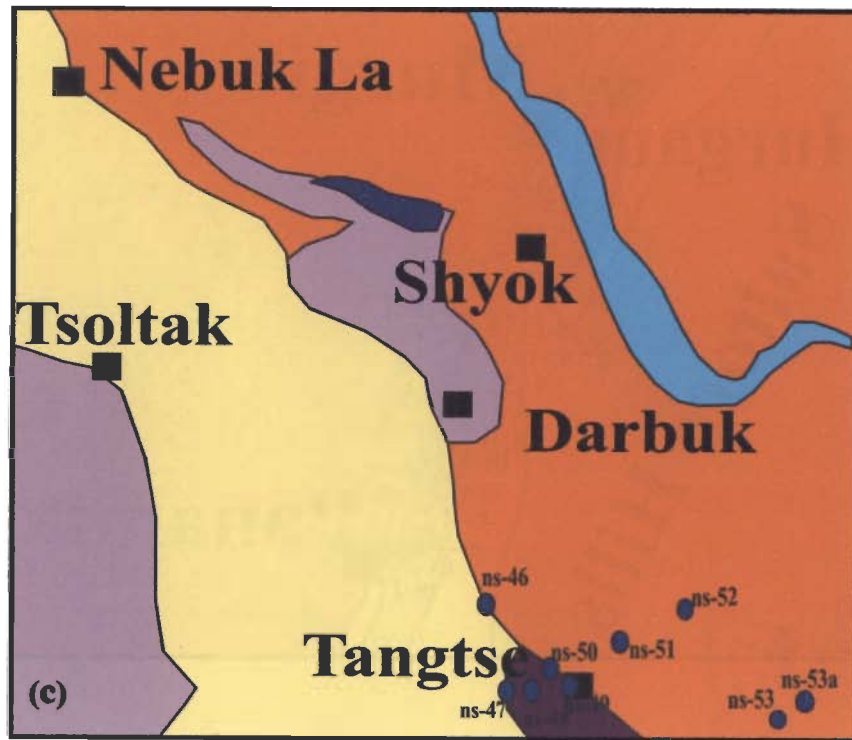


**Figure 4.1** Continued. (c) Pangong Metamorphic Complex (sample with prefix NST are shown as 'ns') (d) Tsoltak volcanics (all samples have prefix NST). For legend see Fig. 4.1a.

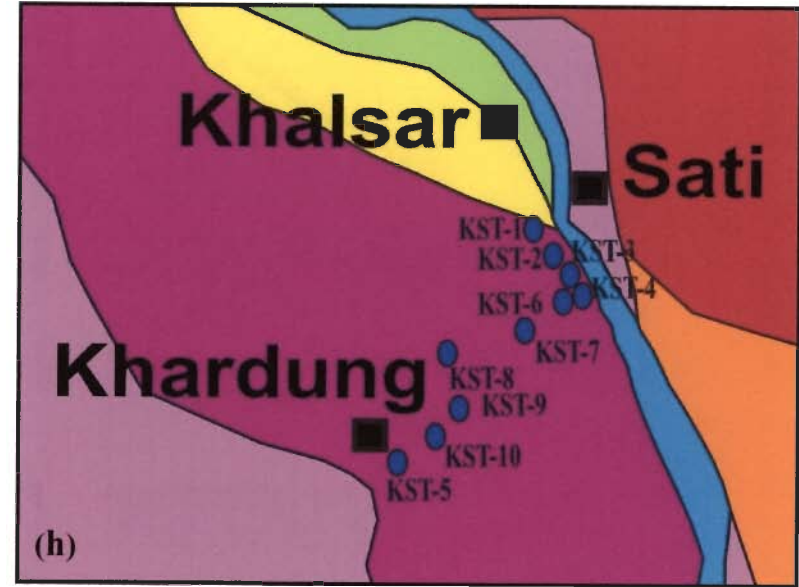
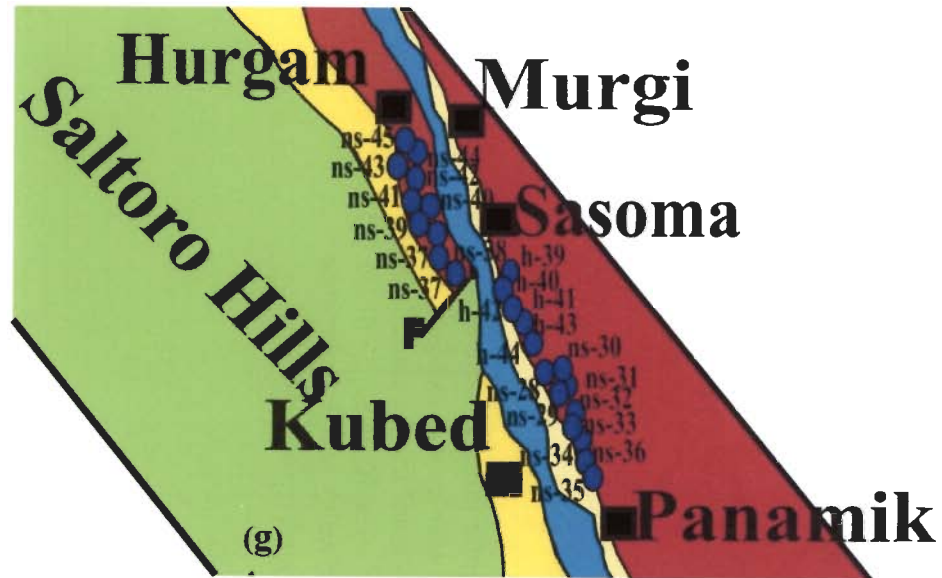


**Figure 4.1** Continued. (g) Karakoram complex (samples with prefix NST are shown as 'ns'). (h) Khardung volcanics. For legend see Fig. 4.1a

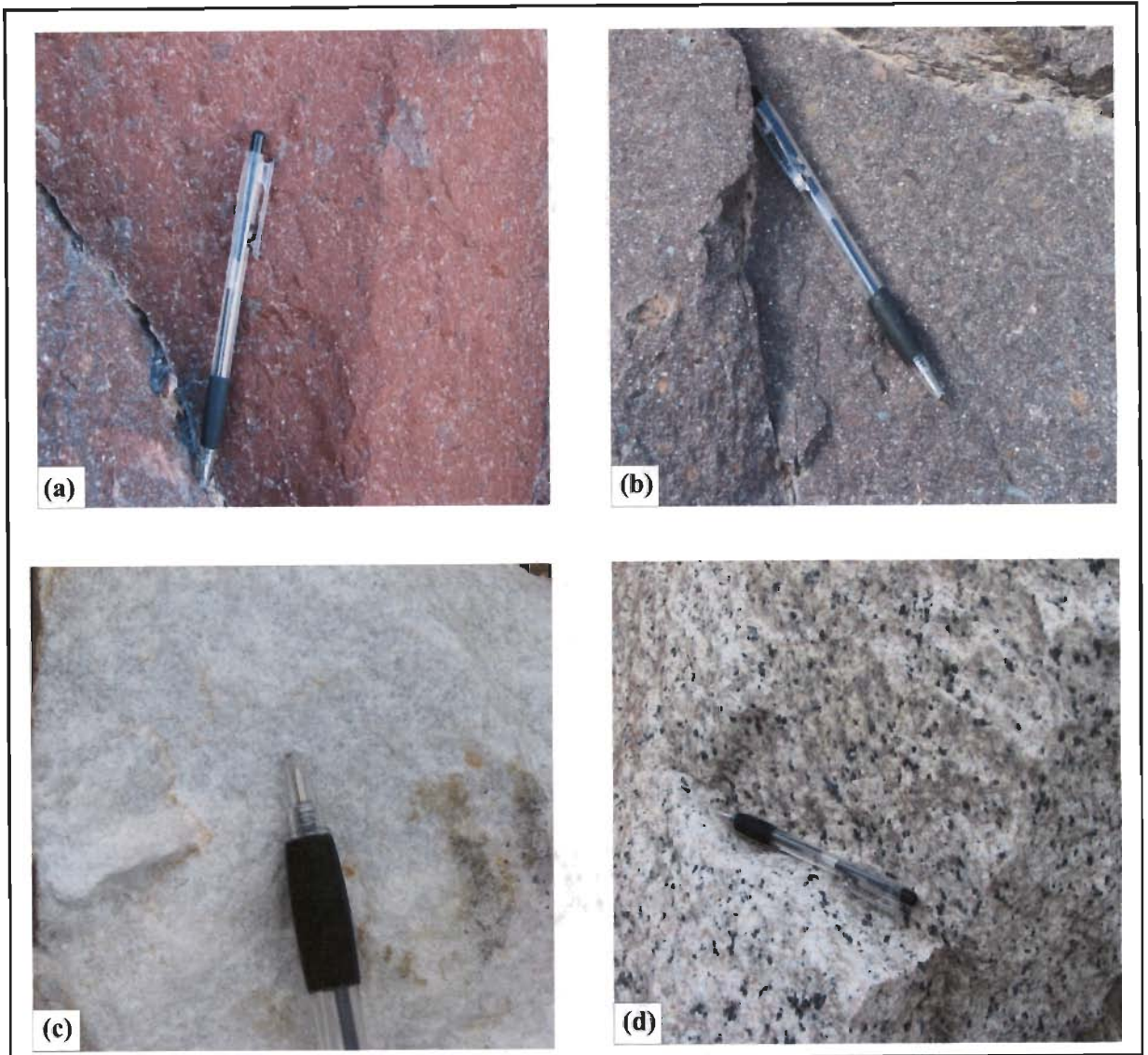


**Figure 4.2** Field photographs of different litho-tectonic units from Shyok Suture Zone.  
(a) Red coloured felsic volcanic rock exposed near Khardung area (b) Greenish grey coloured felsic volcanic rock exposed near Khardung area (c) White coloured rhyolite exposed near Khardung village (d) Light coloured micaceous granite along Hundar river valley near Hundar area

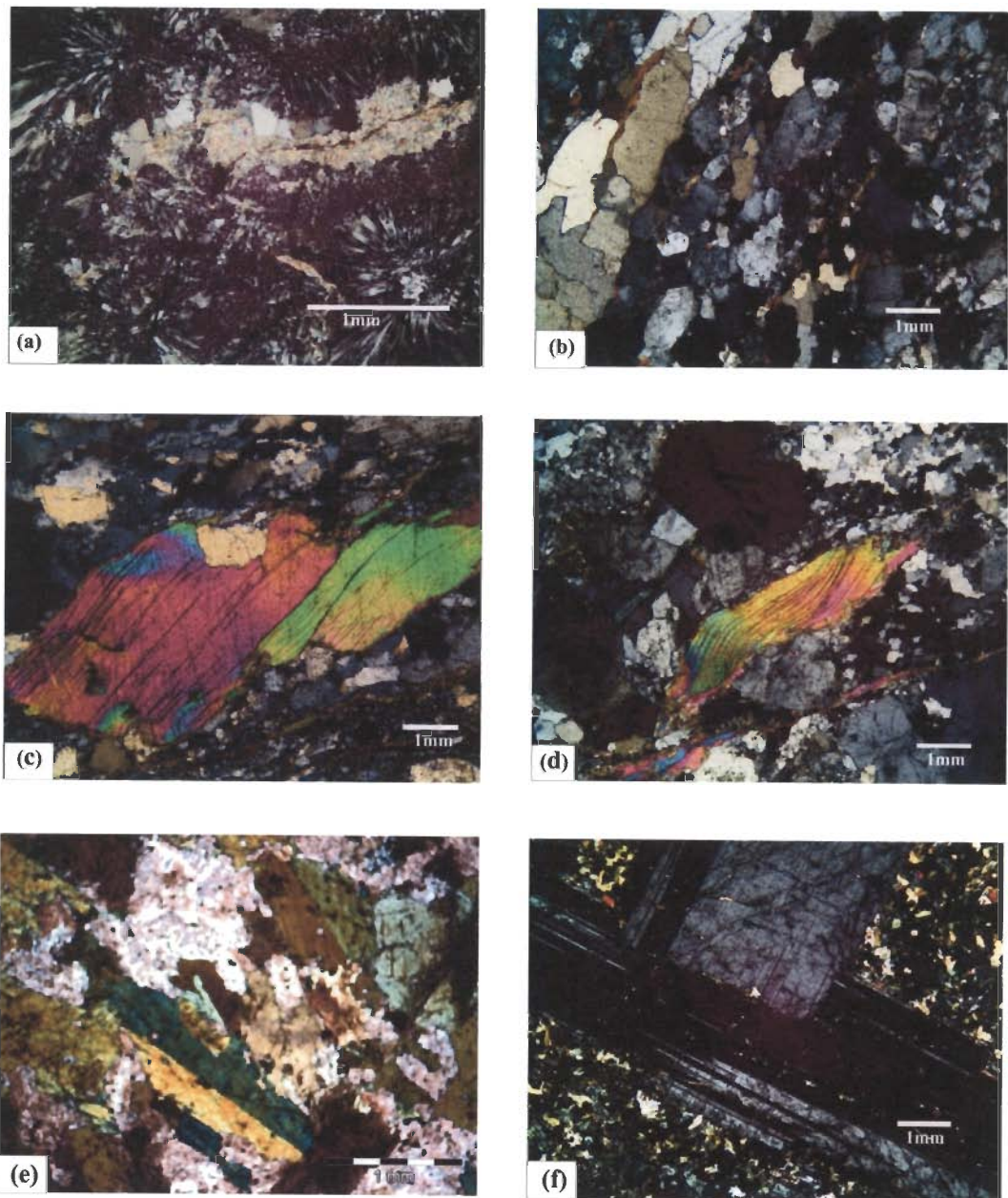


**Figure 4.3** Petromicrographs of samples from different litho-tectonic units.

(a) Phenocryst of spherulitic texture of feldspar in Khardung volcanics, from Khardung area, sample KST-1, under crossed nicols (b) Slightly deformed Karakoram granite forming gneiss from Hurgam area, sample NST-41, under crossed nicols (c) Mica fish trail in granite from Tangtse area, sample NST-46, under crossed nicols (d) Deformed cleavage in mica grain in granite from Tangtse area, sample NST-46, under crossed nicols (e) Actinolite in metbasalt from Shyok area, sample 21, under crossed nicols (f) Large plagioclase phenocryst in fine grained matrix contains small plagioclase crystals in Giant Plagioclase Basalt from Tsoltak area, sample 72-b, under crossed nicols.

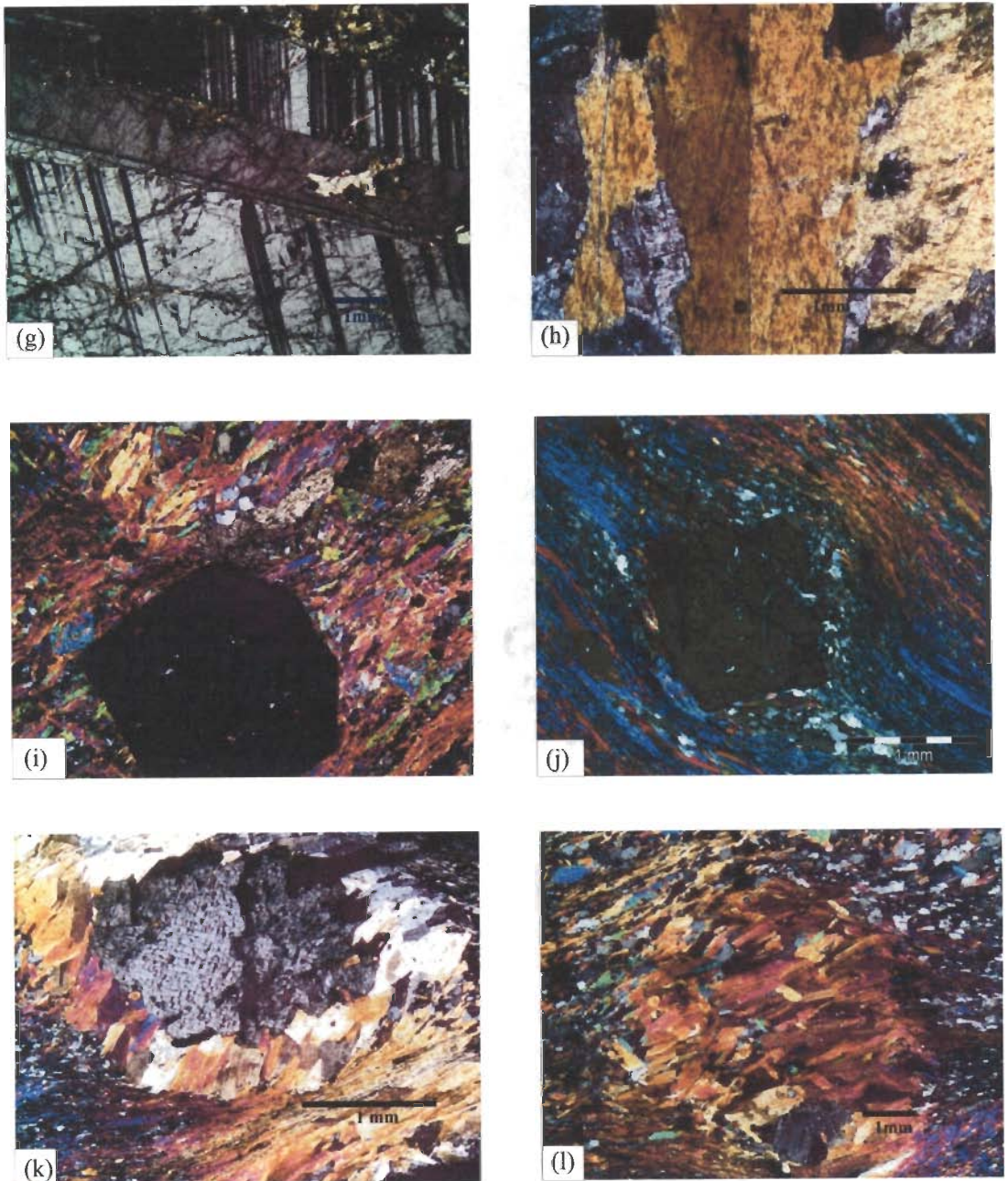


**Figure 4.3** Continued. (g) Pericline twinning in GPB from Tsoltak area, sample 72-d, under crossed nicols (h) Carlsbad type twinning of amphibole in gabbro from Tsoltak area, sample 61, under crossed nicols (i) Sub-idioblastic garnet from Pangong metamorphics, sample 53-a, under crossed nicols (j) Foliation defined by mica swerves around the garnet grain in garnet mica schist from Pangong metamorphics, sample 53-b, under crossed nicols (k) Mica replacing staurolite and foliation mainly defined by muscovite and biotite. Foliation swerves around the staurolite, sample 52-a, under crossed nicols (l) Staurolite replaced by mica grains and forms pseudomorph. Relict of staurolite grain is also visible, sample 52-a, under crossed nicols.

## **Chapter 5**

# **GEOCHEMISTRY**

Rock samples from different litho-tectonic units of SSZ have been analyzed for major, trace and rare earth elements (REE) in order to determine the geochemical characteristics and understand petrogenetic evolution. Petrogenetic modelling using geochemical data involves determining the possible mineralogy and chemical composition of the source region, conditions, mechanics and extent of melting, tectonic setting, and assimilation and/or contamination during magma evolution, ascent and emplacement. The methods of geochemical analyses have been discussed in chapter 3 and analytical results are discussed in this chapter.

### **5.1 MAJOR ELEMENTS CHARACTERISTICS**

Major elements are the essential constituents of rock forming minerals. Concentrations of these elements are usually expressed in terms of oxide percentages and include SiO<sub>2</sub>, TiO<sub>2</sub>, Al<sub>2</sub>O<sub>3</sub>, Fe<sub>2</sub>O<sub>3</sub>, FeO, MnO, MgO, CaO, Na<sub>2</sub>O, K<sub>2</sub>O and P<sub>2</sub>O<sub>5</sub>. The major elements data can be used in rock classification and construction of variation diagrams.

#### **5.1.1 Distribution of major elements**

Bowen, (1928, 1941) described two types of crystallization. In fractional crystallization, crystals are immediately isolated from the system after they are formed. In equilibrium crystallization, crystals react and re-equilibrate with the liquid as the temperature decreases. Olivine and calcic-plagioclase are the minerals to crystallize first from a melt of basaltic composition. Part of olivine crystals may react with the melt and form pyroxene or pyroxene may precipitate on its own as the magma cools or evolves.



Crystallization of pyroxene is followed by formation of amphibole and biotite. Most of the magnesium and calcium leave the melt at the early stage of fractionation as olivine, pyroxene, amphibole and calcic-plagioclase crystallize progressively. The early formed minerals tend to have better formed crystal faces. These euhedral to subhedral crystals commonly occur as phenocrysts. The smaller accessory minerals like zircon, apatite and titanite tend to be euhedral though they form during the later stage of crystallization (Winter, 2001). The composition of plagioclase becomes sodic and at the end of the crystallization quartz and potash feldspar appear with sodic plagioclase. At this stage, the composition of the melt becomes devoid of alkali metals. Iron may be largely concentrated in the early forming minerals. The concentration of aluminium in the melt decreases during fractionation of feldspar and micas. If the oxygen fugacity is low, iron remains longer in the melt otherwise it crystallizes out as Fe-oxides (Presnall, 1979).

As olivine crystallizes from the melt Mg and Fe get into the crystal structure and the Mg and Fe concentration in the residual melt decreases. As pyroxene crystallizes or forms directly from melt, there will be further decrease in Fe and Mg content in the melt. Crystallization of calcic-plagioclase usually follows pyroxenes. Consequently, concentration of alkalis will increase at this stage as Fe and Mg are removed from melt. Ca, Al and Na would increase initially but will start decreasing as pyroxene and plagioclase continues to crystallize. These trends continue with amphibole joining the crystallization process. As micas and other late phases start to crystallize, the concentration of alkalis and Ti will show a reducing trend. During fractionation of olivine, pyroxene, feldspars and Fe-oxide phases, the composition of magma changes from mafic to felsic (Yoder, 1962, 1976; Krauskopf and Bird, 1995; Philpotts, 1995). Fig. 5.1 represents variation diagrams for major element oxides in case of basaltic magma undergoing fractional crystallization and the change in composition of the residual melt.

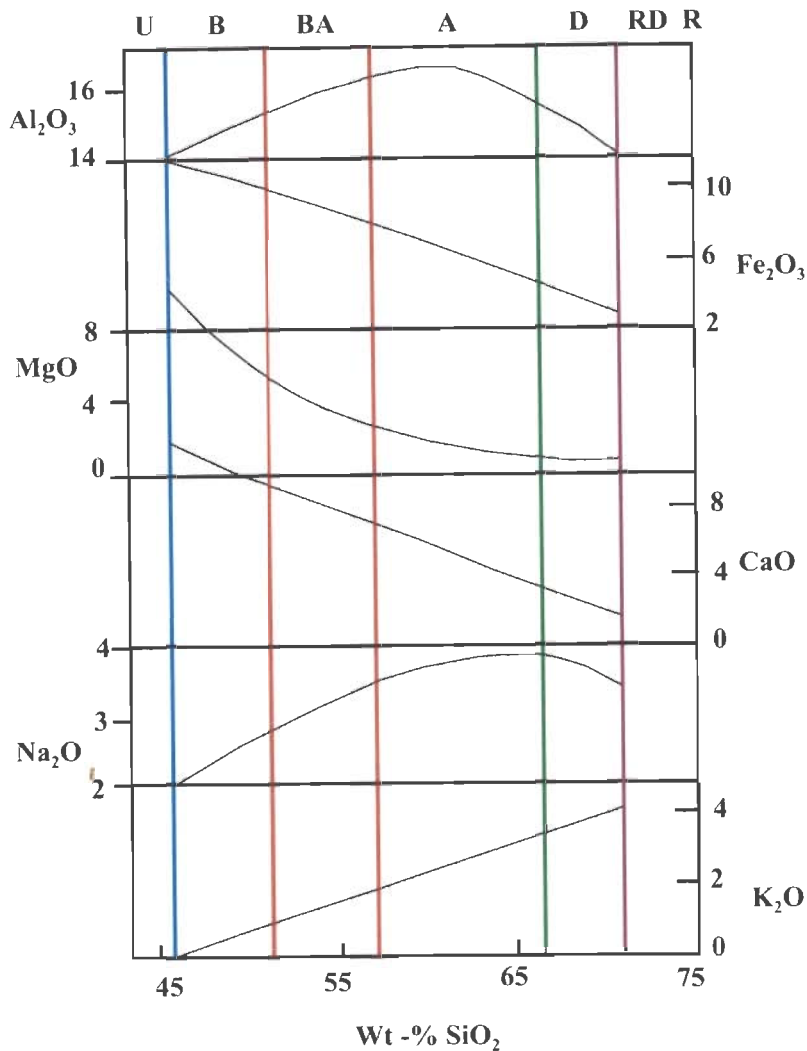


**Figure 5.1** Schematic variation diagrams for major element oxides in case of calc-alkaline volcanic series (data from Ragland, 1989). U: ultra mafic. B: basalt, BA: basaltic andesite, A: andesite, D: dacite, RD: rhyodacite, R: rhyolite.

The sequence of crystallization may not be as simple as described above. With rapid cooling the composition of a mineral may not remain in equilibrium with the melt leading to various possible geochemical distribution patterns. For example, a core and rim with different compositions may develop in porphyroclasts. Sudden decrease in temperature may result in the formation of glass.

In many cases, simultaneous crystallization of several mineral phases takes place. The crystallization of mineral phases at different stages may also be dependent on partial

pressure of H<sub>2</sub>O or oxygen fugacity. The mineral assemblages also depend on the bulk composition of the magma and the temperature of crystallization. The sequence of crystallizations in the case of tholeiitic and calc-alkaline magmas are different and the crystallization trends in these magmas depend on the oxygen fugacity and H<sub>2</sub>O saturation. Iron enrichment during the crystallization of basaltic magma is found to be common for tholeiitic type magmas (Fenner, 1929). Bowen (1928) emphasized the enrichment of alkali feldspar and silica in the residual liquid which is more valid for calc-alkaline magmas. In hydrous conditions, plagioclase crystallizes at higher temperature than pyroxenes in high-aluminum basalt and calc-alkaline andesites (Yoder, 1969). According to Bowen's reaction series, biotite and quartz forms at later stage of fractional crystallization, where volatile and alkali components are enriched. Biotite does not always crystallize at the later stages. In the tholeiitic magma, volatile content is low in the residual liquids compared to the calc-alkaline magma. The crystallization of biotite and quartz occurs at temperatures where K-bearing amphibole is unstable even if the alkali component is very small (Luth, 1967). During the crystallization of calc-alkaline magma, water pressure is high and crystallization temperature is low leading to stabilization of biotite and quartz assemblage. Hence, the assemblage mainly depends on water pressure and temperature of crystallization (Yoder, 1969). The crystallization temperature of amphibole increases with increasing pressure in the presence of H<sub>2</sub>O. Amphibole can crystallize as primary phases at higher depth under hydrous condition (Yoder and Tilley, 1962). Separation of amphibole alone is not effective in generating calc-alkaline trend though fractionation of amphibole is an important phase in calc-alkaline series. Abundance of water in the melt would facilitate the formation of hydrous minerals. At higher pressure (~10-20 kb) garnet and soda rich pyroxenes will replace olivine and plagioclase and the system changes from simple basalt to eclogite. If the magma is

interrupted in ascent at high pressure the compositional variation of residual liquid is controlled by fractionation of eclogite. At intermediate pressure it will be controlled by the fractionation of spinel-lherzolite. All these processes may drastically affect the shape of variation diagrams depicted in Fig. 5.1.

### **5.1.2 Chemical classification of SSZ rocks**












It is difficult to classify rocks in handspecimen and outcrop in the SSZ as the area represents a tectonic mélange (Fig. 2.4). This is owing to the fact that most of the rocks are volcanic or fine grained intrusives with wide variation in physical appearance. The rock types vary continuously from basalt to andesite-rhyolite. Distinguishing mafic from felsic rocks in outcrop and handspecimen may be easy but differentiating samples of intermediate composition is difficult or even impossible in many samples. Therefore, the rocks need to be classified according to their chemical composition. Further, same rock types are repeated in different litho-tectonic zones. For descriptive purpose, the samples are divided into six groups based on geographic locations and litho-tectonic zones from which samples were collected. These are Hundar igneous suite, Khardung volcanics, Shyok volcanics, Nubra volcanics, Tsoltak volcanics and Karakoram complex (see Fig. 4.1).

The total alkali (sum of the  $\text{Na}_2\text{O}$  and  $\text{K}_2\text{O}$ ) vs. silica diagram (TAS) is most frequently used to classify igneous rocks (Le Bas *et al.*, 1986). Volcanic rocks are subdivided into two major series on a TAS diagram, the alkaline and sub-alkaline (originally termed tholeiitic) series (Iddings, 1892). The sub-alkaline field is further divided into five fields as basalt, basaltic andesite, andesite, dacite and rhyolite (Le Bas *et al.*, 1986). The TAS diagram for SSZ samples show that most of the samples plot in the

sub-alkaline field (Fig. 5.2). However, the plot shows continuous variation in chemical composition from basalt through basaltic andesite, andesite, dacite to rhyolite.

In order to distinguish different rock types and samples from different litho-tectonic units in all subsequent geochemical diagrams, a scheme involving symbol for litho-tectonic zones and colour codes for rock types have been evolved (Table 5.1). The litho-tectonic zones represented by Hundar igneous suite, Khardung volcanics, Shyok volcanics, Nubra volcanics, Tsoltak volcanics and Karakoram complex are given circle, inverted triangle, hexagon, diamond, triangle and square, respectively. Rocks with basalt, basaltic andesite, andesite, dacite and rhyolite composition are given blue, red, green, yellow and pink colour codes, respectively. Thus for example, all samples of Khardung volcanics will have inverted triangle symbol. If the sample is basaltic or dacite composition, the inverted triangle will be filled with blue or yellow colour, respectively. Similarly, all samples from Karakoram complex will have square symbol but will have different colour filling depending on rock type.

**Table.5.1** Colour as well as litho-tectonic index

<u>LITHOTECTONIC INDEX</u>		<u>COLOUR INDEX</u>	
	HUNDAR IGNEOUS SUITE		BASALT
	KHARDUNG VOLCANICS		BASALTIC ANDESITE
	NUBRA VOLCANICS		ANDESITE
	TSOLTAK VOLCANICS		DACITE
	SHYOK VOLCANICS		RHYOLITE/GRANITE
	KARAKORAM COMPLEX		

The TAS diagram has been redrawn in Fig. 5.3 incorporating the scheme of symbols and colour coding described above. The Hundar samples (with circle symbols) range in composition from basalt to rhyolite through all the fields. Most of the Khardung samples are restricted to the rhyolite field except one sample each in the andesite and the dacite fields. The Shyok samples also plot in all the fields from basalt to rhyolite but a majority of samples are andesitic in composition. The Nubra samples spread over from basaltic to andesitic fields. Two samples plot even in the alkaline field. The Karakoram samples cover all the compositional fields from basalt to rhyolite but most of the samples plot within the basaltic andesite field. A few samples from Karakoram plot within the alkaline field. Tsoltak volcanics range in composition from basalt to andesite. The SiO<sub>2</sub> content in one sample (sample no. NST-69) from Tsoltak volcanics is 44.2% and has very low alkali content compared to basalts from other areas. This sample is classified as ultramafic rock and has been used as source in petrogenetic modelling (see chapter 6). This sample has not been plotted in the variation diagrams described below. Several other classification schemes are available in the literature. For example, the classification schemes based on least mobile incompatible trace element ratios (Floyd and Winchester, 1975; Nb/Y vs. silica, Winchester and Floyd, 1977) also indicates that most of the samples are sub-alkaline (Fig. 5.4).

In bivariate variation diagrams, geochemical data show as bivariate plots. The oxides of major elements are plotted against the oxide which shows maximum variability in a suite of samples. Bivariate plots using SiO<sub>2</sub> along the X-axis and oxides of other major elements along the Y-axis are often called 'Harker diagrams'. Hence all other major element oxides are plotted against the SiO<sub>2</sub> weight percent and trends are compared with the expected igneous trend of the rocks from mafic to felsic composition (Fig. 5.5). The geochemical data for major elements are given in appendix 2.

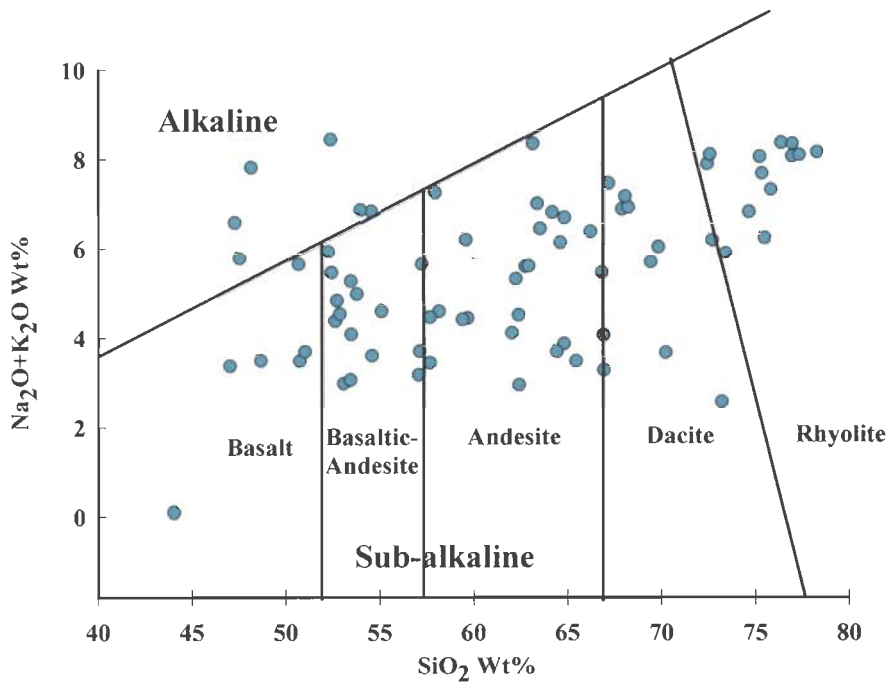


**Figure 5.2** Total alkali versus silica (TAS) diagram of different litho-tectonic units. (Le Bas *et al.*, 1986)

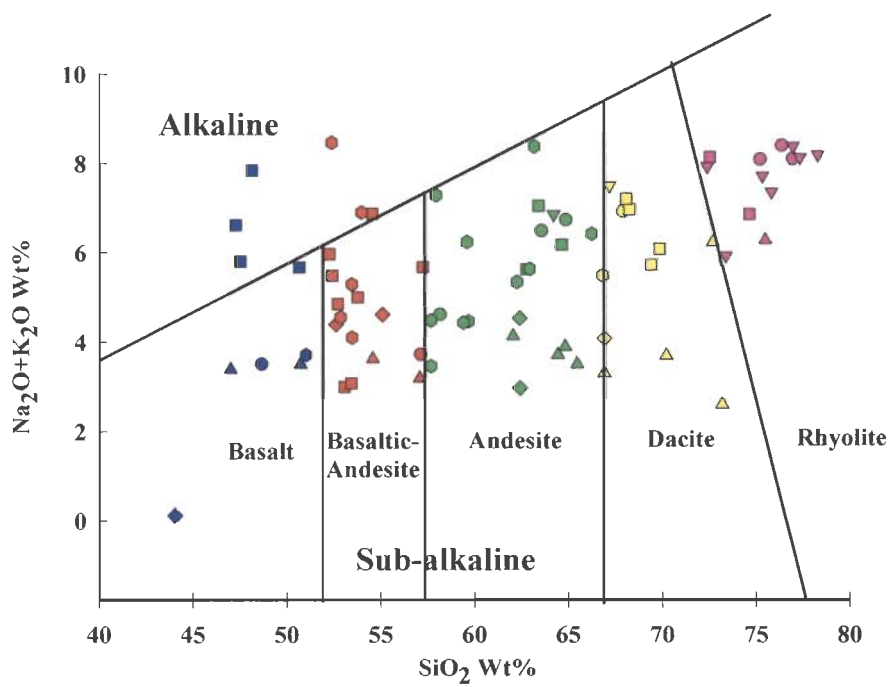


**Figure 5.3** Total alkali versus silica (TAS) diagram of different litho-tectonic units according to their chemical composition (Le Bas *et al.*, 1986).

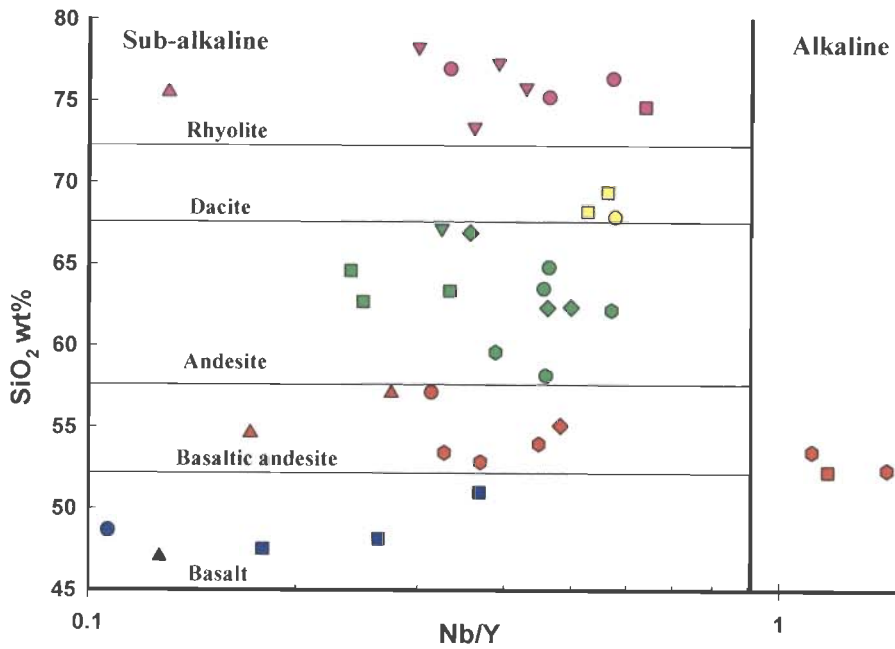


**Figure 5.4** Classification schemes based on least mobile incompatible trace element ratio vs.  $\text{SiO}_2$  wt% (Winchester and Floyd, 1977).

### 5.1.3 Bivariate variation diagrams

#### *MgO-SiO<sub>2</sub> diagram* (Fig. 5.5a)

MgO shows usual negative correlation with  $\text{SiO}_2$ , except for some samples from Nubra and Tsoltak volcanics. For Hundar igneous suite,  $\text{SiO}_2$  varies from about 48% to 77% corresponding to basaltic through intermediate diorite to granite and dacite with concomitant decrease in MgO. Shyok volcanics vary in composition from basalt through basaltic andesite to andesite with  $\text{SiO}_2$  and MgO varying between 47-66% and 2.2-9.3%, respectively. Therefore, Shyok volcanics are relatively more mafic than the Hundar igneous suite. Khardung volcanics are more felsic with  $\text{SiO}_2$  varying between 67 to 78% and MgO is very low or below detection limit. Majority of the Nubra volcanics are basaltic to andesitic in composition.  $\text{SiO}_2$  vary between 52-66% and one or two samples with low MgO plot outside the overall negative trend. For Karakoram rocks, composition



varies from basaltic/gabbroic to granites. MgO goes up to 11.6% for the basalts and ~0.05% for granite.

#### ***CaO-SiO<sub>2</sub> diagram*** (Fig. 5.5b)

CaO shows negative correlation with SiO<sub>2</sub>. Some of the Tsoltak and Nubra volcanics do not strictly follow the general trend. CaO in granites from Hundar area varies from 0.52 -1.43%. In intermediate rocks, CaO varies from 3.67 to 8.35%. Basaltic dyke has approximately 9% CaO content. Shyok volcanics have CaO content 4.4-8.7%. Khardung volcanics have very low CaO. Mafic enclaves in Karakoram complex have high CaO, which goes up to 9.3% whereas the granitoids have concentration, ranges between 1.6-3.49%. For Nubra volcanics it varies from 1% for andesite to 8.4% for basaltic andesite. In Tsoltak volcanics, it varies between 1-7.4% for same range of rock types.

#### ***Fe<sub>2</sub>O<sub>3</sub>-SiO<sub>2</sub> diagram*** (Fig. 5.5c)

Fe<sub>2</sub>O<sub>3</sub> also shows negative trend with SiO<sub>2</sub>. The Fe<sub>2</sub>O<sub>3</sub> concentration in the Hundar igneous suite varies between 1-12% as the rock composition varies from granite to basalt. Khardung volcanics have low concentration of Fe<sub>2</sub>O<sub>3</sub> which varies between 1-4.8% for andesite to rhyolite. Karakoram granites have lower concentration of Fe<sub>2</sub>O<sub>3</sub> but the rocks of intermediate composition and the enclaves have high concentration up to 11%. Tsoltak volcanics have 9% Fe<sub>2</sub>O<sub>3</sub> for basaltic andesite and 2.6% andesite, whereas the basaltic rock has comparatively high Fe<sub>2</sub>O<sub>3</sub> concentration of about 10.6%. In Nubra, basaltic andesite has 13.5% of Fe<sub>2</sub>O<sub>3</sub>.

#### ***MnO-SiO<sub>2</sub> diagram*** (Fig. 5.5d)

The data show quite a bit of scatter and show a weak negative correlation with SiO<sub>2</sub>. In Hundar igneous suite it varies from 0.03 to 0.24% and mafic dyke has 0.36%. In Shyok volcanics it varies from 0.05% for granitoids to 0.16% for basaltic andesite.

Khardung volcanics have MnO concentration 0.01-0.15% for andesite to rhyolite composition. Karakoram dykes and enclaves have MnO content up to 0.2%. In Tsoltak and Nubra volcanics MnO has a maximum value of 0.1%.

***Al<sub>2</sub>O<sub>3</sub>-SiO<sub>2</sub> diagram*** (Fig. 5.5e)

The general convex-upward trend for Al<sub>2</sub>O<sub>3</sub> trend for the samples of SSZ is more or less similar to the expected igneous trend (Fig. 5.1). However, the data show some amount of scatter. Alumina content of Hundar rocks varies from 13-16%. In Shyok volcanics it varies between 12-17.6% for basalt to andesites and 8.6-12 % for the granite and granitoids. In the Khardung volcanics, it varies between 12.5-15%. In the Karakoram granites and intermediate rocks it goes up to 17%. Basaltic rocks of Karakoram complex the alumina ranges from 12-20%. In basaltic andesite to dacite, Al<sub>2</sub>O<sub>3</sub> changes from 12-17%. Tsoltak volcanics also have high alumina content which goes up to 22-23% for andesite samples. Ultramafic sample (NST-69) shows low alumina content about 4%. Nubra volcanics have 12-18% of alumina content for the rocks of basaltic andesite to andesitic composition.

***TiO<sub>2</sub>-SiO<sub>2</sub> diagram*** (Fig. 5.5f)

TiO<sub>2</sub> is generally low in all the rock units and shows a negative correlation with SiO<sub>2</sub>. Rocks of basaltic to andeistic composition have concentration above 1%. In the rocks from Hundar area, TiO<sub>2</sub> varies between 0.09-1.1% for the rock composition granite to basalt. Aplitic dykes of composition varying from dacite to rhyolites from Shyok volcanics rocks with SiO<sub>2</sub> 70-75% have TiO<sub>2</sub> 0.25-0.65%. Rocks of basalt to andesitic composition (47-67% of SiO<sub>2</sub>) have a range of 0.26-1.4 % of TiO<sub>2</sub> concentration. Khardung volcanics have a range of 0.1-0.7% TiO<sub>2</sub> content. Tsoltak volcanics with high SiO<sub>2</sub> content have more than 1% TiO<sub>2</sub>. The basaltic and granitoids rocks of the Karakoram complex have TiO<sub>2</sub> concentration up to 1.64% and 0.5%, respectively. In

Tsoltak area, andesites have  $\text{TiO}_2$  concentration at about 1%. In Nubra area, basaltic andesites with low  $\text{SiO}_2$  content have 1% of  $\text{TiO}_2$ .

#### ***$\text{Na}_2\text{O}-\text{SiO}_2$ and $\text{K}_2\text{O}-\text{SiO}_2$*** (Fig. 5.5 g, h)

$\text{Na}_2\text{O}$  and  $\text{K}_2\text{O}$  do not show distinct correlation with  $\text{SiO}_2$  and the data points are highly scattered. These elements become mobile in case of any fluid influx in the area.

Major element variation diagrams indicate that most of the rock units of SSZ show general magmatic trend.

#### **5.1.4 Triangular variation diagrams**

A commonly used triangular diagram that is used to distinguish between tholeiitic and calc-alkaline magma series is the so-called AFM diagram in which  $A = (\text{Na}_2\text{O} + \text{K}_2\text{O})$ ,  $F = (\text{FeO} + \text{Fe}_2\text{O}_3)$  and  $M = \text{MgO}$  (Kuno, 1968; Irvine and Baragar, 1971). The  $\text{Al}_2\text{O}_3$ - $\text{FeO}$ - $\text{MgO}$  in another example of triangular variation diagram (Pearce *et. al.*, 1977). In this diagram basaltic andesite from different tectonic settings can be discriminated.

#### ***$(\text{Na}_2\text{O} + \text{K}_2\text{O})-(\text{FeO} + \text{Fe}_2\text{O}_3)-\text{MgO}$ (AFM) diagram***

This discrimination diagram (Fig. 5.6) indicates that most of the samples from different litho-tectonic units are sub-alkaline and follow the calc-alkaline trend. Calc-alkaline magmatism is associated with subduction zones and arcs. Hence, SSZ rocks possibly show an arc affinity.

#### ***$\text{Al}_2\text{O}_3$ - $\text{FeO}$ - $\text{MgO}$ diagram***

In the  $\text{Al}_2\text{O}_3$ - $\text{FeO}$ - $\text{MgO}$  triangular diagram, samples with basaltic andesites with  $\text{SiO}_2$  ranging between 51-56 wt% from the whole area are plotted. Majority of the samples are plotted within the field for MORB, island arc and active continental margin (Fig.5.7).

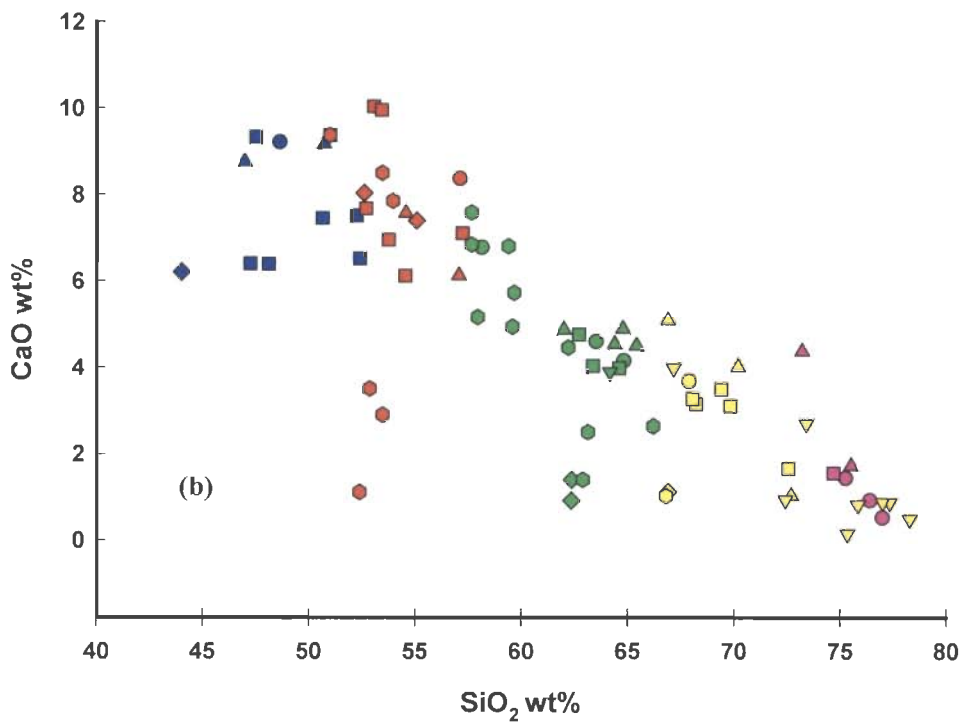
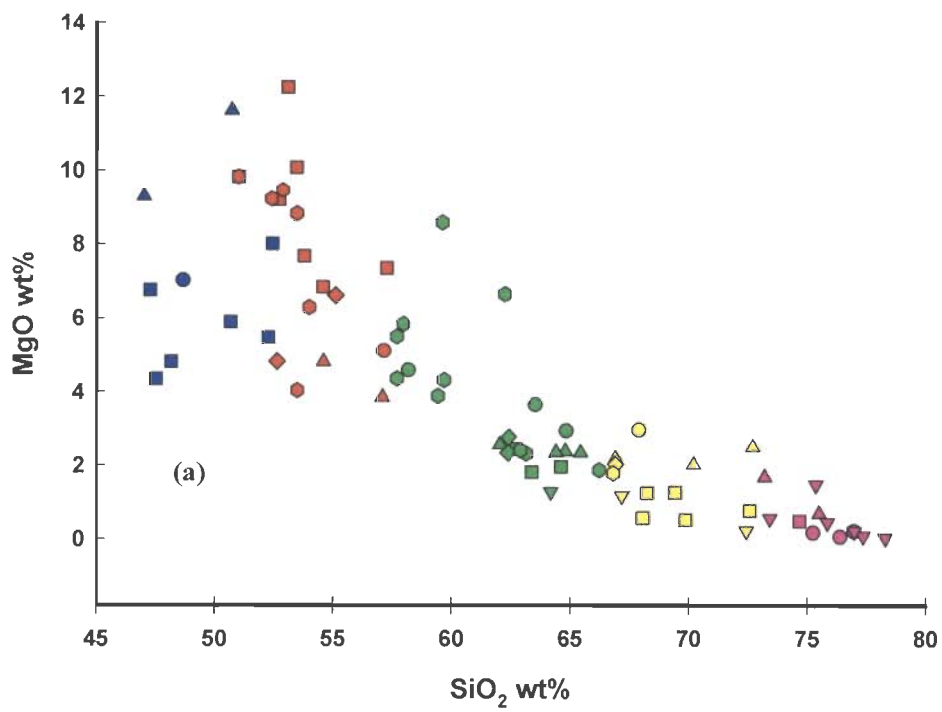


**Figure 5.5** Major element variation diagrams. (a) MgO wt%-SiO<sub>2</sub> wt% (b) CaO wt%- SiO<sub>2</sub> wt%. Symbols as in Table 5.1

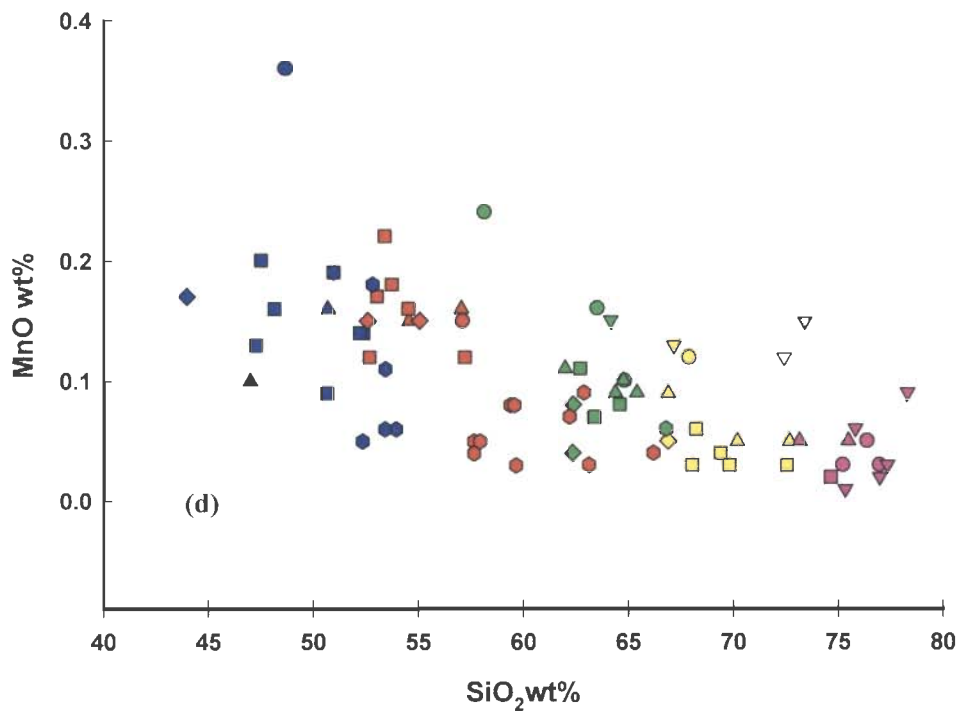
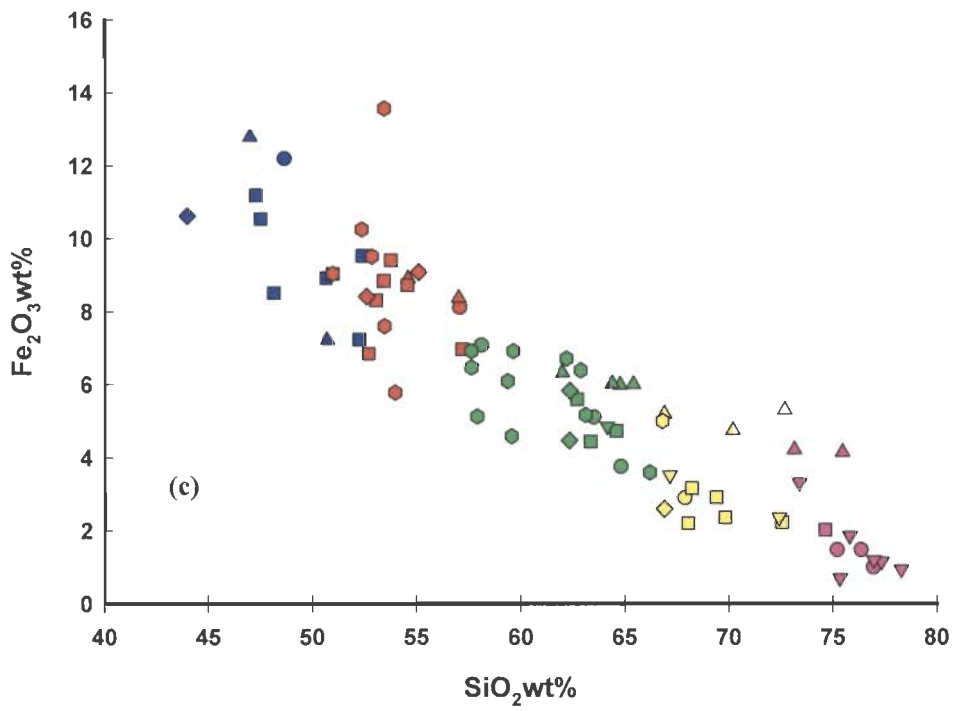


Figure 5.5 Continued. (c)  $\text{Fe}_2\text{O}_3$  wt%- $\text{SiO}_2$  wt% (d)  $\text{MnO}$  wt%- $\text{SiO}_2$  wt%. Symbols as in Table 5.1

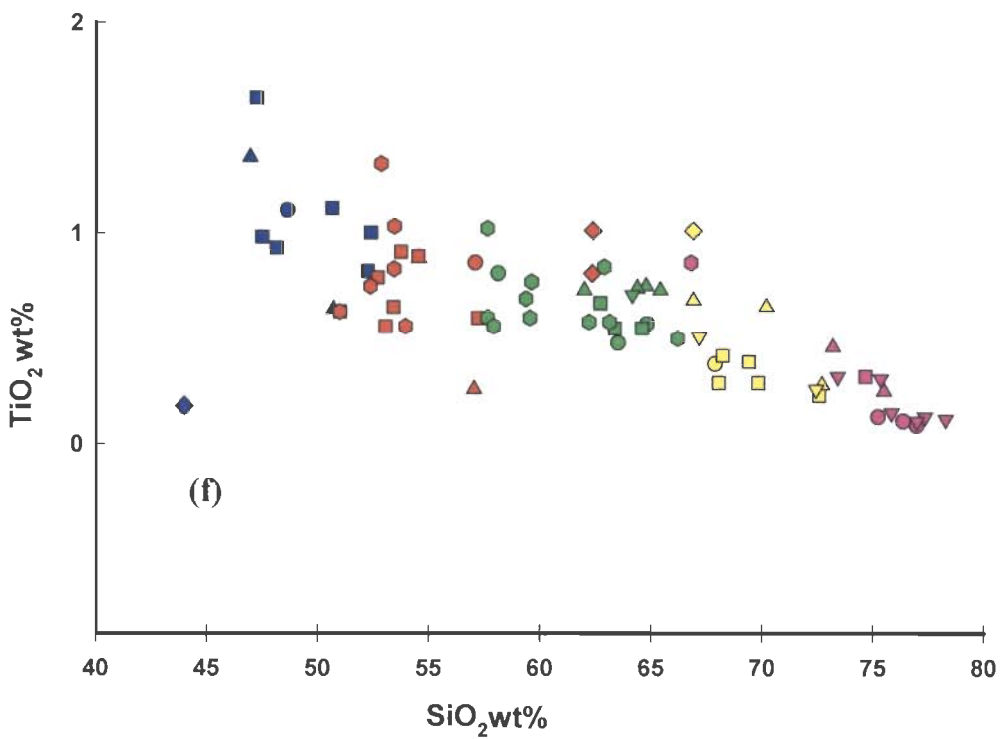
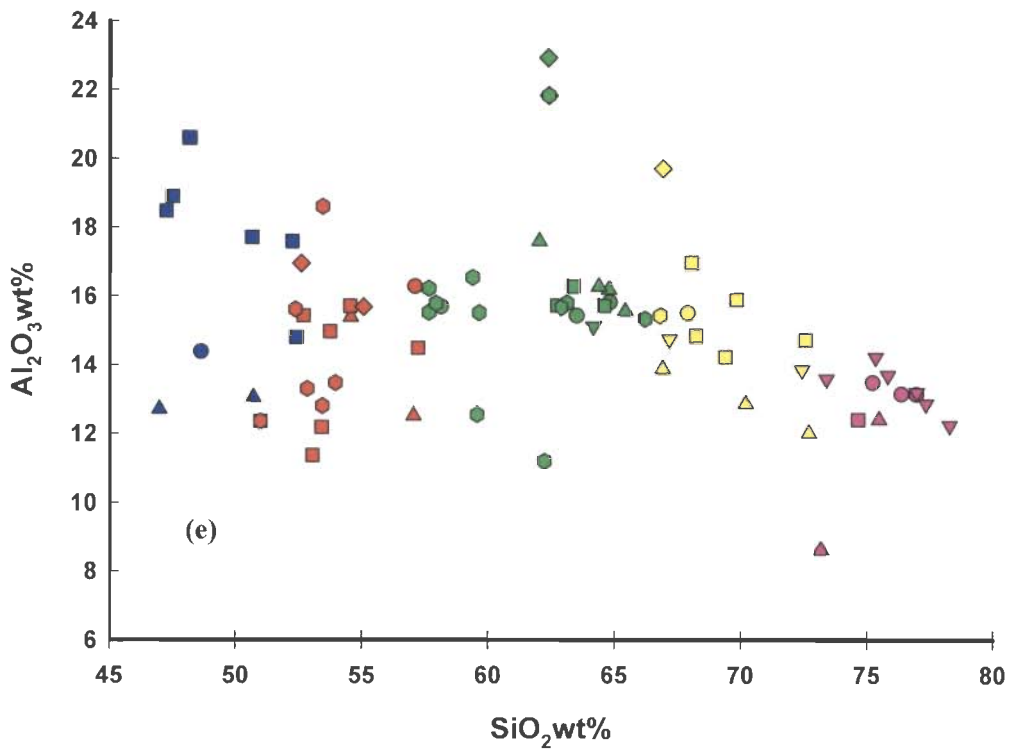


Figure 5.5 Continued. (e)  $\text{Al}_2\text{O}_3$  wt%- $\text{SiO}_2$  wt%. (f)  $\text{TiO}_2$  wt%- $\text{SiO}_2$  wt%. Symbols as in Table 5.1

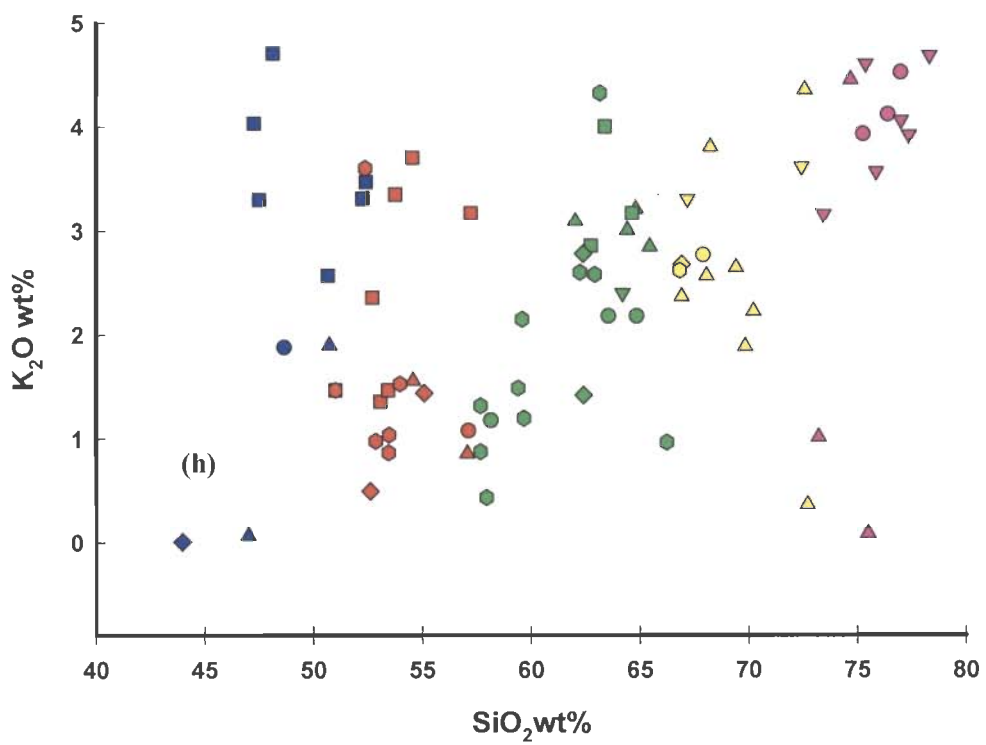
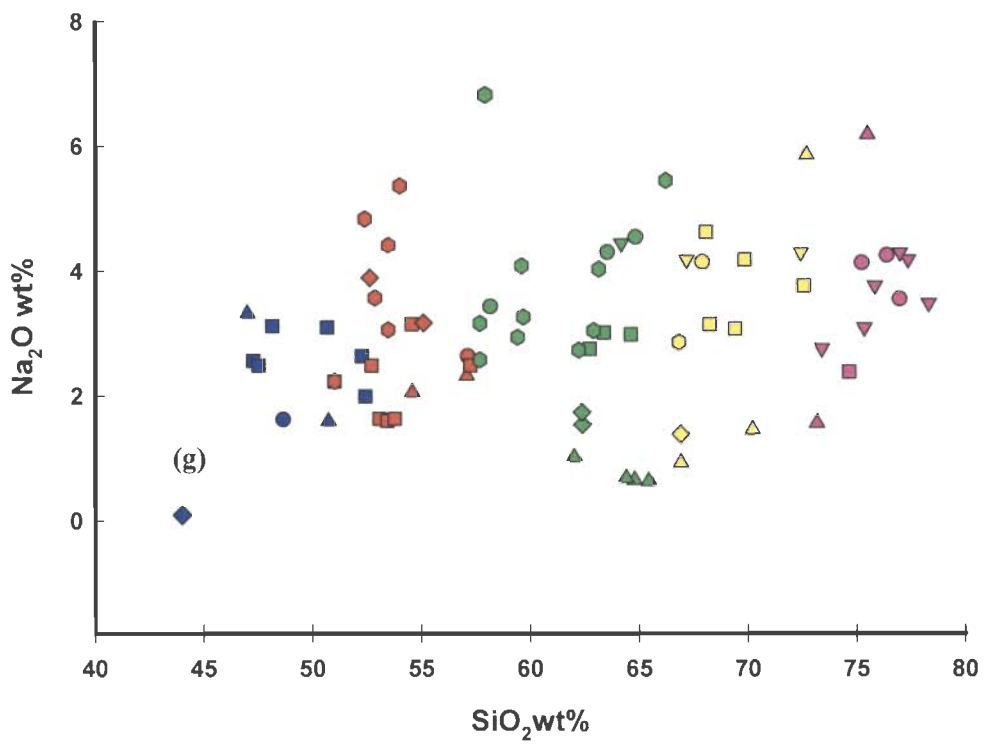
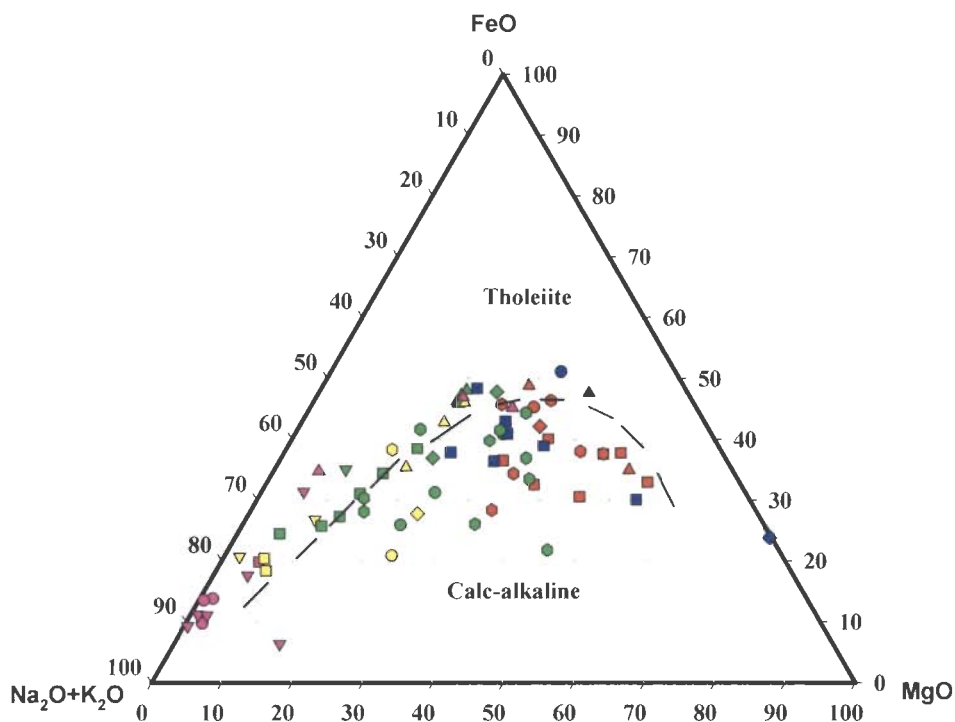
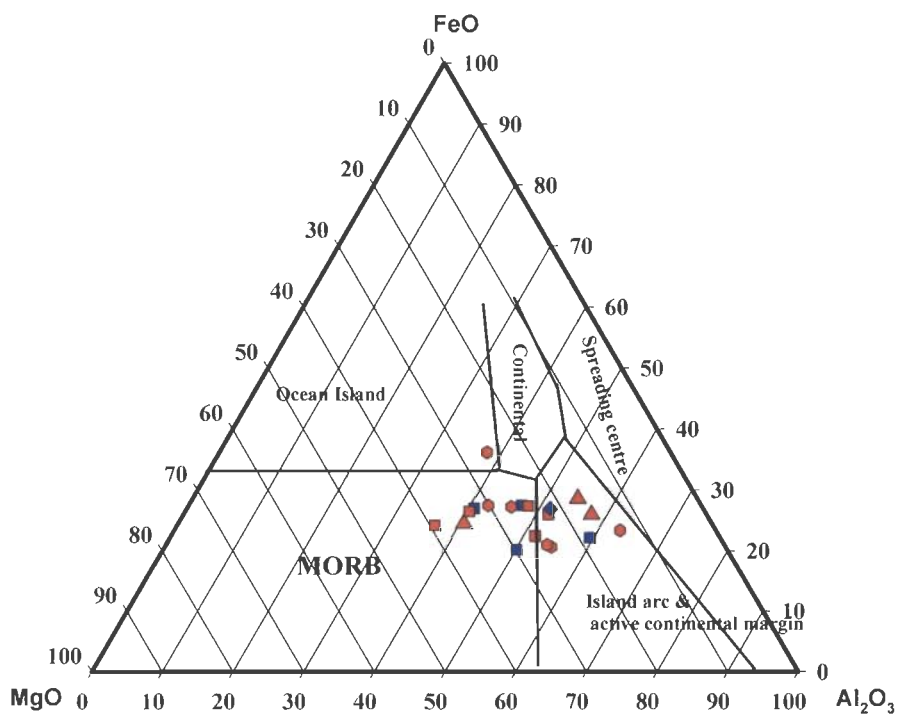


Figure 5.5 Continued. (g)  $\text{Na}_2\text{O}$  wt%- $\text{SiO}_2$  wt% (h)  $\text{K}_2\text{O}$  wt%- $\text{SiO}_2$  wt%.. Symbols as in Table 5.1



**Figure 5.6** AFM diagram distinguishes tholeiitic and calc-alkaline series (Kuno, 1968). Most of the samples plot within the calc-alkaline field. Concentrations are in wt%. Symbols as in Table 5.1



**Figure 5.7**  $\text{Al}_2\text{O}_3$ -FeO-MgO diagram for rocks with silica range 51-56 Wt% (Pearce *et.al.*, 1977). Majority of the samples plot within the field for MORB and island arc and active continental margin. Concentrations are in wt%. Symbols as in Table 5.1



In summary,  $\text{Al}_2\text{O}_3$ ,  $\text{Fe}_2\text{O}_3$ ,  $\text{CaO}$ ,  $\text{MgO}$ ,  $\text{TiO}_2$ ,  $\text{MnO}$  and  $\text{P}_2\text{O}_5$  show negative correlation with  $\text{SiO}_2$ , and alkalis show highly scattered data points (Fig. 5.5). This may indicate fractionation of olivine, pyroxene, feldspars and Fe-Ti oxide phases during the evolution of the magmas. Scattering in  $\text{Na}_2\text{O}$  and  $\text{K}_2\text{O}$  variation diagrams may probably be due to post crystallization alteration or may also be due to the fluid activity in the source area that is commonly expected in most of the arc set up. Major element trends and the triangular diagrams indicate that the rocks have arc affinity and most of the elements preserve their primary magmatic characters.

## 5.2 TRACE ELEMENT CHARACTERISTICS

The trace elements are those elements whose concentrations do not exceed a few thousands parts per million (ppm) by weight in rocks. These elements usually do not form minerals of their own. Trace elements which may be petrogenetic indicators include Rb, Ba, Zr, Y, Nb, REE, Ni, V, and Cr among many others. Different minerals incorporate or exclude different trace elements. For example, olivine selectively incorporates Ni but excludes Rb. The concentration and variation of different trace elements may help us to put constraints on the nature and composition of the mineral assemblages with which the magma may have been in equilibrium. The trace element patterns are also used as a tool to characterize the source for partial melting and to evaluate various igneous processes such as partial melting, magma mixing/contamination, fractional crystallization (McKay, 1989; Green, 1994; Cox *et al.*, 1995).

### 5.2.1 Distribution of trace elements

Distribution of trace element and their geochemical affinities in the common rock forming minerals follows certain crystal-chemical rules. A trace element may substitute

for a major element, if the ionic radii do not differ by more than 15 %. Ions whose charges differ by one unit may substitute for one another provided their radii are similar and the charge difference can be compensated by another substitution (Banno and Matsui, 1973). Two ions that occupy the same position, the one with smaller radius and or higher charge forms the stronger bonds. Even if the size criteria is fulfilled, the substitution is limited if the bonds formed differ in covalent character. If the bond is stronger, ionic substitution is easier. In general, the ionic size, charge and strength of the bond determine the trace element substitution in a mineral. More the similarity in ionic character the more is the probability for a trace element to get into a crystal structure.

Cations with large radii and low electric charges tend to substitute for  $K^+$  ( $1.38 \text{ \AA}^0$ ) and are concentrated in felsic rather than mafic rocks. These are the ions of Rb, Cs, Ba, Pb, etc. and are often called the large ion lithophile elements (LILE). LILE have ionic potential less than  $40 \text{ nm}^{-1}$  (Drake and Weill, 1975). Some cations like U, Th, Pb, Be, Nb, Ta, Zr and Sn with higher radii and higher charges are concentrated at the felsic end of the series not because of substitution but their charge and size make the substitution difficult in early forming minerals. Smaller size and higher charges make the electric field associated with these ions stronger and are often designated as high field strength elements (HFSE). They have the ionic potential higher than  $40 \text{ nm}^{-1}$ . Those LILE and HFSE, which do not fit into the available crystallographic sites in a silicate structure, are described as incompatible elements (Cullers *et al.*, 1973; Krauskopf and Bird, 1995). Those which readily get into the mineral structure are called compatible elements. Elements partitioning between two phases in equilibrium depends on their chemical potential or distribution coefficient ( $K_d$ ). Elements with distribution coefficient (concentration in solid phase/concentration in liquid phase) greater than one are

compatible and less than one are incompatible (Irving, 1978; Hanson, 1980; Wilson, 1989; Wood and Fraser, 1986).

#### **5.2.1.1 Binary plots**

Binary plots have been prepared by using trace and rare earth elements like Ni, La, Nd, Nb and Zr. These elements have different compatibilities with respect to mafic phases in basaltic rocks. In La vs. Nd plot (Fig. 5.8a), Nubra, Shyok and few samples from Tsoltak plot close but slightly above the primitive mantle (P.M.) ratio line (P.M. values after McDonough *et al.*, 1992). Hundar, Khardung and Karakoram samples plot above with higher La/Nd ratios than the primitive mantle ratio line. During the melting of mantle sources, La behaves more incompatibly than Nd. Higher degree of partial melting lowers concentration of La compared to Nd. Hence this plot would probably indicate similar source for all these rocks but Nubra, Shyok and Tsoltak samples represent higher degrees of partial melting than those from Hundar, Khardung and Karakoram or they may have derived from different sources.

There is large variation in Zr/Y ratio with increasing Zr (Fig. 5.8b). Fractionation of olivine and plagioclase can not alter the Zr/Y ratios. It gives restricted Zr/Y ratio with increase of Zr, whereas the fractionation of amphibole and clinopyroxene may raise the ratio with increasing Zr content (Floyd, 1993, Ahmad *et al.*, 1999). As there is change in Zr/Y indicates fractionation of amphibole and clinopyroxene along with olivine and plagioclase. In Ni vs. Ce plot (Fig. 5.8c), mafic and intermediate samples from different rock units have low Ni for the observed concentration of Ce, probably indicates arc affinity for these samples. In general arc rocks have low Ni abundance. In Zr vs. Sr plot (Fig. 5.8d), Sr has large spread compared to Zr. This indicates the mobility of Sr probably due to the fluid activity in the source area or during melting of the source. Post-

crystallization processes or contamination of the source/melt can also mobilize the Sr. Composition of the rocks varies from basaltic andesite to dacite may also attribute this variation.

In Zr vs. Nb (Fig. 5.8e) plot, the majority of the samples plot on Zr side with higher Zr/Nb ratios. This may probably indicate lowering of Nb abundance at a given concentration of Zr, as expected in arc rocks with strong negative Nb anomaly. The Nb anomaly forms due to stability of titanite in the source region. During the generation of arc magma, Nb will stay back in Ti-bearing phases (eg. Rutile, Ilmenite) and thus the melt derived from such source region will have less Nb concentration and shows Nb anomaly in the multi-element pattern. Nb will be always depleted in arcs and therefore arc rocks will have high Zr/Nb ratios. In Zr vs. Nd (Fig. 5.8f) plot the majority of the samples plot on the Nd side and show lower Zr/Nd ratio. During partial melting, Nd behaves more incompatible than Zr and thus the melt will have lower Zr/Nd ratio.

In general, different litho-tectonic units from SSZ may have been derived from same source by varying degrees of partial melting followed by fractional crystallization or they may have derived from different sources. Petrogenetic modelling of different litho-tectonic units are given in chapter 6.

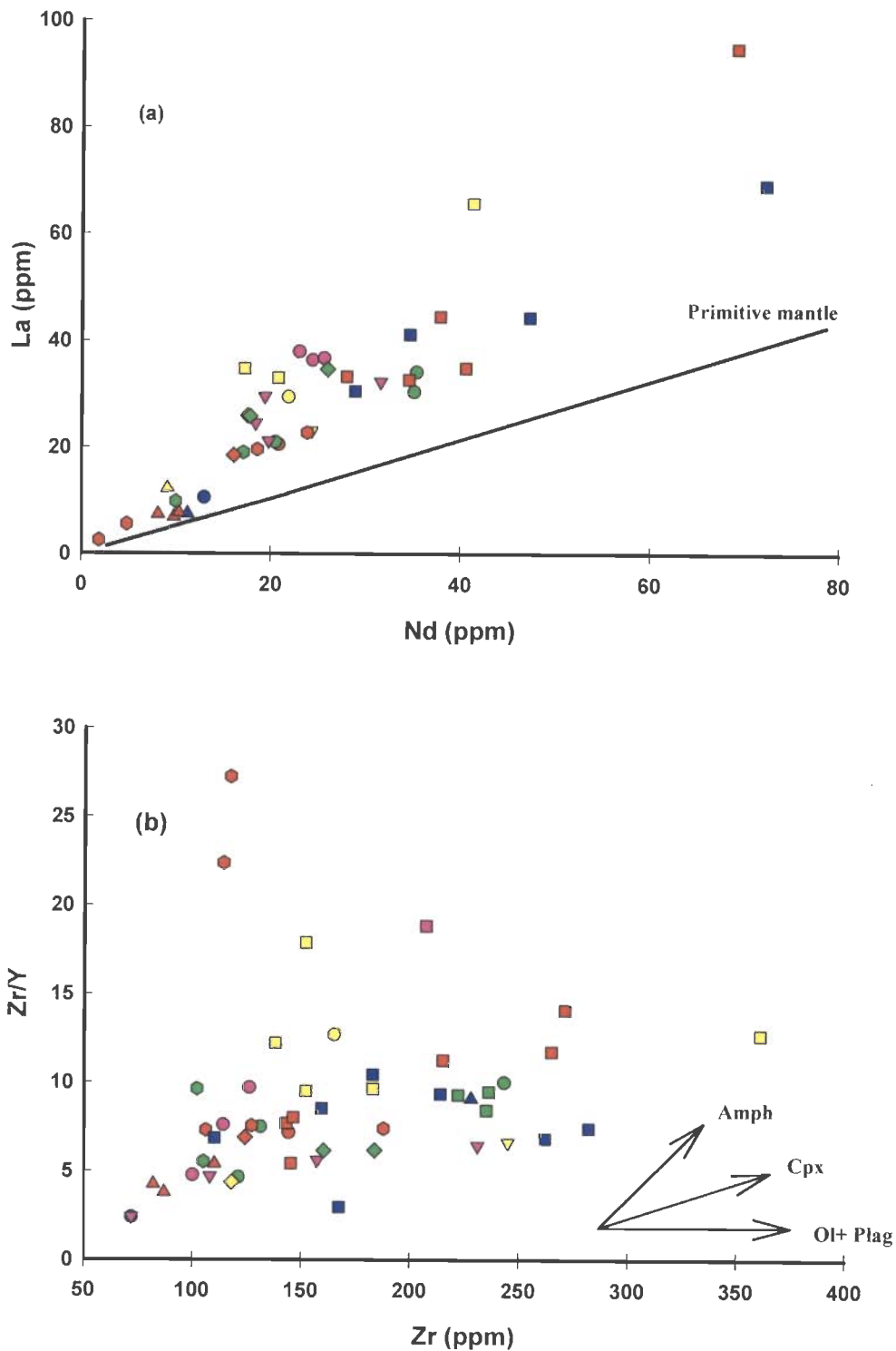
#### **5.2.1.2 Multi-element plots**

Multi-element patterns (Fig. 5.9) of SSZ display enrichment of large ion lithophile elements (LILE) and depletion of high field strength elements (HFSE) with negative Nb, P, Ti, Sr and Eu anomalies. Strontium anomaly indicates the fractionation of feldspar and Ti anomaly indicates the fractionation of titano-magnetite rather than sphene. Sphene fractionation gives rise to the depletion of Y which is not observed in these samples. Presence of Nb, P, and Ti negative anomalies are the indication of subduction

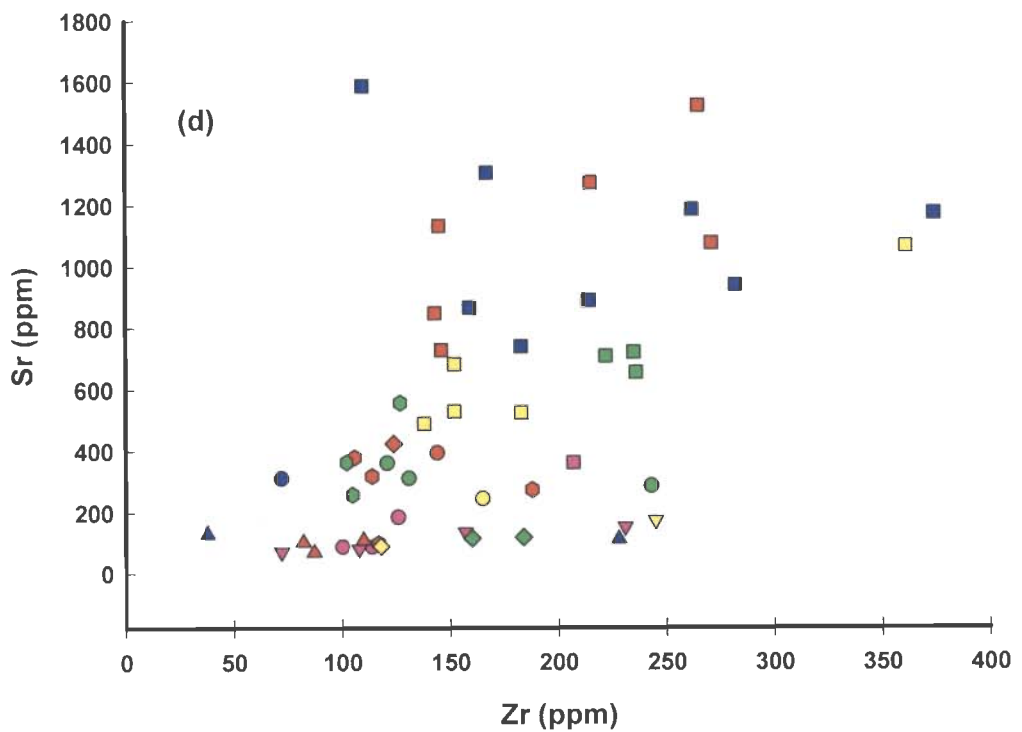
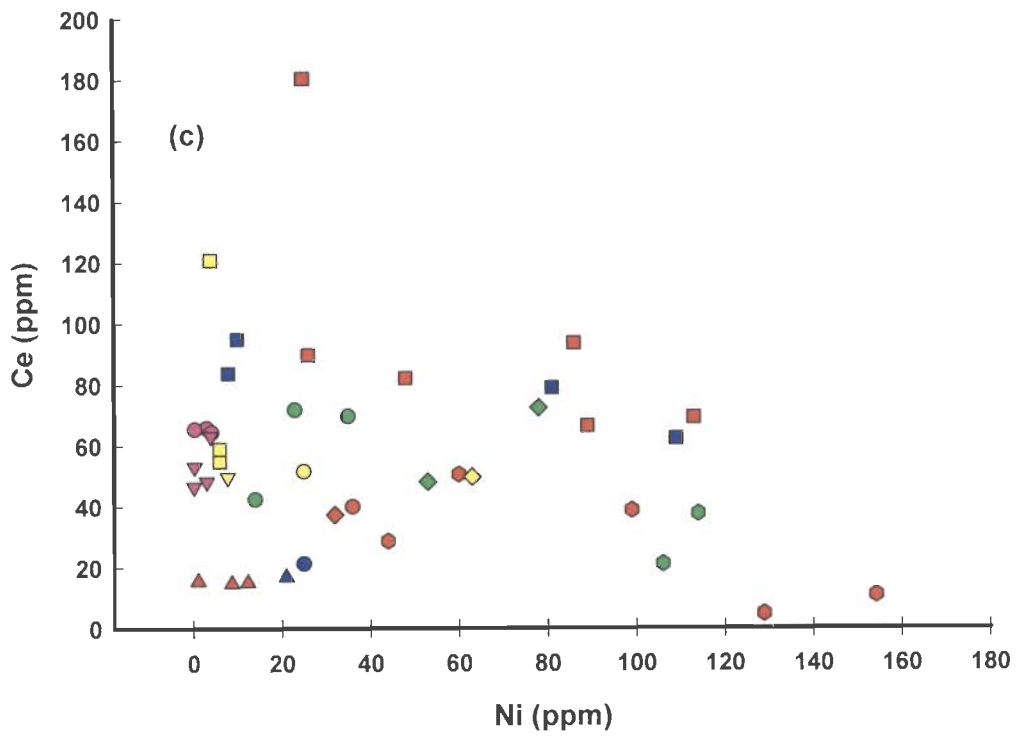
environment and involvement of crustal material. Multi-variate plots and P.M. normalized (P.M values of McDonough *et al.*, 1992) “spidergrams” are used to study the element mobility and also in petrogenetic modelling.

Fig. 5.9 represents the multi-element “spidergrams” of samples from Hundar, Khardung, Shyok, Nubra, Tsoltak and Karakoram area respectively. The samples show calc-alkaline trend with Nb, Sr, P and Ti anomaly, especially in Hundar, Khardung and Karakoram samples. Shyok, volcanics show less enrichment of LILE compared to other litho-tectonic units. Trace elements analytical data are given in appendix 3. Among all the samples from Hundar igneous suite, maximum differentiation is displayed by granite samples. These samples display strong P and Ti anomaly. Almost all the samples follow same trend but with variation in LILE enrichment factor. Mafic dyke sample does not follow the trend and is less differentiated.

Khardung samples also follow the trend of Hundar samples but exhibit strong Sr anomaly compared to Hundar. In Khardung volcanics unit, almost all samples show similar enrichment for LILE except for P and Ti. Shyok volcanics are less differentiated compared to above described groups. Enrichment is less than 10 times compared to these groups. LILE-HFSE of some of the Nubra volcanics are also less differentiated, but LILE enrichment is about 10 times higher than Shyok volcanics. Tsoltak volcanics follow similar trend except NST-71. NST-69 (ultramafic) is less enriched, possibly derived from higher degree of partial melting of mantle source. There is a possibility that the other samples may also have been derived from the same mantle source with more differentiation and enrichment due to the influx of aqueous fluid. LILE-HFSE of Karakoram samples (granodiorites, basaltic andesites, andesites and basalt) are highly differentiated. Most of the samples exhibit strong Nb, P and Ti anomalies.



**Figure 5.8** (a) Large variation in La and Nd indicates varying degrees of partial melting. All the samples plot above the Primitive Mantle line (P.M.) indicating that these rocks are derived from enriched mantle source compared to P.M. (b) Positive relationship of Zr vs. Zr/Y can not be explained by fractionation of olivine and plagioclase alone (inset figure, see the text). Hence the plot indicates fractionation of amphibole and clinopyroxene. Symbols as in Table 5.1.



**Figure 5.8** Continued. (c) Ni vs. Ce plot of basic to intermediate samples shows low Ni (2-150 ppm) for the observed concentration of Ce (20-170 ppm) indicates are affinity. (d) Sr shows large spread (100-1600 ppm) compared to Zr which indicates mobility of Sr. Symbols as in Table 5.1.

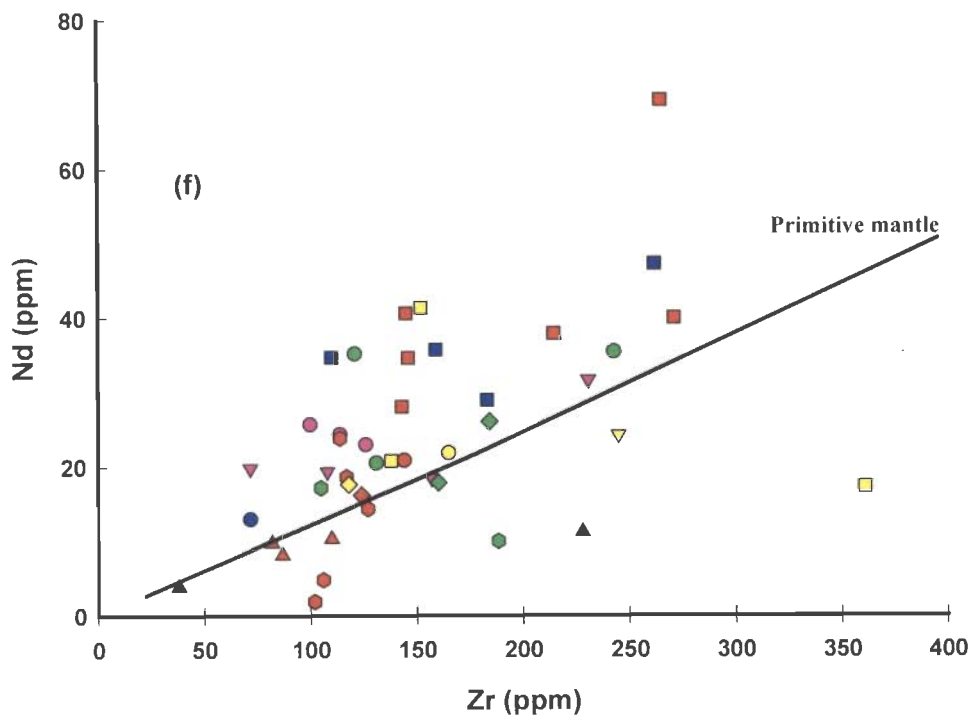
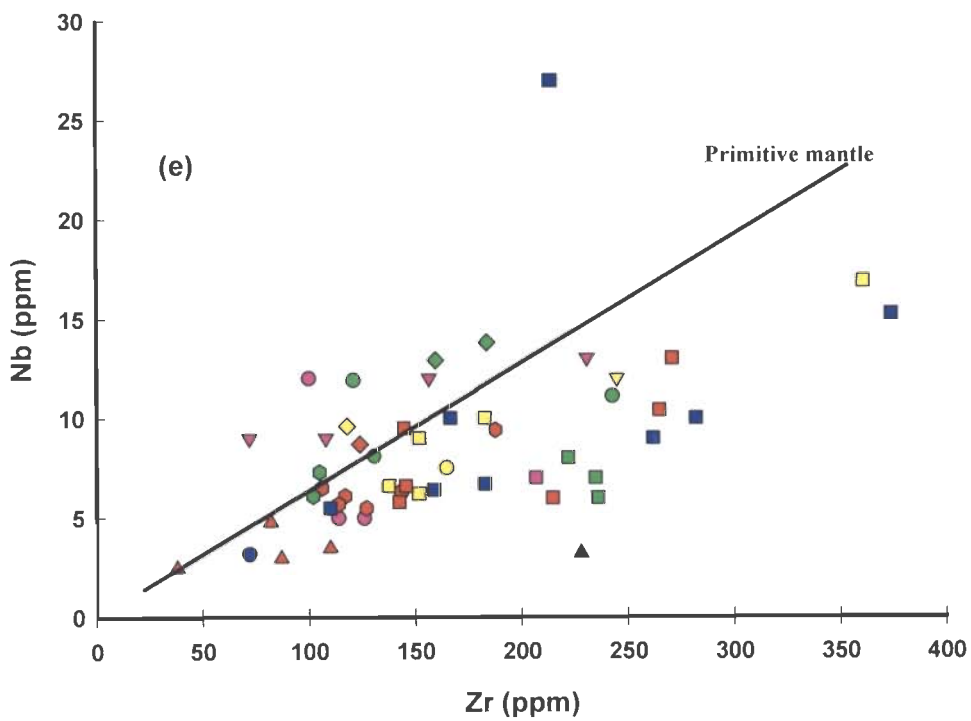


**Figure 5.8** Continued. (e) Majority of the samples plot on Zr side with higher Zr/Nb ratios indicates lower Nb abundance as expected in arc rocks due to the stability of titanite in the source. (f) Zr vs. Nd plot shows majority of the samples plot on the Nd side with lower Zr/Nd ratio indicates neither of these elements controlled by the residual mineralogy. Symbols as in Table 5.1.



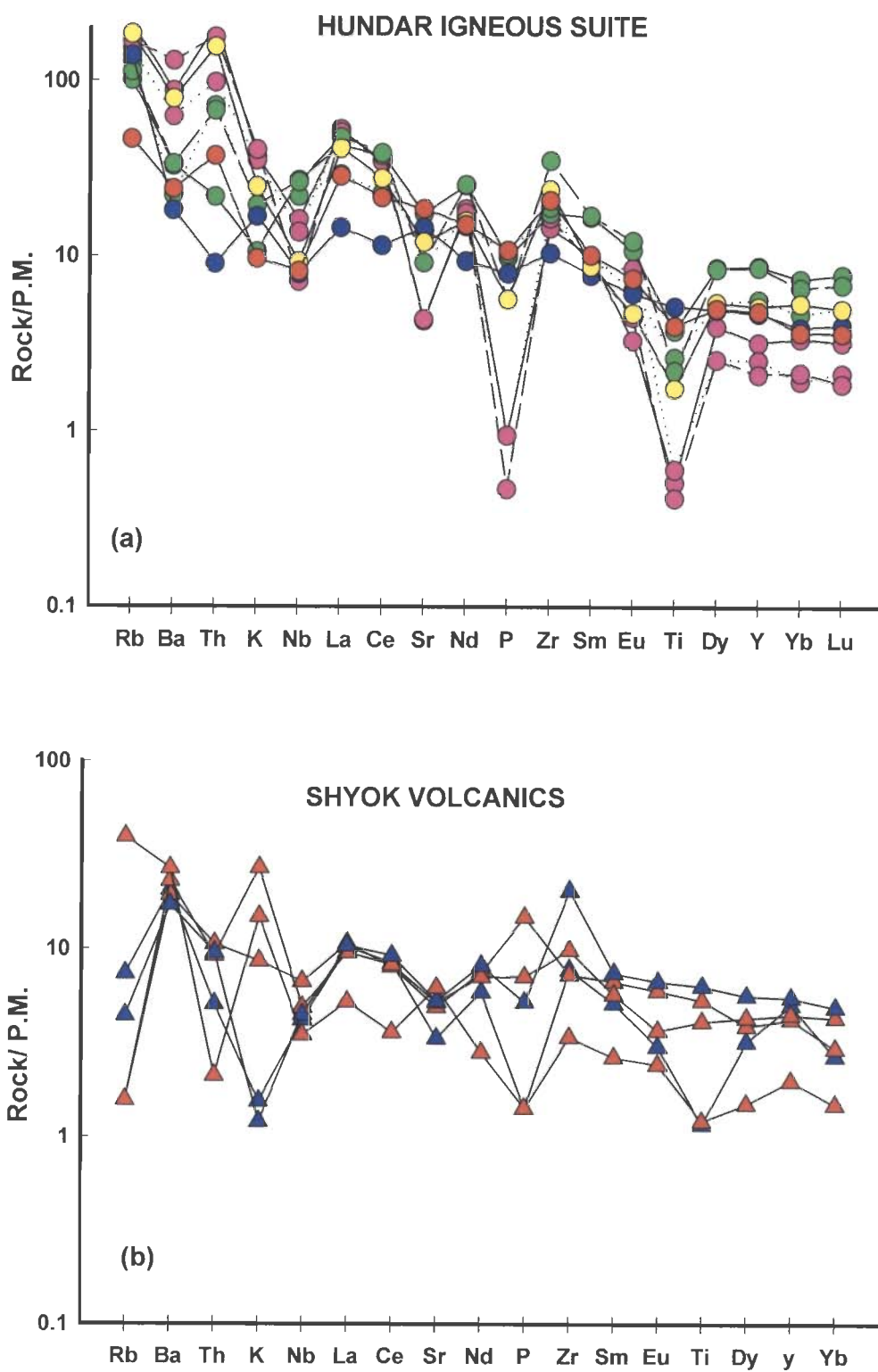


**Figure 5.9** Primitive Mantle (P.M.) normalized multi-element spidergrams (a) Hundar igneous suite samples show Nb, Sr, P and Ti anomalies. Granite samples display strong anomalies especially for P and Ti. (b) Shyok volcanics are ~10 times enriched and show negative Nb, P, and Ti anomalies as expected in arc basalts. Symbols as in Table 5.1.

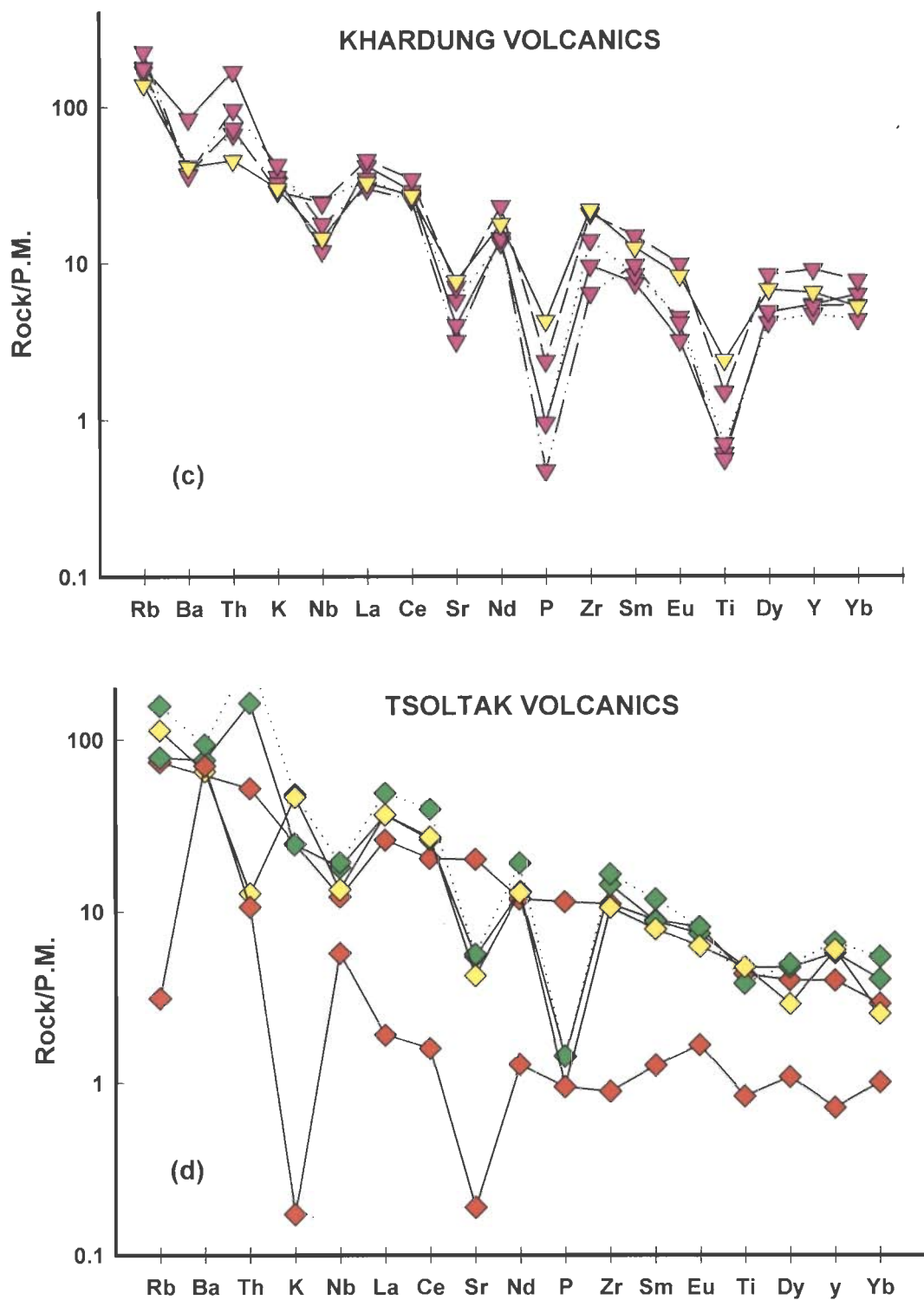


**Figure 5.9** Continued. (c) Khardung volcanics show strong Nb, Sr, P, and Ti anomalies. (d) Tsoltak volcanics also display similar trend of multi-element pattern shown by other litho-tectonic units except two samples. NST-71, basaltic andesite shows lower abundance compared to other samples. Symbols as in Table 5.1.

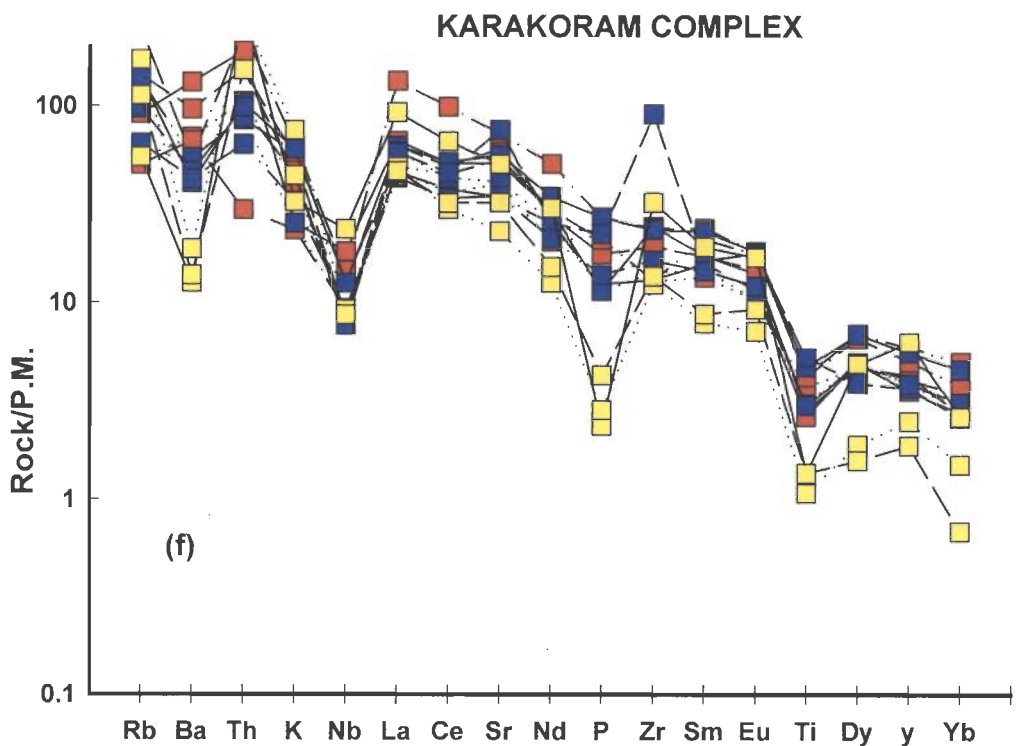
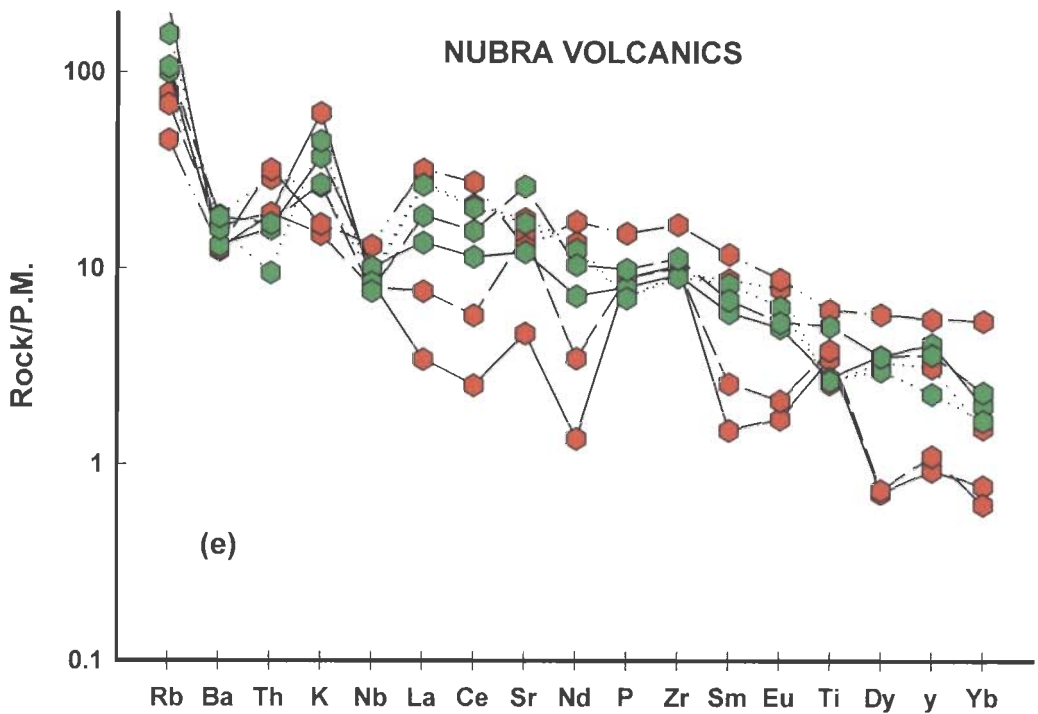


**Figure 5.9** Continued. (e) Multi-elements pattern of Nubra volcanics show highly differentiated. (f) Karakoram samples are also highly differentiated. They show Nb, P and Ti anomalies similar to other litho-tectonic units. Symbols as in Table 5.1.

### 5.2.2 Rare Earth Element abundances

The REE are particularly useful in petrogenetic study because they are less mobile and geochemically very similar. Except for Eu and Ce the REE are trivalent under most geologic condition. The REEs are a group of fifteen elements with atomic numbers from 57 (La) to 71 (Lu). REEs with lower atomic numbers are generally referred to as the light REE (LREE); those with higher atomic numbers are the heavy REE (HREE). The REE include those elements that have two electrons in the 6s energy level and one electron in the 5d level; with increasing atomic number additional electrons are added to the 4f energy level. As the 4f level fills the ionic radii are systematically reduced (from La to Lu) as a result of 'Lanthanide contraction' (Mc Kay, 1986; Cox *et al.*, 1989).

A given REE has geochemical characters very similar to those of the nearest atomic neighbor, but differing systematically from those of the REE with greater or smaller atomic numbers. The REE have greater abundance in minerals with cation radius of about 0.9 to 1 Å<sup>0</sup>. High oxidation state and ionic radii make REE group incompatible in common minerals. Hence the REEs by and large remain in liquid during fractional crystallization. Slight difference in ionic size makes the LREE somewhat more incompatible than HREE. During crystallization of magma the LREEs concentrate more in the residual fluid and during melting in the earliest melt than the HREEs. This small difference makes the REE a useful tool in the studies of the source and magmatic processes responsible for the emplacement of various igneous rocks (Hanson and Langmuir, 1978; Hanson, 1980).

Analytical result of REE is displayed as chondrite normalized data. For the purpose of plotting, the analyzed concentrations of the element in the rocks are divided by average concentrations of the elements in chondrite. This has the effect of smoothing out the saw tooth distribution. Smooth pattern shown by normalized data can be easily

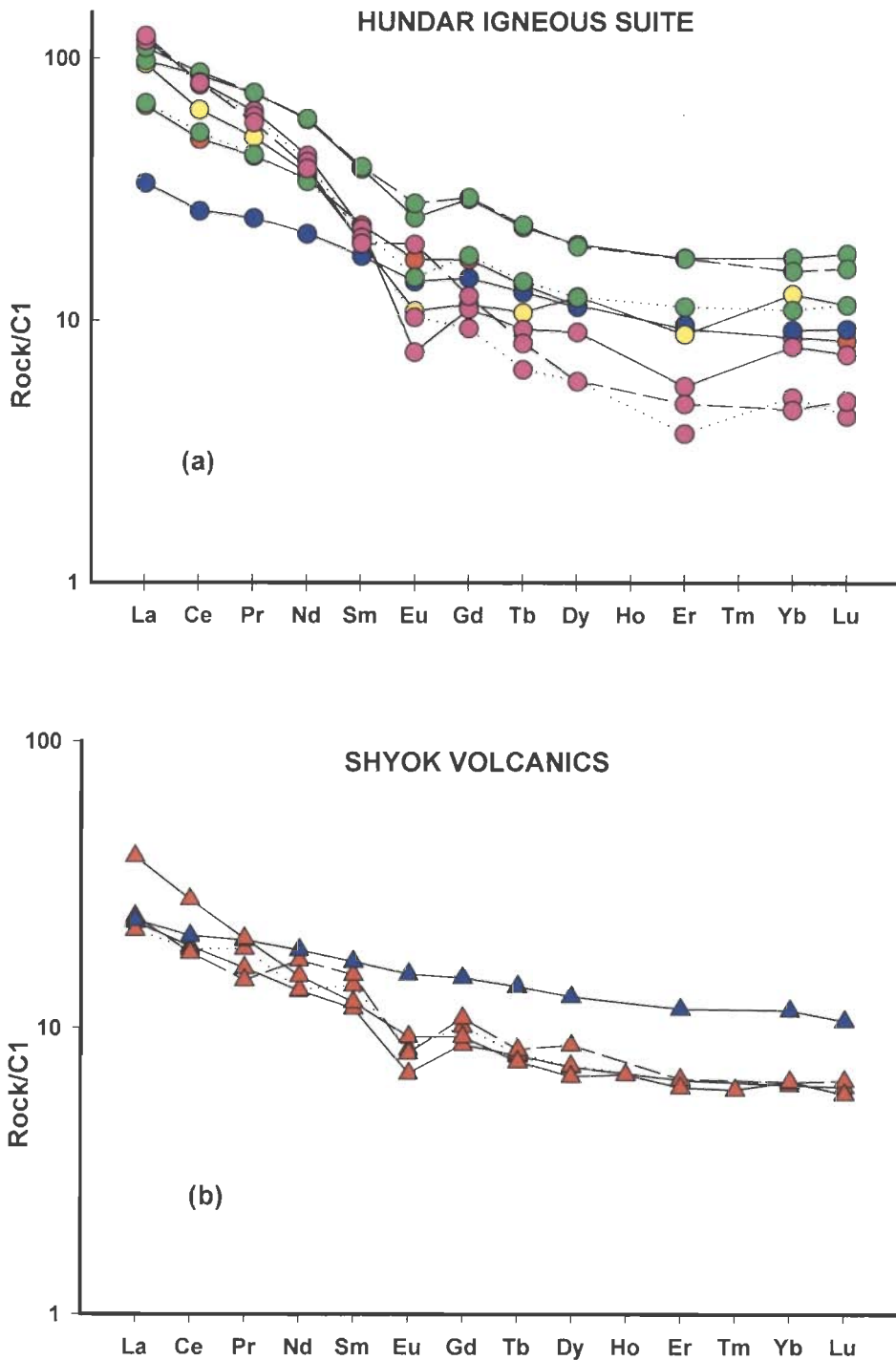
interpreted. Chondrites have been used because they are primitive solar material which may have been the same parental material of the earth. Though the REEs are trivalent ions, Eu and Ce show additional stable oxidation state as  $2^+$  and  $4^+$  respectively. The divalent Eu ion readily substitutes for  $\text{Ca}^{2+}$  and  $\text{Sr}^{2+}$ . When plagioclase crystallizes from a mafic melt it removes the Eu from the liquid (Goldschmidt, 1937; Drake and Weill, 1975).

Fig. 5.10 shows REE patterns from Hundar, Khardung, Shyok, Nubra, Tsoltak and Karakoram areas. Chondrite normalized REE plots exhibit enrichment of light REE and fractionation of middle and heavy rare earth elements. Shyok volcanics exhibits slightly less enriched pattern for LILE without large variation from Gd to Lu. The rocks with an unusual abundance of LILE and LREE are considered as the product of extreme differentiation as either final residual liquid or initial melt during melting. It is also influenced by the presence or absence of water during melting and contamination of crustal material. The concentration of trace elements and REE are used in working out the details of rock history. Mineral composition of the starting material and the extent of melting are important factor which influences the melt chemistry. Detailed petrogenetic modelling of different litho-tectonic units and the source characterization is given in next chapter. Rare earth element data are given in appendix 4. The enrichment factor of each group is given in Table 5.2.

Hundar granites are more HREE differentiated as compared to the andesite. Basaltic andesite as the LREE enrichment more than 10 times that of the HREE. Khardung volcanics also have LREE/HREE ratio of  $\sim 10$  with Eu negative anomaly. Eu negative anomaly indicates the fractionation of feldspar. The LREE enrichment is about ten times compared to HREEs. Although these samples have different extent of differentiation they have similar REE patterns. It is possible that they may have originated

by different extent of partial melting of the same source. HREE depleted pattern indicates the possibility of amphibole fractionation. In the case of Shyok volcanics REEs show comparatively less enriched pattern with considerably less differentiation. Nubra volcanics show Eu positive anomaly which indicates the presence of plagioclase feldspar. Petrographic study also confirms the presence of feldspar in the rocks. Tsoltak volcanics also show similar pattern with Eu positive anomaly. NST-69 (ultramafic) sample may represent a primary magma derived from the mantle with approximately 5 times enrichment compared to the mantle. It also shows Eu positive anomaly, which indicates alteration. Karakoram granitoids are highly fractionated samples. La/Yb ratio is ~70 in these samples. The fractionated pattern indicates possibility of garnet as a fractionated phase which removes considerable amount of HREE.

Geochemical studies of the samples from different litho-tectonic units of SSZ indicate that majority of rocks show calc-alkaline characteristics and have arc affinity. LILEs and LREEs are enriched in most of the samples. The samples may have been derived from same source by different extent of partial melting and fractionation of different mineral phases. Fluid interaction at the source region during melting or during the transport of magma is suspected for changing the geochemical signature of the rock units. Contamination of the melt due to sediment input or due to incorporation of crustal rocks is also considered as responsible for the geochemical characteristics of the rocks from SSZ. Detailed petrogenetic modelling for each litho-tectonic unit is attempted to understand these possibilities (see chapter 6).



**Figure 5.10** Chondrite normalized REE patterns for different litho-tectonic units (a) Among Hundar samples granites display more LREE enrichment, more than 10 times compared to HREEs. Basaltic dyke shows less differentiation. Most of the samples show Eu negative anomaly except for one granite sample. (b) Shyok volcanics also follow similar pattern as Hundar samples. Enrichment of LREEs is comparatively less (~20-30 times to C1). Except for basaltic dyke other samples display Eu negative anomaly. Symbols as in Table 5.1.

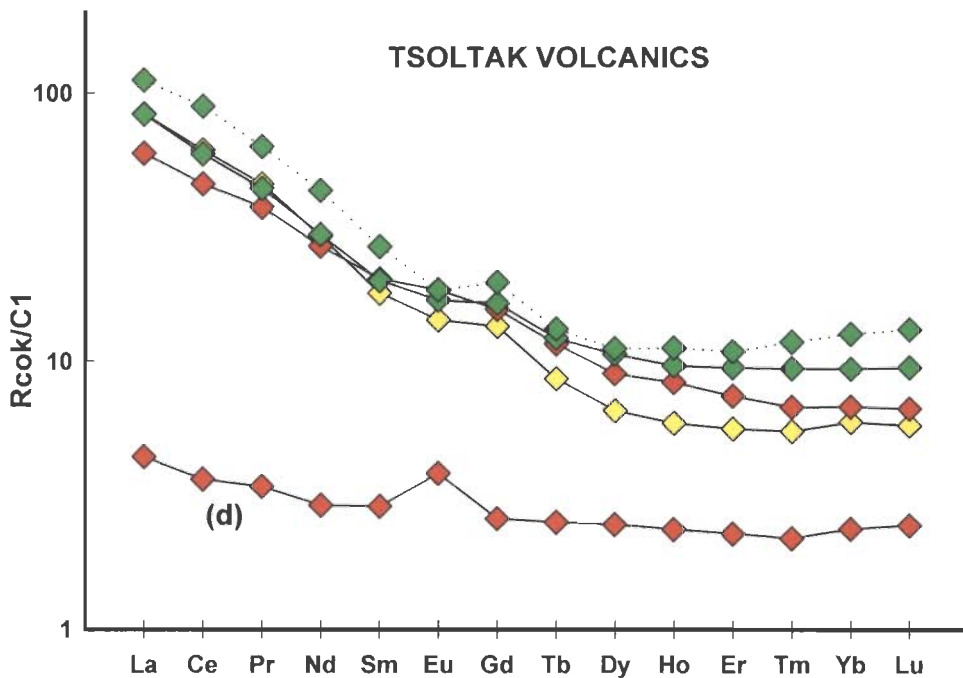
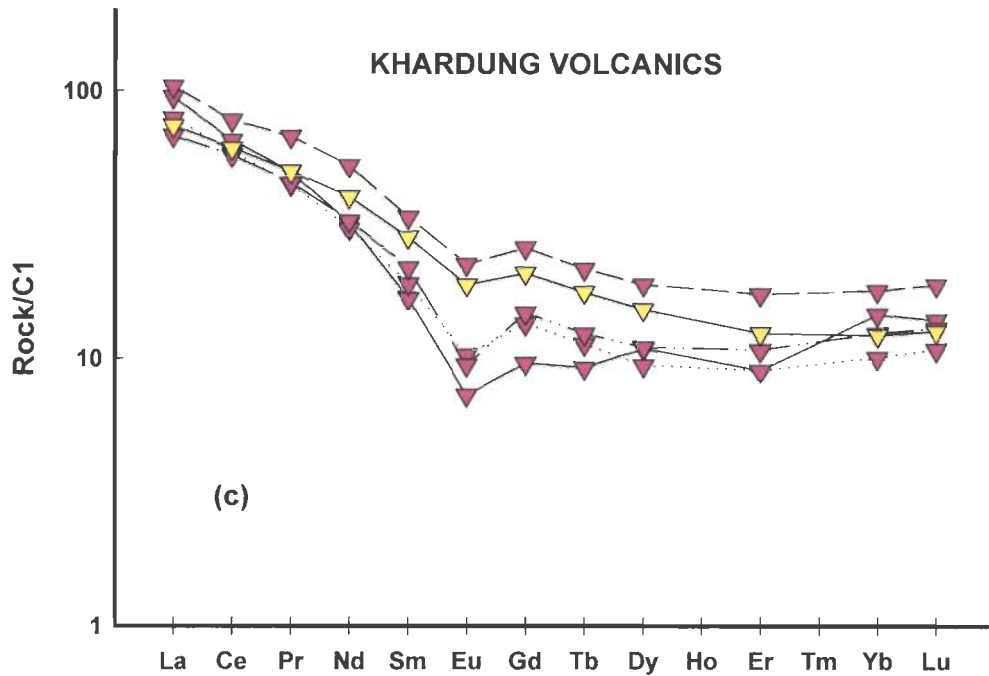


**Figure 5.10** Continued. (c) Khardung volcanics have similar REE pattern with Hundar igneous suite and Shyok volcanics. They also have LREE /HREE ratio of ~10 with Eu negative anomaly with similar REE patterns. (d) Tsoltak volcanics also have LREE enrichment.. Samples show Eu positive anomaly indicates presence of plagioclase feldspar. Ultramafic sample has very less enrichment of REEs. Eu anomaly may indicate alteration. Symbols as in Table 5.1.



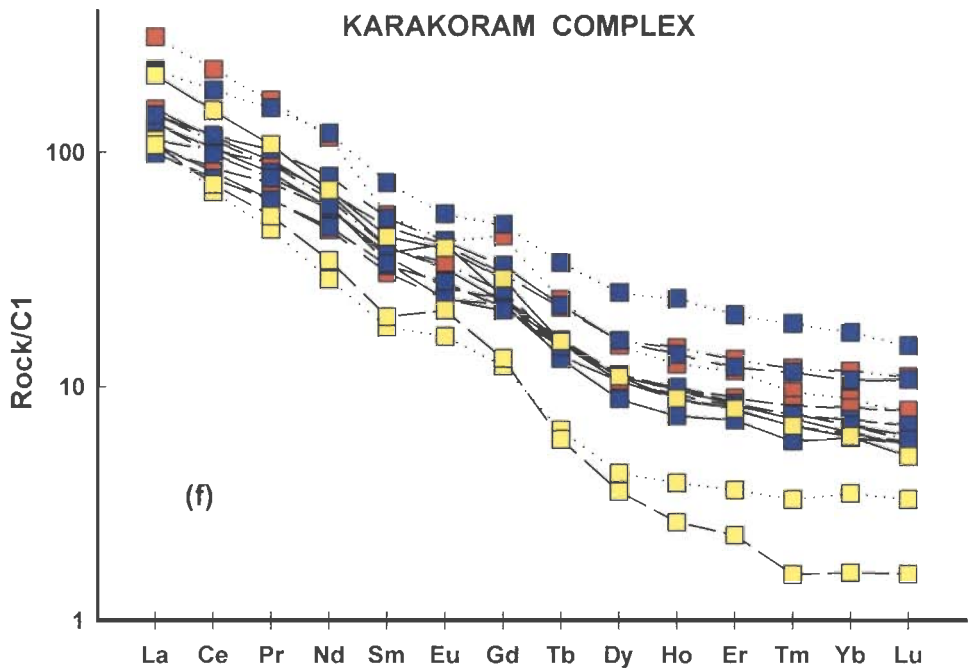
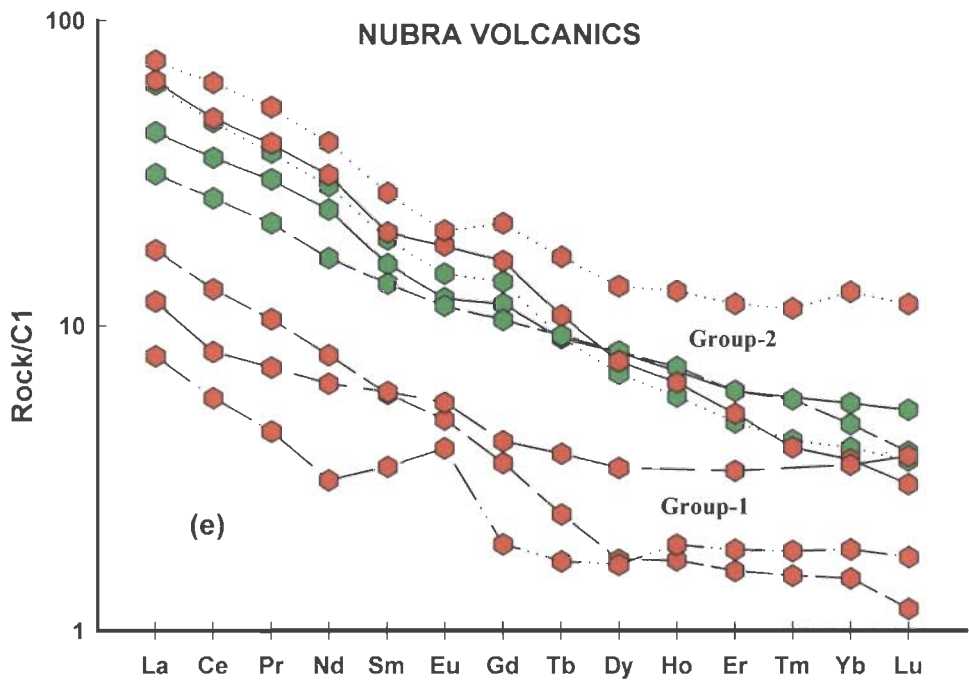


**Figure 5.10** Continued. (e) Nubra volcanics show two groups. One group has LREE/HREE ratio  $\sim 10$  and another group has the LREE enrichment more than 10 times compared to HREE. Group-2 shows similar pattern as Tsoltak volcanics with similar LREE/HREE differentiation. (f) Granodiorites of Karakoram complex are highly differentiated samples. LREE enrichment is up to  $\sim 20$  times in these samples. These samples also show Eu positive anomaly. Symbols as in Table 5.1.

**Table 5.2.** REE data showing relative enrichment of LREE and HREE

		$\Sigma$ LREE	$\Sigma$ HREE	(La/Sm)N	(Dy/Yb)N	(La/Yb)N
<b>Hundar igneous suite</b>	HST-18	140.67	9.33	5.243842	1.134898	14.80804
	HST-3	137.11	6.63	5.613379	1.152551	22.88478
	HST-9	138.45	7.65	6.165166	1.284614	26.63767
	HST-12	113.59	12.37	4.751613	0.980978	7.523387
	HST-6	92.23	12.83	2.853557	1.326825	7.654518
	HST-17	52.17	12.29	1.890722	1.227513	3.64344
	HST-15	153.25	22.79	2.578015	1.12827	5.647996
	HST-10	94.43	14.28	3.02137	1.120348	6.152749
<b>Khardung volcanics</b>	HST-7	159.71	22.3	2.83647	1.242044	7.093598
	KST- 5	111.86	11.89	5.623167	0.746323	6.478407
	KST-4	110.07	16.77	2.613425	1.247428	6.083543
	KST-3	101.1	11.47	4.116387	0.933801	7.804108
	KST-2	143.52	21.93	3.062619	1.051938	5.77267
	KST-1	98.01	13.3	3.09262	0.885319	5.473625
<b>Shyok volcanics</b>	HST-29	35.66	7.9	2.002971	1.155538	3.708065
	HST-22	42.4	13.83	1.402495	1.116938	2.073145
	HST-21	37.23	10.21	1.684023	0.968988	2.172756
	HST-27	38.46	10.46	1.604243	1.275755	3.533704
	HST-32	16.7	3.91	1.983051	0.978048	3.435616
<b>Nubra volcanics</b>	HST-38	63.9	8.71	2.707485	1.471595	7.729978
	NST-1	10.53	1.93	2.305516	0.893523	4.313088
	NST- 7	86.89	9.08	3.14821	2.101134	17.42688
	NST-17	23.69	2.25	2.959643	1.151573	11.9006
	NST- 20	82.97	8.20	3.221233	1.751467	15.49669
	NST -27	110.05	16.19	2.711905	1.045721	5.721093
	NST-15	46.89	8.16	2.283276	1.734127	6.597563
<b>Karakoram complex</b>	HST-43	201.61	13.51	3.833752	1.742236	23.81982
	HST-40	173.55	13.1	3.968848	1.650096	19.65132
	NST- 41	142.83	13.15	3.501824	1.544555	15.72409
	NST- 44	192.82	13.81	3.666768	1.68244	22.78456
	NST-31A	211.97	19.62	2.728457	1.476968	13.48052
	NST-31B	180.45	19.35	2.345028	1.359441	9.722463
	NST -28	179.42	12.68	3.568746	1.456559	21.86815
	NST- 29	154.09	14.27	2.940742	1.396305	13.0468
	NST -35	378.13	21.69	5.663619	1.690531	34.64573
	NST -42	137.71	13.36	2.989864	1.536835	13.69767
	NST -43	117.09	6.45	6.243748	1.222664	32.02281
	NST -45	124.56	5.70	5.358537	2.228145	66.46743
	NST- 40	252.33	14.82	4.862701	1.801952	34.67613
<b>Tsolatak volcanics</b>	NST- 64	103.26	8.63	4.64117	1.104252	14.08207
	NST- 67	102.17	12.52	4.149877	1.135043	8.870696
	NST- 68	147.08	14.67	4.156561	0.881211	8.822377
	NST- 69	7.28	2.64	1.524927	1.039554	1.844876
	NST- 71	81.77	10.69	2.933053	1.32791	8.803055

## **Chapter 6**

# **PETROGENETIC MODELLING**

Quantitative petrogenetic modelling using the trace element distribution coefficient in ( $K_d$ ) mineral melt system is used to decipher the degrees of partial melting, fractional crystallization and finger printing the source characteristics of rocks. The processes of petrogenetic modelling using major and trace elements is very complex. The rock suite of interest can be derived from a magma which could have formed by partial melting of a source rock followed by fractional crystallization and/or AFC (assimilation fractionation crystallization) and/or other petrogenetic processes such as magma mixing and post-crystallization alteration. The quantitative modelling is difficult because the mineral-melt of many trace elements vary with composition, temperature, pressure, presence of fluid and the oxygen fugacity during melting and crystallization. Therefore, least mobile trace elements, including REEs are used for the geochemical modelling. The REEs are relatively less mobile even under granulite grade of metamorphism (Balakrishnan and Rajamani, 1987). However, LREE are shown to be mobile by many other workers particularly under hydrous conditions (*e.g.*, Geen and Watson, 1982). There are several magmatic processes that are responsible for the diversification of magma. Fractional crystallization and partial melting are considered as the most common processes and an attempt has been made in this study to quantify the extent of these processes using trace element modelling.

If the minerals undergo melting in the same proportions as in the original source it is called modal melting. This type of melting occurs very rarely and in general the rocks undergo non-modal melting. The behavior of trace element during non-modal partial melting processes is usually described by equilibrium batch melting and fractional melting (incremental batch melting) equations. During equilibrium melting, the melt

remains at the site of melting and is in chemical equilibrium with the solid residue until the mechanical condition allows it to escape as a single batch of primary magma. However, in fractional melting small fraction of melt is removed continuously and completely. Batch melting equation can be written as:

$$C_L/C_0 = 1/F + D - FD$$

where,  $C_L$  = concentration of element in the melt produced by partial melting

$C_0$  = concentration of element in the original unmelted source,

$F$  = fraction of the melt produced by partial melting

$D$  = bulk distribution coefficient

Trace element behavior during magmatic evolution undergoing crystal fractionation can be described by the fractional (Rayleigh) crystallization equation as follows:

$$C_L/C_0 = F^{(D-1)}$$

where,  $C_L$  = concentration of element in the remaining melt

$C_0$  = concentration of element in the parent melt

$F$  = fraction of the melt remaining,

$D$  = bulk distribution coefficient of fractionating assemblages

Comparison of the trace element behavior produced by varying degree of partial melting and fractional crystallization of an assumed source with composition of the samples from SSZ emphasis petrogenetic processes that resulted in the formation of different lithological units in the SSZ.

## 6.1 MINERAL COMPOSITION AND MELT CHEMISTRY

When a mineral is added or removed from a basaltic melt there will be a net change in the bulk composition of the melt. Olivine has least effect on the enrichment of the REEs, while garnet has maximum effect on the HREE. Plagioclase crystallization is

likely to produce a distinct Eu anomaly. Fractionation of plagioclase depletes the melt in CaO and Al<sub>2</sub>O<sub>3</sub>, whereas olivine fractionation leads to depletion of MgO, FeO, Fe<sub>2</sub>O<sub>3</sub>, Ni, Co and Cu but Na<sub>2</sub>O, Al<sub>2</sub>O<sub>3</sub>, CaO and REEs get enriched (Hanson, 1980; Green, 1980; Henderson, 1984).

Clinopyroxene fractionation may deplete CaO and MgO along with Cr and Sc. Fractionation of augite leads to higher depletion CaO than pigeonite. Ni strongly fractionates into olivine compared to pyroxene. Hence, the ratio of Ni to Cr or Sc provides the effect of olivine and augite in a partial melt or a rock produced by fractional crystallization. Sm, Lu and Eu enter Ca sites while La gets enriched in the liquid. Garnet removes HREE from the melt and gives a negative slope to REE pattern. LREE enrichment due to low degree of partial melting also results a negative slope but it shows minor HREE variation (McKay, 1989). Co and Sc prefer to enter garnet rather than olivine and clinopyroxene. With increasing fractionation, La/Sm ratio will increase along with the incompatible element such as Zr, Ti, P, Y, Nb etc. (Neuman *et al.*, 1954; Wilson, 1989; Winter, 2001).

Feldspar is an important fractionating phase at shallower depth (up to 40 km). Feldspar fractionation has a minor effect on the REE pattern of the melt, except for the negative Eu anomaly in the melt. Thus the shape of the REE pattern of some mantle derived basalts indicates their depth of origin. The presence of garnet leads to the depletion of the HREE and also contributes a positive Eu anomaly in the melt. The presence of clinopyroxene leads to the enrichment of LREE rather than the middle or HREE and contribute positive Eu anomaly. The fractionation of hornblende will lead to the depletion of middle REE but biotite has little effect on REE. Fractional crystallization of amphibole would result in low K/Rb ratio in the evolved melt. Zircon has very large K<sub>d</sub>

(distribution coefficient) for heavy REE, but its low abundance could lead to minor depletion of the HREE in the melt (Hanson, 1980).

Partitioning of trace elements including the REEs can be used to characterize the source rock or to identify minerals particular mineral involved in either partial melting or fractional crystallization processes. REE can also be used to distinguish between high pressure and low pressure melting.

## **6.2. PETROGENETIC MODEL OF SUBDUCTION ENVIRONMENT**

It is generally agreed that the process of magma generation in subduction environment is a multi-stage multi-source phenomenon (Hawkesworth *et al.*, 1994; Dupuy and Dostal, 1982; Arculus and Powell, 1986). The process of subduction transports cold oceanic lithospheric plate into the mantle. This plate is composed of depleted mantle lherzolite of oceanic lithosphere, oceanic crust comprising basalt and gabbro, serpentinised bodies and oceanic sediments (Wilson, 1991).

During subduction, oceanic slab is progressively heated up with increasing pressure and prograde metamorphic reactions occur. The effect of this metamorphism initiates slab dehydration by releasing H<sub>2</sub>O as a separate fluid phase. The presence of this fluid phase is critical in modelling of island arc magma genesis. Recent models favoured multi-stage multi-source phenomena, involving the mantle wedge in petrogenesis (Green and Watson, 1982; Wilson and Davidson, 1984; Johnston, 1986; Ellam and Hawkesworth, 1988). The potential sources for the generation of arc magmas include:

- 1) Oceanic lithosphere. It probably comprises lherzolite and hurzbergite of refractory nature.
- 2) A zone of asthenospheric upper mantle. The lherzolite of this zone may be considerably more fertile.

3) The oceanic crust which consists of variably metamorphosed ocean floor basalt, and oceanic sediments ranging from pelagic clay to terrigenous clastic sediments.

Along with these components, sea water incorporated during the hydrothermal alteration and ocean floor metamorphism or direct circulation within the arc crust also play an important role in modifying the rock chemistry.

In general, the arc magma could be generated through partial melting of amphibolite/eclogite with or without fluid, lherzolite of the mantle wedge with aqueous fluid and lherzolite modified by the reaction with magma derived by the partial melting of the slab (McDonough and Frey, 1989; Parkinson and Pearce, 1998; Rapp *et al.*, 1999). The slab derived fluids have the effect of lowering the mantle solidus, thereby promoting melting (Pearce and Parkinson, 1993). All these processes are taken into accounting petrogenetic modelling of different rock units in the SSZ.

### **6.2.1 Hundar igneous suite**

Hundar igneous suite consists of different rock types from basaltic andesite to granite in composition. Samples from Hundar area show enrichment of large ion lithophile elements (LILE), depletion of high field strength elements (HFSE) and exhibit strong negative Nb, Sr, P, Ti anomalies (Fig. 5.9a). Nb anomaly and LILE concentration indicate the possibility of crustal contamination of the magma (Wilson, 1989). Most of the elements plotted in the “spidergram” (Fig. 5.9a) are incompatible elements for mantle phases (olivine, orthopyroxene and clinopyroxene). LREEs are also enriched with moderate fractionation for middle and heavy rare earth elements (Fig. 5.10a). Basaltic andesites, andesites and granites are treated separately for modelling.

#### ***Partial Melting***

Plank and Langmuir, (1998) assess the importance of sediments to arc volcanism and crust–mantle recycling. The global subducting sediments (GLOSS, Plank and



Langmuir, 1998) have composition similar to upper continental crust (UCC) but there are differences in the enrichment and depletion of some elements. In Hundar igneous suite, the andesites and basaltic andesites have Sr and Zr differentially enriched compared to the arc magma (Sr = 112, Zr = 67). Concentrations of Sr and Zr in andesite and basaltic andesite sample are Sr = 360, Zr = 121 and Sr = 393, Zr = 144 respectively. It appears that these elements are decoupled during melting. During metamorphism, the H<sub>2</sub>O-rich fluid induces enrichment of alkalis, Th, U, and Sr, and LILE in the melt (Sorensen and Grossman, 1989). HREE and HFSE are largely retained in slab residues during very high degrees of H<sub>2</sub>O saturated melting (Spandler *et al.*, 2007).

The element recycling through subduction zones is fundamental to arc magma genesis. Hence during the melting of mantle rocks along with the subducting sediment the Sr can be mobilized by the fluid whereas the Zr will be retained in the residue. The melt produced in the arc by metasomatism thus result in high Sr and relatively less Zr. The subduction of part of the primitive arc along with the sediment also can give same result. Therefore, a source with a mixture of 20% sediment and 80% basalt composition (primitive arc) for the basaltic andesite in Hundar igneous suite is considered to be a reasonable assumption. As the Shyok volcanics appear to be more primitive, basaltic rock from Shyok volcanics is taken as one of the components for mixing. This mixing could be through addition of sediment in the source area or the contamination of the mantle derived melt. Concentration of Sr and Zr in sediment is taken from the GLOSS (Plank and Langmuir, 1998). Concentrations of Sr and Zr in the mixed source are given in Table 6.1. The input of Zr is considered as less than the calculated value for the sediment and basaltic melt mixing at 2:8 proportions because the mobility of Zr is much less compared to Sr.

Partial melting (25%-30%) of a mixed source which consists of 60% clinopyroxene+ 30% garnet + 10% plagioclase is considered to account for the formation of the basaltic andesite (HST-15), which has 360 ppm Sr and 121 ppm Zr (Fig. 6.1). The water from metasomatised regions of the mantle may return to the crust through andesite magmatism (López *et al.*, 2005). 30% partial melting of the mixed source produce REE pattern nearly same as basaltic andesite (HST-6) and quite similar to andesite (HST-10) (Fig. 6.2). Figs. 6.1 and 6.2 clearly indicate that about 25-30% melting of 80% +20% sediment mixed source can produce basaltic andesite rocks in the Hundar area. However, it has been suggested that hydrous fluid derived from metamorphism of sinking slab and involved in melting of mantle wedge can have almost similar trace element effect on mixing of terrigenous sediments and basalt (Wilson, 1989; Bignold *et al.*, 2006). This indicates the hydrous fluids derived from the sinking slab not only cause melting of the mantle wedge, but also transport mobile elements such as Sr from the slab to the mantle wedge through fluids and induce melting of the arc which can produce magmas of andesites composition.

**Table 6.1** Concentration of Sr and Zr in melts derived by different amount of partial melting for 80% basalt+20%sediment source. Source:  $C_0(\text{Sr})=170$  ppm,  $C_0(\text{Zr})=42$  ppm,  $D(\text{Sr})=0.24232$ ,  $D(\text{Zr})=0.06336$ .

	Partial melting of mixed source (80% basalt+20% sediments)					
	10%	20%	30%	35%	40%	50%
Concentration of Sr, ppm	534.44	431.63	361.99	334.97	311.70	273.68
Concentration of Zr, ppm	267.48	167.54	121.97	107.37	95.89	78.99

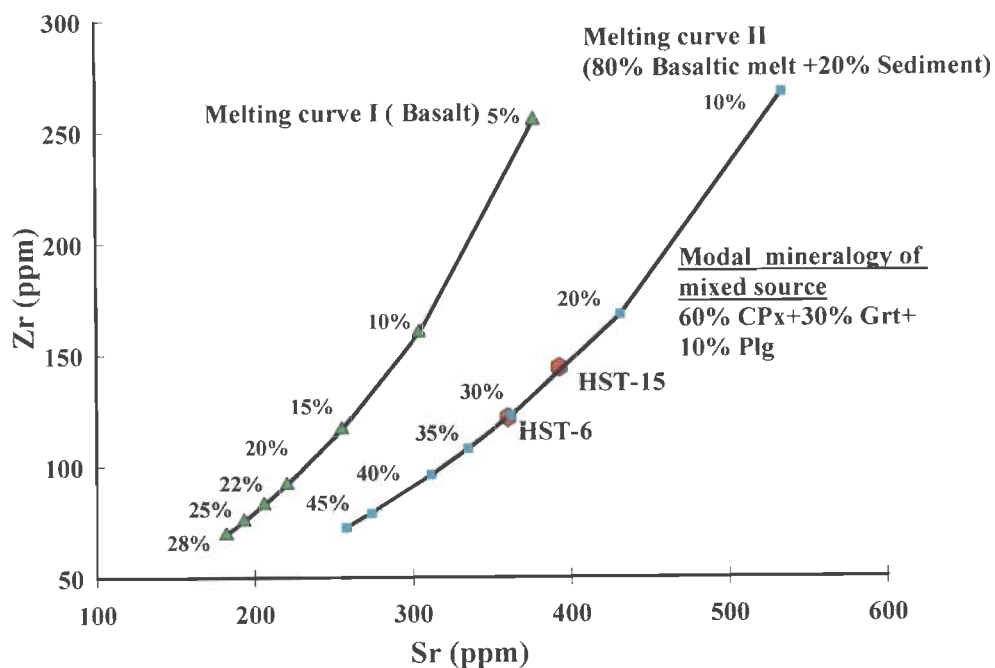


**Figure 6.1** The melting (curve-I) of basalt and basaltic source with sediment input (curve-II). Green triangles and cyan squares indicate different degrees of partial melting. Red hexagons are the basaltic andesite samples from Hundar igneous suite.

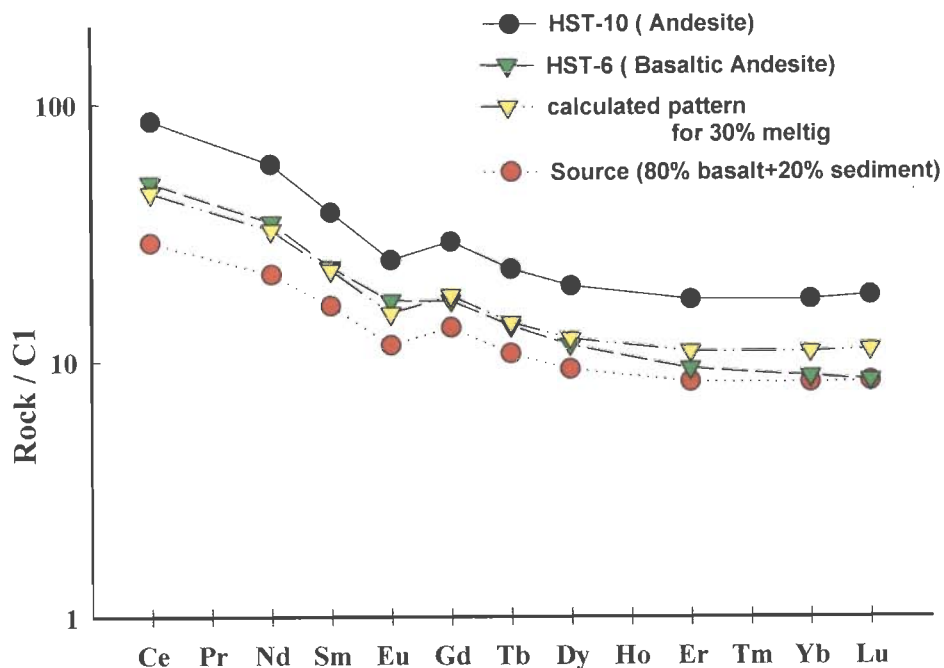


**Figure 6.2.** Chondrite normalized REE pattern of the assumed source (basalt+sediment) along with basaltic andesite and andesite samples from the Hundar area.

### 6.2.2 Shyok Volcanics

“Spidergram” of Shyok volcanics shows slightly less enriched LILE pattern compared to other rock units (Fig. 5.9b). REE pattern of the samples from Shyok also shows lower LREE/HREE ratios compared to other litho-tectonic units (Fig. 5.10b).

#### *Partial melting and Fractional crystallization*

The Ni concentration in the sample (HST-22, used for modelling) is very low (21 ppm) compared to the average concentration in peridotite (1890 ppm). Concentration of Ce in this sample is very high (17 ppm) as compared to the average concentration in peridotite (0.89 ppm). Hence it is reasonable to assume a mixed source with equal proportion of basalt and peridotite (garnet lherzolite) (Fig. 6.3). Mixing of the basaltic magma (Ce = 10.2 ppm, Ni = 42 ppm) in peridotite will increase the Ce and decrease the concentration of Ni in mixed source (Ce = 5.54 ppm, Ni = 966 ppm). Partial melting (25%) of a source with peridotite and basalt in equal proportion (50%+50%) is modelled for the possible parent magma that can produce the basalt (HST-22) leaving 60% olivine + 25% clinopyroxene + 12% orthopyroxene + 3% garnet as residue, ( $K_d$  values from Hanson, 1980; Bedard, 1994). Concentrations of Ce and Ni in the mixed source (peridotite + basalt) are given in Table 6.2. As these rocks are subduction related where mantle wedge is normally a possible source and therefore, fluids released from the slab can enrich LREE and LILE but not HFSE. 5 to 55% fractionation trend involving olivine and clinopyroxene in equal proportion, amphibole and plagioclase in 4:6 proportions and clinopyroxene and plagioclase combination in different proportions are similar and leads to samples from Shyok area (Fig. 6.3). Thus the fractional crystallization of different phases in different proportions from a parent magma, which produced from a mixed source of peridotite and basaltic melt, could be accounted for the rare element abundance in Shyok volcanics (Fig. 6.4). Fractional crystallization of clinopyroxene along with

plagioclase in 2:8 proportions is modeled for the formation of other basaltic andesite samples from Shyok area (Fig. 6.5).

**Table 6.2** Concentration of Ce and Ni in melts derived by different amount of partial melting for mixed source (basalt + peridotite). Source:  $C_0(\text{Ce})= 5.1445$  ppm,  $C_0(\text{Ni})= 966$  ppm,  $D(\text{Ce})=0.04384$ ,  $D(\text{Ni})= 4.651$ .

	Partial Melting of mixed source (basalt +peridotite)				
	10%	15%	20%	25%	40%
Concentration of Ce	36.90	27.47	21.88	18.19	12.07
Concentration of Ni	225.39	235.41	246.38	258.41	302.76

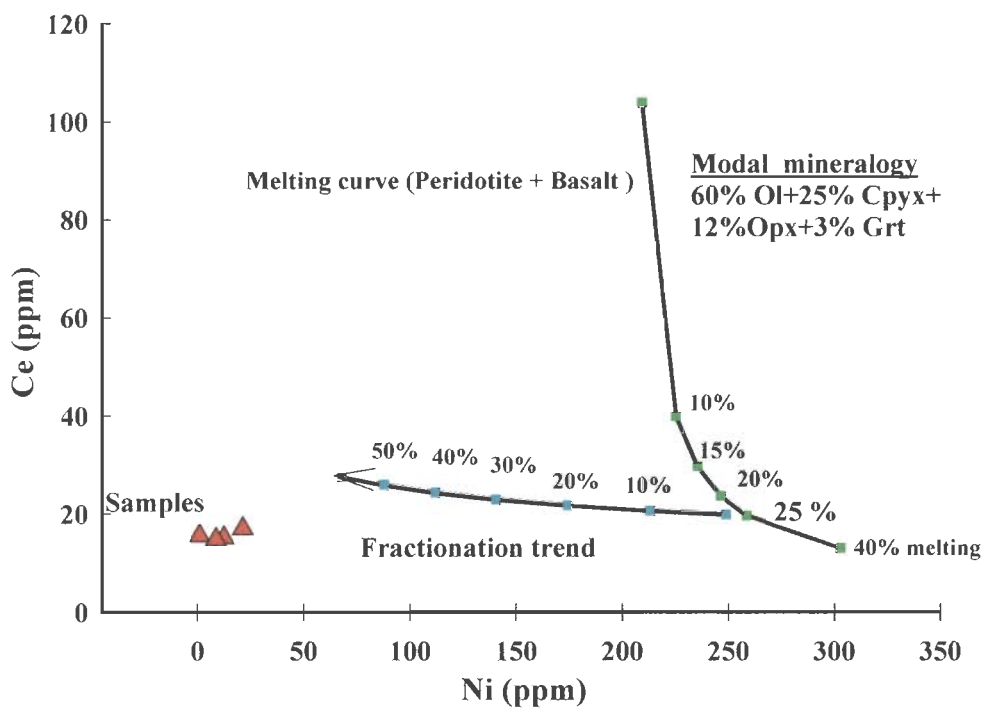


**Figure 6.3** Melting of a contaminated mantle source and the fractionation of olivine and pyroxene result the samples of Shyok area. Green and cyan squares indicate different degrees of partial melting and fractionation respectively. Red triangle indicates the samples from Shyok volcanics. 25% partial melting of the mixed source along with fractionation of olivine and clinopyroxene in equal proportion, amphibole and plagioclase in 4:6 proportion and clinopyroxene and plagioclase in different proportions give the rock with Ce and Ni concentration similar to the Shyok samples.

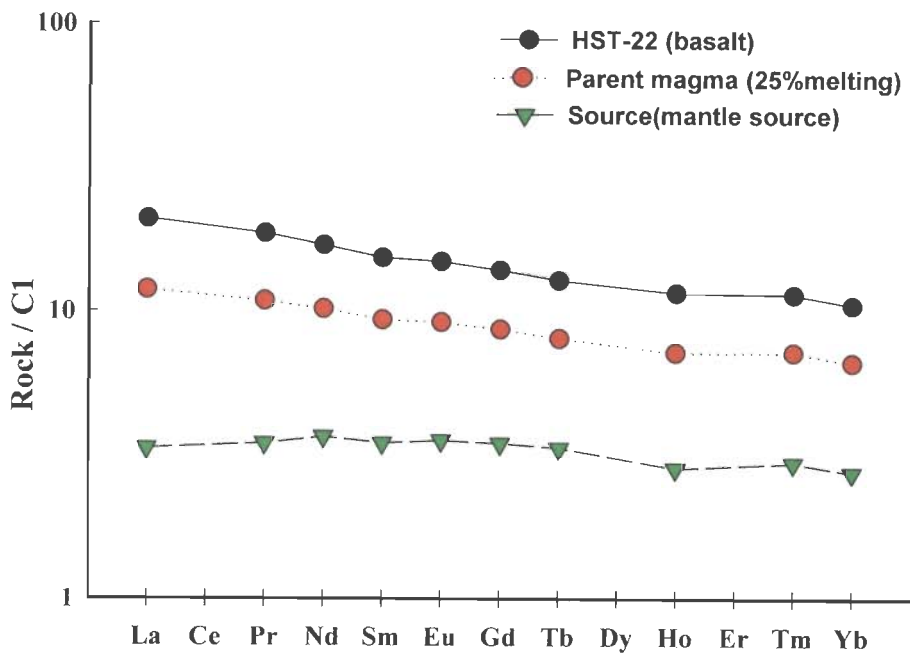


**Figure 6.4** Mixed source (50%peridotite+50%basalt), parent magma formed by 25% melting of this mixed source and fractionation of the mineral phases (clinopyroxene and olivine) from the magma gives HST-22.

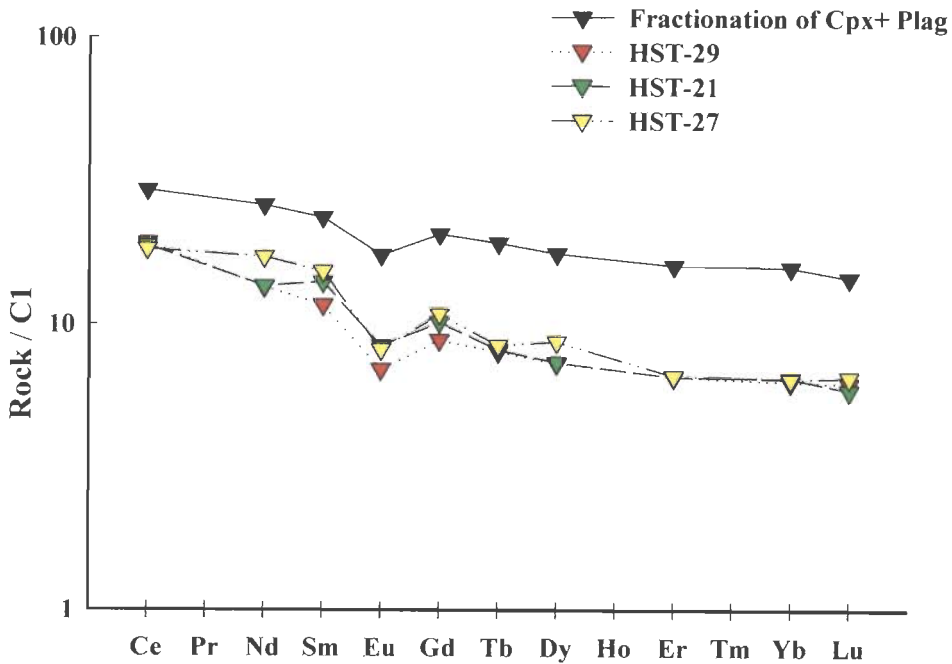


**Figure 6.5** Chondrite normalized REE pattern of the basaltic andesites of the Shyok area. Black inverted triangles indicate fractionated melt leaving clinopyroxene and plagioclase in residue. The REE pattern of the melt is similar to the basaltic andesite from Shyok area but slightly enriched.

### 6.2.3 Khardung Volcanics

Similar to Hundar igneous suite Khardung volcanics also exhibit negative Nb, Eu and Sr anomaly (Fig. 5.9c). LREE are enriched and HREE are moderately fractionated (Fig. 5.10c). Khardung volcanics are dominantly felsic volcanics. Experimental studies by Condie (1986), Rapp *et al.* (1991) and Rapp and Watson (1995) show that low degree of partial melting of basalt can give rise to intermediate and high silica melts. Amphibole is the dominant residual phase during low degree of partial melting of basalt in hydrous condition. Under this condition plagioclase becomes unstable. During dehydration melting, plagioclase becomes stable and amphibole becomes unstable (Beard and Lofgren, 1991).

#### *Partial melting*

An attempt is made to model the REE abundance in the felsic melt in Khardung formation by partial melting of basalt which is similar to the Shyok volcanics (*e.g.*, HST-22). As the rocks of Khardung felsic volcanics have negative Eu anomaly, plagioclase is considered as a fractionating phase. Fractional crystallization of plagioclase along with clinopyroxene and amphibole in different proportions depletes the LREE concentration of the residue and give more or less a flat pattern whereas the sample from Khardung (KST-4) has depleted HREE pattern compared to the residual melt left after fractional crystallization. Therefore, the possibility of fractionation is ruled out.

Partial melting of the assumed source (subducted oceanic crust of basaltic composition, or subduction of part of the primitive arc) at shallow depth can leave a residue with clinopyroxene and plagioclase. Plagioclase and clinopyroxene can not deplete the HREE in considerable amount (Fig. 6.6). Therefore, the melting is assumed to have occurred at higher depth (higher pressure) which can leave a residue with either amphibole or clinopyroxene along with garnet (Fig. 6.7). Garnet will remove considerable

amount of HREE from the melt. Different degree of partial melting of basalt leaving a residue with amphibole/clinopyroxene + plagioclase + garnet in 70:25:5 proportions can account for the formation of felsic magma from a basaltic melt. As Shyok volcanics are considered as primitive arc magmas, basaltic rock from this area is considered as the source. 20% to 30% melting of the basalt with amphibole + plagioclase + garnet residue gives a melt which has similar concentration of REE as in KST-4 (Fig. 6.8). Fractionation of some accessory phases like sphene and different extent of partial melting leaving residue in varying proportions may be responsible for the formation of other felsic rocks in the area.

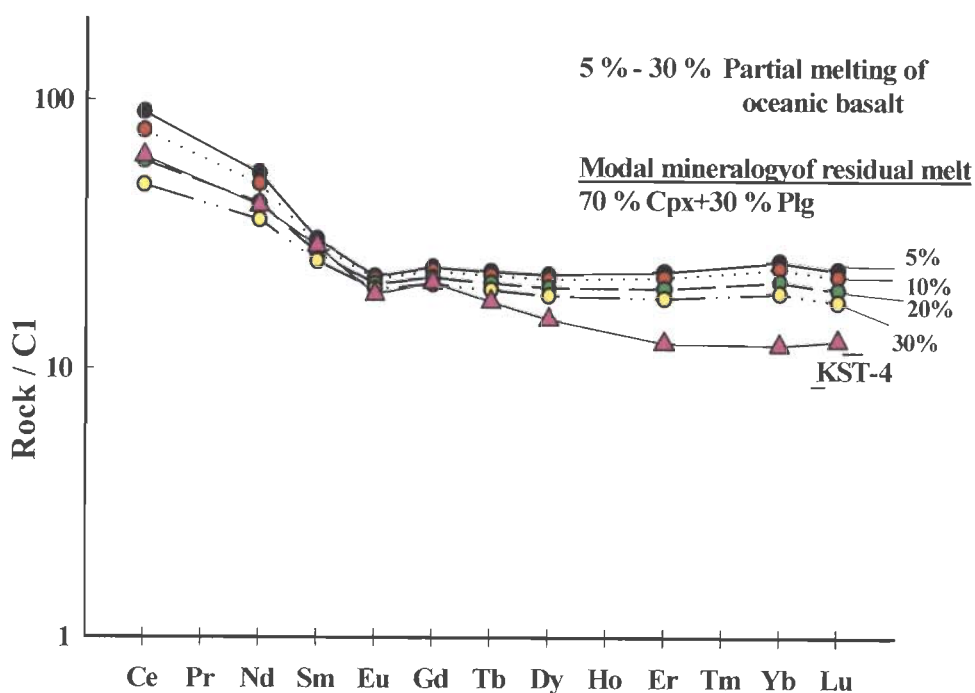


**Figure 6.6** Partial melting of the subducted oceanic crust (basalt) or the subducted primitive arc at shallow depth with fractionation of clinopyroxene and plagioclase can not deplete the HREEs. REE pattern of the sample from Khardung volcanics (KST-4) has more depleted HREEs than the melt produced by the assumed source.



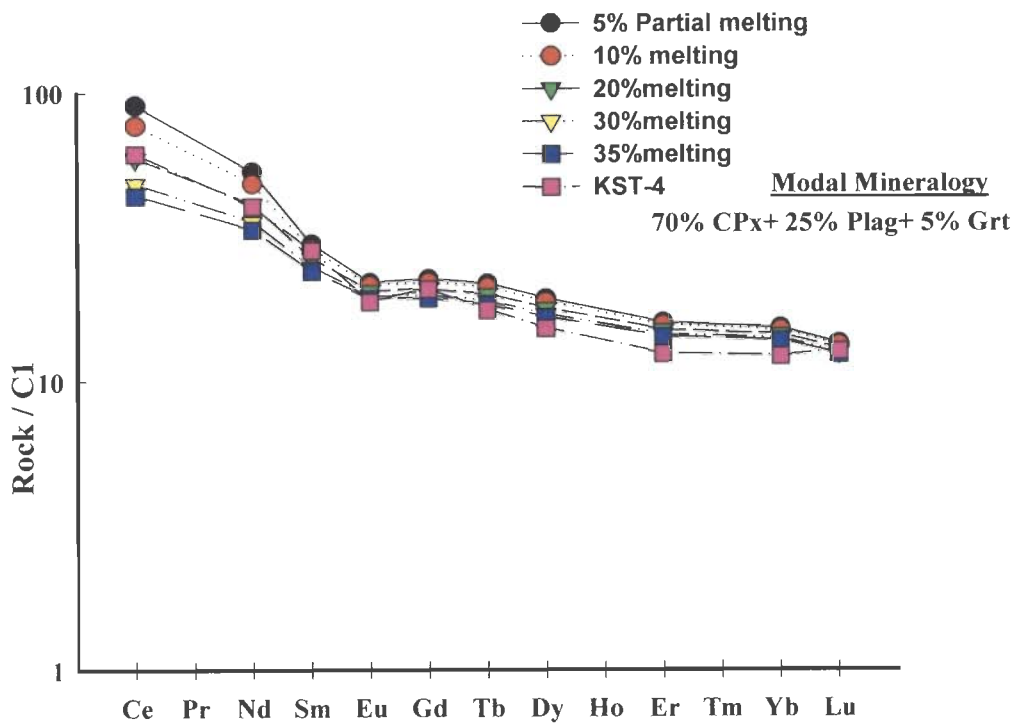


**Figure 6.7** Different degrees of partial melting of the assumed source (basalt) at greater depth with Cpx-Plg-Grt in the residue. REE pattern of the sample KST-4 is matching with the pattern of the melt.

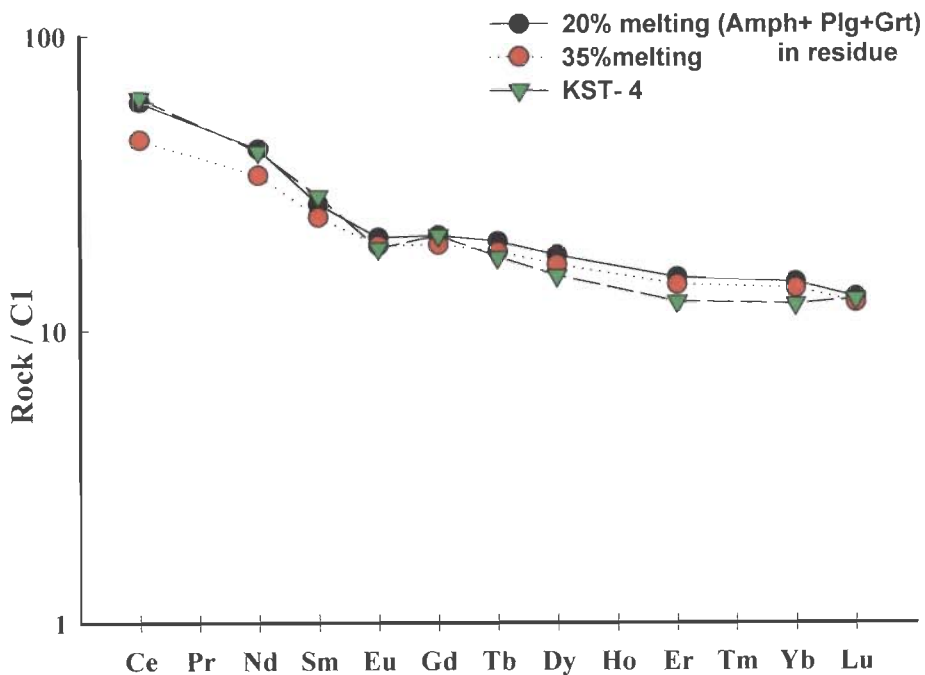


**Figure 6.8** Felsic magma formed generated the melting of same source (basalt) composition leaving a residue with amphibole (instead of clinopyroxene) and plagioclase along with garnet.

#### 6.2.4 Tsoltak volcanics

Tsoltak volcanics are associated considered as a well developed ophiolite sequence of Nubra ophiolite mélange. NST-69 is an ultramafic rock with very high MgO wt% (30.4 wt %) which is very similar to the MgO in mantle source (39.22 % in peridotite, after Rapp *et al.*, 1999).

Average major element composition of the mantle peridotite rocks from the ophiolite belts in western Qinghai-Tibetan Plateau (Qiu *et al.*, 2007) and composition of pyrolite (Ringwood, 1975) are compared with the sample NST-69 of the study area (Table 6.3). Mantle pyrolite forms at the asthenosphere (upper part of the mantle). The major element concentrations in NST-69 are similar to the mantle pyrolites from other ophiolites. Therefore NST-69 may possibly represent peridotite from the mantle wedge. The volcanic unit in the Tsoltak area probably represents the rocks derived from this source.

Andesitic magma could be generated directly by partial melting of hydrous lherzolite at depths less than 40 km. Such magmas reach the surface after extensive crystal fractionation (Wilson, 1985). Hence considering a source similar to mantle lherzolite is reasonable. The Mg number ( $Mg_{\#}$ ), and MgO content of mantle peridotites are regarded as indicative of the degree of mantle depletion, or the degree of partial melting. The larger the  $Mg_{\#}$  the higher the MgO content and greater the degree of partial melting and also the residual mantle may be more depleted (Qiu *et al.*, 2007). The average MgO content is 30% in the Tsoltak ultramafic sample (NST-69). This indicates higher degree of partial melting. Hence modelling of lherzolite with high degree of partial melting in the mantle wedge is attempted for Tsoltak volcanics. Presence of  $H_2O$  facilitate the partial melting in mantle wedge.

REE patterns for the melts derived the by partial melting of NST-69 (similar to lherzolite) originally consisting of 50% olivine+ 20% orthopyroxene+ 20% clinopyroxene + 10% garnet are modelled for the Tsoltak volcanics. The calculations were carried out using the  $K_d$  values given by Hanson (1980). 10-25% of partial melting of the mantle derived source and subsequent fractionation give the REE concentrations similar to the volcanics in Tsoltak area (Fig. 6.9). However, the LREEs in the Tsoltk volcanics do not exactly match with calculated REE pattern.

If a hydrous fluid containing light REE and LILE introduced into the mantle wedge during the process of oceanic crust subduction, the REE signature of rocks could be changed to a great extent. Since the REE abundance in the mantle source is very low, the addition of a hydrous fluid containing light REEs and LILE may results in light REE enrichment. Therefore, the fluid interaction my explain slight LREE mismatch between calculated and Tsoltak REE pattern.

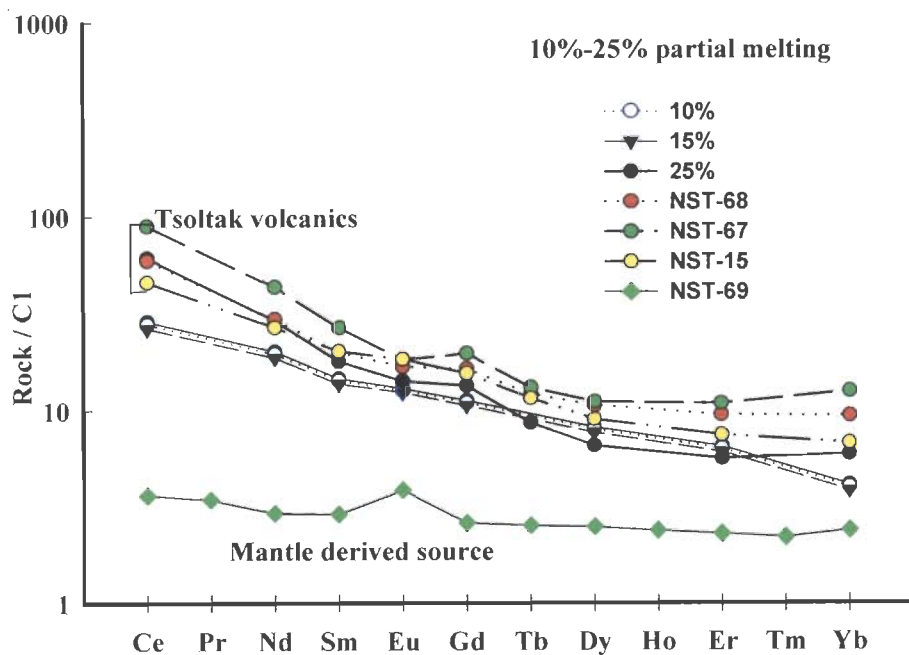


**Figure 6.9** Partial melting of the mantle derived source give the REE pattern similar to the Tsoltak volcanics. Source enriched by fluids can have more enriched LREE to match the patterns better.

**Table 6.3** Major element data of mantle pyrolite from different ophiolites along with sample NST-69 from Tsoltak volcanics.

	SiO <sub>2</sub>	TiO <sub>2</sub>	Al <sub>2</sub> O <sub>3</sub>	Fe <sub>2</sub> O <sub>3</sub>	FeO	MnO	MgO	CaO	Na <sub>2</sub> O	K <sub>2</sub> O	P <sub>2</sub> O <sub>5</sub>
Qiu <i>et al.</i> ,2007											
Bangonghu	46.1	0.09	1.27	1.52	6.62	0.11	43.44	0.68	0.1	0.05	0.03
Shiquanhe	45.15	0.06	1.48	1.62	7.02	0.11	43.93	0.38	0.13	0.08	0.03
Yarlung Zangpo	45.44	0.08	1.45	1.56	7.19	0.12	42.92	1.15	0.05	0.02	0.03
PulanDangqiong	44.58	0.04	1.1	1.22	6.82	0.12	45	0.98	0.08	0.02	0.02
Ringwood, 1975	45.48	0.72	3.57	0.46	8.1	0.14	37.67	3.1	0.57	0.13	0.06
(NST-69)	44	0.18	3.88	1.4	9.19	0.17	30.49	6.2	.1	.01	.02

### 6.2.5 Nubra ophiolite volcanics

Nubra samples display LILE enriched pattern with depletion of HFSE. REEs are not fractionated and LREEs are slightly enriched (Figs. 5.9e, 5.10e). NST-1 is similar to NST-69 of Tsoltak volcanics in REE pattern and may also represent a mantle source. Hence, the same mantle derived source (NST-69) of Tsoltak is taken as the source for modelling Nubra volcanic rocks.

#### *Partial melting*

At 3% to 15 % melting of the source (NST-69 from Tsoltak volcanics), the calculated concentrations of the REEs in the melt are found to be very similar to the REE concentrations of andesite (sample NST-15) from Nubra volcanics. NST-1 may be derived by higher degree of partial melting of NST-69 (Fig. 6.10). The variations in REE pattern from Nubra volcanics (Fig. 5.10e and 6.11) can be explained by Fig. 5.8b indicating fractionation of olivine, clinopyroxene, amphibole and plagioclase. Partial melting of mantle derived source and subsequent fractionation of clinopyroxene, amphibole and plagioclase. REE pattern of Tsoltak volcanics are very similar to Nubra ophiolite volcanics (Fig. 6.11). All these evidence suggest that Nubra ophiolite volcanics in the Nubra valley are possibly the extension of ophiolite mélange of Chang La ultramafics

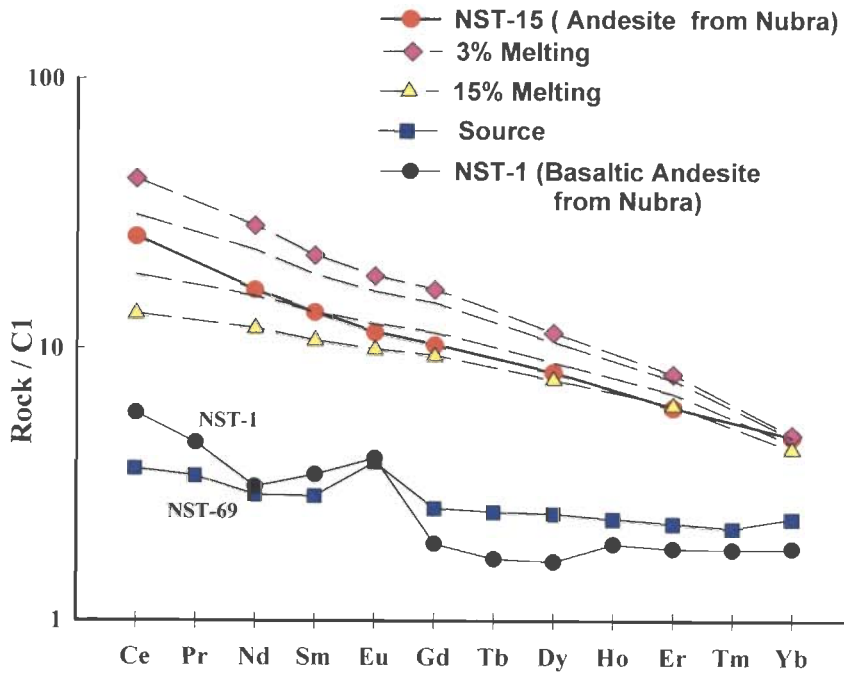


**Figure 6.10** NST-69 from Tsoltak volcanics is considered as the mantle derived source. Higher degree of partial melting of this source gives the REE pattern similar to basaltic andesite. 3-15% of melting of the same source gives similar REE pattern for andesite from Nubra.

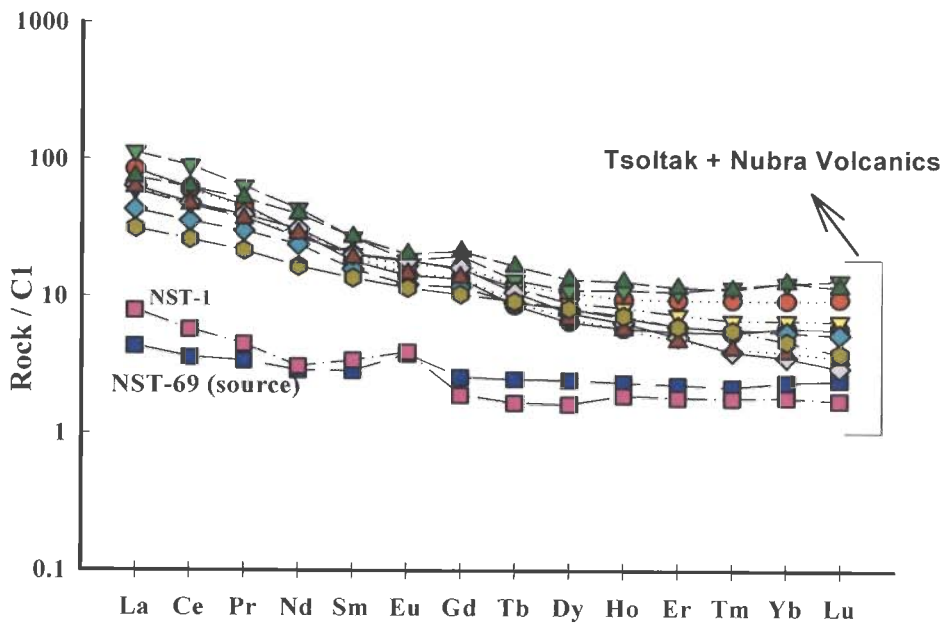


**Figure 6.11** Tsoltak and Nubra volcanics show similar REE patterns. Different degrees of partial melting of same source may result in generation of the patterns

### 6.2.6 Karakoram complex

There are different hypothesis about the formation of granodiorite. One hypothesis is that the granodiorites represent recycled products of an older crust (Armstrong, 1968, McCulloch and Wasserburg, 1978; Allegre and Othman, 1980). It has been suggested that that the genesis of voluminous granodioritic batholith requires the participation of hydrous mafic magma derived from mantle (Moyen *et al.*, 2001). Partial melting of basaltic magma can enrich the silica content and give felsic rocks (Rapp and Watson, 1995). Detailed petrogenetic modelling of Karakoram complex has not been done because it is not part of SSZ. However a preliminary modelling of diorite and dykes from the complex has been attempted.

The major, trace as well as the REE chemistry suggest mafic dykes and diorite from Karakoram suggest that fractional crystallization can be a plausible mechanism by which the diorite and granodiorite are related. There is a decrease in  $TiO_2$  and an increase in  $SiO_2$  in granodiorite compared to the diorite (Fig, 5.5e). This can be expected when hornblende and biotite constitute the fractionation phases. This possibility has been tested by fractionating 10% biotite. Garnet is considered as one of the phases because of the depletion of HREE, which can not be attributed to plagioclase alone. Hence, 30% amphibole, 40% plagioclase and 20% clinopyroxene along with 5% garnet is fractionated from the diorite to get the granodiorite. Basaltic melt with 20-30 % sediment input in the source is considered for REE modelling.

The mafic dykes in Karakoram complex is considered as the extension of the dyke activity in the Nubra area. On this assumption, the model for Nubra ophiolite volcanics is applied for the mafic dykes in this area. The model indicates that the mafic dykes of the Karakoram area also have resulted from the similar mafic magmatism of Nubra area, and the magma is derived from the mantle source by fractionation of olivine and pyroxene

(Fig.6.13). As the granites of Karakoram batholith is very massive, modelling with few samples may not be appropriate. Hence, petrogenetic modelling is not attempted for the granites and granitoids of Karakoram batholith

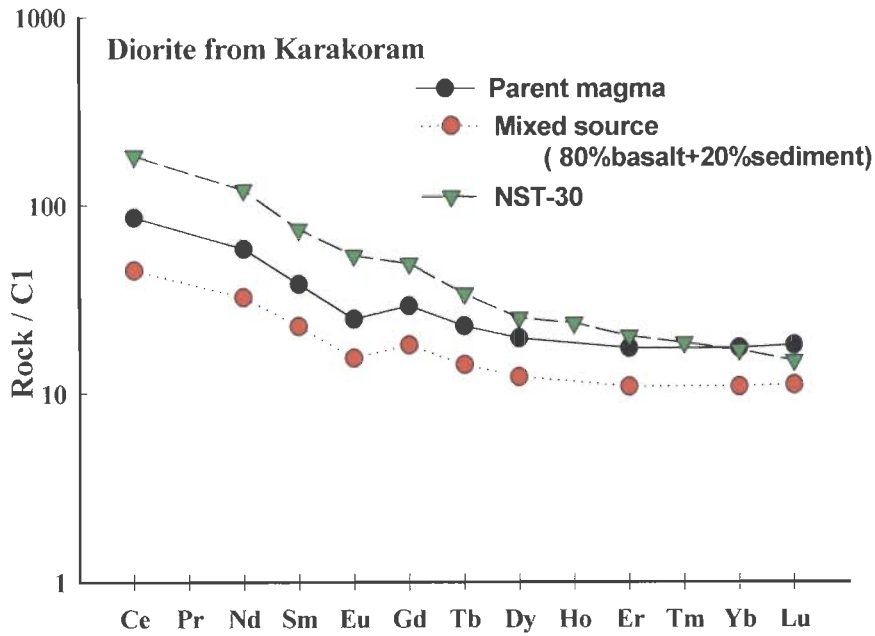


Figure 6.12 The sediment input in the source for diorite in Karakoram area.

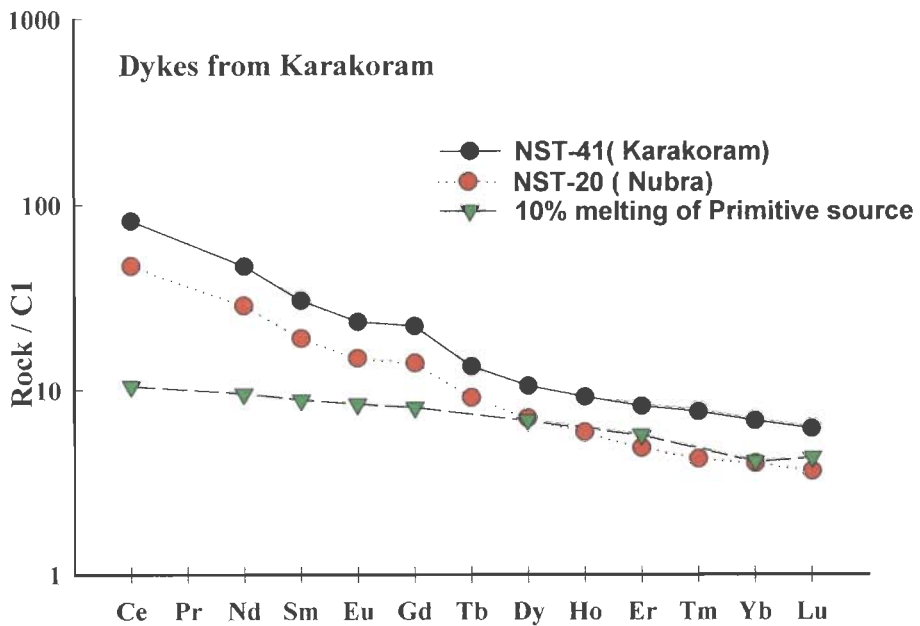


Figure 6.13 Melting of mantle derived source and the REE pattern of basic volcanics from Nubra and Karakoram dyke.

### 6.3 SUMMARY

The possible sources for the generation of magmas in subduction setting are attempted for the petrogenetic modelling of SSZ. Mantle peridotite, oceanic crust and oceanic lithosphere along with subducting sediments and fluids in different combinations are tried to verify source characteristics for different litho-tectonic units.

Petrogenetic modelling from different litho-tectonic units of SSZ indicates that magma could have been generated by the partial melting of peridotite of the mantle wedge with aqueous fluid. Recycling of the primitive arc and incorporation of continental crust and the crustal derived sediment with the magma also played an important role in the genesis of the rock units in the study area. The source of primitive arc magma (Shyok volcanics) is modelled with mixed components as peridotite of the mantle wedge and the subducted oceanic slab. Hundar igneous suite and more felsic Khardung volcanics could have been formed by the recycling of the primitive arc (similar to Shyok volcanics). Petrogenetic modelling is not attempted for the granites and granitoids of Karakoram batholith.

Most of the rock units in the SSZ have clear evidence of contamination. Metasomatism of arc component with enriched aqueous fluid is also found to be a possible process that may change the geochemical signature of the rock. The REE characteristics of the rock units from SSZ indicate the possibility of an Andean type setting where crustal contamination or sediment involvement is prominent. Figs. 6.14 summarizes source characteristics of the study area. For comparison, the source characteristics of adjacent area in Pakistan are shown in Fig. 6.15 (Bignold *et al.*, 2006)



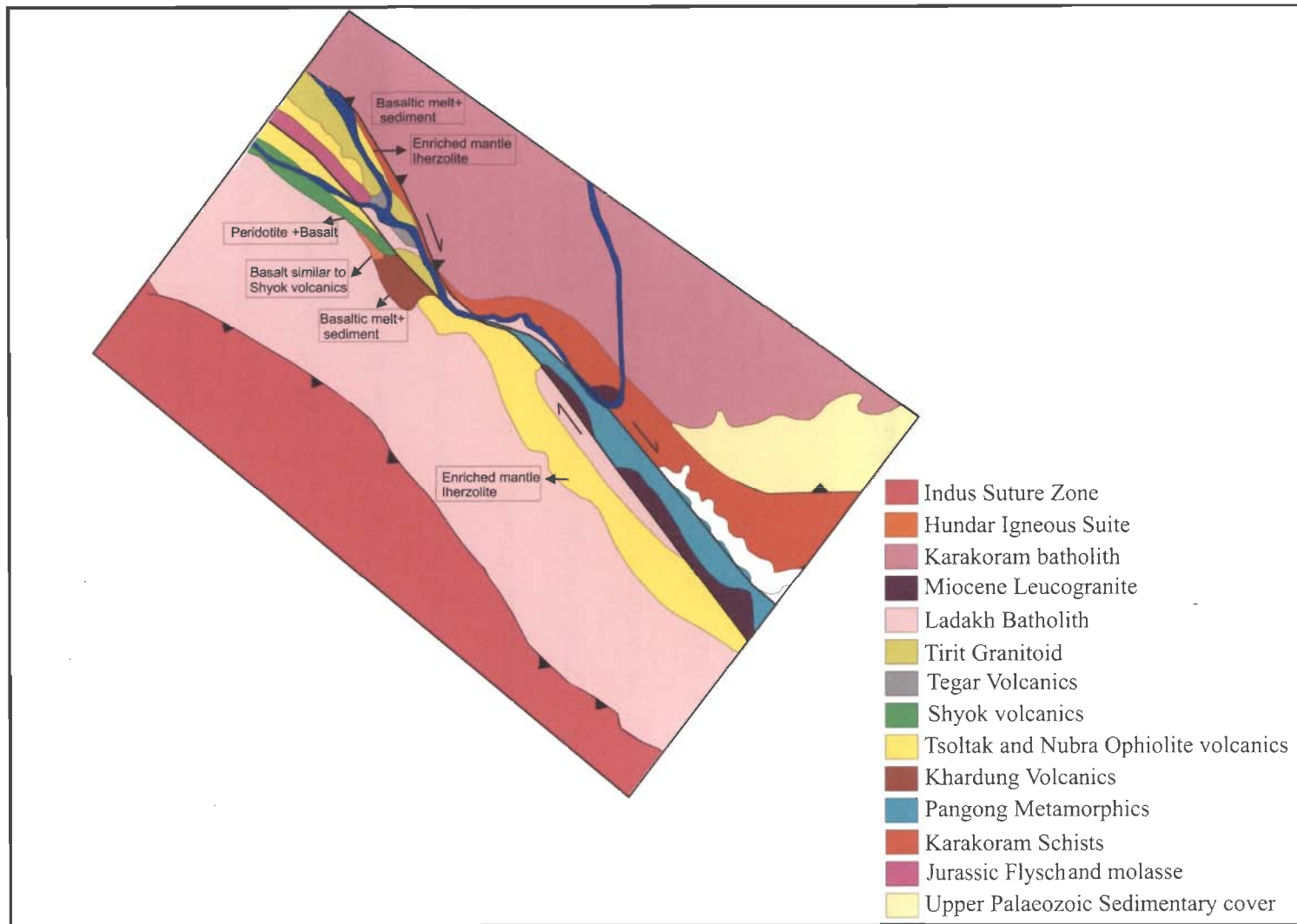


**Figure 6.14** Source characteristics of different litho-tectonic units of SSZ

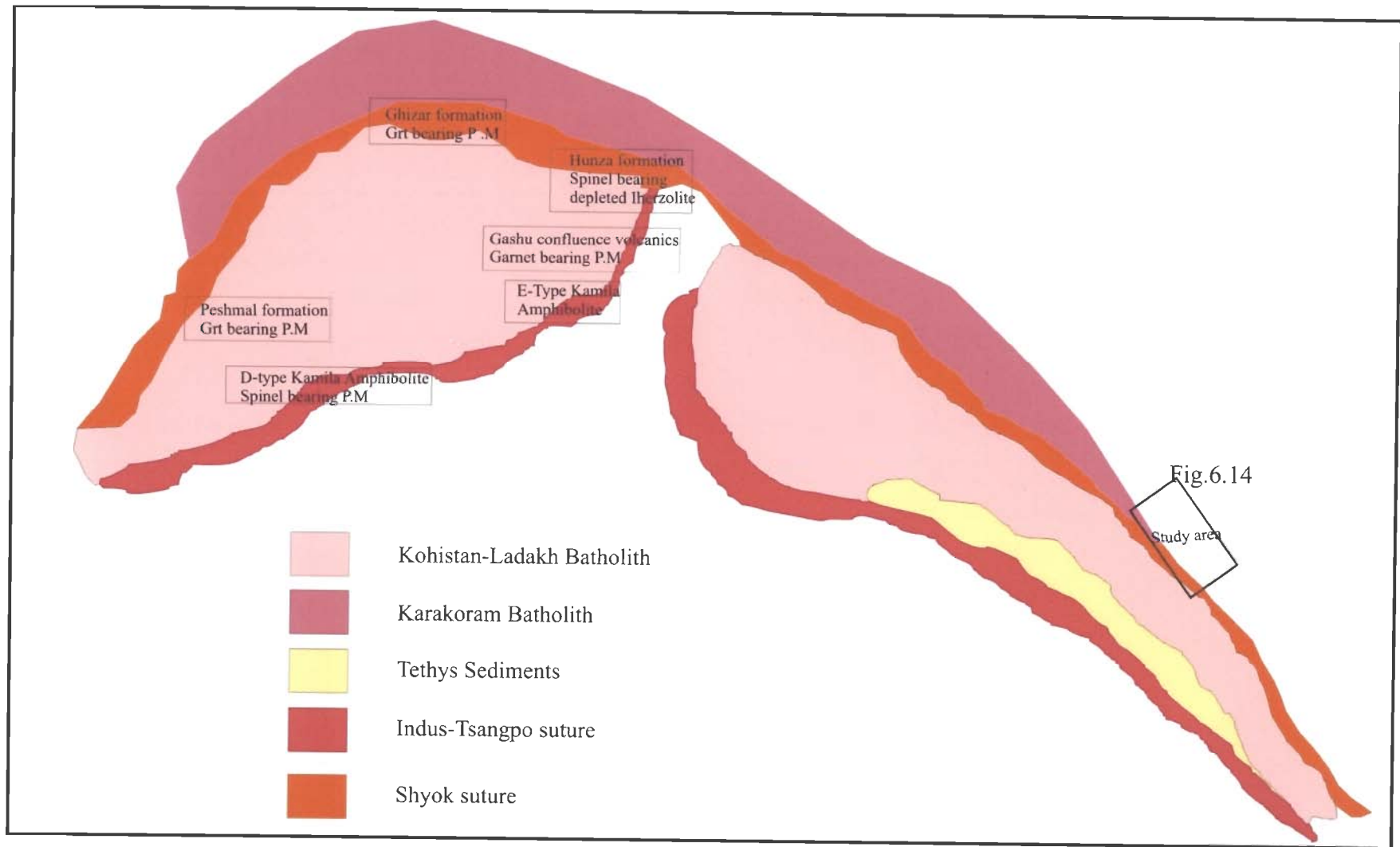


**Figure 6.15** Source characteristics of different rock units from Pakistan area (Bignold *et al.*, 2006)

## **Chapter 7**

# **ISOTOPE GEOCHEMISTR**

Rb-Sr, Sm-Nd and various other isotopic systems can be used for dating rocks and minerals which are useful in determining ages of various geological events and understand petrogenesis. Rb-Sr and Sm-Nd methods of dating can be employed for rocks varying in composition from mafic to felsic spectrum. Micas and K-feldspar are used for mineral dating using Rb-Sr method. Garnet, clinopyroxene and plagioclase are used in basic rocks for dating purpose. REEs are less mobile than alkali metals and alkaline earths during metamorphism, hydrothermal alteration and chemical weathering. The Sm-Nd method therefore can be used to date rocks that are not suitable for dating by Rb-Sr method (Faure, 1986; Patchett, 1989).

### 7.1 Rb-Sr SYSTEMATICS

Sr has four naturally occurring isotopes,  $^{88}\text{Sr}$ ,  $^{87}\text{Sr}$ ,  $^{86}\text{Sr}$  and  $^{84}\text{Sr}$ . Rb has two naturally occurring isotopes  $^{85}\text{Rb}$  and  $^{87}\text{Rb}$ .  $^{87}\text{Rb}$  is radioactive and decays to stable  $^{87}\text{Sr}$  by emission of a negative beta particle. Hence, the total concentration of  $^{87}\text{Sr}$  present in the rock is  $^{87}\text{Sr}$  produced by the decay of  $^{87}\text{Rb}$  through time added to the initial concentration of  $^{87}\text{Sr}$  present at the time of formation. The equation can be written as

$$^{87}\text{Sr} = (^{87}\text{Sr})_i + ^{87}\text{Rb} (e^{\lambda t} - 1)$$

where  $\lambda$  is the decay constant,  $\lambda = 1.47 \times 10^{-11} \text{ y}^{-1}$ , and  $t$  is age

It is convenient to determine the ratios of these isotopes with  $^{86}\text{Sr}$  which is stable and not produced by the decay of any naturally occurring isotope of any other element. Therefore the equation can be rewritten as:

$$^{87}\text{Sr}/^{86}\text{Sr} = (^{87}\text{Sr}/^{86}\text{Sr})_i + ^{87}\text{Rb}/^{86}\text{Sr} (e^{\lambda t} - 1)$$

where 't' is in the geological past

## 7.2 Sm-Nd SYSTEMATICS

$^{147}\text{Sm}$  decays to  $^{143}\text{Nd}$  by the emission of alpha particle. The decay of  $^{147}\text{Sm}$  and growth of radiogenic  $^{143}\text{Nd}$  is described by the equation

$$^{143}\text{Nd}/^{144}\text{Nd} = (^{143}\text{Nd}/^{144}\text{Nd})_i + ^{147}\text{Sm}/^{143}\text{Nd}(e^{\lambda t} - 1)$$

where  $\lambda = 6.54 \times 10^{-12} \text{ y}^{-1}$ . Age determination by the Sm-Nd method is usually made by analyzing separated minerals or comagmatic suite of rocks by plotting the  $^{147}\text{Sm}/^{143}\text{Nd}$  on the x-axis and  $^{143}\text{Nd}/^{144}\text{Nd}$  on the y-axis to construct isochron. Similarly, for Rb-Sr method,  $^{87}\text{Rb}/^{86}\text{Sr}$  is plotted on the x-axis and  $^{87}\text{Sr}/^{86}\text{Sr}$  on the y-axis. Slope of the isochron is related to the age of the mineral or the rock.

### 7.2.1 Evolution of Sm-Nd and Rb-Sr systematics

Isotopic evolution of Nd in the earth is described in terms of a model called CHUR, which is Chondritic Uniform Reservoir. This model assumes that the Nd has evolved in the Earth from a uniform reservoir whose Sm/Nd ratio is equal to the chondrite (0.1967, Winter, 2005). Partial melting of the CHUR gives rise to magma having lower Sm/ Nd ratio than CHUR (higher Nd and lower Sm). The igneous rocks that are derived from this magma should have lower present day  $^{143}\text{Nd}/^{144}\text{Nd}$  than CHUR. The residual solid left behind after the partial melting of CHUR will have higher Sm/Nd ratio and therefore, higher  $^{143}\text{Nd}/^{144}\text{Nd}$  ratios than CHUR. The chondritic reservoir remain undisturbed whose isotopic composition evolved without interruption (Fig. 7.1).

Nd gets concentrated in the liquid relative to Sm in the course of fractional crystallization of magma and the crustal rocks have lower  $^{147}\text{Sm}/^{143}\text{Nd}$  ratio than the rocks derived from the upper mantle. During partial melting of rocks in the mantle or crust the silicate liquid will be enriched in Nd relative to Sm. The reason is that  $\text{Nd}^{3+}$  has larger radius than  $\text{Sm}^{3+}$  which gives it a lower ionic potential than  $\text{Sm}^{3+}$ . Therefore  $\text{Nd}^{3+}$

forms weaker bonds that can be broken very easily than those of  $\text{Sm}^{3+}$  (Allegre *et al.*, 1980, 1984; Albarede and Brouxel, 1987).

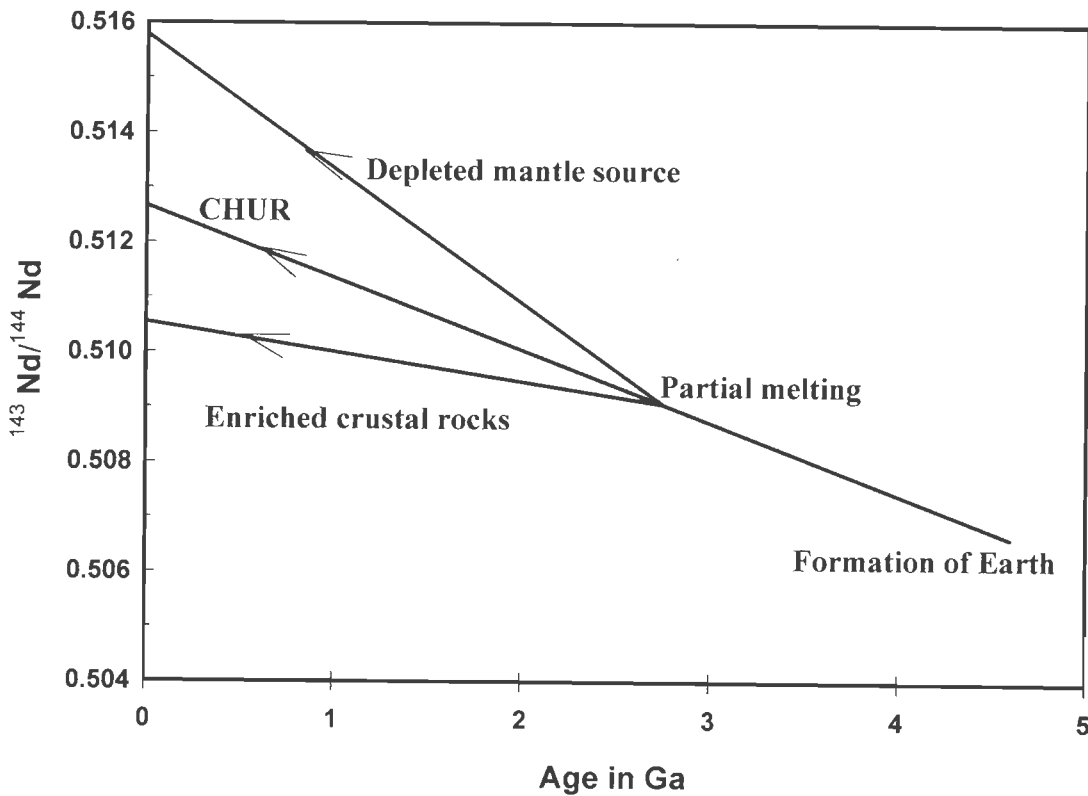


**Figure. 7.1** Shows the Nd isotope evolutionary curves for CHUR, depleted mantle and enriched crust. Partial melting of CHUR gives rise to depleted mantle rocks with high present day  $^{143}\text{Nd}/^{144}\text{Nd}$  values. Enriched crustal rocks have lower  $^{143}\text{Nd}/^{144}\text{Nd}$  ratio than CHUR

The isotopic evolution of the undisturbed part of the CHUR serves as the reference for the isotopic evolution of the magmas derived from the crust or mantle reservoir. This reference parameter is called ' $\epsilon$ '. This parameter is introduced by De-Paolo and Wasserberg (1976). The  $\epsilon$  value is used to compare the  $^{143}\text{Nd}/^{144}\text{Nd}$  ratios of the rocks in the crust with the corresponding ratios of CHUR at the time of the crystallization of the rocks, or to compare the initial ratio of  $^{143}\text{Nd}/^{144}\text{Nd}$  is higher or lower than the CHUR. If the  $\epsilon$  is positive, it indicates the rock derived from the residual solid or mantle which has higher Sm/Nd and such part of the reservoir is said to be 'depleted' (depleted in LILE). If

$\epsilon$  is negative, it indicates the rock derived from the old crustal rock with lower  $^{147}\text{Sm}/^{143}\text{Nd}$  ratio than the reservoir and said to be 'enriched'.  $\epsilon$  expressed as

$$\epsilon^t_{\text{CHUR}} = \left[ \frac{(^{143}\text{Nd}/^{144}\text{Nd})_i}{I^t_{\text{CHUR}}} - 1 \right] \times 10^4 \text{ and } \epsilon^0_{\text{CHUR}} = \left[ \frac{(^{143}\text{Nd}/^{144}\text{Nd})_{\text{Measu.}}}{I^0_{\text{CHUR}}} - 1 \right] \times 10^4$$

where,  $I^t_{\text{CHUR}}$  is the  $^{143}\text{Nd}/^{144}\text{Nd}$  ratio of CHUR at any time 't' in the past and  $I^0_{\text{CHUR}}$  is the  $^{143}\text{Nd}/^{144}\text{Nd}$  ratio of CHUR at the present time (0.512638, Winter, 2005)

$$I^t_{\text{CHUR}} = I^0_{\text{CHUR}} - (^{147}\text{Sm}/^{143}\text{Nd})_{\text{CHUR}} \times (e^{\lambda t} - 1)$$

Bulk of the earth's crust differentiated from the mantle early in geologic time. The  $\text{Rb}^+$  ion is large and close to  $\text{K}^+$  ion in geochemical character hence would be concentrated in the relatively silica rich differentiates that formed crust. The  $\text{Sr}^{2+}$  ion is small and doubly charged resembles  $\text{Ca}^{2+}$  ion in its geochemical behavior and would distribute itself evenly between crust and mantle. The greater concentration of Rb in the crust means that production of  $^{87}\text{Sr}$  would be faster and  $^{87}\text{Sr}/^{86}\text{Sr}$  in the crustal material would be higher than the ratio in the mantle. Earth's mantle and all its derivative products are considered to be originated from a hypothetical Uniform Reservoir (UR) (McCulloch and Wasserburg, 1978; De-Paolo, 1988).

The primordial  $^{87}\text{Sr}/^{86}\text{Sr}$  ratio of the Earth is same as that of basaltic achondrite because they show evidence of silicate liquid origin and resembles the terrestrial igneous rocks. The initial  $^{87}\text{Sr}/^{86}\text{Sr}$  ratio is therefore deduced from the basaltic achondrite called 'BABI' (basaltic achondrite best initial, value is  $0.698990 \pm 000047$ , Faure, 1986). During fractional crystallization of magma, strontium tends to be concentrated in plagioclase, whereas the rubidium remains in the liquid phase. Therefore the  $^{87}\text{Rb}/^{87}\text{Sr}$  ratio of the residual magma may increase gradually in the course of progressive plagioclase crystallization (Jacobsen and Wasserburg, 1984; Hofmann, 1988). Similar to Sm-Nd systematics, the  $\epsilon$  value is used to compare the Sr isotopic ratio of the rock and

corresponding ratio of 'BABI' at the time of crystallization. Epsilon value at present time is expressed as:

$$\epsilon_{UR}^0 = \left[ \frac{(^{87}\text{Sr}/^{86}\text{Sr})_{\text{Measu.}}}{(^{87}\text{Sr}/^{86}\text{Sr})_{UR}} - 1 \right] \times 10^4$$

### 7.2.2 Isotope studies of Shyok suture zone rocks

A total of 22 samples representing different litho-tectonic units, including four samples from Ladakh batholith, have been analyzed for Rb-Sr and Sm-Nd isotopes. The data from the SSZ are highly scattered in both the Rb-Sr or Sm-Nd isotope diagrams and no meaningful age can be extracted from these diagrams (Figs. 7.2, 7.3). However, the data are useful in evaluating the petrogenetic history of the rock units. The variation in isotope ratios in this area may be due to various reasons including source heterogeneity in terms of isotope ratios, extensive crustal contamination, magma mixing, fluid activity and others. Isotopic data of Rb- Sr and Sm- Nd are given in appendix 4.

The intrusive samples of Hundar area do not define collinear array either in the Rb-Sr or Sm-Nd isotope evolution diagrams indicating multiplicity of sources for magmas representing these samples. They have  $\epsilon_{Nd}$  (t =110 Ma) varies from -1.9 to +3.4 while the  $\epsilon_{Sr}$  varies from -4 to +31. The trend shown by these samples in the  $\epsilon_{Nd}$  vs.  $\epsilon_{Sr}$  diagram, plot close to the mantle array and partly with samples with high  $^{143}\text{Nd}/^{144}\text{Nd}$ . The magmas represented by the samples of the Hundar igneous suite appear to be derived from variably enriched sources.

The samples of Ladakh pluton have extended  $\epsilon_{Nd}$  (-7 to +2) and  $\epsilon_{Sr}$  (+2 to +150) values. Few samples of Ladakh batholith plot along with mantle array and leucogranite samples have high  $\epsilon_{Sr}$  and low  $\epsilon_{Nd}$ . These samples probably indicate the melting of part of the arc itself with some influence of older crust such as Higher Himalayan Crystalline (Ahmad *et al.*, 2000). The isotopic age of granite and diorite of Hundar suite is calculated by K-Ar



method and have yielded an age of 64 to 66 Ma, indicating late Cretaceous igneous activity in the area and oldest age data in Hundar area is 65.8 Ma (Thanh *et al.*, 2005). These age data indicate cooling ages for these rocks, thus their crystallization ages will be slightly higher. The presented K-Ar age data for the magmatic rocks of the Hundar intrusives (igneous suite) indicate that these rocks are much older than the dominant magmatic phase (~50-58 Ma) of the Ladakh batholith and therefore could be unrelated (Thanh *et al.*, 2005; Ahmad *et al.*, 2008). The felsic rocks from the Khardung area give the K-Ar ages of 50-51Ma. (Thanh *et al.*, 2005). It indicates that the Khardung volcanics erupted ~16 million years after the igneous activity in Hundar area and probably contemporaneous with magmatism associated with Ladakh batholith emplacement. These age data indicate that subduction related igneous activity in Shyok area took place, at least for, from 64 Ma to 68 Ma before the collision event between Indian and Asian continents.

Limited data on Shyok volcanic sample follow the trends shown by samples of the other suites from this area although they plot along the mantle array with highly variable Sm/Nd and Rb/Sr ratio than CHUR. This indicates that Shyok volcanics may have had a mantle source history. As there are less number of samples the trend is not obvious. However, one sample from the Shyok area shows more depleted  $\epsilon_{Nd}$  value.

Nubra ophiolite mélangé is exposed north of the Karakoram Fault and the basic dykes across the Karakoram Fault appear to be in continuation of basic volcanics of the Nubra ophiolitic mélangé. However, the basic volcanics from the mélangé have positive  $\epsilon_{Nd}$  of +3.3 at 110 Ma, where as the basic dykes along the Karakoram Fault yielded  $\epsilon_{Nd}$  value as -4.9. These  $\epsilon_{Nd}$  values indicate that there are two different episodes of basic magmatism in the Nubra-Karakoram area across the Karakoram Fault and they might have evolved independently.

Rocks with positive  $\epsilon_{Nd}$ , and  $\epsilon_{Sr}$  from Hundar, Nubra, Khardung and Ladakh batholith probably originated from the sources with Sm/Nd and Rb/Sr ratios greater than CHUR values. The elemental characteristics do not agree with the positive  $\epsilon_{Nd}$  and  $\epsilon_{Sr}$  enrichments. This type of enrichment indicates that the isotopic and element ratios are decoupled. The decoupling is possible only due to the enrichment of Rb rather than Sm. Enrichment of Rb in the rock could be due to any heterogeneity in the source. Either it could be incorporated in the source due to mixing with enriched material including aqueous fluids or due to crustal contamination of mantle derived magma during their ascent. Enrichment of trace and REE behavior of the samples from SSZ also agree with the heterogeneity in the source.

The trend shown by the samples of the SSZ in the  $\epsilon_{Nd}$  vs.  $\epsilon_{Sr}$  diagram indicates that these rocks were variably contaminated. Samples from various lithotectonic units of SSZ exhibit a general trend along a line a line indicating mixing of depleted mantle component (DMM) and old crustal component. Most of the samples in the SSZ plot along this mixing line (Fig. 7.4). Leucogranites of Ladakh batholith and granites of Karakoram pluton samples have lower slope and indicate involvement of sediment in the magma generation or contamination of magma by older crust. The mixing line is similar to the mixing hyperbola given by McCulloch and Chappell (1982) and Bignold *et al.* (2006). Karakoram dykes and enclaves, Karakoram pluton and leucogranites of Ladakh plutons are traced towards the crustal component of the mixing line. Sediment derived (S-type) granites are already reported from Ladakh batholiths and Karakoram batholith which is derived from the partial melting of crustal sediments. The isotopic study of the rocks from SSZ indicates source multiplicity, either by mixing of crustal material due to subduction during melting or during the transport of magma to the surface.

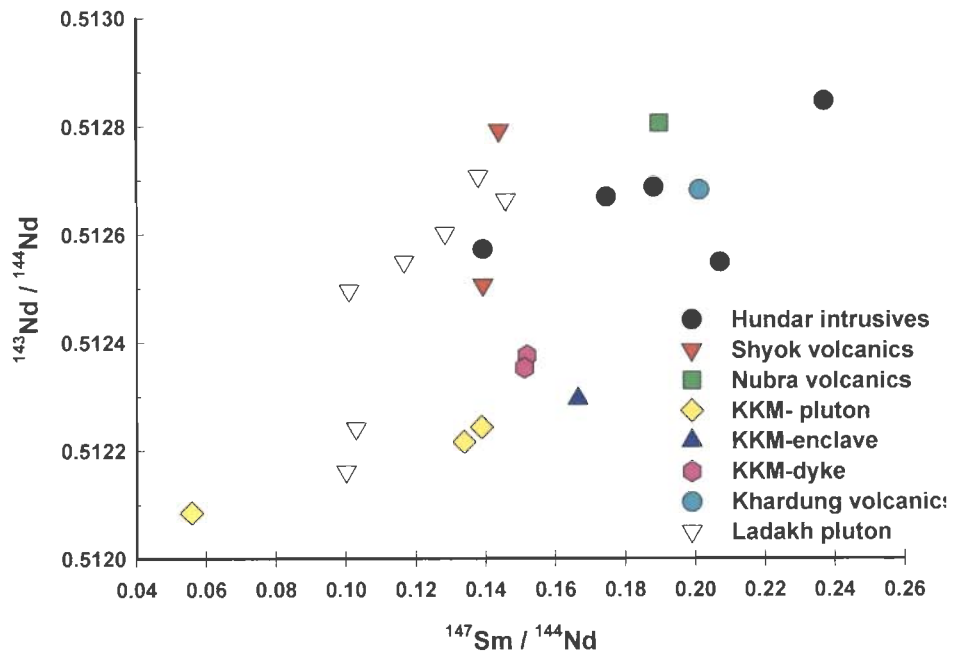


Figure 7.2 No meaningful isochron can be derived from the diagram.

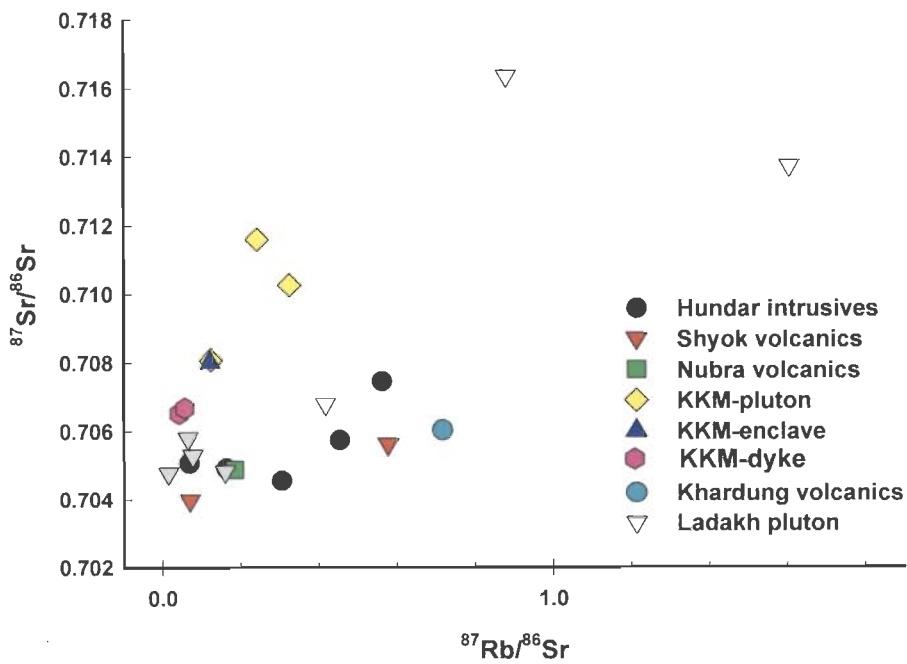
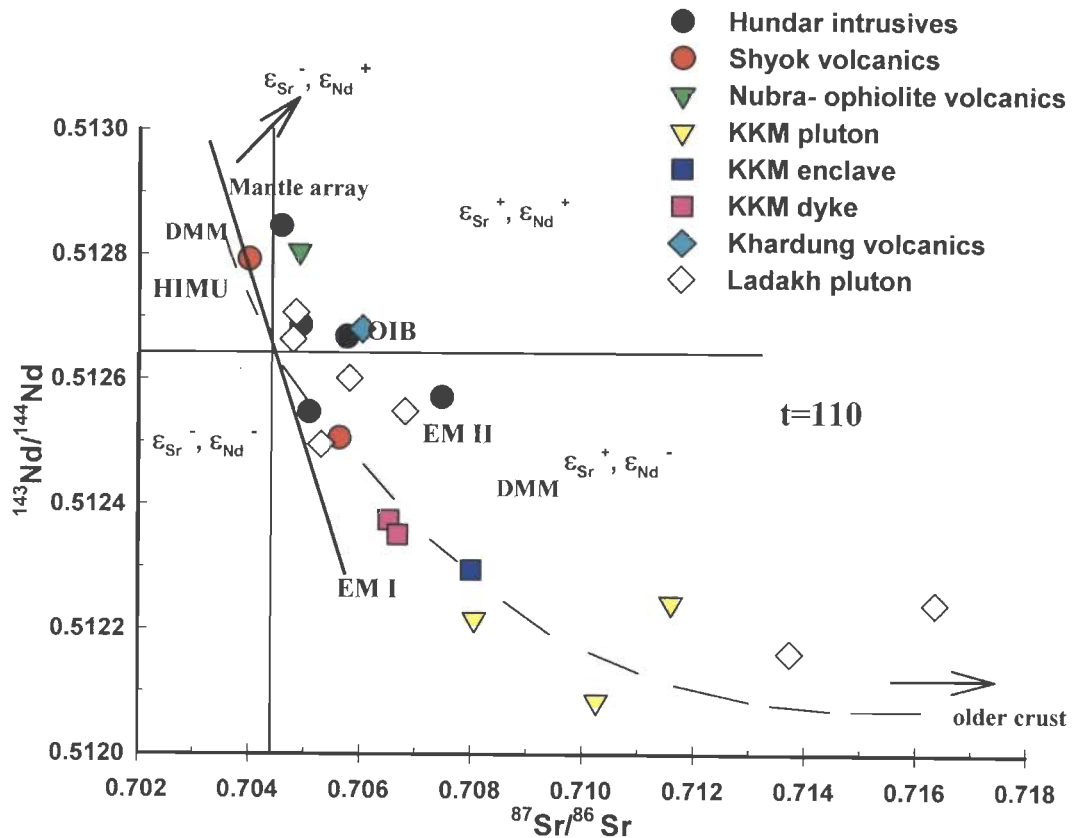


Figure 7.3 No meaningful isochron can be derived from the diagram.



**Figure 7.4** Shows the Sr-Nd isotopic plot of different litho-tectonic units of SSZ. All the rock samples are plotting along the mixing line of depleted mantle source and an older crustal rock. Contamination is obvious in these suture zone samples. KKM in the plot denotes Karakoram area.

### 7.3 COMPARISON WITH ROCKS FROM OTHER TECTONIC SETTINGS

In a Nd vs Sr isotopic plot (Fig .7.5, after Rolland *et al.*, 2000) samples from the Southern Group represents the immature arc tholeiites samples and are plot along the mantle array with high  $^{143}\text{Nd}/^{144}\text{Nd}$  and low  $^{87}\text{Sr}/^{86}\text{Sr}$ . Northern Group represent the back basin between Ladakh and Asian margin and are plotting away from the mantle array with high  $^{143}\text{Nd}/^{144}\text{Nd}$  and high  $^{87}\text{Sr}/^{86}\text{Sr}$  ratios. Kamila amphibolite and Chilas complex are the mafic and ultramafics at the southern part of Kohistan arc. Eastern Ladakh represents the Shyok volcanics of Shyok-Nubra area. Different groups (after Rolland *et al.*, 2000) plot within different quadrants indicate that the rocks from SSZ have

isotopically different source characteristics. Similar distinctions are described by Ahmad *et al.* (2005, 2008) based on trace element ratios. Kohistan island arc rocks which are considered as an intra-oceanic origin (Bignold *et al.*, 2006) are also plotted with the Shyok Suture Zone rocks at  $t = 110$  Ma for comparison (Fig. 7.6). These rocks plot along the mantle array with Shyok volcanics of SSZ.

In cogenetic suites of rocks, if fractional crystallization is accompanied by crustal contamination (AFC), the  $^{87}\text{Sr}/^{86}\text{Sr}$  ratio will increase with increase of  $\text{SiO}_2$ . The rocks from Hundar igneous suit show large variation in  $\text{SiO}_2$ . As the  $\text{SiO}_2$  increases  $^{87}\text{Sr}/^{86}\text{Sr}$  ratio also increases (Fig. 7.7). The  $^{143}\text{Nd}/^{144}\text{Nd}$  ratios also show variation with  $\text{SiO}_2$ . This indicates the possibility of source enrichment and/or crustal contamination.

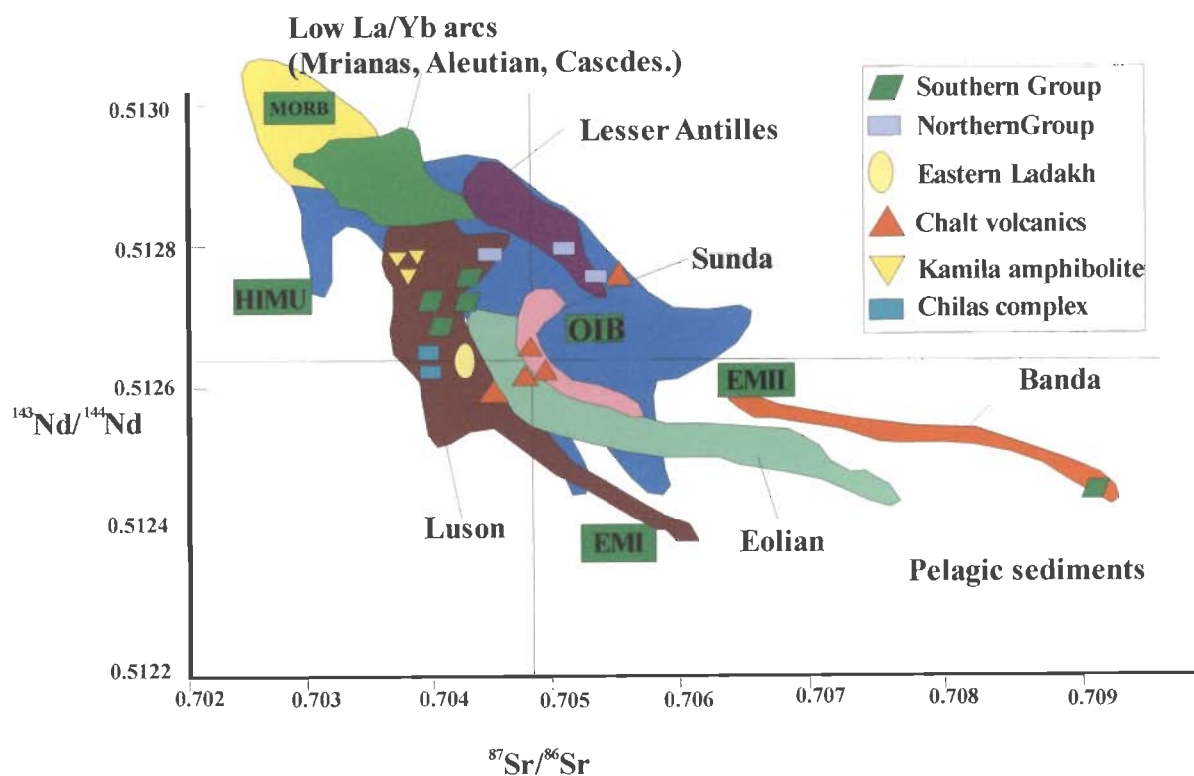


**Figure 7.5** Comparison of isotopic ratios of other tectonic setting and suture zone rocks from Pakistan (modified after Rolland *et al.*, 2000).

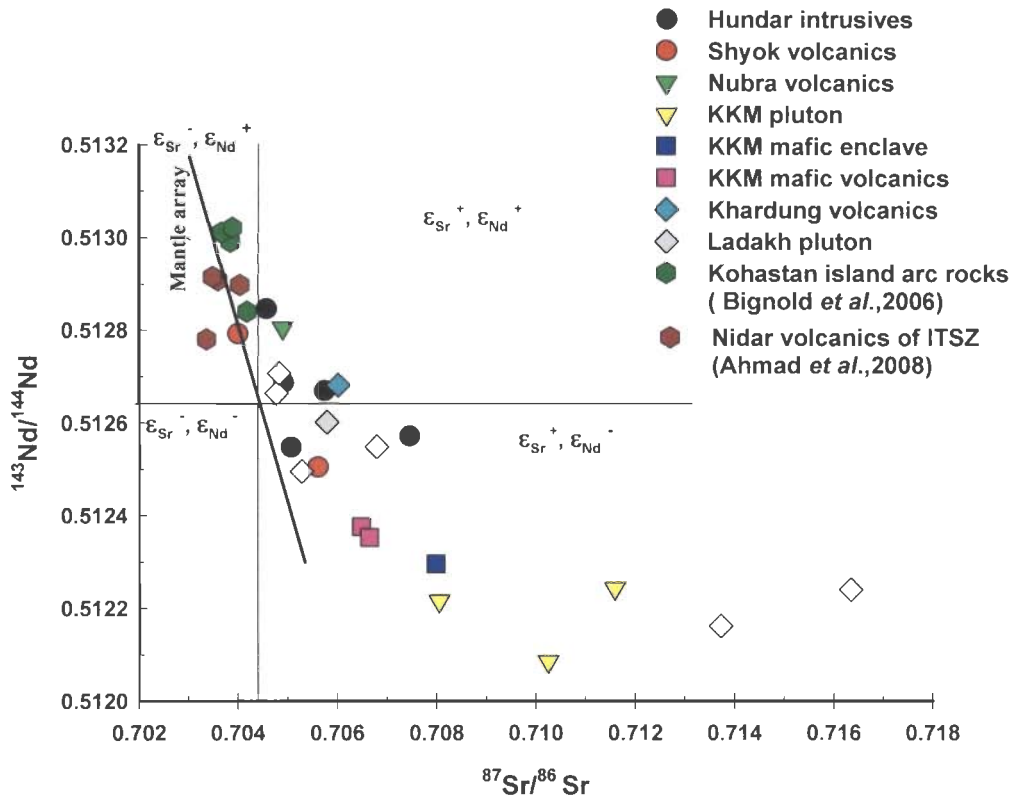


**Figure 7.6** Isotopic ratios of Kohistan island arc rocks along with Shyok suture zone rocks ( $t=110\text{Ma}$ ). KKM denotes Karakoram area

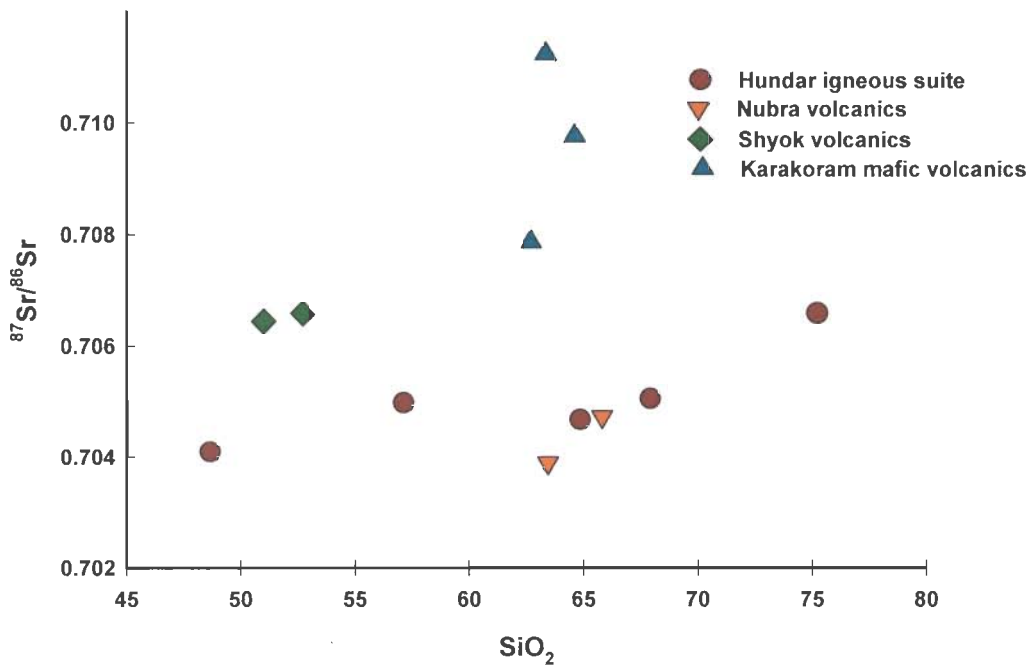


**Figure 7.7**  $^{87}\text{Sr}/^{86}\text{Sr}$  ratio increases with increase of  $\text{SiO}_2$ , indicates the possibility of source enrichment and/or crustal contamination.

## **Chapter 8**

# **DISCUSSION AND CONCLUSIONS**

### 8.1 DISCUSSION OF THE RESULTS

The following are major observations on the geochemical characteristics of the rocks of SSZ

- (1) The SSZ rocks have dominantly calc-alkaline magmatic characteristics.
- (2) These rocks exhibit strong P, Nb, Sr, and Ti anomalies, commonly observed in island arc setting.
- (3) In general, they have higher concentrations of K, Rb, Zr, and Th as compared to Primitive Mantle (P.M.).
- (4) All litho-tectonic units of SSZ show enrichment of LILE and LREEs as compared to Primitive Mantle and Chondrite (C1).
- (5) The Khardung felsic volcanics are SiO<sub>2</sub> rich rocks (dacite and rhyolite) within the calc-alkaline series. The SiO<sub>2</sub> wt% goes up to 78 % in these volcanics.
- (6) Shyok volcanics appear to be more primitive among other rock units from SSZ. They probably represent the initial pulse of magmatism in the SSZ similar to Dras-Nidar volcanics from the ITSZ.
- (7) Nubra and Tsoltak ophiolitic volcanics are similar in petrography and geochemical characteristics.
- (8) Different rocks from Hundar igneous suite display similar REE and isotopic characteristic with Khardung volcanics. This similarity of the plutonic rocks from Hundar and the volcanic rocks from Khardung units strengthen the possibility that they have undergone similar petrogenetic evolution.
- (9) The SSZ rock units exhibit wide range of <sup>87</sup>Sr/<sup>86</sup>Sr and <sup>143</sup>Nd/<sup>144</sup>Nd ratios, indicating geochemical heterogeneity in source region.



- (10) Isotopic ratios of samples from SSZ plot along mixing hyperbola of depleted MORB mantle (DMM) and older enriched continental crust.
- (11) Crustal contamination is obvious in all the rock units. However, it is not clear in Shyok volcanics.

Most of the rocks from SSZ rocks belong to calc-alkaline magma series which is recognized in both island arc and continental arc setting. As these rock units have strong Nb, P and Ti negative anomalies in these rocks indicates stabilization of titanites in subduction zone environment. Two possible subduction settings are intra oceanic (island arc/Mariyana Type) and ocean-continent subduction (active continental margin or Andean type). The volcanism associated with island arc and active continental margins are broadly similar in many aspects, but the passage of magma through the continental crust produces geochemical complexities to the magmatism associated with active continental margins.

The SSZ rock units have higher concentrations of K, Sr, Rb, Zr, Th, and higher LILE-LREE concentrations as compared to P.M. This is a distinct feature of continental margin volcanic suite compared to oceanic island arc magmas. The rock units in the study area also show LILE and LREE enrichment. The enrichment may be due to addition of sediment in the source region or contamination of mantle derived magma during passage through older crust. Interaction of continentally derived sediments with magma in the source region is also possible in island arc setting. In most of the cases it is impossible to separate the effects of crustal contamination and sediment input in the magma/source. Geochemical and isotopic characteristics of the rock units indicate crustal/sediment involvement as a major petrogenetic process.

The Shyok volcanics appear to be more primitive rock unit in the study area. The LILE and LREE enrichment in these volcanics are relatively less compared to other litho-

tectonic units. These volcanics show geochemical similarities with Dras and Nidar volcanics of ITSZ rocks which represent the initial pulses of the arc magmatism in Kohistan-Ladakh area (comparison is given in the following section). Nubra and Tsoltak volcanics associated with ophiolitic mélanges are similar in petrography and geochemistry. Major, trace and REE characteristics of these volcanics indicate that these are possibly same units but probably separated due to movement along the Karakoram Fault.

Published age data from Hundar and Ladakh indicate that the rocks from Hundar igneous suite are older (65.8 Ma) than the major magmatic episode of the Ladakh plutons (55Ma) Field relation also indicates that Ladakh batholith (granitoid) has intrusive relationship with Hundar igneous suite. Hundar igneous suite which ranges in composition from gabbro to granite shows similar REE and isotopic characteristics as Khardung volcanics. These characteristics suggest similar petrogenetic histories. Khardung volcanics give a younger K-Ar age data (~50 Ma) than Hundar igneous suite, but contemporaneous with Ladakh batholith.,

## **8.2 COMPARISON OF SHYOK AND INDUS SUTURE ZONE ROCK UNITS**

The ITSZ is compared with similar rock units from SSZ to evaluate relation between the two suture zones. For this purpose, the volcanic rocks associated with the ophiolite mélanges from both the suture zones are considered. The ITSZ is represented here by the mafic volcanic rocks associated with Nidar ophiolite sequence and the SSZ is represented by the volcanic rocks such as Nubra mélange volcanics and Tsoltak mélange volcanics associated with Nubra-Tsoltak ophiolite mélange. Based on geochemical and isotopic data Ahmad *et al.* (2005, 2008) have demonstrated that Nidar ophiolite was emplaced in

an intra-oceanic subduction environment whereas the SSZ ophiolite volcanics were emplaced in an Andean type tectonic setting.

Nb, Zr and Y are equally immobile during extreme degree of alteration and thus their ratios are unaffected. Hence, these elements and their ratios are used for the comparison. Figs. 8.1 and 8.2 show Zr/Nb-Zr/Y ratio plots of different ophiolite mélanges of ITSZ and SSZ in adjacent areas (Ahmad *et al.*, 2008). Within the Zildat ophiolites the rock units display two trends; one group with restricted Zr/Nb ratio and another with large variation in Zr/Y ratio. Shergol and Zildat ophiolites represent E-MORB-OIB type rocks and indicate the origin at varying depth. The rocks from Nidar ophiolites, have restricted Zr/Y ratio and variable Zr/Nb ratio and represent N-MORB, island arc volcanics and gabbros (Ahmad *et al.*, 2008). The SSZ rock units from east and west of Ladakh batholith form separate group which do not follow any of the trends shown by ITSZ rocks.

Volcanic rocks associated with the ophiolite mélange from Nubra and Tsoltak areas do not fall within the field defined by the rock units from ITSZ, but Shyok volcanics shows similar geochemical pattern to that of Nidar ophiolite volcanics (Fig. 8.3). In La-Y diagram (Fig. 8.4), plot, the rocks of intermediate composition and mafic volcanics of SSZ are plotted along with the same rock types from ITSZ. Shyok volcanics follow the similar trend of Nidar volcanics with restricted La with some variation in Y.

The rocks from Nidar ophiolite of ITSZ show restricted variation of the REE abundance, whereas the SSZ rocks show wide variation. Chondrite normalized REE pattern of Nidar volcanics shows flat to slightly depleted LREE patterns with less fractionation (Fig. 8.5). Shyok volcanics show similar geochemical characteristics as the Nidar volcanics, but the REE pattern is slightly enriched and comparatively more differentiated (Fig. 8.6) Mafic volcanics from Nubra and Tsoltak ophiolite mélange of SSZ show similar LREE enriched pattern (Figs. 8.7, 8.8).

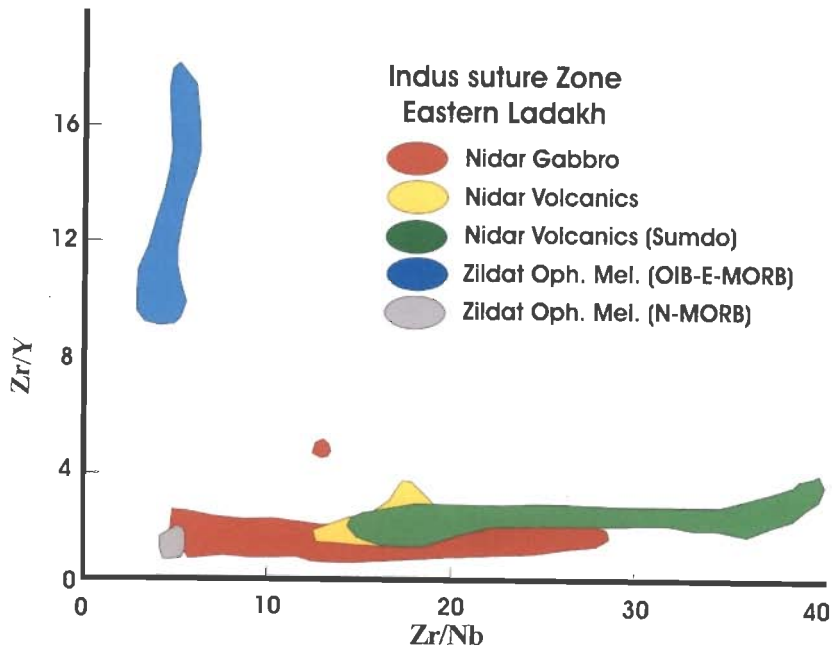


**Figure 8.1** Zr/Nb vs. Zr/Y plot shows Nidar and Zildat ophiolites of ITSZ. Gabbro and volcanics from Nidar ophiolites have wide Zr/Nb with restricted Zr/Y ratios. Ophiolite rocks from Zildat have restricted Zr/Nb ratios with wide range of Zr/Y ratios (after Ahmad *et al.*, 2008).

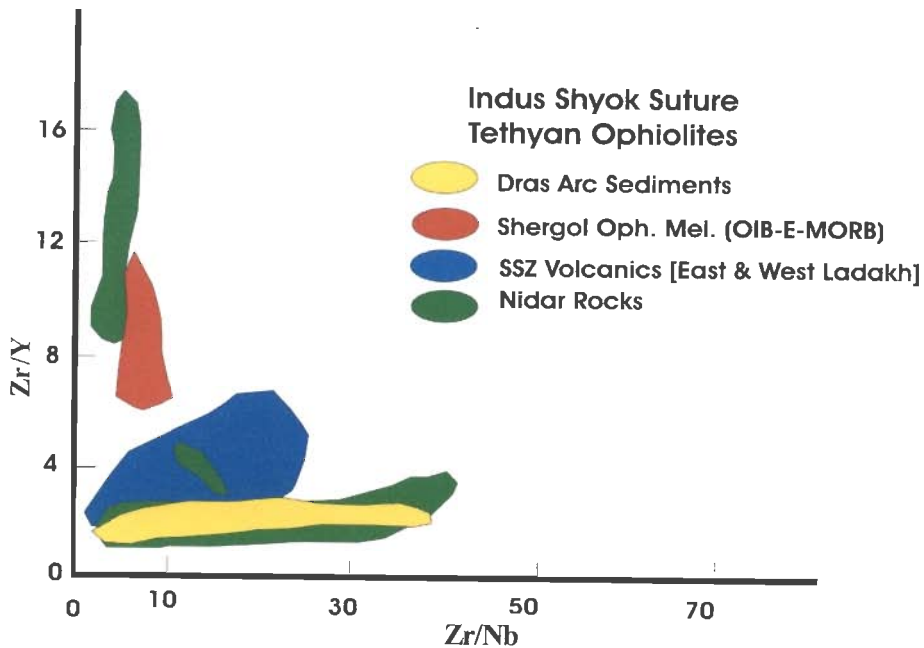


**Figure 8.2** Zr/Nb vs. Zr/Y plot shows Nidar and Zildat ophiolites of ITSZ along with SSZ volcanics. A group of rocks from Nidar ophiolite and the Dras arc sediments have wide Zr/Nb with restricted Zr/Y ratios. Ophiolite rocks from Zildat and Shergol have restricted Zr/Nb ratios with wide range of Zr/Y ratios. SSZ volcanics from eastern and western Ladakh area are not following both these trends (after Ahmad *et al.*, 2008).

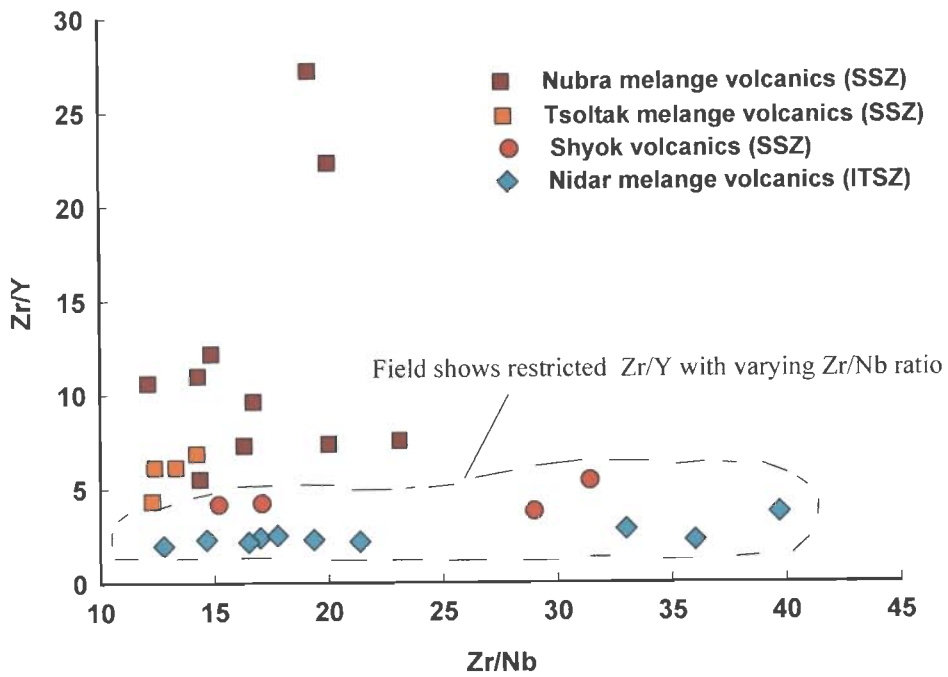


**Figure 8.3** Zr/Nb vs. Zr/Y plot shows comparison of Nidar ophiolites of ITSZ and Tsoltak, Nubra and Shyok volcanics of SSZ. Field outlined with dashes indicates arc-N-MORB field after Ahmad *et al.* (2008).

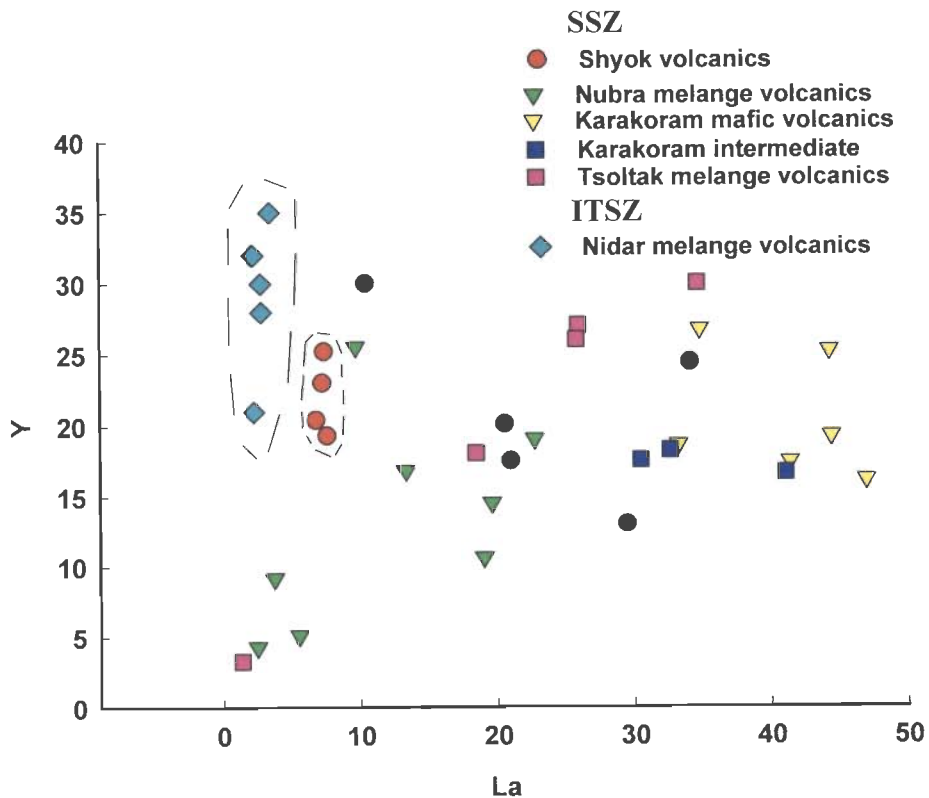


**Figure 8.4** La vs. Y plot shows comparison between intermediate and mafic volcanic rocks from SSZ and ITSZ. Shyok volcanics from SSZ show similar trend with Nidar volcanics from ITSZ. Shyok and Nidar volcanics have restricted La with wide range of Y.

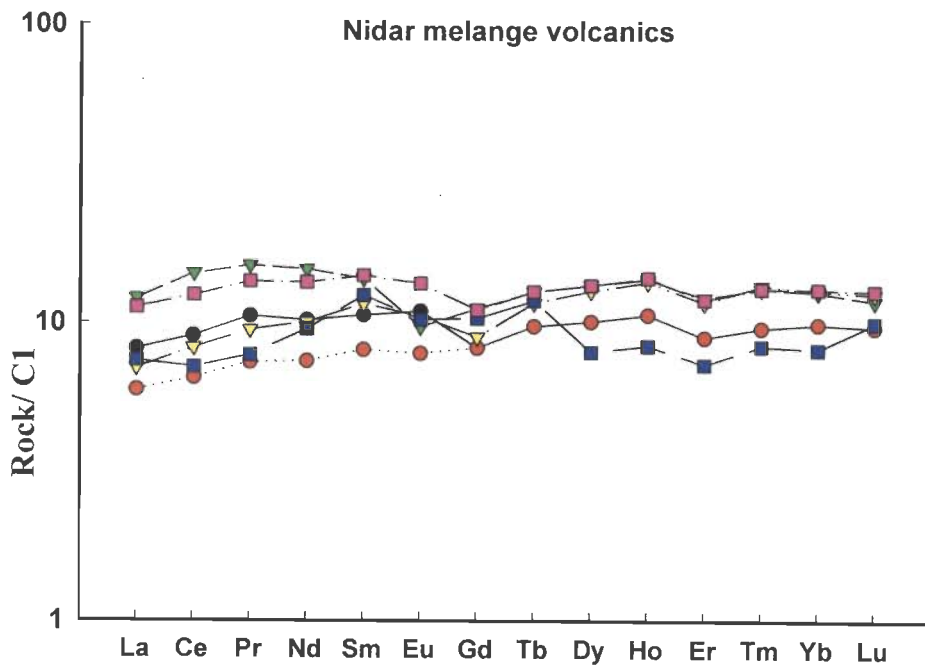


**Figure 8.5** Chondrite normalized REE pattern of Nidar mafic volcanics (Ahmad *et al.*, 2008). Show slightly depleted LREE pattern with less differentiation

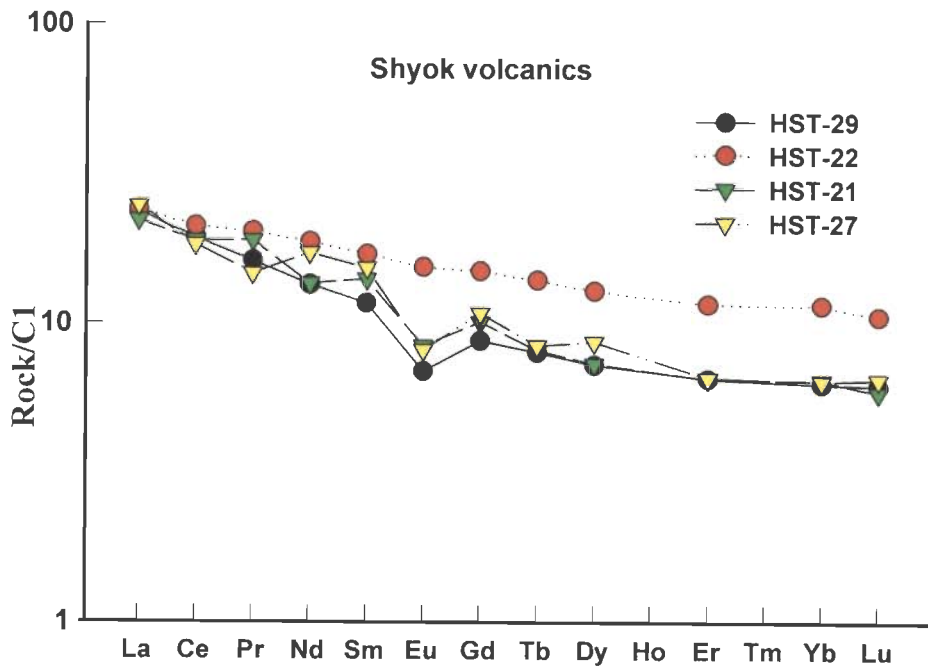


**Figure 8.6** Chondrite normalized REE pattern of Shyok volcanics shows enriched and more differentiated pattern compared to Nidar ophiolite volcanics.

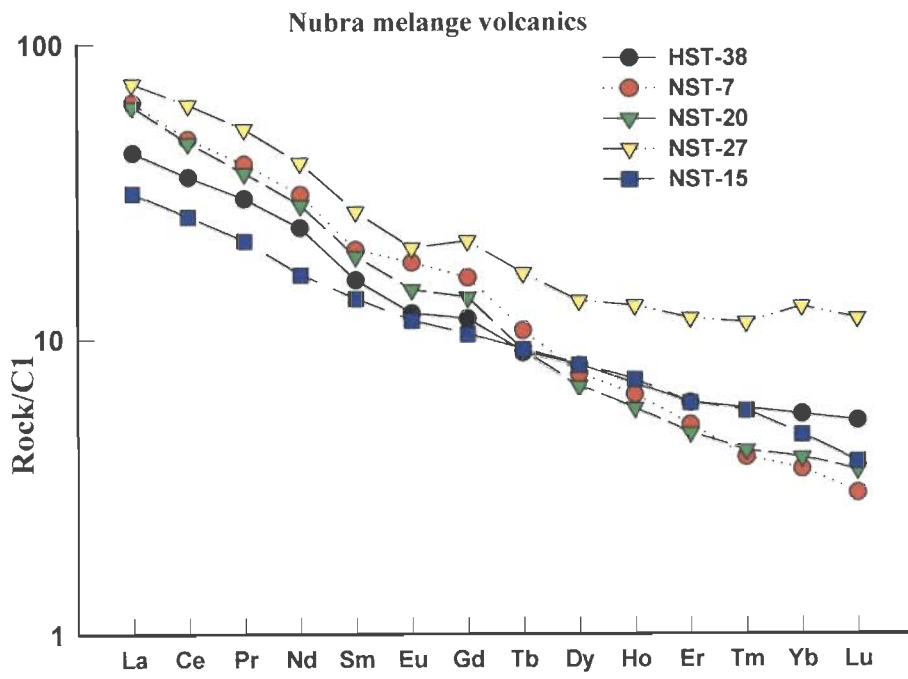


**Figure 8.7** Chondrite normalized REE pattern of Nubra mélangé volcanics show highly enriched and differentiated pattern compared to Nidar ophiolite volcanics from ITSZ.

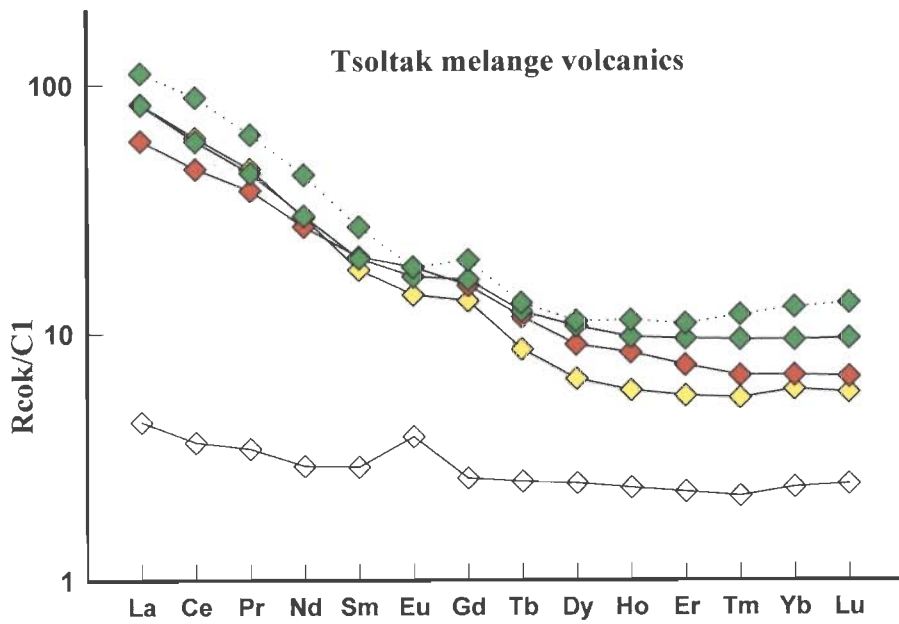


**Figure 8.8** Chondrite normalized REE pattern of Tsoltak mélangé volcanics show highly enriched pattern compared to Nidar ophiolite volcanics.

Nb and Ce are more incompatible than Zr and Y for mantle phases. Thus the smallest degree of melt will show the largest values of Ce/Y and the smallest values of Zr/Nb. Zr/Nb-Ce/Y ratio plot (Fig. 8.9) for the ITSZ rocks (Chalt and Jutal groups) suggest that they are associated with intra-oceanic subduction (Clift *et al.*, 2000). The Khardung group with higher Ce/Y values indicates Andean type setting during collision. Range of higher Ce/Y values in Kohistan batholith suggest transition from intra-oceanic to Andean type setting. Fig. 8.10 shows higher Ce/Y ratios for Nubra, Tsoltak and Khardung volcanics of SSZ and plot within the field defined for Andean type arc setting by Clift *et al.* (2000). Ahmad *et al.*, (2005, 2008) also suggest that the Nidar ophiolite volcanics originated in an intra-oceanic tectonic set up. These evidence indicate that the SSZ is formed in a different tectonic setting, probably represent an Andean type rather than an intra-oceanic island arc setting

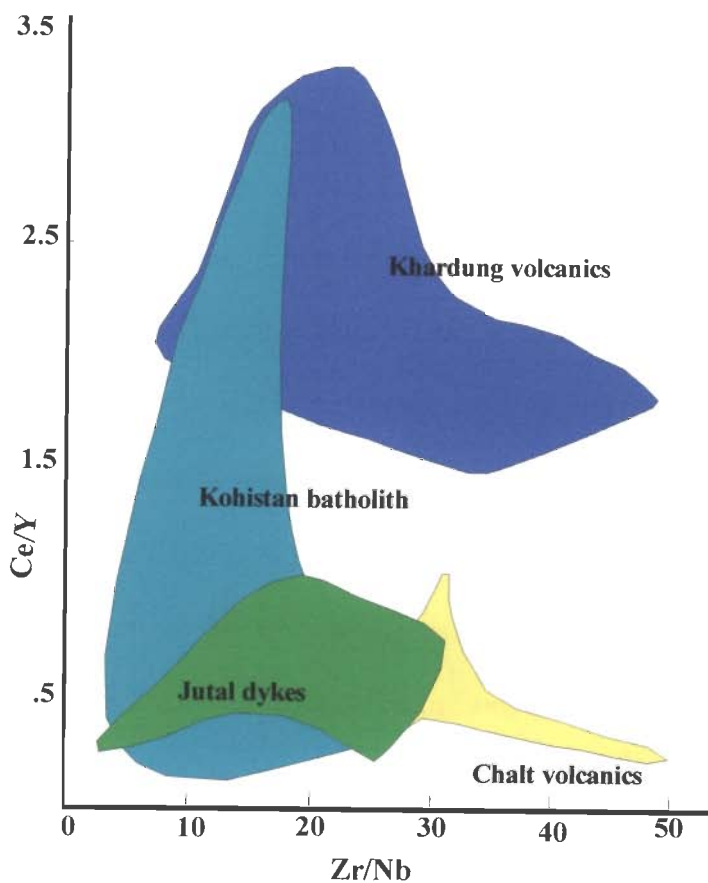
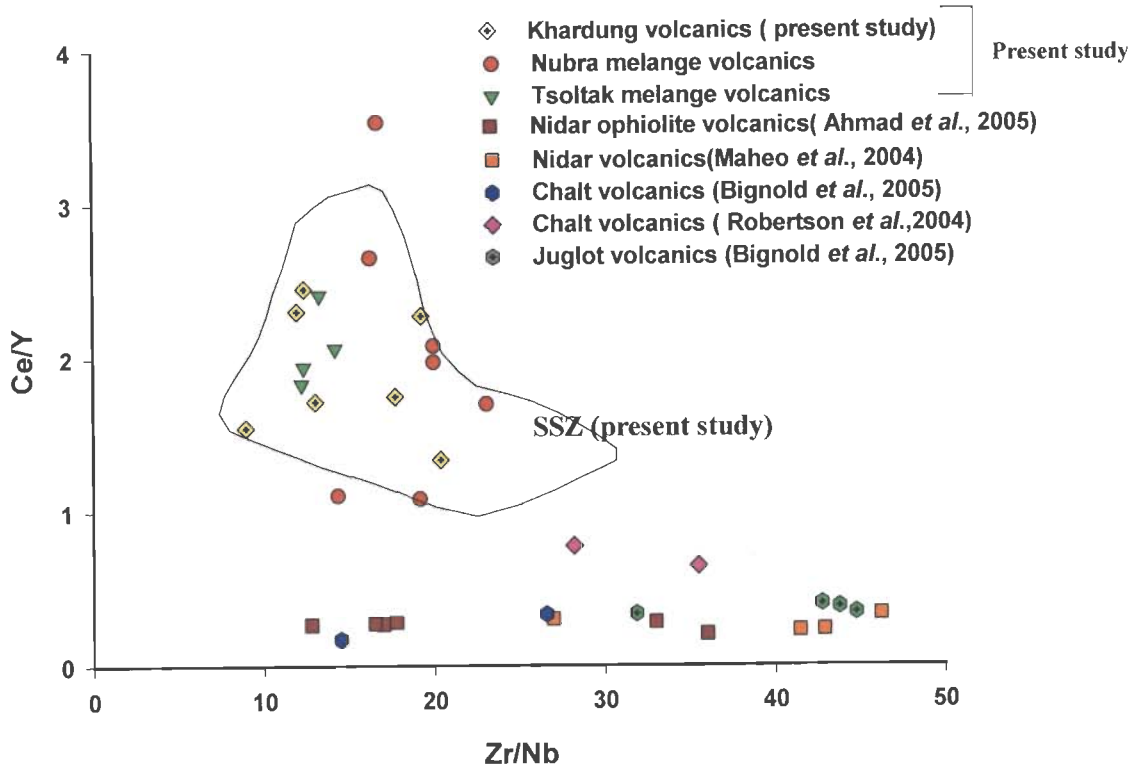


Figure 8.9 Zr/Nb vs. Ce/Y plot of volcanics from ITSZ and SSZ (Clift *et al.*, 2000)





**Figure 8.10** Zr/Nb vs. Ce/Y plot of volcanics from ITSZ and SSZ. The volcanic rocks from ITSZ are not plotting in the field defined (by Clife *et al.*, 2000) for Andean type arc setting with high Ce/Y ratio.

The REE pattern of Shyok volcanics, Nubra volcanics and Tsoltak volcanics of the present area are compared with that of Nidar volcanics of the ITSZ in Figs. 8.5-8.8. As the rock units from SSZ and ITSZ exhibit diverse geochemical characteristics they might have formed in different tectonic set up. The dominant factors that control the geochemical characteristics of the magmas in the SSZ are an enriched source composition and/or crustal influence in the magma genesis. Enrichment of the mantle source is considered to have occurred by incorporation of subducted sediments into the mantle wedge above a subducted slab of Indian lithosphere during India–Asia convergence, or enrichment occurred during the ascent of magma through the continental crust. As the

ITSZ is formed in intra-oceanic regime, the enriched source characteristics of SSZ indicate that it is formed in an Andean type setting.

Rare earth element modelling indicates enrichment of LREE in the melt derived from the mantle peridotites. Since the REE abundance of mantle peridotite is low, the addition of a hydrous fluid containing a large amount of light REEs and LILE ions may change the REE signature of the rock, resulting in light REE enrichment and an increase in total REE. The enrichment may also be due to different geological processes, crustal contamination of the mantle derived source, later metasomatism of the arc by the fluids released during the subduction of oceanic crust and addition of subducted sediments to the source. In an ocean–continent subduction, crustal contamination during the extrusion is also a possible process that can add higher LREE and LILE contribution to the rock. When a hot magma moves up into the crust, some of the low melting components may mobilize and are likely to be incorporated in the magma.

It has been shown by Ahmad *et al.* (2008) that, the geochemical evolution of the arc magma of the ITSZ changes from initial mafic (Dras-Nidar) to more intermediate (Ladakh batholith) to more felsic magmatism at the final stages (Khardung volcanics). However, the relation between Hundar igneous suite, Khardung volcanics and Ladkh batholith is not properly established. Figs. 8.11 and 8.12 show similar REE pattern of Hundar and Khardung units. Hundar igneous suite represents intrusive plutonic rocks and Khardung volcanics of the study area occurs as pyroclastic flow with very high SiO<sub>2</sub> content (up to 76%) varying in composition from dacite to rhyolite. Isotopic study and petrogenetic modelling indicate that the Khardung volcanics and Hundar intrusives are derived by the melting of part of the older oceanic arc itself. Recycling of the arc may be responsible for the enrichment of the traces and isotopes of these rock units. The assumed source composition for petrogenetic modelling matches with the mixed source of depleted

arc component (equivalent to Shyok volcanics or Dras volcanics) from the Ladakh-Kohistan arc and sediments (equivalent to more evolved calc-alkaline component of the arc). The rock units; Hundar and Khardung therefore indicate the maturation of the oceanic arc towards south of the SSZ.

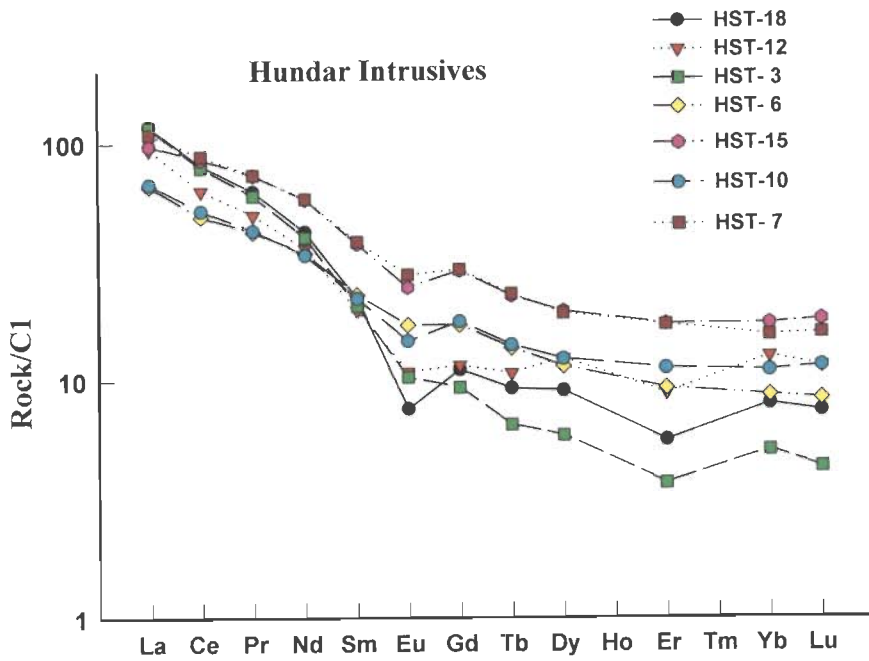


Figure 8.11 C1 normalized REE pattern of Hundar igneous suite/intrusives

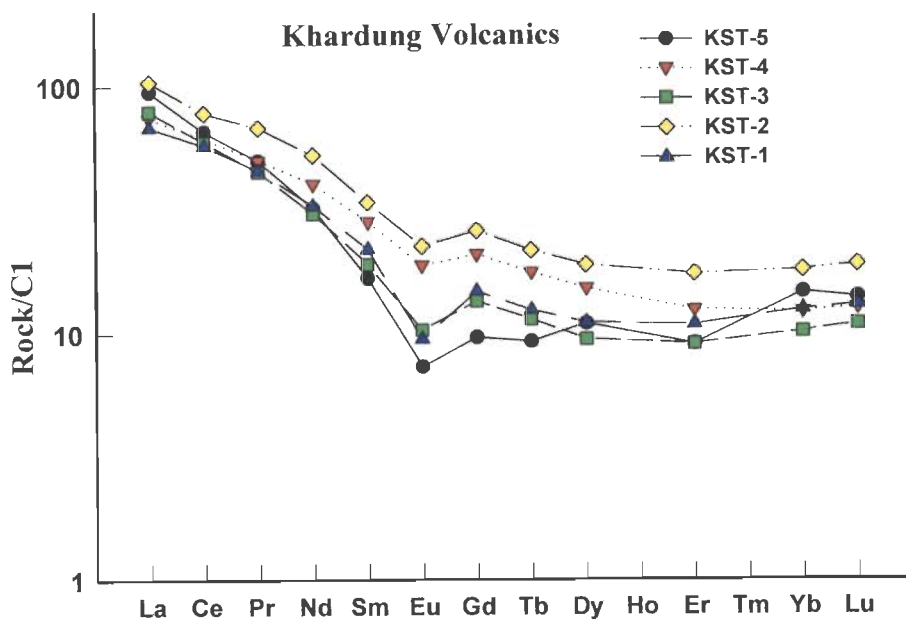


Figure 8.12 REE pattern of Khardung volcanics is similar to Hundar igneous suite.

## 8.3 CONCLUSIONS

### (a) Geochemical implications

- 1) Petrogenetic modelling indicates that the SSZ rocks could have been generated by partial melting of peridotite of the mantle wedge with the influx of aqueous fluid.
- 2) Involvement of subducted sediment at the source region during melting or crustal contamination during transport of the magma to the surface appears to be responsible for LILE-LREE enrichment.
- (3) Fluid released during the subduction of the oceanic crust also played important role in the mobility of elements.
- (4) Recycling of the arc is responsible for the enrichment of trace elements and isotopes in the rock units, which represent different stages of maturation of the island arc.
- (5) Geochemical similarity of Shyok volcanics with the rock units from ITSZ indicates that they are the initial pulses of the arc magmatism. Shyok volcanics form the base for more evolved calc-alkaline arc components.
- (6) Similarity in geochemical characteristics petrogenetic evolution and petrography indicate the possibility that Nubra and Tsoltak are part of same ophiolite mélange that are now separated due to the movement along the Karaoram Fault.
- (7) Isotopic study of the rocks from SSZ indicates isotopically heterogeneous source, either by mixing of older crustal material with depleted mantle source, when the melting of source during subduction or during the transport of magma to the surface.

### (b) Geodynamic implications

- (1) ITSZ represents an intra-oceanic setting where as the SSZ represents an Andean type setting.
- (2) There is no indication of back-arc magmatism in the study area although continental arc and back arc basin are reported from the Pakistan and Tibet areas. It indicates that

the more mature arc and back-arc setting is probably displaced along the Karakoram Fault towards east which gives an apparent impression that the back-arc basin closes towards east.

- (3) The rock units exposed in the study area probably represent the fore arc and the accretionary complex of an Andean type setting.
- (4) Isotopic and geochemical characteristics suggest that Khardung volcanics and Hundar igneous suite are formed by melting of arc components from primitive Kohistan-Ladakh island arc. Hundar, Ladakh and Khardung magmatism represent the maturation of the island arc. Major episode of Ladakh magmatism occurred after the magmatism in Hundar area, where as the Khardung forms the acidic pyroclastic flow when the Ladakh batholith was emplaced at deeper level.

The evidence enumerated here confirm that an active continental margin (Andean type subduction) existed between the Kohistan-Ladakh and Karakoram during Cretaceous time. Shyok volcanics may be the basement on which the calc-alkaline arc evolved. The arc and back arc basin is well exposed in the northern (Pakistan) area; where as in the Indian part, because of the Karakoram Fault more mature arc and the back-arc unit have shifted towards NE (Lhasa side) which looks more like a narrow back-arc basin closing towards SE as described by Rolland *et al.* (2000, 2002). Phillips *et al.* (2004) show that the SSZ extends further towards east. The rock units exposed in the study area therefore represent fore arc and the accretionary complex of an Andean type setting.

Tectonic evolution of SSZ is depicted Fig. 8.13 in which there is intra-oceanic subduction within the Neo-Tethys ocean gave in to Kohistan-Ladakh batholith (Fig. 8.13a). The northern part of the oceanic crust subducts beneath the Eurasian plate along the SSZ and gave rise to the Shyok volcanics and Karakoram batholith (Fig. 8.13b). Fig.

8.13c represents present-day scenario of SSZ and remnants of the obducted oceanic crust preserved as the ophiolites in ITSZ

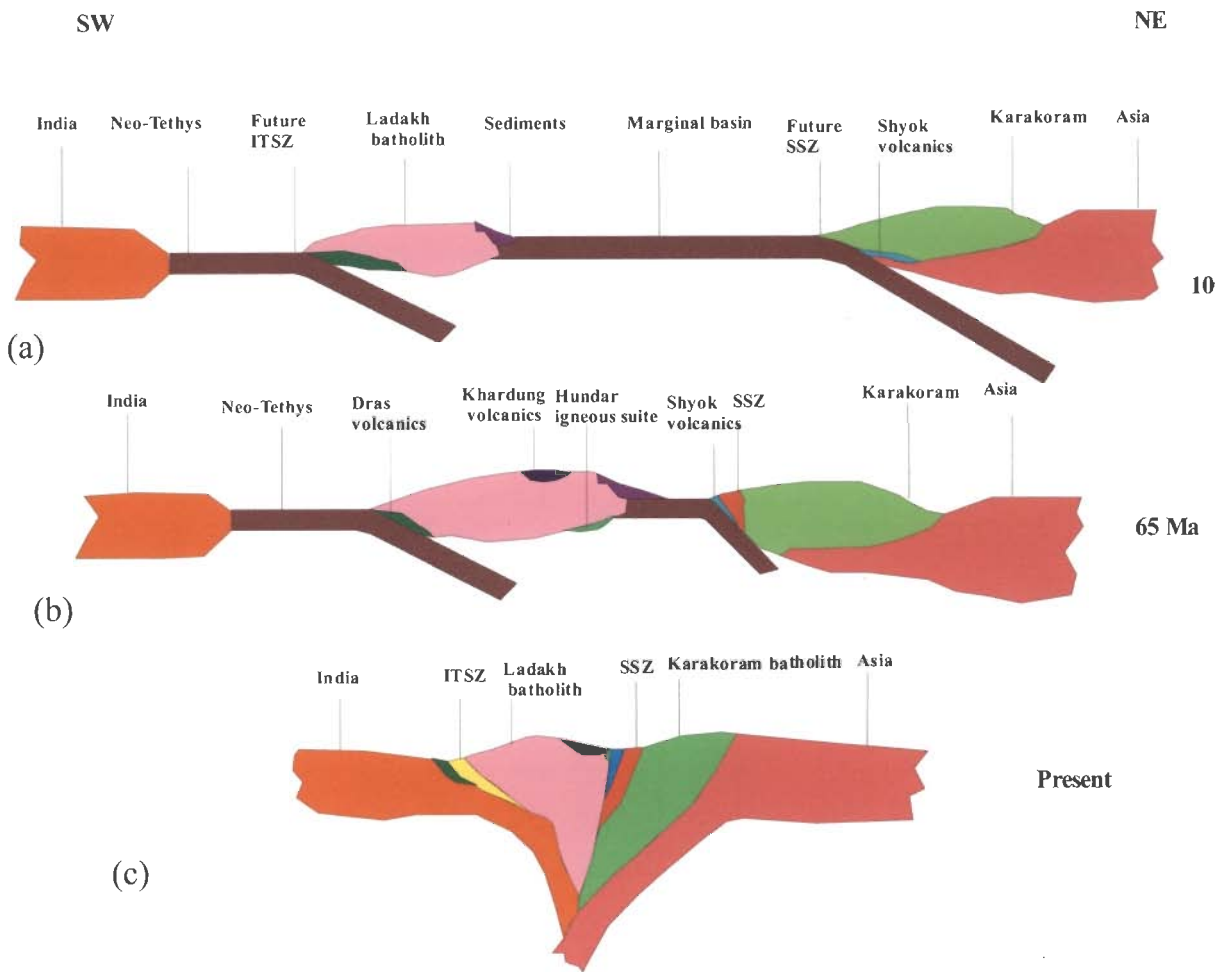


**Figure 8.13** Tectonic evolution of Shyok Suture Zone (modified after Dunlap and Wysoczanski, 2002 and Ahmad *et al.*, 2008).

## **REFERENCES**

## REFERENCES

- Ahmad, T., Harris N.B.W., Tanaka, T., Bickle, M.J., Chapman, H., Khanna, P.P., Bunbury, J., 2003. Nd-Sr isotopic and geochemical constrains on the source characteristics and petrogenesis of arc volcanics from the Shyok Suture Zone, Ladakh, India. In: Himalayan Tectonics (The HIMPROBE results), IIT Roorkee 10-13.
- Ahmad, T., Harris, N.B.W., Bickle, M., Chapman, H., Bunbury, J., Prince, C., 2000. Isotopic constraints on the structural relationships between the Lesser Himalayan Series and the High Himalayan Crystalline Series, Garhwal Himalaya. *Geol. Soc. Am. Bull.* 112, 467-477.
- Ahmad, T., Harris, N.B.W., Islam, R., Khanna, P.P., Sachan, H.K., Mukharjee, B.K., 2005. Contrasting mafic magmatism in the Shyok and Indus Suture Zones: Geochemical constraints. *Him. Geol.* 26, 33-40.
- Ahmad, T., Islam, R., Khanna, P. P., Thakur, V.C., 1996. Geochemistry, Petrogenesis and tectonic significance of the basic volcanic units of the Zildat ophiolitic mélange, Indus suture zone, eastern Ladakh (India). *Geody. Acta* 9, 222-233.
- Ahmad, T., Mukherjee, P.K. and Trivedi, J.R., 1999. Geochemistry of Precambrian mafic magmatic rocks of the western Himalaya, India: Petrogenetic and tectonic implications. *Chem. Geol.* 160, 103-119.
- Ahmad, T., Thakur, V.C., Islam, R., Khanna, P.P., Mukherjee, P.K., 1998. Geochemistry and geodynamic implications of magmatic rocks from the Trans-Himalayan arc. *Geochem. J.* 32, 383-404.
- Ahmad, T., Tanaka, T., Sachan, H.K., Asahara, Y., Islam, R., Khanna, P.P., 2008. Geochemical and isotopic constraints on the age and origin of the Nidar Ophiolitic Complex, Ladakh, India: Implications for the Neo-Tethyan subduction along the Indus suture zone. *Tectonophysics* 451, 206–224.
- Albarede, F. Brouxel, M., 1987. The Sm/Nd secular evolution of the continental crust and the depleted mantle. *Earth Planet. Sci. Lett.* 82, 25-35.
- Allègre, C.J., 1984. Structure and evolution of the Himalaya-Tibet orogenic belt. *Nature* 145, 17-22.



- Allegre, C.J., Ben Othman, D., 1980. Nd-Sr isotopic relationship in granitoid rocks and continental crust development: a chemical approach to orogenesis. *Nature* 286, 335-342.
- Allegre, C.J., Rousseau, D., 1984. The growth of the continental through geological time studied by Nd isotope analysis of Shales. *Earth Planet. Sci. Lett.* 67, 19-34.
- Ananad, R., 2007. Geochemical and geochronological studies on metavolcanics of the Hutti Schist Belt and granitoids around the schist belts of the Eastern Dharwar Craton, India. Unpubl. Ph.D thesis. University of Pondicherry, Pondicherry.
- Arculus, R.J., Powell, R., 1986. Source component mixing in the regions of arc magma generation. *J. Geophys. Res.* 91, 5913–5926.
- Argand, E., 1924. La tectonique de l' Asie. International Geological Congress Report Session 13, 170–372.
- Armstrong, R.L., 1968. A model for the evolution of strontium and lead isotope in a dynamic Earth. *Rev. Geophy.* 6, 175-199.
- Atchison, J.C., Ali, J.R., Davis, A.M., 2007. When and where did India and Asia collide?. *J. Geophy. Res.* 112, 139-160.
- Auden, J.B., 1935. Transverse in the Himalayas. *Rec. Geol. Surv. India* 69, 123-167.
- Balakrishnan, S., Rajamani, V., 1987. Geochemistry and petrogenesis of granite gneisses around the Kolar schist belt, South India: Constraints for the evolution of the crust in the Kolar area. *J. Geol.* 95, 219-240.
- Balram, V., Ramesh, S.L., Anjaniah, K.V., 1995. Comparative study of sample decomposition procedure in the determination of trace and rare earth elements in anorthosite and related rocks by ICP-MS. *J. Analy. Chem.* 353, 176-182.
- Banno, S. Matsui, Y., 1973. On the formulation of partition coefficient for trace element distribution between minerals and magma. *Chem. Geol.* 11, 1-15.
- Barnicoat, A.C., Trealar, P.J., 1989. Himalayan metamorphism-an introduction, *J. Metamorph. Petrol.* 7, 3-8.
- Beard, J.S., Lofgren, G.E., 1991. Dehydration melting and water saturated melting of basaltic and andesitic greenstones and amphibolites at 1, 3 and 6.9 kb. *J. Petrol.* 32, 365–401.
- Beck, R.A., Burbank, D.W., Sercombe, W.J., Riley, G.W., Barndt, J.K., Berry, J.R., Afzal, J., Khan, A.M., Jurgen, H., Metje, J., Cheema, A., Shafique, N.A., Lawrence, R.D., Khan, M.A., 1995. Stratigraphic evidence for an early collision between northwest India and Asia. *Nature* 375, 55-58.

- Bedard, J., 1994. A procedure for calculating the equilibrium distribution of trace elements among the minerals of cumulate rocks, and the concentration of trace elements in the coexisting liquids. *Chem. Geol.* 118, 143-153.
- Besse, J. Courtillot, V., 1984. Paleomagnetic estimates of crustal shortening in the Himalayan thrusts and Zangbo suture, *Nature* 311, 621-626.
- Bhandari, A.K., Srimal, N., Redcliff, R.P., Srivastava, D.K., 1978. Geology of part of Shyok and Nubra valleys, Ladakh District, J& K-a preliminary report. Abstract, 9<sup>th</sup> Sem. Him. Geol. Dehradun.
- Bhargava, O.N., Bassi, U.K., 1999. Western Himalaya Tethyan Eocambrian-Mesozoic basin and events. In: *Geodynamics of the NW Himalaya*. Jain, A.K., Manickavasagam, R.M. (Editors). *Gond. Res. Group Mem.* 6, 51-59.
- Bhat, M.I., Le Fort, P., 1992. Sm-Nd age and petrogenesis of Rampur metavolcanic rocks, NW Himalaya: Late Archaean relics in the Himalayan belt. *Precamb. Res.* 56, 191-210.
- Bhatia, S.B., Bhargava, O.N., 2006. Biochronological continuity of the Paleogene sediments of the Himalayan Foreland Basin: palaeontological and other evidences. *J. Asian Earth Sci.* 26, 477-487.
- Bilchert, J.S., 1993. Manual for Sr and Nd isotope Gechemistry, Unpubl. manual, Copenhagen.
- Bignold, S.M., Treloar, P.J., Petford, N., 2006. Changing sources of magma generation beneath intra-oceanic island arcs: An insight from the juvenile Kohistan island arc, Pakistan Himalaya. *Chem. Geol.* 233, 46-74.
- Blattner, P., Dietrich, V., Gansser, A., 1983. Contrasting O<sup>18</sup> enrichment and origins of High Himalaya and Trans Himalaya intrusives. *Earth Planet. Sci. Lett.* 65, 276-286.
- Bowen, N.L., 1928. *The evolution of the igneous rocks*. Princeton University Press, Princeton. 332.
- Bowen, N.L., 1941. Certain singular points on crystallization curves of solid solutions. *Nat. Acad. Sci. Proc.* 27, 301-309.
- Brookfield, M.E, Reynolds, P.H., 1990. Moicene <sup>40</sup>Ar/<sup>39</sup>Ar ages from the Karakoram Batholith and Shyok mélangé, northern Pakistan, indicate late Tertiary uplift and southward displacement. *Tectonophysics*, 172, 155-168.

- Brookfield, M.E., Reynolds, P.H., 1981. Late Cretaceous emplacement of the Indus suture zone ophiolitic mélanges and an Eocene-Oligocene magmatic arc on the northern edge of the Indian plate. *Erath Planet. Sci. Lett.* 55, 157-162.
- Burchfiel, C.B., Chen, Z., Hodges, K.V., Liu, Y., Royden, L.H., Deng, C., Xu, J., 1992. The South Tibetan Detachment System, Himalayan Orogen: Extension Contemporaneous with and Parallel to Shortening in a Collisional Mountain Belt. *Geol. Soc. Am. Spec. Paper* 269, 41.
- Burchfiel, C.B., Royden, L.H., 1985. North-South extension within the convergent Himalayan region. *Geology* 13, 679-682.
- Burg, J.P., 1983. Carte Géologique du Sud du Tibet. Ministry of Geology Cent. Nat. Res. Sci. Paris 420, 123-130.
- Burg, J.P., Chen, G.M., 1984. Tectonics and structural zonation of southern Tibet, China. *Nature* 311, 219-223.
- Cannat, M., Mascle, G., 1990. Reunion extraordinaire de la société géologique de France en Himalaya du Ladakh. *Bull. Soc. Geol. France* 4, 553-582.
- Carter, A., Roques, D., Bristow, C., Kinny, K., 2001. Understanding Mesozoic accretion in Southeast Asia: significance of Triassic thermotectonism (Indosinian Orogeny) in Vietnam. *Geology* 29, 211-214.
- Casnedi, R., Desio, A., Forcella, F., Nicoletti, M., Petruciani, C., 1978. Absolute age of some granitoid rocks between Hindu Raj and Gilgit river (western Karakoram). *Acad. Nazio. dei Lincei.* 64, 204-210.
- Cawood, P. A., Buchan, C., 2007. Linking accretionary orogenesis with supercontinent assembly. *Earth Sci. Rev.* 89, 217-256.
- Chandra, R., Upadhyay R., Sinha, A.K., 1999. Subduction and collision related magmatism in the Shyok Suture and eastern Karakoram. *Palaeobotanist* 48, 183-209.
- Chaudhuri, B.K., 1983. Structure, metamorphism and deformation history of the Pangong Tso area, eastern Ladakh. In: *Geology of Indus Suture Zone of Ladakh*. Thakur, V.C., Sharma, K.K. (Editors), W.I. H.G., Dehradun 107-116.
- Clift, P.D., Degnan, P.J., Hannigan, R., Blusztajn, J., 2000. Sedimentary and geochemical evolution of the Dras forearc basin, Indus Suture, Ladakh Himalaya, India. *Geol. Soc. Am. Bull.* 112, 450- 466.

- Condie, K.C., 1986. Origin and early growth rate of continents. *Precamb. Res.* 32, 261-278.
- Corfield, R., Searle, M., Green, O., 1999. Photang thrust sheet: an accretionary complex structurally below the Spontang ophiolite constraining timing and tectonic environment of ophiolite obduction, Ladakh Himalaya, NW India. *J. Geol. Soc. London* 156, 1031–1044.
- Corfield, R., Searle, M., Pedersen, R.B., 2001. Tectonic setting and obduction history of the Spontang ophiolite, Ladakh Himalaya, NW India. *J. Geol.* 109, 715–736.
- Corfield, R.I., Searle, M.P., Pederson R.B., 2001. Tectonic setting, origin, and obduction history of the Spontang ophiolite, Ladakh Himalaya, NW India. *J. Geol.* 109, 715-736.
- Coulon, C., Maluski, H., Bollinger, C., Wang, S., 1986. Mesozoic and Cenozoic volcanic rocks from central and southern Tibet:  $^{39}\text{Ar}$ – $^{40}\text{Ar}$  dating, petrological characteristics and geodynamical significance. *Earth Planet. Sci. Lett.* 79, 281–302.
- Coward, M.P., Jan, M.Q., Rex, D., Tarney, J., Triwall, M., Windley, B.F., 1982. Structural evolution of a crustal section in the western Himalaya. *Nature* 295, 22-24.
- Coward, M.P., Windley, B.F., 1986. Collision tectonics in the NW Himalayas. *Geol. Soc. Spec. Publ.* 19, 203-219.
- Coward, M.P., Windley, B.F., Broughton, R.D., Lu, I.W., Petterson, M.G., Pudsey, C.J., Rex, D.C., Khan, M.A., 1986. In: Collision tectonics in the NW Himalayas. Coward, M.P., Ries, A.C. (Editors). *Collision Tectonics*, *Geol. Soc. Lond. Spec. Publ.* 19, 203-209.
- Cox, K.G., Bell, J.D., Pankhurst, R.J., 1989. *The Interpretation of Igneous rocks*. George Allen and Union Publishers Ltd. London, U.K.
- Crawford, M.B., Windley, B.F., 1990. Leucogranites of the Himalaya/ Karakoram, magmatic evolution within collisional belts and the study of collision-related Leucogranite petrogenesis. In: *Collision magmatism*. Le Fort, P., Pearce, J.A., Pecher, A.J. (Editors). *Volcanol. Geotherm. Res. Spec. Issue* 44, 1-19.
- Cullers, R.L., Medaris, L.G., Haskin, L.A., 1973. Experimental studies of the distribution of rare earth as trace elements among silicate minerals and liquid and water. *Geochem. Cosmochim. Acta* 37, 1499-1512.

- Dasgupta, S., Ganguly, J., Neogi, S., 2004. Inverted metamorphic sequence in the Sikkim Himalayas: Crystallization history,  $P$ - $T$  gradient, and implications. *J. Metamorph. Geol.* 22, 395-412.
- De Paolo, D.J., 1988. Neodymium isotope geochemistry-an introduction. Springer-Verlag, New York. 187.
- De Paolo, D.J., Wasserberg, G.J., 1976. Nd isotopic variations and petrogenetic models. *Geophys. Res. Lett.* 3, 249-252.
- de Sigoyer, J., Guillot, S., Lardeaux, J.M., Mascle, G., 1997. Glaucophane bearing eclogites in the Tso Moriri dome (eastern Ladakh, NW Himalaya). *Eur. J. Mineral.* 9, 1073-1083.
- Debon, F., Khan, N.A., 1996. Alkaline orogenic plutonism in the Karakorum batholith: the upper Cretaceous Koz Sar complex (Karambar valley, N. Pakistan). *Geod. Acta* 9, 145-160.
- Debon, F., LeFort, P., Sonet, J., Dautel, D., Zirmann, J.M., 1986. Granites of western Karakoram and northern Kohistan (Pakistan): A composite Mid-Cretaceous to Upper Cenozoic magmatism. *Lithos* 20, 19-40.
- Deniel, C., Vidal, P., Fernandez, A., Le Fort, P., Peucat, J., 1987. Isotopic study of the Manaslu granite (Himalaya, Nepal): Inference on the age and source of Himalayan leucogranites. *Contrib. Mineral. Petrol.* 96, 78-92.
- Desio, A., 1976. Some geotectonic problems of Kashmir Himalaya- Karakoram-Hindukush and Pamir area. In: Coll. In. Geotectonica, Della zone orogeniche, Kashmir Himalaya-Karakoram-Hindukush-Pamir. Farah, A. (Editor). *Acad. Nazio. dei Lincei* 115-129.
- Desio, A., 1977. On the geology of Deosai plateau, Kashmir. *Mem. Acad. Nazio. dei Lincei* 15, 1-19.
- Desio, A., 1979. Geological evolution of the Karakoram. In: *Geodynamics of Pakistan*. Farah, A., Dejong, K.A. (Editors). *Geol. Surv. Pakistan* 8, 111-124.
- Desio, A., Tongiorigi, E., Ferrara, G., 1964. On the geological age of some granites of Karakoram, Hinduush and Badakshan (central Asia), Himalayan and Alpine orogeny. 22<sup>nd</sup> Int. Geol. Cong. India 479-496.
- Dewey, J.F., Bird, J.M., 1970. Mountain belts and its new global tectonics, *J. Geophys. Res.* 75, 2625-2647.
- Dewey, J.F., Shackelton, R.M., Chang, C. and Sun, Y., 1988. The tectonic evolution of the Tibetan Plateau. *Phil. Trans. Royal Soc. London* 327, 379-413.

- Dezes, P., Vannay, J.C., Steck, A., Bussy, F., Cosca, M., 1999. Synorogenic extension: quantitative constraints on the age and displacement of the Zaskar shear zone (Northwest Himalaya). *Geol. Soci. Am. Bull.* 111, 364-374.
- Dèzes., P., 1999. Tectonic and metamorphic Evolution of the Central Himalayan Domain in Southeast Zaskar (Kashmir, India). *Mémo. de Géol. (Lausanne)* 32, 1015-3578.
- Dietrich, A., Frank, W., Gansser, A., Honegger, K.H., 1983. A Jurassic–Cretaceous island arc in the Ladakh Himalayas. *J. Volcanol. Geotherm. Res.* 18, 405-433.
- Drake, M.J., Weill, D.F., 1975. Partition of Sr, Ba, Ca, Y,  $\text{Eu}^{2+}$ ,  $\text{Eu}^{3+}$ , and other REE between plagioclase feldspar and magmatic liquid: An experimental study. *Geochem. Cosmochim. Acta* 39, 689-71.
- Dunlap, W.J., Wysoczanski, R., 2002. Thermal evidence for early Cretaceous metamorphism in Shyok suture zone and age of the Khardung volcanic rocks, Ladakh, India. *J. Asian Earth Sci.* 20, 481-490.
- Dupuy, C., Dostal, J., 1984. Trace element geochemistry of some continental tholeiites. *Earth Planet. Sci. Lett.* 67, 61-67.
- Ehiro, M., Kojima, S., Sato, T., Ahmad, T., Ohtani, T., 2007. Discovery of Jurassic ammonids from Shyok suture zone to the northeast of Chang La Pass, Ladakh, northwest India and its tectonic significance. *Island Arc* 16, 124-132.
- Ellam, R.M., Hawkesworth, C.J., 1988. Is average continental crust generated on subduction zones?. *Geology* 16, 314-317.
- Ernst, W.G., 1963. Petrogenesis of glaucophane schist. *J. Petrol.* 4, 1–13.
- Ernst, W.G., 1970. Tectonic contact between the Franciscan mélangé and the Great Valley Sequence-Crustal expression of a late Mesozoic Benioff zone. *J. Geophys. Res.* 75, 888–901.
- Ernst, W.G., 1999. Metamorphism, partial preservation and exhumation of ultra high-pressure belts. *Island Arc* 8, 125–153.
- Faure, G., 1986. Principles of isotope geology. John Wiley & Sons Publications. New York.
- Fenner, C.N. 1929. Crystallization of Basalts. 5<sup>th</sup> Sem. *Am. J. Sci.* 18, 225-253.
- Floyd, P.A., 1993. Geochemical discrimination and petrogenesis of alkalic basalt sequences in part of the Ankara mélangé, central Turkey. *J. Geol. Soc. London* 150, 541-550.

- Floyd, P.A., Winchester, J.A., 1975. Magma type and tectonic setting discrimination, using immobile elements. *Earth Planet. Sci. Lett.* 27, 211-218.
- Frank, W., Gansser, A., Trommsdorff, V., 1977a. Geological observations in the Ladakh area (Himalayas)-a preliminary report. *Schwe. Miner. Petro. Mitte.* 57, 89-113.
- Frank, W., Thoni, M., Purtscheller, F., 1977b. Geology and petrography of Kulu-south Lahul area, Himalaya. *Coll. Int. Cent. Nat. Res. Sci.* 268, 147-160.
- Gaetani, M., Garzanti, E., 1991. Multicyclic history of the northern India continental margin (northwestern Himalaya). *Am. Assoc. Petrol. Geol. Bull.* 75, 1427-1446.
- Gahlaut, V.K., Chander, R., 1992. On the active tectonics of Dehradun region from observations of ground elevation changes. *J. Geol. Soc. India* 39, 61-68.
- Gansser, A., 1964. *Geology of Himalayas*. Interscience, London.
- Gansser, A., 1974. The ophiolitic mélange, a world-wide problem on Tethyan examples. *Eclog. Geol. Helv.* 67, 479-507.
- Gansser, A., 1977. The great suture zone between Himalaya and Tibet-a preliminary account. *Coll. Int. Cent. Nat. Res. Sci.* 33, 181-192.
- Gansser, A., 1980. The significance of Himalayan suture zone. *Tectonophysics* 62, 37-40.
- Gansser, A., 1981. The timing and significance of orogenic events in Himalayas, in *Geology. Geological history and origin of Qinghai -Xizang plateau*, Beijing. *Science* 195, 23-30.
- Garzanti, E., Le Fort, P., Sciunnach, D., 1999. First report of Lower Permian basalts in South Tibet: tholeiitic magmatism during break-up and incipient opening of Neotethys. *J. Asian Earth Sci.* 17, 533-546.
- Gautham, P., Upreti, B.N., Arita, K., 1995. Palaeomagnetism and petrochemistry of the Dawar Khola volcanics central Nepal, Sub-Himalaya. *J. Geol. Soc. Nepal Spec. Issue* 11, 179-195.
- Girardeau, J., Marcoux, J., Allegre, C.J., Bassoulet, J.P., Tang, Y., Xiao, X., Zhao, Y., Wang, X., 1984. Tectonic environment and geodynamic significance of the Neo-Cimmerian Dongqiao ophiolite, Bangong-Nujiang suture zone, Tibet. *Nature* 307, 27-31.
- Goldschmidt, V.M., 1937. The principle of distribution of chemical elements in minerals and rocks. *J. Chem. Soc.* 9, 655-672.
- Golonka, J., Krobicki, M., 2001. Upwelling regime in the Carpathian Tethys: a Jurassic-Cretaceous palaeogeographic and paleoclimatic perspective. *Geol. Quarterly* 45, 15-32.

- Gradstein, F.M., Ogg, J.G., Smith, A.G., Agterberg, F.P., Bleeker, W., Cooper, R.A., Davydov, V., Gibbard, P., Hinnov, L.A., House, M.R., Lourens, L., Luterbacher, H.P., McArthur, J., Melchin, M.J., Robb, L.J., Shergold, J., Villeneuve, M., Wardlaw, B.R., Ali, J., Brinkhuis, H., Hilgen, F.J., Hooker, J., Howarth, R.J., Knoll, A.H., Laskar, J., Monechi, S., Plumb, K.A., Powell, J., Raffi, I., Röhl, U., Sadler, P., Sanfilippo, A., Schmitz, B., Shackleton, N.J., Shields, G.A., Strauss, H., Van Dam, J., Kolfshoten, T., Veizer, J., Wilson, D., 2004. A Geologic Time Scale. Cambridge University Press, Cambridge.
- Grasemann, B., Fritz, H., Vannay, J.C., 1999. Quantitative kinematic flow analysis from the Main Central Thrust Zone (NW-Himalaya, India): implications for a decelerating strain path and the extrusion of orogenic wedges. *Jour. Struct. Geol.* 21, 837–853.
- Green, T.H., 1980. Island arc arc and continent-building magmatism: a review of petrogenetic models based on experimental petrology and geochemistry. *Tectonophysics* 63, 367-385.
- Green, T.H., 1994. Experimental studies of trace-element partitioning applicable to igneous petrogenesis—Sedona, 16 years later. *Chem. Geol.* 117, 1–36.
- Green, T.H., Watson, E.B., 1982. Crystallization of apatite in natural magmas under high pressure hydrous conditions, with particular reference to orogenic rock series. *Contrib. Mineral. Petrol.* 79, 96-105.
- Guillot, S., Replumaz, A., Hattori, K.H., Strzeczynski, P., 2007. Initial geometry of western Himalaya and ultrahigh-pressure metamorphic evolution. *J. Asian Earth Sci.* 30, 557–564.
- Gulliot, S., Garzanti, E., Baratoux, D., Marquer, D., Maheo, G., De Sigoyer, J., 2002. Reconstructing the total shortening history of the NW Himalaya. *Geochem. Geophys. Geosys.* 41, 10-29.
- Gupta, K.R., Sharma, K.K., 1978. Some observations on the geology of Indus Shyok valleys between Leh and Panamik, District Ladakh, Jammu and Kashmir, India. *Rec. Res. Geol.* 7, 133-143.
- Gurnis, M., 1988. Large-scale mantle convection, the aggregation and dispersal of supercontinents. *Nature* 332, 695–699.
- Haines, S.S., Klemperer, S.L., Brown, L., Jingru, G., Mechie, J., Meissner, F., Ross, A., Wenjin, Z., 2003. INDEPTH III seismic data: from surface observations to deep crustal processes in Tibet. *Tectonics* 22, 101-110.



- Hanson, C.R., 1989. The northern suture in the shigar valley, Baltistan, northern Pakistan. *Geol. Soc. Am. Spec. Publ.* 232, 203-215.
- Hanson, G.N., Langmuir, C.H., 1978. Modelling of major and trace elements in mantle-melt systems using trace element approaches. *Geochem. Cosmochim. Acta* 42, 725-741.
- Hanson, G.N., 1980. Rare earth elements in petrogenetic studies of igneous systems. *Ann. Rev. Earth Planet. Sci. Lett.* 8, 371-406.
- Harrison, T.M., Mc Keegan, K.D., Lefort, P., 1995. Detection of inherited monazite in the Manaslu leucogranite by Pb/Th ion microprobe dating: crystallization age and tectonic implications. *Earth Planet. Sci. Lett.* 133, 271-282.
- Hawkesworth, C.J., Gallagher, K., Hergt, J.M., Mc Dermott, F., 1994. Destructive plate margin magmatism: geochemistry and melt generation. *Lithos* 33, 169-188
- Hayden, H.H., 1904. The geology of Spiti with parts of Bushahr and Rupshu. *Mem. Geol. Surv. India* 6, 1-121.
- Heim, A., Gansser, A., 1939. Central Himalaya-Geological observations of Swiss Expedition. *Soc. Helv. Sci. Nat.* 73, 245.
- Henderson, P., 1984. *Rare Earth Element Geochemistry*. Elsevier, Amsterdam
- Herren, E., 1987. Zaskar shear zone: north-east south-west extension within the Higher Himalayas (Ladakh, India). *Geology* 15, 409-413.
- Hirn, A., Lepine, J.C., Jobert, G., Sapin, M., Wittlinger, G., Xin, X.Z., Yuan, G.E., Jing, W.X., Wen, T. J., Bai, X.S., Pandey, M.R., Tater, J.M., 1984. Crustal structure and variability of the Himalayan border of Tibet. *Nature* 307, 23-25.
- Hodges, K.V., 2000. Tectonics of the Himalayas and southern Tibet from two perspectives. *Geol. Surv. Am. Bull.* 112, 324-350.
- Hoffman, P.F., 1991. Did the breakout of Laurentia turn Gondwanaland inside-out? *Science* 252, 1409-1412.
- Hofmann, A.W., 1988. Chemical differentiation of the Earth: the relationship between mantle, continental crust, and oceanic crust. *Earth Planet. Sci. Lett.* 90, 297-314.
- Honegger, K., Le Fort, P., Mascle, G., Zimmermann, J.L., 1989. The blueschists along the Indus Suture Zone in Ladakh, NW Himalaya. *J. Metamorph. Geol.* 7, 57-72.
- Honegger, K.H., Dietrich, V., Frank, W., Gansser, A., Thommsdorf, M., Thommsdorf, K., 1982. Magmatism and metamorphism in the Ladakh Himalayas (the Indus-Tsangpo Suture Zone). *Earth Planet. Sci. Lett.* 60, 253-292.

- Hooper, P.R., Subbarao, K.V., and Beane, J.E., 1988. The giant plagioclase basalts (GPBs) of the Western Ghats, Deccan Traps. In: Deccan Flood Basalts. Subbarao, K.V. (Editor). Geol. Soc. India 10, 135-143.
- Iddings, J.P., 1892. The origin of igneous rocks. Bull. Phil. Soc. Washington 12, 89-214.
- Irvine, T.N., Baragar, W.R.A., 1971. A guide to the chemical classification of common volcanic rocks. Can. J. Earth Sci. 8, 523-548.
- Irving, A.J., 1978. A review of experimental studies of crystal/liquid trace element partitioning. Geochem. Cosmochim. Acta 42, 743-770.
- Jacobsen, S.B., Wasserberg, G.J., 1984. Isotopic evolution of chondrites and achondrites, Earth Planet Sci. Lett. 67, 137-150.
- Johnston, A.D., 1986. Anhydrous *P-T* phase relations of near-primary high-alumina basalt from the South Sandwich Islands. Implications for the origin of island arcs and tonalite-trondhjemite series rocks. Contrib. Mineral. Petrol. 92, 368-382.
- Kapp, P., Murphy, M.A., Yin, A., Harrison, T.M., 2003. Mesozoic and Cenozoic tectonic evolution of the Shiquanhe area of western Tibet. Tectonics 22, 3.1–3.21.
- Khadri, S.F.R., Subbarao, K.V., Hooper, P.R., Walsh, J.N., 1988. Stratigraphy of Thakurvadi Formation, Western Deccan Basalt Province. Geol. Soc. India Mem.10, 253-279.
- Khan, M.A., Jan, M.Q., Windley, B.F., Tarney, J., Thirlwall, M.F., 1989. The Chilas mafic-ultramafic igneous complex; the root of the Kohistan island arc in the Himalaya of northern Pakistan. Geol. Soc. Am. Spec. Publ. 232, 75-94.
- Klootwijk, C., Sharma, M.L., Gergan, J., Tirkey, B., Shah, S.K., Agarhwal, V., 1979. The extend of Greater India-II. Palaeomagnetic data from the Ladakh intrusives at Kargil, Northwestern Himalayas. Earth Planet. Sci. Lett. 44, 47-64.
- Klootwijk, C.T., Gee, J.S., Peirce, H.W., Smith, G.M., McFadden, P.L., 1992. An early India-Asia contact: palaeomagnetic constraints from Ninetyeast Ridge, ODP Leg.121. Geology 20, 395-398.
- Krauskopf, K.B., Bird, D.K., 1995. Introduction to geochemistry. McGraw-Hill, New York.
- Kuno, H., 1968. Plateau basalts. In: In the Earth's crust and upper mantle. Hart, P. (Editor). Am. Geophys. Union. Geophys. Monogr. 13, 10-14.
- Lacassin, R., Valli, F., Arnaud, N., Leloup, P.H., Paquette, J.L., Haibing, L., Tapponnier, P., Chevalier, M.-L., Guillot, S., Maheo, G., Zhiqin, X., 2004. Large-scale

- geometry, offset and kinematic evolution of the Karakorum Fault, Tibet. *Earth Planet. Sci. Lett.* 219, 255–269.
- Le Bas, M.J., Le Maitre, R.W., Streckeisen, A., Zanettin, B., 1986. Chemical classification of volcanic rocks based on the total alkali-silica diagram, *J. Petrol.* 27, 745-750.
- Le Fort, P., 1975. Himalaya, the collided range, present knowledge of continental arc. *Am. J. Sci.* 275, 1-44.
- Le Fort, P., Cuney, M., Deniel, C., Lanords, C.F., Sheppard, N.F., Upreti, B. N. Vidal, P., 1987. Crustal generation of the Himalayan leucogranite. *Tectonophysics* 134, 39-57.
- Le Fort, P., Michard, A., Sonet, J., Zimmermann, J.L., 1983. Petrography, geochemistry and geochronology of some samples from Karakoram axial batholith, North Pakistan. In: *Granites of Himalayas, Karakoram and Hindu Kush*. Shams, F.A. (Editor). Punjab University, Lahore 377-387.
- Le Fort., 1975. Himalayas: the collided range, present knowledge of the continental arc, *Am. J. Sci.* 275, 1–44.
- Li, P., Rui, G., Junwen, C., Ye, G., 2004. Paleomagnetic analysis of eastern Tibet: implications for the collisional and amalgamation history of the Three Rivers Region, SW China. *J. Asian Earth Sci.* 24, 291-310.
- Li, X. Powell, C.M., 2001. An outline of the palaeogeographic evolution of the Australian region since the beginning of the Neoproterozoic. *Earth Sci. Rev.* 53, 237–277.
- Li, Z.X., Bogdanova, S.V., Collins, A.S., Davidson, A., De Waele, B., Ernst, R.E., Fitzsimons, I.C.W., Fuck, R.A., Gladkochub, D.P., Jacobs, J., Karlstrom, K.E., Lu, S., Natapov, L.M., Pease, V., Pisarevsky, S.A., Thrane, K., Vernikovsky, V., 2008. Assembly, configuration, and break-up history of Rodinia: A synthesis. *Precamb. Res.* 160, 179-210.
- Li, Z.X., Li, X.H., Kinny, P.D., Wang, J., 1999. The breakup of Rodinia: did it start with a mantle plume beneath South China? *Earth Planet. Sci. Lett.* 173, 171–181.
- Liu, G.H., Einsele, G., 1994. Sedimentary history of the Tethyan basin in the Tibetan Himalayas. *Geol. Rundsch.* 83, 32–61.
- Lo'pez , S. Castro, A., Garcí'a-Casco, A., 2005 Production of granodiorite melt by interaction between hydrous mafic magma and tonalitic crust. Experimental constraints and implications for the generation of Archaean TTG complexes. *Lithos* 79, 229–250.

- Luth, W.C., 1967. Studies in the system  $\text{KAlSi}_3\text{O}_8\text{-Mg}_2\text{SiO}_4\text{-SiO}_2\text{-H}_2\text{O}$ , Inferred phase relations and petrologic applications. *J. Petrol.* 8, 372-416.
- Maekawa, H.S., Masaya, I., Teruaki, F., Fryer, P., Julian, A., 1993. Blueschist metamorphism in an active subduction zone. *Nature* 364, 520–523.
- Mahéo, G., Bertrand, H., Guillot, S., Villa, I.M., Keller, F., Capiez, P., 2004. The south Ladakh ophiolites (NW Himalaya, India): an intra-oceanic tholeiitic origin with implication for the closure of the Neo-Tethys. *Chem. Geol.* 203, 273–303.
- Mahéo, G., Guillot, S., Blichert-Toft, J., Rolland, Y., Pêcher, A., 2002. A slab break off model for the Neogene thermal evolution of South Karakoram and South Tibet. *Earth Planet. Sci. Lett.* 195, 45–58.
- Mahéo, G., Fayoux, X., Guillot, S., Garzanti, E., Capiez, P., Mascle, G., 2005. Relicts of an intra-oceanic arc in the Sapi-Shergol mélange zone (Ladakh, NW Himalaya, India): implications for the closure of the Neo-Tethys Ocean. *J. Asian Earth Sci.* 20, 1–13.
- Mahoney, J. B., Weis, D., Kieffer, B., Friedman, R., Pretorius, W., Scoates, J., Goolaerts, A. and Maerschalk, C., 2003. Ongoing Isotopic characterization of USGS Standards: MC-ICPMS and TIMS data from the Pacific Centre for Isotopic and Geochemical Research, University of British Columbia. (Abst.) Abstracts with Programs, *Ann Meet. Geol. Soc. Am.* 35, 243.
- Mathur, N.S., 1983. Age of Kargil Formation, Ladakh Himalaya. In: *Geology of Indus Suture Zone of Ladakh*. Thakur, V.C., Sharma, K.K. (Editors). W.I.H.G., Dehradun 145-150.
- Matte, P., Mattauer, M., Oliver, J.M., Griot, D.A., 1996. Continental subduction beneath Tibet and the Himalayan orogeny: a review. *Terra Nova* 9, 264-270.
- McCulloch, M.T., Chappell, B.W., 1982. Nd isotopic characteristics of S and I type granites. *Earth Planet. Sci. Lett.* 58, 51-64.
- McCulloch, M.T., Wasserberg, G.J., 1978. Sm-Nd and Rb-Sr chronology of continental crust formation. *Science* 200, 1003-1011.
- McDonough, W.F., Frey, F. A., 1989. Rare Earth Elements in upper mantle rocks. In: *Geochemistry and Mineralogy of Rare Earth Elements*. Lipin B.R., Mc Kay, G.A. (Editors). *Mineral. Soc. Am.* 21, 99-139.
- McDonough, W.F., Sun, S.-s., Ringwood, A.E., Jagoutz, E., Hofmann, A.W., 1992. Potassium, rubidium and cesium in the Earth and Moon and the evolution of the mantle of the Earth. *Geochim. Cosmochim. Acta* 56, 1001-1012.

- McKay, G., 1986. Crystal liquid partitioning of REE in basaltic systems: Extreme fractionation of REE in olivine. *Geochim. Cosmochim. Acta* 50, 69-79.
- McKay, G.A., 1989. Partitioning of rare earth elements between major silicate elements and basalt melts. *Geochim. Cosmochim. Acta* 72, 45-74.
- Medlicott, H.B., 1864. On the geological structure and relation of the southern portion of the Himalayan Range between the rivers Ganges and Ravee. *Mem. Geol. Surv. India* 26, 191-198.
- Metcalf, I., 1999. The Tethys: How many? How old? How deep? How wide?. In: *Proceedings of the International Symposium on Shallow Tethys (ST)*. Ratanasthein, B., Rieb, S.L. (Editors). Chiang Mai, Thailand 5, 1-15.
- Metcalf, I., 1998, Gondwanaland dispersion, Asian accretion and evolution of eastern Tethys. *J. African Earth Sci.* 26, 9-19.
- Molnar, P., Tapponier, P., 1975. Cenozoic tectonics of Asia: effects of a continental collision. *Science* 189, 419-426.
- Moyen, J.F., Martin, H., Jayananda, M., 2001. Multi-element geochemical modelling of crust-mantle interactions during late-Archaean crustal growth: the Closepet granite (South India). *Precamb. Res.* 112, 87-105.
- Mukhopadhyay, D.K., 2001. Extreme heterogeneity in Sr isotopesystematic in the Himalayan leucogranites: A possible mechanism of partial melting based on thermal modeling. *Proc. Indian Acad. Sci. (Earth Planet. Sci.)* 110, 161-169.
- Mukhopadhyay, D.K., 2003. A melting mechanism for the Himalayan leucogranite. In: *Granitoids of the Himalayan Collisional Belt*. Singh, S. (Editor). *J. Virtual Exp.* 11, 83-95.
- Nakata, T., Otsuki, K., Khan, S.H., 1990. Active faults, stress field and plate motion along the Indo-Eurasian plate boundary. *Tectonophysics* 181, 141-154.
- Nance, R.D., Worsley, T.R., Moody, J.B., 1988. The super-continent cycle. *Sci. Am. Bull.* 259, 72-79.
- Neuman, H., Mead, J. Vitaliano, C.J., 1954. Trace element variation during fractional crystallizations calculated from the distribution law. *Geochim. Cosmochim. Acta* 6, 90-99.
- Ni, J., Barazangi, M., 1984. Seismotectonics of the Himalayan collision zone: Geometry of the underthrusting Indian plate beneath the Himalaya. *J. Geophys. Res.* 89, 1147-1163.

- Ni, J; Barazangi, M., 1985. Active tectonics of the western Tethyan Himalaya above the underthrusting Indian plate: The Upper Sutlej river basin as a pull-apart structure. *Tectonophysics* 112, 277-295.
- O'Brein, 2001. Subduction followed by collision: Alpine and Himalayan examples. *Phys. Earth Planet. Inter.* 127, 277–291.
- Otofujii, Y., Mu, C.L., Tanaka, K., Miura, D., Inokuchi, H., Kamei, R., Tamai, M., Takemoto, K., Zaman, H., Yokoyama, M., 2007. Spatial gap between Lhasa and Qiangtang blocks inferred from Middle Jurassic to Cretaceous paleomagnetic data. *Earth Planet. Sci. Lett.* 262, 581-593.
- Parkash, B., Sharma, R.P., Roy, A.K., 1980. The Siwalik Group (molasse) sediments shed by collision of continental plates. *Sediment. Geology* 25, 127–159.
- Parkinson, I.J., Pearce. J.A., 1998. Peridotites from the Izu Bonin Mariana forearc (ODP Leg 125): evidence for mantle melting and melt-mantle interaction in a supra-subduction zone setting. *J. Petrol.* 39, 1577-1618.
- Patchett, P.J., 1989. Radiogenic isotopic geochemistry of rare earth elements. In: *Geochemistry and mineralogy of rare earth elements*, Lipin, B.R., Mc Kay, G.A. (Editors). Mineral. Soc. Am. Washington, D.C. 21, 25-43.
- Patel, R.C., Singh, S., Asokan, A., Manickavasagam, R.M., Jain, A.K., 1993. Extensional tectonics in the Collisional Zaskar Himalayan belt. In: *Himalayan Tectonics*. Treolar, P.J., Searle, M.P. (Editors). *Geol. Soc. Spec. Publ.* 74, 445-459.
- Patel, R.C; Jain, A.K., 1997. Deformation and strain patterns of the Panjal Traps in the Tethyan Sedimentary Zone, Zaskar, NW Himalaya. In: *Geodynamic domains in Alpine-Tethys*. Sinha, A.K., Sassi, F.P., Papanikolaou, D.P. (Editors). Oxford and IBH Publishing Co. 69-100.
- Patra, B.A., Vijan, A.R., Singh, S., Jain, A.K., 2003. Rb-Sr biotite ages: constraints on cooling and unroofing history of Pangong–Injection Complex, Eastern Ladakh, India. In: *Himalayan Tectonics (HIMPROBE results)*, IIT Roorkee 6-7.
- Patriat, P., Achache, J., 1984. India-Eurasia collision chronology has implication for crustal shortening and driving mechanisms of plates. *Nature* 311, 615-621.
- Pearce, J.A. Gale, G.H., 1977. Identification of ore deposition environment from trace element geochemistry of associated igneous host rocks. In: *Volcanic Processes in Ore Genesis*. *Geol. Soc. Lond. Spec. Publ.* 7, 14-24.

- Pearce, T.H., Gorman, B.E., Birkett, T.C., 1977. The relationship between major element chemistry and tectonic environment of basic and intermediate volcanic rocks. *Earth Planet Sci. Lett.* 36, 121-132.
- Pearce, J.A., Parkinson, I.J., 1993. Trace element models for mantle melting: application to volcanic arc petrogenesis. In: *Magmatic processes and plate tectonics*. Pitchard, H.M., Alabaster, T., Harris, N.B.W., Neary, C.R. (Editors). *Geol. Soc. Lond. Spec. Publ.* 76, 373-403.
- Pedersen, R.B., Searle, M.P., Corfield, R.I., 2001. U–Pb zircon ages from the Spong tang ophiolite, Ladakh Himalaya. *J. Geol. Soc. London* 158, 513–520.
- Petterson, M.G., Crawford, M.B., Windley, B.F., 1993. Petrogenetic implications of neodymium isotope data from the Kohistan batholith, North Pakistan. *J. Geol. Soc. London* 150, 125–129.
- Petterson, M.G., Treloar, P.J. 2004. Volcanostratigraphy of arc volcanic sequences in the Kohistan arc, North Pakistan: volcanism within island arc, back-arc basin, and intra-continental tectonic settings. *J. Volcanol. Geotherm. Res.* 130, 147–178.
- Petterson, M.G., Windley, B.F., 1985. Rb-Sr dating of the Kohistan arc-Batholith in the Trans-Himalaya of N Pakistan and tectonic implications. *Earth Planet. Sci. Lett.* 74, 45-75.
- Phillips, R.J., Parrish, R. R., Searle, M. P., 2004. Age constraints on ductile deformation and long-term slip rates along the Karakoram fault zone, Ladakh. *Earth Planet. Sci. Lett.* 226, 305–319.
- Philpotts, A.R., 1991. *Principles of Igneous and Metamorphic Petrology*, Prentice-Hall Publishing Co.
- Pierce, J.A., Mei, H., 1988. Volcanic rocks of the Tibetan geotraverse Lhasa-Golmud. *Phil. Trans. Royal Soc. London* 327, 203–213.
- Pilgrim, G.E., 1910. Preliminary note on a revised classification of the Tertiary fresh water deposits of India. *Rec. Geol. Surv. India* 40, 185–188.
- Pilgrim, G.E., 1913. The correlation of the Siwaliks with the mammalian horizons of Europe. *Rec. Geol. Surv. India* 43, 264–325.
- Pilgrim, G.E., West, W.D., 1928. The structure and correlation of Simla rocks. *Geol. Surv. India Mem.* 53, 1-140.
- Plank, P., Langmuir, C.H., 1998. The chemical composition of subducting sediment and its consequences for the crust and mantle. *Chem. Geol.* 145, 325–394.

- Powell, C.M., Conaghan, P.J., 1973. Plate tectonics and the Himalayas. *Earth Planet. Sci. Lett.* 20, 1-12.
- Powell, C.M., Conaghan, P.J., 1975. Tectonic models for the Tibetan Plateau. *Geology* 4, 727-731.
- Pozzi, J.P., Westphal, M., Zhou, Y.X., Xing, L.S., Chen, X.Y., 1972, Position of the Lhasa Block, South Tibet, during the late Cretaceous. *Nature* 297, 319-321.
- Presnall, D.C., 1979. Fractional crystallization and partial fusion. In: *The evolution of igneous rocks*. Yoder, H.S. (Editor) Fifteenth Anniversary Perceptives. Princeton University Press. Princeton. N.J.
- Pudsey, C.J., 1986. The Northern Suture, Pakistan: margin of a Cretaceous island arc. *Geol. Mag.* 123, 405-423.
- Pudsey, C.J., Coward, M.P., Luff, I.W., Shackleton, R.M., Windley, B.F., Jan, M.Q., 1985. Collision zone between Kohistan arc and the Asian plate in NW Pakistan. *Trans. Royal Soc. Edinburgh Earth Sci.* 76, 463-479.
- Qiu, R.Z., Zhou, S., Li, T.D., Deng, J.F., Xiao, Q.H., Wu, Z.X. Cai, Z.Y., 2007. The tectonic setting of ophiolites in the western Qinghai-Tibet Plateau, China. *J. Asian Earth. Sci.* 29, 215-228.
- Radhakrishna, T., 1987. Collision tectonics in the Himalaya as evidenced by the Indus and Shyok rock assemblages. *Tectonophysics* 134, 1-16.
- Radhakrishna, T., Rao, V.D., Murali, A.V., 1984. Geochemistry of Dras volcanics, the evolution of the Indus ophiolites. *Tectonophysics* 108, 135-153.
- Rai, H. 1989. The Dras volcanic series of the Indus suture zone-a tectonic melange of off-scraped ophiolite and island arc volcanics. *Ophioliti*, 14, 221-234.
- Rai, H., 1979. Lapilli structure and its significance on palaeo-environment of Khardung volcanics, Ladakh, India. *Him.Geol.* 9, 529-536.
- Rai, H., 1982. Geological evidences against the Shyok palaeosuture, Ladakh Himalaya, *Nature* 297, 142-144.
- Rai, H., 1983. Geology of the Nubra valley and its significance on the evolution of the Ladakh Himalaya. In: *Geology of Indus Suture Zone of Ladakh*. Thakur, V.C, Sharma, K.K. (Editors). W.I.H.G., Dehradun 79-97.
- Rai, H., 1986. Some geological observations on the area between Khalsar and Durbuk in the Shyok valley, Ladakh. *J. Geol. Soc. India* 27, 513-516.



- Rai, H., 1999. Geological and tectonic evolution of the Shyok Suture Zone, Ladakh. In: Geodynamics of the NW Himalaya. Jain, A.K., Manickavasagam, R.M. (Editors) Gond. Res. Group Mem. 6, 159-166.
- Rangland, P.C., 1989. Basic analytical petrology. Oxford University Press. New York.
- Rao, D.R., Rai, H., 2006. Signatures of rift environment in the production of garnet-amphibolites and eclogites from Tso-Morari region, Ladakh, India: A geochemical study. Gond. Res. 9, 512-523.
- Rapp, R.P., Shimizu, N., Norman, M.D., Applegate, G.S., 1999. Reaction between slab-derived melts and peridotite in the mantle wedge: experimental constraints at 3.8 GPa. Chem. Geol. 160, 335-356.
- Rapp, R.P., Watson, E.B., 1995. Dehydration melting of metabasalt at 32 kbar: Implications for continental growth and crust- mantle recycling. J. Petrol. 36, 891-931.
- Rapp, R.P., Watson, E.B., Miller, C.F., 1991. Partial melting of amphibole/eclogite and the origin of Archean trojhemites and tonolites. Precamb. Res. 94, 4619-4633.
- Rashid, S.A., Sharma, K.K., 2005. Palaeo-proterozoic clastic sedimentary rocks from Chakrata Formation, Lesser Himalaya: implications for crustal evolution and weathering history in the Himalayas. J. Asian Earth Sci. 21, 285-295.
- Ray, S., 1947. Zonal metamorphism in the eastern Himalaya and some aspects of local geology. Quart. J. Geol. Met. Soc. India 19, 117-138.
- Raz, U., Honegger, K., 1989. Magmatic and tectonic evolution of the Ladakh block from field studies. Tectonophysics 161, 107-118.
- Replumaz, A., Tapponnier, P., 2003. Reconstruction of the deformed collision zone between India and Asia by backward motion of lithospheric blocks, J. Geophys. Res. 108, 22-85.
- Reuber, I., 1987. Tectogenesis of the Dras Volcanic arc, Ladakh- Himalaya. Terra Cognita 7, 111-112.
- Reuber, I., 1989. The Dras Arc: two successive volcanic events on eroded oceanic crust. Tectonophysics 161, 107-118.
- Reuber, I., Colchen, M., Mevel, C., 1987. The geodynamic evolution of the south-Tethyan margin in Zaskar, NW Himalaya, as revealed by the Spontang ophiolitic mélange. Geodin. Acta 1, 283-296.

- Reynolds, P.H., Brookfield, M.E., McNutt, R.H., 1983. The age and nature of Mesozoic Tertiary magmatism across the Indus suture zone in Kashmir and Ladakh, *Geol. Rundsch.* 72, 981-1004.
- Ricou, L.E., 1994. Tethys reconstructed- plates, continental fragments and their boundaries from 260-Ma. from Central America to South Eastern Asia. *Geodin. Acta* 7, 169-218.
- Ringwood, A.E., 1975. *Composition and Petrology of the Earth's Mantle*. McGraw-Hill, New York, N.Y.
- Robertson, A.H.F., Collins, A.S., 2002. Shyok suture zone, N Pakistan: Late Mesozoic – Tertiary evolution of a critical suture separating the oceanic Ladakh Arc from the Asian continental margin. *J. Asian Earth. Sci.* 20, 309-351.
- Rolfo, F., Lombardo, B., Compagnoni, R., Le Fort, P., Lemmenicier, Y., Pecher, A., 1997. Geology and metamorphism of the Ladakh terrane and Shyok Suture Zone in the Chogo Lungma-Turmik area (northern Pakistan). *Geodin. Acta* 10, 251-270.
- Rolland Y., Pêcher, A., 2001. Reply to the comments on “Middle Cretaceous back-arc formation and arc evolution along the Asian margin: the Shyok Suture Zone on northern Ladakh (NW Himalaya)” by Weinberg and Dunlap. *Tectonophysics* 340, 269– 271.
- Rolland, Y., 2002. From intra oceanic convergence to post collisional evolution example of Indian Asian convergence in NW Himalaya, from Cretaceous to present. In: *Reconstruction of the evolution of the Alpine-Himalayan orogeny*. Rosenbaum, G., Lister, G. S. (Editors). *J. Virtual Expl.* 8, 75-98.
- Rolland, Y., Pecher, A., Picard, C., 2000. Middle Cretaceous back arc formation and arc evolution along the Asian margin: the Shyok suture zone in northern Ladakh (NW Himalaya). *Tectonophysics* 325, 145-173.
- Rolland, Y., Picard, C., Pêcher, A., Lapierre, H., Bosch, D., Keller, F., 2002. The Cretaceous Ladakh Arc of NW Himalaya—slab melting and melt mantle interaction during fast northward drift of Indian Plate. *Chem. Geol.* 182, 139–178.
- Rollinson, H.R., 1993. *Using Geochemical Data: Evolution, Presentation, and Interpretation*. Longmans. Essex. Singapore. Publication Ltd.
- Rowley, D.B., 1996. Age of initiation of collision between India and Asia; a review of stratigraphic data. *Erath Planet. Sci. Lett.* 145, 1-13.
- Roy, A.B., 1999. Assembly and Breakup of Supercontinents: A story of the Changing Map Patterns of the Earth. *Resonance* 228, 42-48.

- Saini, N.K., Mukharjee, P.K., Rathi, M.S., Khanna, P.P., Purohit, K.K., 1998. A new geochemical reference sample of granite (DGH) from Delhousie, Himachal Himalaya. *J. Geochem. Soc. India* 52, 603-606.
- Saini, N.K., Purohit, K.K., Rathi, M.S., Khanna, P.P., Mukharjee, P.K., Rai, H., 1992. A new metabasic reference sample (MB-H) from Himalayan orogenic belt. *J. Geol. Soc. India* 37, 453-456.
- Scaillet, B., Holtz, F., Pichavant, P., Schmidt, M., 1996. Viscosity of Himalayan leucogranites: Implications for mechanisms of granitic magma ascent. *J. Geophys. Res.* 101, 27691-27699.
- Scaillet, B., Pecher, A., Rochette, P., Champenois, M., 1995. The Gangotri granite (Garhwal Himalaya): laccolithic emplacement in an extending collisional belt. *J. Geophys. Res.* 100, 585-607.
- Scharer, U., 1984. The effect of initial  $^{230}\text{Th}$  disequilibrium on young U-Pb young ages: the Makalu case, Himalaya. *Earth Planet. Sci. Lett.* 67, 191-204.
- Scharer, U., Hamet, J., Allegre C.J., 1984. The Trans Himalaya (Gangdese) plutonism in the Ladakh region: a U-Pb and Rb-Sr study. *Earth Planet. Sci. Lett.* 67, 327-339.
- Scotese, C., 2001, Palaeomap Palaeogeographic Atlas, Palaeomap project, University of Texas, Arlington.
- Searle, M. P., Asif, M., Khan, M., Fraser, J.E., Gough, S.J., Qasim Jan, M., 1999. The Tectonic evolution of the Kohistan-Karakoram collision belt along the Karakoram High Way transect, north Pakistan. *Tectonics* 18, 929-949.
- Searle, M.P., 1983. Stratigraphy, structure and evolution of the Tibetan-Tethys zone in zaskar and Indus suture zone in the Ladakh Himalayas. *Trans. Roy. Soc. Edinburgh. Earth Sci.* 73, 205-219.
- Searle, M.P., 1986. Structural evolution and sequence of thrusting in Higher Himalaya; Tibetan-Thethys and Indus suture zone of Zaskar and Ladakh, W Himalaya, *J. Struct. Geol.* 8, 923-936.
- Searle, M.P., 1991. *Geology and tectonic of the Karakoram mountains.* Wiley, London.
- Searle, M.P., 2001. Dating the Indian continental subduction and collisional thickening in the northwest Himalaya: Multichronology of Tso Morari eclogite: comment and reply. *Geology* 191-192.
- Searle, M.P., Crawford, M.B., Rex, A.J., 1992. Field relations, geochemistry, origin and emplacement of the Baltoro granite, Central Karakoram. *Trans. Roy. Soc. Edinburgh. Earth Sci.* 83, 519-538.

- Searle, M.P., Rex, A.J., Tirrul, R., Rex, D.C., Barnicoat, A., Windley, B.F., 1989. Metamorphic, magmatic and tectonic evolution of the central Karakorum in the Biafo-Baltoro-Hushe regions of northern Pakistan. *Geol. Soc. Am. Spec. Paper* 232, 47–74.
- Searle, M.P., Weinberg, R.F., Dunlap, W.J., 1998. Transpressional tectonics along the Karakoram Fault zone, N–Ladakh controlling on Tibetan extrusion. *Geol. Soc. Spec. Publ.* 135, 307–326.
- Searle, M.P., Windley, B.F., Coward, M.P., Cooper, D.J.W., Rex, A.J., Rex, D.C., Litingdong., Xiao Xumang ja, M.Q., Thakur, V.C., Kumar, S., 1987. The closing of Tethys and tectonics of the Himalaya. *Geol. Soc. Am. Bull.* 98, 678–701.
- Seeber, L., Armbruster, J., Quittmeyer, R., 1981. Seismicity and continental subduction in the Himalayan arc. In: Zagros, Hindu Kush, Himalaya, Geodynamic Evolution. Gupta, H.K., Delany, F.M. (Editors). *Geodynamics Seminar, Amer. Geophy. Union, Washington, D.C. (Geol. Soci. Am.)* 3, 215–242.
- Sen, G., 2001. Generation of Deccan Trap magmas. *Proc. Indian Acad. Sci.* 111, 409–431.
- Sengör, A.M.C., 1984. The Cimmeride orogenic system and the tectonics of Eurasia. *Geol. Soc. Am. Spec. Paper* 195, 82–84.
- Sengör, A.M.C., Altmer, D., Cin, A., Ustaomer, T., Hsu, K.J., 1988. Origin and assembly of the Tethyside collage at the expanse of Gondwanaland. In: *Gondwana and Tethys*. Audley-Charles, M.G., Hallam, A. (Editors). *Geol. Soc. Spec. Publ.* 37, 119–181.
- Shams, F.A., 1972. Glaucophane-bearing rocks from near Topsin, first record from Pakistan. *Pakistan J. Sci. Res.* 24, 343–345.
- Sharma, K.K., 1987. Crustal growth and two-stage India-Eurasia collision in Ladakh. *Tectonophysics* 134, 17–28.
- Sharma, K.K., 1990. Petrology, geochemistry and geochronology of Ladakh batholith and its role in the evolution of Ladakh magmatic Arc. In: *Geology and Geodynamic Evolution of the Himalayan collision zone*. Sharma, K.K (Editor). *Phys. Chem. Earth.* 17, 173–194.
- Sharma, K.K., Choubey, V.M., Chatti, H.R., 1991. Geological setting of the ophiolites and magmatic arc of Lohit Himalaya (Arunachal Pradesh) India with special reference to their petrochemistry. In: *Geology and Geodynamic Evolution of the*

- Himalayan Collision Zone, Part-2. Sharma, K.K. (Editor). *Phys. Chem. Earth.* 18, 221–236.
- Sharma, K.K., Choubey, V.M., 1983. Petrology, geochemistry and geochronology of the southern margin of the Ladakh batholith between Upshi and Chumangtang. Thakur, V.C., Sharma, K.K. (Editors). 14<sup>th</sup> Sem. *Him. Geol. W.I.H.G.*, Dehradun 41-60.
- Sharma, K.K., Gupta, K.R., 1978. Some observations on the geology of the Indus and Shyok valleys between Leh and Panamik, District Ladakh, Jammu and Kashmir, India. *Rec. Res. Geol.* 7, 133-143.
- Sharma, K.K., Gupta, K.R., 1983. Calc-alkaline island arc volcanism in Indus–Tsangpo Suture Zone. In: *Geology of Indus Suture Zone of Ladakh.* Thakur, V.C., Sharma, K.K. (Editors). 14<sup>th</sup> Sem. *Him. Geol. W.I.H.G.*, Dehradun 71-78.
- Sharma, K.K., Kumar, S., 1978. Contribution to geology of Ladakh, northwestern Himalaya. *Him. Geol.* 8, 353-287.
- Sharma, K.K., Sinha, A.K., Bagdasarian, G.P., Guhasian, R.C., 1978. Potassium-Argon dating of Dras volcanics, Shyok volcanics and Ladakh granite, Ladakh, Northwest Himalaya. 9<sup>th</sup> Sem. *Him. Geol. W.I.H.G.*, Dehradun 8, 288-295.
- Shi, G.R., Archbold, N.W., 1998. Permian marine biogeography of SE Asia. In: *Biogeography and Geological Evolution of SE Asia.* Hall, R., Blundell, D. (Editors). Backhuys Publishers, Amsterdam, Netherlands 57–72.
- Sinha, A.K., Misra, M., 1992. Emplacement of the ophiolite melange along continental collision zone of Indus Suture Zone in Ladakh Himalaya, India. *J. Him. Geol.* 3, 179-189.
- Sinha, A.K., Upadhyay, R., 1997. Subduction accretion and subduction kneding : A possible mechanism for incorporation of sedimentary sequence within the ophiolitic mélangé belt in the western Himalaya, India. *J. Him. Geol.* 1, 259-264.
- Sinha-Roy, S., 1976. On the origin of ophiolite complexes in the southern Tethys region: Discussion. *Tectonophysics* 34, 257-265.
- Sinha-Roy, S., 1981. Reactivated Tibetan block in a Tethyan context. *J. Struct. Geol.* 3, 459-465.
- Sinha–Roy, S., 1982. Himalyan Main Central Thrust and its implications for Himalyan inverted metamorphism. *Tectonophysics* 84, 197-224.

- Sorensen, S.S., Grossman, J.N., 1989. Enrichment in trace elements in garnet amphibolites from a paleo-subduction zone: Catalina schist, southern California. *Geochim. Cosmochim. Acta* 53, 3155–3177.
- Sorkhabi, R.B., Valdiya, K.S., Arita, K., 1999. Cenozoic uplift of the Himalayan orogen: chronologic and kinematic patterns. In: *Geodynamics of the NW Himalaya*. Jain, A.K., Manickavasagam, R.M. (Editors). *Gond. Res. Group Mem.* 6, 189-206.
- Spandler, C., Mavrogenes, J., Hermann, J., 2007. Experimental constraints on element mobility from subducted sediments using high-P synthetic fluid/melt inclusions. *Chem. Geol.* 239, 228-249.
- Spring, L., Bussy, F., Vannay, J.C., Huon, S., Cosca, M.A., 1993. Early Permian granitic dykes of alkaline affinity in the Indian High Himalaya of Upper Lahaul and SE Zaskar: Geochemical characterization and geotectonic implications. In: *Himalayan Tectonics*. Treloar, P.J., Searle, M.P. (Editors). *Geol. Soc. Lond. Spec. Publ.* 74, 251–264.
- Srikantia, S., Razdan, M.L., 1981. Shilakong ophiolite nappe of Zaskar Mountains. Ladakh Himalaya. *J. Geol. Soc. India* 22, 227-234.
- Srikantia, S.V., Ganesan, T.M., Wangdus, C., 1982. A note on the tectonic frame work and geological set up of the Pangong–Chusul sector, Ladakh Himalaya. *J. Geol. Soc. India* 23, 354-357.
- Srimal, N., 1986. India-Asian collision: Implications from the geology of the eastern Karakoram. *Geology* 14, 523-527.
- Srimal, N., Basu, A.R., 1987. Tectonic interference from Oxygen isotopes in volcano-plutonic complexes of the India-Asia collision zone, NW India. *Tectonics* 6, 261-273.
- Stampfli, G.M., Borel, G.D., 2001. A plate tectonic model for the Paleozoic and Mesozoic constrained by dynamic plate boundaries and restored synthetic oceanic isochrones. *Earth Planet. Sci. Lett.* 196, 17–33.
- Steck, A., Spring, L., Vannay, J.C., Masson, H., Stutz, E., Bucher, H., Marchant, R., Tieche, J.C., 1993. Geological transect across the northwestern Himalaya in eastern Ladakh and Lahul (A model for continental collision of India and Asia). *Eclog. Geol. Helv.* 86, 219-263.
- Stille, H., 1958. 'Die assyntische Tektonik im geologischen Erdbild, *Beih. Geol. J.* 22, 13-28.

- Subbarao, K.V., Bodas, M.S., Hooper, P.R. Walsh, J.N., 1988. Petrogenesis of Jawhar and Igatpuri Formations Western Deccan Basalt Province. *Geol. Soc. India Mem.* 10, 253-279.
- Sun, X.M., Nie, Z.T., Liang, D.Y., 1994. On the time and tectonic significance of ophiolitic mélange in Jinsha river belt, northwest Yunnan. *J. Graduate Sch.* 8, 241–245.
- Sun, X.M., Zhang, B.M., Nie, Z.T., Liang, D.Y., 1997. Formation age and environment of ophiolite and ophiolitic mélange in Jinshajiang belt, Northwestern Yunnan. *Geol. Rev.* 43, 113–120.
- Talukdar, S.C., Majumdar, A.K., 1983. Geology of Abor volcanic rocks, Siang district, Arunachal Pradesh. *Proceeding of Symposium on Geology and mineral Resources. NE Himalaya. Geol. Surv. India* 43, 135-138.
- Tewari, A.P., 1964. On the Upper Tertiary deposits of Ladakh Himalaya and correlation of various geotectonic units of Ladakh with those of the Kumaun-Tibet region. *Int. Geol. Cong., Session-XXII.* 11, 37-58.
- Thahirkheli, R.A.K., Tapponnier, P., Proust, F., 1982. Geology of the Himalaya, Karakoram, and Hindu Kush in Pakistan. *Geol. Bull., University of Peshawar, Spec. Issue* 11, 1-189.
- Thahirkheli, R.A.K., Mattaue, M., Proust, F., Tapponnier, P., 1979. The India Eurasia suture zone in Northern Pakistan : synthesis and interpretation of recent data at plate scale. In: *Geodynamics of Pakistan.* Farah, A., De Jong, K.A. (Editors). *Geol. Surv. Pakistan Spec. Mem. Quetta* 125-130.
- Thakur, V.C., 1981, Regional framework and geodynamic evolution of the Indus-Tsangpo suture zone in the Ladakh Himalaya: *Trans. Royal Soc. Edinburgh. Earth Sci.* 72, 89–97.
- Thakur, V.C., 1993. *Geology of Western Himalaya.* Phys. Chem. Earth. Pergamon Press, New York. 19, 355.
- Thakur, V.C., Bagati, T.N., 1983. An arc trench gap sediments. In: *Geology of Indus Suture Zone of Ladakh.* Thakur, V.C., Sharma, K.K. (Editors.). 14<sup>th</sup> Sem. Him. Geol. W.I.H.G., Dehradun 9-19.
- Thakur V.C., Jain, A.K., 1975. Some Observations on deformation, metamorphism and tectonic significance of the rocks of some parts of the Mishmi Hills, Lohit district (NEFA), Arunachal Pradesh. *Him. Geol.* 5, 339–363.

- Thakur, V.C., Misra, D.K., 1984. Tectonic frame work of the Indus suture zone in eastern Ladakh (N-W Himalaya). *Tectonophysics* 101, 207-220.
- Thakur, V.C., Viridi, N.S., 1979. Lithostratigraphy and structural frame work, deformation and metamorphism of Se region of Ladakh, Kashmir Himlaya. *J. Geol. Soc. India* 22, 46-50.
- Thakur, V.C., Viridi, N.S., Rai, H., Gupta, K.R., 1981. A note on the geology of Nubra-Shyok area of Ladakh, Kashmir, Himalaya. *J. Geol. Soc. India* 22, 46-50.
- Thanh, N.X., Itaya, T., Ahmad, T., Kojima, S., Ohtani, T., Ehiro, M., 2005. Mineral chemistries and K-Ar ages of Hunda granite - diorite complex in the Shyok Suture Zone, Ladakh Himalaya, India. 19<sup>th</sup> General Meet. Int. Mineral. Assoc., Japan 324.
- Treloar, P.J., Petterson, M.G., Jan, M.Q., Sullivan, M.A., 1996. A re-evaluation of the stratigraphy and evolution of the Kohistan arc sequence, Pakistan Himalaya: implications for magmatic and tectonic arc building processes. *J. Geol. Soc. London* 153, 681-693.
- Treloar, P.J., Rex, D.C., Guise, P.G., Coward, M.P., Searle, M.P., Windley, B.F., Petterson, M.G., Jan, M.Q., Luff, I.W., 1990. K-Ar and Ar-Ar geochronology of the Himalayan collision in NW Pakistan: constraints on the timing of suturing, deformation, metamorphism and upliftment. *Tectonics* 8, 884-909.
- Upadhyay, R., Sinha, A.K., Chandra, R., Rai, H., 1999. Tectonic and magmatic evolution of the eastern Karakoram, India. *Geodin. Acta* 12, 341-358.
- Valdia, K.S., 1980. Geology of Kumaun Lesser Himalaya. *Him.Geol. W.I.H.G., Dehradun* 9, 291.
- Valdiya, K.S., 1989. Trans-Himadri intracrustal fault and basement upwarps south of Indus-Tsangpo Suture Zone. *Geol. Soc. Am. Spec. Publ.* 232, 153-168.
- Valdiya, K.S., 1997. Himalaya, the Northern Frontier of East Gondwanaland. *Gond. Res.* 1, 3-9.
- Van der Voo, R., Spakman, W., Bijwaard, H., 1999. Tethyan subducted slabs under India. *Earth. Planet. Sci. Lett.* 171, 7-20.
- Vannay, J.C., Grassemann, B., 1998. Inverted metamorphism in the High Himalaya of Himachal Pradesh (NW India): phase equilibria versus thermo barometry. *Schweiz. Miner. Petro. Mitt.* 78, 107-132.



- Vannay, J.C., Spring, L., 1993. Geochemistry of the continental basalts within the Tethyan Himalaya of Lahul-Spiti and SE Zaskar, northwestern India. *Geol. Soc. Spec. Publ.* 74, 237–249.
- Veevers, J.J., 2004. Gondwanaland from 650–500 Ma assembly through 320 Ma merge in Pangea to 185–100 Ma breakup: supercontinental tectonics via stratigraphy and radiometric dating. *Earth Sci. Rev.* 68, 1–132.
- Wadia, D.N., 1937. The Cretaceous volcanic series of Astor-Deosai, Kashmir and its intrusion. *Rec. Geol. Surv. India* 72, 151-161.
- Wadia, D.N., 1931. The syntaxis of the northwest Himalaya: its rocks, tectonics and orogeny. *Rec. Geol. Surv. India* 65, 189-220.
- Wang, X.F., Metcalfe, I., Jian, P., He, L.Q., Wang, C.S., 2000. The Jinshajiang–Ailaoshan Suture zone: tectonostratigraphy, age and evolution. *J. Asian Earth Sci.* 18, 675–690.
- Weinberg, R.F., Dunlap, W.J., 2001. Comment on “Middle Cretaceous back-arc formation and arc evolution along the Asia margin: the Shyok Suture Zone in northern Ladakh (NW Himalaya)” by Rolland and Pêcher. *Tectonophysics* 340, 265–268
- Weinberg, R.F., Dunlap, W.J., 2000. Growth and deformation of the Ladakh batholith, NW Himalayas: implications for timing of continental collision and origin of calc-alkaline batholiths. *J. Geol.* 108, 303-320.
- Weinberg, R.F., Dunlap, W.J., Whitehouse, M., 2000. New field, structural and geochronological data from the Shyok and Nubra valleys, northern Ladakh: Linking Kohistan to Tibet. In: *Tectonics of the Nanga Parbat Syntaxis and the Western Himalaya*. Khan, M.A., Jan, M.Q., Treloar, P.J., Searle, M.P. (Editors). *Geol. Soc. London Spec. Publ.* 170, 253-275.
- Weinberg, R.F., Searle, M.P., 1998. Pangong Injection Complex, Indian Karakoram: a case of pervasive granite flow through hot viscous crust. *J. Geol. Soc. London* 155, 883-891.
- Wilson, M., Davidson, J.P., 1984. The relative roles of crust and upper mantle in the generation of oceanic island arc magmas. *Phil. Trans. Res. Soc. London* 310, 661-674.
- Wilson, M., 1989. *Igneous Petrogenesis. A Global tectonic approach*. Harper Collins Academic, London.

- Winchester, J.A., Floyd, P.A., 1977. Geochemical discrimination of different magma series and their differentiation products using immobile elements. *Chem. Geol.* 20, 325–344.
- Winter, J.D., 2001. *Igneous and Metamorphic Petrology*. Prentice Hall, New Jersey.
- Wood, B.J., Fraser, D.G., 1986. *Elementary Thermodynamics for Geologists*. Oxford University Press.
- Xu, R.H., Schärer, U., Allegre, C.J., 1985. Magmatism and metamorphism in the Lhasa Block (Tibet): a geo-chronological study. *J. Geol.* 93, 41–57.
- Yin, A., Harrison, T.M., 2000. Geologic evolution of the Himalayan-Tibetan orogen. *Ann. Rev. Earth Planet. Sci. Lett.* 28, 211–280.
- Yoder H.S., Tilley, C.E., 1962. Origin of basalt magmas: an experimental study of natural and synthetic rock system. *J. Petrol.* 3, 342-532.
- Yoder, H.S., 1969. Calc-alkaline andesite: Experimental data bearing on the origin of their assumed characteristics. In: *Proceedings of Andesites Conference*. Birney, A.R.M (Editor). State of Oregon. Dep. Min. Geol. India. Publ. 77-89.
- Yoder, H.S., 1976. *Generation of Basaltic Magmas*. N.A.S. Washington, D.C.
- Zanchi, A., Poli, S., Fumagalli, P., Gaetani, M., 2000. Mantle exhumation along the Tirich Mir Fault Zone, NW Pakistan: pre-Mid Cretaceous accretion of the Karakoram Terrane to the Asian Margin. *J. Geol. Soc. Lond. Spec. Publ.* 170, 237-252.
- Zeitler, P.K., Chamberlain, L.P., 1991 Petrogenetic and tectonic significance of young leucogranites from the northwestern Himalaya, Pakistan. *Tectonics* 10, 729-741.
- Zhong, S., Zhang, N., Li, Z.X., Roberts, J.H., 2007. Supercontinent cycles, true polar wander, and very long-wave length mantle convection. *Earth Planet. Sci. Lett.* 261, 551–564.

# **APPENDICES**

**APPENDIX 1**  
**SAMPLE LOCATIONS AND FIELD DESCRIPTIONS**

S.N	Sample No.	Location	Description	Litho-tectonic unit/ Location
1	HST-1/04	N-34 <sup>0</sup> 34'00.2" E-77 <sup>0</sup> 27'27.3"	Volcanic sand stone / tuff grayish, thick bedded tuff is fine grained where as the sand stone is coarse grained (Along Hundar river valley near Hundar village).	Hundar igneous suite along Hundar valley
2	HST-2/04	N-34 <sup>0</sup> 34'00.2" E-77 <sup>0</sup> 27'27.3"	Dyke cutting through the granite and sand stone	Hundar igneous suite
3	HST-3/04	N-34 <sup>0</sup> 34'5.4" E-77 <sup>0</sup> 27'27.3"	Granite body intruded in to the volcanic tuff and sand stone which in turn intruded by the dyke.	Hundar igneous suite
4	HST-4/04	N-34 <sup>0</sup> 34'12.6" E-77 <sup>0</sup> 27'29.3"	Volcanic sand stone. Fine grained grayish in colour.	Hundar igneous suite
5	HST-5/04	N-34 <sup>0</sup> 34'19.3" E-77 <sup>0</sup> 27'26.3"	Fine grained diorite. Dark in colour with mineral fabric (formed by amphiboles) but not very prominent.	Hundar igneous suite
6	HST-6/04	N-34 <sup>0</sup> 34'21.9" E-77 <sup>0</sup> 27'25.0"	Fine grained gabbro with intrusion of granite. Miner logically this rock has mica, pyx/ amph, Qtz and feldspar	Hundar igneous suite
7	HST-7/04	N-34 <sup>0</sup> 34'23.9" E-77 <sup>0</sup> 27'24.4"	Coarse grained gabbro with ophitic and sub-ophitic texture. This coarse grained gabbro is surrounded by fine grained gabbro.	Hundar igneous suite
8	HST-8/04	N-34 <sup>0</sup> 34'23.9" E-77 <sup>0</sup> 27'24.4"	Fine grained gabbro comparable with HST-6 with same mineralogy.	Hundar igneous suite
9	HST-9/04	N-34 <sup>0</sup> 34'25.5" E-77 <sup>0</sup> 27'23.7"	Pink granite intruded into the diorite. Intrusive contact clearly visible. Granite has K-feld, plag, Qtz. etc.	Hundar igneous suite
10	HST-10/04	N-34 <sup>0</sup> 34'25.5" E-77 <sup>0</sup> 27'23.7"	Fine grained diorite in which the pink granite is intruded. Diorite has elongated mineral (amph) fabric.	Hundar igneous suite
11	HST-11/04	N-34 <sup>0</sup> 34'35.5" E-77 <sup>0</sup> 27'23.5"	Pink coloured granite intruded into the diorite	Hundar igneous suite
12	HST-12/04 13/04	N-34 <sup>0</sup> 34'33.7" E-77 <sup>0</sup> 27'23.2"	Fine grained diorite in which the granite has been intruded	Hundar igneous suite
13	HST-14/04	N-34 <sup>0</sup> 34'33.7" E-77 <sup>0</sup> 27'23.2"	Felsic granite intruding in to the diorite	Hundar igneous suite

14	HST-15/04	N-34°34'34.5" E-77°27'24.3"	Medium grained gabbro, greenish black in colour	Litho-tectonic unit/ Location
15	HST-16/04	N-34°34'44.2" E-77°27'28.3"	Felsic micaceous granite that intrudes into all rock units include volcanic sandstone and tuff	Hundar igneous suite
16	HST-17/04 18/04	N-34°35'03.2" E-77°27'32.3"	Andesitic dyke cutting through the felsic granite	Hundar igneous suite
17	HST-19/04	N-34°35'03.7" E-77°27'32.6"	Fine grained bluish green volcanic sandstone with bedding.	Hundar igneous suite
18	HST-20/04	N-34°35'03.7" E-77°27'32.6"	Very fine grained volcanic tuff, dark in colour.	Hundar igneous suite
19	HST-21/04	N-34°36'14.2" E-77°27'15.6"	Basalt from Shyok volcanics' with well developed schistosity. Epidotization found long the schistosity plane	Shyok volcanics from north of Hundar village
20	HST-22/04 22/04	N-34°36'14.2" E-77°27'15.6"	More massive basalt with less shearing	Shyok volcanics
21	HST-23/04	N-34°36'14.2" E-77°27'15.6"	Basalt with epidotization. Small vesicles are found to be filled with secondary minerals.	Shyok volcanics
22	HST-24/04	N-34°32'46.6" E-77°33'5.9"	Fine grained gabbro, highly sheared.	Shyok volcanics
23	HST-25/04	N-34°32'46.6" E-77°33'5.9"	Coarse grained gabbro	Shyok volcanics
25	HST-26/04 27/04, 28/04	N-34°32'45.5" E-77°33'12.1"	Fine grained basalt with no vesicles.	Shyok volcanics
27	HST-29/04	N-34°32'45.5" E-77°33'12.1"	Basic/mafic dyke cutting through the gabbro.	Shyok volcanics
28	HST-30/04	N-34°32'40.8" E-77°34'11.4"	Micaceous granite highly sheared at the periphery more massive and less sheared towards the centre.	Shyok volcanics
29	HST-31/04 32/04	N-34°32'40.8" E-77°34'11.4"	Fine grained basalt with no vesicles.	Shyok volcanics
30	HST-33/04	N-34°31'49.2" E-77°37'29.1"	Coarse grained gabbro with blebs of mafic minerals (amphiboles)	Shyok volcanics from E of Diskit village.
31	HST-34/04	N-34°31'50.9" E-77°36'0.5"	Volcanic sandstone associated with red shale and gabbro.	Nubra volcanics along Khalsar-Panamik road.

32	HST-35/04	N-34 <sup>0</sup> 31'50.9" E-77 <sup>0</sup> 36'0.5"	Very fine grained red shale found to be associated with volcanic sandstone	Nubra volcanics
33	HST-36/04 37/04	N-34 <sup>0</sup> 42'37.5" E-77 <sup>0</sup> 34'26.1"	Conglomerate small pebbles are associated with red shale and sandstone.	Nubra volcanics
34	HST-38/04	N-34 <sup>0</sup> 42'37.5" E-77 <sup>0</sup> 34'26.1"	Vesicular basalt greenish grey in colour .Vesicles are filled with secondary minerals	Nubra volcanics
35	HST-39/04	N-34 <sup>0</sup> 42'37.5" E-77 <sup>0</sup> 34'26.1"	Massive, dark coloured basalt	Nubra volcanics
36	HST-40/04 41/04	N-34 <sup>0</sup> 47'18.5" E-77 <sup>0</sup> 30'51.9"	Basalt found to be associated with volcanic sandstone.	Karakoram complex along the KF zone
37	HST-42/04 43/04, 44/04	N-34 <sup>0</sup> 47'44.4" E-77 <sup>0</sup> 30'33.9"	Basic/mafic dykes of few m. thickness are cutting through the Karakoram granitoid	Karakoram complex
38	KST-1/04	N-34 <sup>0</sup> 28'7.4" E-77 <sup>0</sup> 42'41.6"	Pink felsic volcanics. Individual grains area not visible.	Khardung volcanics from Khardung area
39	KST-2/04	N-34 <sup>0</sup> 28'7.4" E-77 <sup>0</sup> 42'41.6"	Green coloured, medium grained pyroclastic rock show banding.	Khardung volcanics
40	KST-3/04	N-34 <sup>0</sup> 27'22.4" E-77 <sup>0</sup> 43'20.8"	Red coloured volcanics. Big plagioclase grains re visible with naked eye.	Khardung volcanics
41	KST-4/04	N-34 <sup>0</sup> 26'12.7" E-77 <sup>0</sup> 40'14.8"	Dark coloured massive volcanics without any bedding	Khardung volcanics
42	KST-5/04	N-34 <sup>0</sup> 23'51.4" E-77 <sup>0</sup> 39'40.8"	White coloured rhyolite	Khardung volcanics
43	KST-6/04	N-34 <sup>0</sup> 22'53.2" E-77 <sup>0</sup> 39'24.9"	White coloured rhyolite.	Khardung volcanics
44	KST-7/04	N-34 <sup>0</sup> 25'22.6" E-77 <sup>0</sup> 39'34.5"	Mafic dyke traversing Khardung volcanics	Khardung volcanics
45	KST-8/04	N-34 <sup>0</sup> 26'58.5" E-77 <sup>0</sup> 43'08.7"	Fine grained rhyolitic rock	Khardung volcanics
46	KST-9/04	N-34 <sup>0</sup> 27'10.3" E-77 <sup>0</sup> 43'19.9"	Reddish brown fine grained rhyolitic flow	Khardung volcanics
47	KST-10/04	N-34 <sup>0</sup> 27'14.6" E-77 <sup>0</sup> 43'23.7"	Green coloured, medium grained pyroclastic rock	Khardung volcanics
48	NST-1/06, 2/06,	N-34 <sup>0</sup> 45'7.1" E-77 <sup>0</sup> 33'11.7"	Metabasalt sample collected from Nubra volcanics	Nubra volcanics near Sasoma
49	NST-3/06, 4/06	N-34 <sup>0</sup> 45'7.8" E-77 <sup>0</sup> 33'6.7"	Metabasalt surrounded by finely bedded tuffaceous rock	Nubra volcanics

50	NST-5/06	N-34 <sup>0</sup> 45'7.8" E-77 <sup>0</sup> 33'6.7"	Volcanic sand stone	Nubra volcanics
51	NST-6/06	N-34 <sup>0</sup> 45'7.8" E-77 <sup>0</sup> 33'6.7"	Slightly deformed metabasalt	Nubra volcanics
52	NST-7/06,	N-34 <sup>0</sup> 45'7.8" E-77 <sup>0</sup> 33'6.7"	Tuffaceous rock surrounding metabasalt	Nubra volcanics
53	NST-8/06,	N-34 <sup>0</sup> 45'7.8" E-77 <sup>0</sup> 33'6.7"	Basalt, less deformed and un-metamorphosed	Nubra volcanics
54	NST-9/06	N-34 <sup>0</sup> 45'5.8" E-77 <sup>0</sup> 33'1.7"	Metabasalt with less schistosity	Nubra volcanics
55	NST-10/06, 11/06	N-34 <sup>0</sup> 45'5.6" E-77 <sup>0</sup> 33'1.0"	Unmetamorphosed basalt with epidote veins	Nubra volcanics
56	NST-12/06	N-34 <sup>0</sup> 45'5.4" E-77 <sup>0</sup> 33'0.1"	Highly schistose meta basalt with blebs of amphiboles	Nubra volcanics
57	NST-13/06, 14/06,	N-34 <sup>0</sup> 45'5.4" E-77 <sup>0</sup> 33'0.1"	Metabasalt collected 2m way from previous location	Nubra volcanics
58	NST-15/06	N-34 <sup>0</sup> 45'0.7" E-77 <sup>0</sup> 33'13.5"	Low grade metabasalt	Nubra volcanics
59	NST-16/06	N-34 <sup>0</sup> 44'59.0" E-77 <sup>0</sup> 33'30.1"	Fine grained metabasalt from 20m E of previous location	Nubra volcanics
60	NST-17/06	N-34 <sup>0</sup> 44'56.8" E-77 <sup>0</sup> 33'15.6"	Undeformed, fine grained massive basalt	Nubra volcanics
61	NST-18/06	N-34 <sup>0</sup> 44'56.9" E-77 <sup>0</sup> 33'18.8"	Fine grained, low grade slightly schistose metabasalt	Nubra volcanics
62	NST-19/06	N-34 <sup>0</sup> 44'54.8" E-77 <sup>0</sup> 33'19.4"	Fresh massive basalt with epidote veins	Nubra volcanics
63	NST-20/06	N-34 <sup>0</sup> 44'52.4" E-77 <sup>0</sup> 33'20.9"	Massive basalt	Nubra volcanics
64	NST-21/06, 22/06	N-34 <sup>0</sup> 44'51.5" E-77 <sup>0</sup> 33'23.3"	Fine grained schistose metabasalt with specs of chlorites	Nubra volcanics
65	NST-23/06, 24/06	N-34 <sup>0</sup> 44'46.7" E-77 <sup>0</sup> 33'27.9"	Schistose metabasalt with blebs of amphiboles	Nubra volcanics
66	NST-25/06	N-34 <sup>0</sup> 44'44.5" E-77 <sup>0</sup> 33'26.4"	Metabasalt with nicely developed schistosity	Nubra volcanics
67	NST-26/06, 27/06	N-34 <sup>0</sup> 44'42.9" E-77 <sup>0</sup> 33'24.8"	Blue coloured fresh metabasalt with less developed schistosity	Nubra volcanics
68	NST-28/06	N-34 <sup>0</sup> 48'28.4" E-77 <sup>0</sup> 30'10.6"	Greenish grey diorite	Karakoram complex along Kubet-Gonbo road
69	NST-29/06, 30/06	N-34 <sup>0</sup> 48'22.4" E-77 <sup>0</sup> 30'13.0"	Diorite with less mafic minerals, relatively light coloured	Karakoram complex

70	NST-31/06	N-34 <sup>0</sup> 48' 19.0" E-77 <sup>0</sup> 30' 14.3"	Dyke intruding into the deformed Karakoram granite	Karakoram complex
71	NST-32/06	N-34 <sup>0</sup> 48' 19.0" E-77 <sup>0</sup> 30' 14.3"	Porphyritic Karakoram granite	Karakoram complex
72	NST-33/06	N-34 <sup>0</sup> 48' 16.8" E-77 <sup>0</sup> 30' 13.0"	Augen gneiss in which plagioclases are deformed into augen shape	Karakoram complex
73	NST-34/06	N-34 <sup>0</sup> 48' 16.8" E-77 <sup>0</sup> 30' 13.0"	Granite is highly deformed into mylonite	Karakoram complex
74	NST-35/06, 36/06	N-34 <sup>0</sup> 48' 11.5" E-77 <sup>0</sup> 30' 13.3"	Dark coloured medium grained diorite into which the granite has intruded	Karakoram complex
75	NST-37/06,	N-34 <sup>0</sup> 48' 10.2" E-77 <sup>0</sup> 30' 14.6"	Porphyritic granite developed gneissosity	Karakoram complex
76	NST-38/06	N-34 <sup>0</sup> 48' 10.2" E-77 <sup>0</sup> 30' 14.6"	Felsic tuff associated with volcanic sandstone	Karakoram complex along Kubed-Charasa road
77	NST-39/06	N-34 <sup>0</sup> 48' 10.2" E-77 <sup>0</sup> 30' 14.6"	Leuco-granite associated with deformed volcanic sand stone	Karakoram complex
78	NST-40/06	N-34 <sup>0</sup> 47' 16.2" E-77 <sup>0</sup> 30' 40' 9"	Felsic tuff associated with volcanic sandstone	Karakoram complex
79	NST-41/06	N-34 <sup>0</sup> 47' 18.9" E-77 <sup>0</sup> 30' 43.2"	Mafic dyke about 4m width cutting into the diorite	Karakoram complex
80	NST-42/06	N-34 <sup>0</sup> 47' 18.9" E-77 <sup>0</sup> 30' 43.2"	Diorite with dyke intrusion	Karakoram complex
81	NST-43/06	N-34 <sup>0</sup> 47' 40.3" E-77 <sup>0</sup> 30' 27.0"	Granite without porphyry. Slightly developed mineral lineation is present	Karakoram complex
82	NST-44/06	N-34 <sup>0</sup> 47' 42.8" E-77 <sup>0</sup> 30' 29.6"	Fine grained mafic dyke dark in colour	Karakoram complex
83	NST-45/06	N-34 <sup>0</sup> 47' 42.8" E-77 <sup>0</sup> 30' 29.6"	Less deformed granite away from Karakoram Fault zone	Karakoram complex, along Hurgam-Panamik road
84	NST-46/06	N-34 <sup>0</sup> 02' 48.1" E-78 <sup>0</sup> 09' 28.4"	Deformed leucogranite	Tangtse area
85	NST-47/06	N-34 <sup>0</sup> 01' 30.6" E-78 <sup>0</sup> 10' 16.9"	Ladakh granite, deformed along southern strand of KF	Tangtse area
86	NST-48/06	N-34 <sup>0</sup> 01' 30.7" E-78 <sup>0</sup> 10' 26.8"	Calc-silicate with patches of granite within it.	Tangtse area
87	NST-49/06	N-34 <sup>0</sup> 01' 32.1" E-78 <sup>0</sup> 11' 56.5"	Granites are intercalated with mafic layers, biotites are concentrated in this layer	Tangtse area



88	NST-50/06	N-34 <sup>0</sup> 02'20.9" E-78 <sup>0</sup> 13'13.8"	Gneiss with alternate felsic and mafic bands	Tangtse area
89	NST-51-a/06, 51-b/06	N-34 <sup>0</sup> 00'50.6" E-78 <sup>0</sup> 17'40.8"	Carbonaceous shale	Pangong meatmorphics
90	NST-52-a/06	N-34 <sup>0</sup> 00'08.2" E-78 <sup>0</sup> 20'16.6"	Garnet-muscovite schist	Pangong meatmorphics
91	NST-52-b/06	N-34 <sup>0</sup> 00'08.2" E-78 <sup>0</sup> 20'16.6"	Garnet-staurolite-muscovite schist	Pangong meatmorphics
92	NST-52-c/06	N-34 <sup>0</sup> 00'08.2" E-78 <sup>0</sup> 20'16.6"	Garnet-muscovite schist	Pangong meatmorphics
93	NST-52-c/06	N-34 <sup>0</sup> 00'08.2" E-78 <sup>0</sup> 20'16.6"	White coloured Marble	Pangong meatmorphics
94	NST-53/06 (a,b,c)	N-33 <sup>0</sup> 58'47.9" E-78 <sup>0</sup> 22'11.8"	Kyanite schist and other metapellites	Pangong meatmorphics
95	NST-54/06	N-33 <sup>0</sup> 58'47.9" E-78 <sup>0</sup> 22'11.8"	Granite which is more felsic cutting across garnet-biotite bearing granite	Part of Karakoram complex from Shyok village to Pangong
96	NST-55/06	N-33 <sup>0</sup> 58'47.9" E-78 <sup>0</sup> 22'11.8"	Amphibolite rock cut by aplitic dykes	Part of Pangong metamorphics
97	NST-56/06	N-34 <sup>0</sup> 05'55.3" E-77 <sup>0</sup> 59'9.7"	Altered dunite	Tsoltak area
98	NST-57/06	N-34 <sup>0</sup> 05'56.1" E-77 <sup>0</sup> 59'25.7"	Ultramafics (Herzburgite)	Tsoltak area
99	NST-58/06, 59/06	N-34 <sup>0</sup> 05'57.3" E-77 <sup>0</sup> 59'27.7"	Ultramafics (Pyroxenite)	Tsoltak area
100	NST-60/06	N-34 <sup>0</sup> 05'58.3" E-77 <sup>0</sup> 59'28.7"	Fine grained basalt with less vesicles	Tsoltak area
101	NST-61/06, 62/06	N-34 <sup>0</sup> 05'58.8" E-77 <sup>0</sup> 59'29.2"	Coarse grained gabbro	Tsoltak area
102	NST-63/06	N-34 <sup>0</sup> 05'59.5" E-77 <sup>0</sup> 59'31.1"	Fine grained dark coloured basalt	Tsoltak area
103	NST-64/06	N-34 <sup>0</sup> 05'59.9" E-77 <sup>0</sup> 59'31.7"	Vesicular basalt	Tsoltak area
104	NST-65/06	N-34 <sup>0</sup> 06'01.0" E-77 <sup>0</sup> 59'32.7"	Vesicular basalt, vesicles are filled with secondary minerals(zeolites)	Tsoltak area
105	NST-66/06	N-34 <sup>0</sup> 06'02.5" E-77 <sup>0</sup> 59'33'.1"	Ultramafic rock (pyroxenite)	Tsoltak area
106	NST-67/06	N-34 <sup>0</sup> 06'02.5" E-77 <sup>0</sup> 59'33.1"	Light green coloured and altered dunite forming serpentinite.	Tsoltak area

107	NST-68/06	N-34 <sup>0</sup> 06'02.8" E-77 <sup>0</sup> 59'34.1"	Basalt with vesicles filled with zeolites	Tsoltak area
108	NST-69/06	N-34 <sup>0</sup> 06'03.2" E-77 <sup>0</sup> 59'35.5"	Fine grained felsic volcanics	Tsoltak area
109	NST-71/06	N-34 <sup>0</sup> 06'03.8" E-77 <sup>0</sup> 59'36.0"	Dolerite with ophitic and sub-ophitic texture	Tsoltak area
110	NST-72/06 (a, b, c, d)	N-34 <sup>0</sup> 06'04.2" E-77 <sup>0</sup> 59'37.8"	Giant plagioclase basalt with big plagioclase laths	Tsoltak area

Note. The number after slash indicates year of collection of sample.

APPENDIX 2

MAJOR ELEMENT DATA IN WT%, FROM DIFFERENT LITHO-TECTONIC UNITS OF SSZ  
ANALYZED USING XRF AT W.I.H.G., DEHRA DUN

Litho-tectonic units	Sample	SiO <sub>2</sub>	TiO <sub>2</sub>	Al <sub>2</sub> O <sub>3</sub>	Fe <sub>2</sub> O <sub>3</sub>	MnO	MgO	CaO	Na <sub>2</sub> O	K <sub>2</sub> O	P <sub>2</sub> O <sub>5</sub>	LOI
Hundar igneous suite	HST-9	75.23	0.13	13.52	1.47	0.03	0.18	1.43	4.13	3.94	0.02	0.12
	HST-18	76.37	0.11	13.19	1.47	0.05	0.07	0.92	4.25	4.13	0.02	0.78
	HST-3	76.96	0.09	13.18	1	0.03	0.22	0.52	3.55	4.53	0.01	1.02
	HST-7	63.53	0.48	15.47	5.09	0.16	3.63	4.57	4.3	2.18	0.12	0.68
	HST-10	64.83	0.57	15.86	3.75	0.1	2.92	4.13	4.54	2.18	0.22	1.88
	HST-12	67.89	0.38	15.54	2.89	0.12	2.96	3.67	4.14	2.77	0.12	0.90
	HST-15	58.14	0.81	15.71	7.07	0.24	4.58	6.76	3.43	1.18	0.21	2.48
	HST-6	57.11	0.86	16.3	8.1	0.15	5.1	8.35	2.64	1.08	0.23	1.56
	HST-17	48.66	1.11	14.4	12.17	0.36	7	9.19	1.63	1.88	0.17	3.51
Shyok volcanics	HST-32	75.49	0.25	12.44	4.11	0.05	0.69	1.72	6.18	0.09	0.03	0.22
	HV-1	73.19	0.46	8.62	4.18	0.05	1.67	4.35	1.57	1.02	0.1	.69
	HV-7	70.2	0.65	12.89	4.74	0.05	2.02	4.01	1.46	2.23	0.13	1.52
	HV-4	66.91	0.68	13.91	5.19	0.09	2.19	5.09	0.93	2.37	0.15	2.5
	HV-3	65.43	0.73	15.6	5.98	0.09	2.33	4.48	0.65	2.85	0.14	1.27
	HV-2	64.79	0.75	16.23	5.97	0.1	2.37	4.86	0.67	3.22	0.15	1.04
	HV-5	64.4	0.74	16.32	6.01	0.09	2.34	4.51	0.7	3.01	0.15	2.08
	HV-6	62.02	0.73	17.62	6.3	0.11	2.57	4.84	1.03	3.1	0.15	1.62
	HST-29	57.06	0.26	12.55	8.36	0.16	3.85	6.12	2.33	0.86	0.03	1.49
	HST-21	54.57	0.88	15.41	8.9	0.15	4.8	7.56	2.06	1.56	0.15	3.93
	HST-27	52.62	1.14	16.96	8.41	0.15	4.81	8.02	3.89	0.5	0.31	3.06
	HST-22	47.01	1.36	12.73	12.76	0.1	9.27	8.74	3.32	0.07	0.11	4.58

Litho-tectonic units	Sample	SiO <sub>2</sub>	TiO <sub>2</sub>	Al <sub>2</sub> O <sub>3</sub>	Fe <sub>2</sub> O <sub>3</sub>	MnO	MgO	CaO	Na <sub>2</sub> O	K <sub>2</sub> O	P <sub>2</sub> O <sub>5</sub>	LOI
<b>Khardung volcanics</b>	KST-1	78.28	0.12	12.28	0.94	0.09	0.05	0.49	3.48	4.69	0.01	0.26
	KST-2	73.41	0.32	13.63	3.3	0.15	0.57	2.7	2.76	3.17	0.05	0.19
	KST-3	75.83	0.15	13.74	1.85	0.06	0.46	0.82	3.76	3.58	0.02	0.19
	KST-4	67.17	0.51	14.77	3.51	0.13	1.17	3.98	4.17	3.31	0.09	2.14
	KST-5	77.34	0.13	12.91	1.15	0.03	0.1	0.87	4.18	3.93	0.02	0.20
	KST-6	76.97	0.11	13.24	1.19	0.02	0.23	0.87	4.29	4.07	0.01	0.49
	KST-8	75.35	0.31	14.26	0.7	0.01	1.46	0.15	3.09	4.61	0.05	1.7
	KST-9	64.18	0.71	15.16	4.84	0.15	1.27	3.87	4.44	2.4	0.22	2.37
	KST-10	72.43	0.26	13.88	2.35	0.12	0.23	0.93	4.29	3.62	0.05	1.63
<b>Karakoram Complex</b>	NST-37	68.23	0.42	14.88	3.16	0.06	1.25	3.15	3.14	3.81	0.14	1.57
	NST-32	63.38	0.55	16.32	4.43	0.07	1.81	4.01	3.02	4.01	0.2	1.61
	NST-33	74.66	0.32	12.44	2.01	0.02	0.49	1.55	2.39	4.46	0.06	1.28
	NST-34	62.73	0.67	15.75	5.58	0.11	2.43	4.73	2.76	2.86	0.26	1.68
	NST-38	64.61	0.55	15.76	4.72	0.08	1.95	3.96	2.99	3.18	0.22	1.81
	NST-39	69.4	0.39	14.25	2.91	0.04	1.26	3.49	3.07	2.65	0.13	2.07
	NST-43	72.57	0.23	14.75	2.22	0.03	0.77	1.66	3.76	4.36	0.06	1.12
	NST-40	69.83	0.29	15.92	2.36	0.03	0.52	3.1	4.18	1.89	0.05	1.39
	NST-45	68.05	0.29	17.01	2.2	0.03	0.57	3.26	4.62	2.57	0.09	0.73
	NST-28	50.67	1.12	17.72	8.91	0.09	5.88	7.44	3.1	2.57	0.47	3.68
	NST-29	53.07	0.56	11.4	8.31	0.17	12.25	10.01	1.64	1.36	0.26	2.35
	NST-35	54.55	0.89	15.73	8.72	0.16	6.83	6.11	3.15	3.71	0.57	1.87
	NST-42	50.73	0.64	13.08	7.22	0.16	11.62	9.15	1.6	1.9	0.29	3.11
	NST-30	47.28	1.64	18.48	11.18	0.13	6.74	6.39	2.57	4.04	0.68	2.86
	NST-36A	52.26	0.82	17.6	7.24	0.14	5.47	7.5	2.64	3.32	0.47	2.37
	NST-36B	48.16	0.93	20.64	8.51	0.16	4.8	6.38	3.12	4.71	0.27	2.43
	NST-36C	47.52	0.98	18.9	10.53	0.2	4.34	9.31	2.49	3.31	0.41	1.77
	HST-40	51.01	0.63	12.38	9.03	0.19	9.82	9.35	2.24	1.47	0.24	1.58
	NST-41	53.43	0.65	12.21	8.84	0.22	10.08	9.93	1.61	1.47	0.24	2.17
	HST-43	52.71	0.79	15.45	6.85	0.12	9.19	7.66	2.49	2.36	0.46	2.96
NST-44	57.23	0.6	14.52	6.96	0.12	7.34	7.09	2.49	3.18	0.37	1.77	
NST-31A	52.42	1	14.82	9.52	0.14	7.99	6.51	2	3.48	0.57	1.56	
NST-31B	53.76	0.91	14.99	9.4	0.18	7.66	6.94	1.64	3.36	0.44	1.45	

Litho-tectonic units	Sample	SiO <sub>2</sub>	TiO <sub>2</sub>	Al <sub>2</sub> O <sub>3</sub>	Fe <sub>2</sub> O <sub>3</sub>	MnO	MgO	CaO	Na <sub>2</sub> O	K <sub>2</sub> O	P <sub>2</sub> O <sub>5</sub>	LOI
Tsoltak volcanics	NST-64	66.91	1.01	19.75	2.6	0.05	2.02	1.12	1.39	2.68	0.02	1.4
	NST-67	62.4	1.01	21.91	5.81	0.08	2.76	1.39	1.55	1.42	0.03	1.5
	NST-68	62.37	0.81	22.98	4.46	0.04	2.35	0.91	1.75	2.78	0.03	3.15
	NST-71	55.08	0.92	15.7	9.07	0.15	6.6	7.38	3.17	1.44	0.24	1.52
	NST-69	44	0.18	3.88	10.61	0.17	30.49	6.2	0.1	0.01	0.02	2.69
Nubra volcanics	NST-7	53.97	0.56	13.5	5.79	0.06	6.28	7.84	5.36	1.53	0.15	4.3
	NST-17	53.45	0.83	12.83	13.53	0.06	8.81	2.89	4.42	0.87	0.19	3.05
	NST-20	62.23	0.58	11.23	6.68	0.07	6.65	4.43	2.74	2.6	0.15	1.7
	NST-27	52.86	1.33	13.33	9.5	0.18	9.45	3.49	3.57	0.98	0.32	3.51
	NST-15	59.57	0.6	12.58	4.59	0.08	8.57	4.94	4.08	2.15	0.17	2.41
	HST-38	53.43	1.1	17.12	7.11	0.05	7.72	4.19	4.47	1.56	0.21	3.78
	NST-1	52.39	0.75	15.63	10.24	0.05	9.21	1.11	4.84	3.61	0.19	1.55
	NST-2	66.21	0.5	15.38	3.59	0.04	1.86	2.63	5.44	0.97	0.133	3.18
	NST-3	57.66	1.02	16.24	6.91	0.05	4.35	6.83	2.58	0.88	0.27	3.23
	NST-4	62.91	0.84	15.7	6.36	0.09	2.39	1.39	3.05	2.58	0.21	4.35
	NST-5	57.66	0.6	15.55	6.46	0.04	5.49	7.57	3.16	1.32	0.18	1.81
	NST-6	59.65	0.77	15.54	6.91	0.03	4.31	5.72	3.26	1.2	0.2	2.57
	NST-8	66.81	0.86	15.47	4.99	0.06	1.78	1.02	2.86	2.62	0.16	3.26
	NST-9	59.39	0.69	16.56	6.09	0.08	3.88	6.79	2.94	1.49	0.13	1.87
	NST-10	53.47	1.03	18.62	7.6	0.11	4.03	8.48	3.06	1.04	0.21	2.46

APPENDIX 3

TRACE ELEMENT CONCENTRATIONS IN PPM, ANALYZED USING XRF AT W.I.H.G., DEHRA DUN

Lithotectonic Units	Sample No.	Sc	Co	Ni	Cu	Zn	Ga	Pb	Th	Rb	U	Sr	y	Zr	Nb
Hundar igneous suite	HST-18	1		3	15	29	14.7	20	15.4	138	0.1	89	21	100	12
	HST-3			4	56	76	11	26	15.5	103	2	87	15	114	5
	HST-9	1			8	20	13.8	14	9	80	4.5	184	13	126	5
	HST-12	8	10	25	44	79	13.5	6.9	12	112	4	244	13	165	8
	HST-6	26	31	36	60	87	16.4	10.8	6.8	30	1.2	393	20.1	144	6
	HST-17	37	33	25	37	125	15.9	6.6	0.3	83	2.7	310	30	72	3
	HST-15	21	24	35	31	98	16.8	11.5	3.4	54	2	360	26	121	12
	HST-10	11	12	14	15	63	15.6	6.5	9.9	75	2.6	310	17.5	131	8
	HST-7	18	18	23	22	80	19	14	6	61	2	285	24	243	11
Khardung volcanics	KST-8	4	1	4	6	19	10	5.8	7.2	119	5.6	73	22	191	10
	KST-6	3	1	6	2	8	13	9.5	13	111	5.4	84	19	102	8
	KST-5			0.5	37	30	13	14	13	104	0.1	80	23	108	9
	KST-4	7		7.8	23	69	16	15	5	93	1.9	172	37	245	12
	KST-3	0.7		3	41	58	14	17	11.7	101	8.6	135	28	157	12
	KST-2	5		4	30	86	15	18	9.7	112	0.8	152	36	231	13
	KST-1	0.5		0	26	38	12	12	14	142	2.5	72	30	72	9
Shyok volcanics	HST-29	6.7	13	1	24	23	13.7	3	3.5	2	1.5	71	23	87	3
	HST-22	38	29	21	16	37	17	2.7	0.9	2		112	25	228	3
	HST-27	8	6	10	16	21	13.8	0.5	1	1	0.5	104	19	82	4.8
	HST-21	15	10	12	13	18	14.6	1.8	0.9	1	0.5	110	20.4	110	3.5
	HST-32	28	35	165	20	65	11	5		25	0.7	132	9	38	2.5
Nubra volcanics	HST-38	17	28	44	92	37	17.7	9.8	1.6	68	2.4	555	16.8	127	5.5
	NST-20	13	23	114	26	29	10.5	2.9	0.9	100	1.8	361	10.6	102	6
	NST-1	10	26	129	14	45	18	1.5	1.8	133	2.6	99	4	117	6
	NST-15	17	15	106	14	45	12.8	2	1.5	64	1.8	257	19	105	7.5
	NST-27	15	23	60	10	91	12.3	3.6	3	29	0.7	273	25.5	188	9.4
	NST-17	16	34	154	23	36	15.9	4	1.8	44	1.5	317	5	114	5.7
	NST-7	17	17	99	6	24	11	1.5	2.7	50	1.8	378	14.5	106	6.5

Lithotectonic Units	Sample No.	Sc	Co	Ni	Cu	Zn	Ga	Pb	Th	Rb	U	Sr	y	Zr	Nb
Tsoltak volcanics	NST-64	17	9	63	15	42	15.8	24.5	1	72	1.8	89	27	118	9.6
	NST-67	26	12	53	18	59	20.8	24.9	15.5	50	1.5	115	26	160	12.9
	NST-68	12	17	78	39	60	21.8	19.5	29.6	100	1.7	119	29.9	184	13.8
	NST-69	44	71	737	17	42	0.5	1.6	1	2		4	3.5	10	4
	NST-71	24	29	32	81	74	14.6	8	4.9	47	1.6	423	18	124	8.7
Karakoram Complex	HST-43	25	31	86	86	79	15.5	12.7	17.8	58	2	1074	16	271	13
	HST-40	33	35	81	43	90	14.5	12	8	36	1	864	17.5	159	6.5
	NST-41	30	39	89	176	81	12.6	11	9.9	34	1.9	846	18.6	143	5.8
	NST-44	18	23	26	11	50	12.7	14.9	14.5	91	2.7	1270	19	215	6
	NST-31A	20	25	10	22	76	15.4	17	9.7	89	2	1183	25.2	262	9
	NST-31B	25	27	48	59	77	14.5	19	8	86	1.9	1130	26.7	145	9.5
	NST-40	6	1	6	1	16	13.9	7.8	31	35	0.9	1063	28.5	361	16.9
	NST-43	5	7	6	1	16	12.8	22.3	26.5	109	4.4	487	11.5	138	6.6
	NST-45	6	1	4	4	41	17	32.4	14	72	3.6	681	8.5	152	6
	HST-37	4	8	11	5	35	13	30	23	97	4	523	19	183	10
	HST32	9	12	14	15	46	15	20	16	112	3	705	24	222	8
	HST-33	3	5	10	18	16	10	21	47	76	4	361	11	207	7
	HST-34	15	15	15	17	59	15	16	16	89	2	717	28	235	7
	HST-38	10	10	15	13	48	14	14	16	86	3	652	25	236	6
	HST-39	7	8	11	2	25	12	10	21	92	2	528	16	152	9
	NST-36A	24	26	56	18	79	15	13	20	121	4	890	23	214	27
	NST-36B	25	20	20	13	119	21	21	7	193	0	938	38	282	10
	NST-36C	32	22	6	36	106	20	63	7	162	3	1303	56	167	10
	NST-30	31	30	5	10	101	22.5	28	13.6	127	1	1169	38.2	374	15.3
	NST-28	14	26	8	36	69	17.6	20	9.3	62	3.8	1585	16.6	110	5.5
	NST-29	34	36	113	22	73	9.6	13	2.8	32	1.9	726	18	146	6.6
	NST-35	19	25	25	35	82	16.6	24	22.5	156	1.5	1518	22.6	265	10.5
	NST-42	24	33	189	35	68	10.6	6	6	41	1.9	736	17.5	183	6.7

**APPENDIX 4**

**REE DATA OF SAMPLES IN PPM., ANALYZED BY ICP-MS, AT W.I.H.G., DEHRA DUN**

	La	Ce	Pr	Nd	Sm	Eu	Gd	Tb	Dy	Er	Yb	Lu
<b>Hundar igneous suite</b>												
HST-18	36.68	65.69	7.71	25.63	4.4	0.56	2.88	0.44	2.92	1.18	1.67	0.24
HST-3	36.32	64.26	7.38	24.32	4.07	0.76	2.43	0.31	1.9	0.78	1.07	0.14
HST-9	37.93	65.3	6.98	22.93	3.87	1.44	3.23	0.39	1.9	1.01	0.96	0.16
HST-12	29.46	51.45	6.13	21.85	3.9	0.8	3	0.51	3.99	1.86	2.64	0.37
HST-6	20.55	39.88	5.2	20.81	4.53	1.26	4.45	0.65	3.7	1.95	1.81	0.27
HST-17	10.43	21.27	3.02	12.94	3.47	1.04	3.78	0.61	3.65	2.02	1.93	0.3
HST-15	30.41	69.5	9.01	35.09	7.42	1.82	7.55	1.08	6.31	3.64	3.63	0.58
HST-10	20.99	42.26	5.27	20.46	4.37	1.08	4.6	0.67	3.97	2.37	2.3	0.37
HST-7	34.09	71.61	9.05	35.34	7.56	2.06	7.63	1.1	6.2	3.62	3.24	0.51
<b>Khardung volcanics</b>												
KST- 5	29.5	53.06	6.1	19.36	3.3	0.54	2.5	0.44	3.53	1.9	3.07	0.45
KST-4	23.1	49.64	6.13	24.25	5.56	1.39	5.42	0.84	4.92	2.62	2.56	0.41
KST-3	24.54	48.14	5.51	18.4	3.75	0.76	3.51	0.54	3.05	1.9	2.12	0.35
KST-2	32.28	63.08	8.29	31.58	6.63	1.66	6.75	1.03	6.11	3.66	3.77	0.61
KST-1	21.19	46.5	5.56	19.75	4.31	0.7	3.85	0.59	3.56	2.27	2.61	0.42
<b>Nubra volcanics</b>												
HST-38	13.3	28.63	3.66	14.32	3.09	0.9	3.04	0.43	2.63	1.28	1.16	0.17
NST-1	2.46	4.69	0.55	1.87	0.67	0.29	0.50	0.08	0.53	0.39	0.39	0.06
NST- 7	19.62	38.62	4.80	18.60	3.92	1.34	4.189	0.51	2.46	1.08	0.76	0.10
NST-17	5.47	10.63	1.28	4.79	1.163	0.36	0.92	0.12	0.55	0.33	0.31	0.04
NST- 20	19.06	37.51	4.47	17.14	3.72	1.08	3.59	0.43	2.24	1.01	0.83	0.12
NST -27	22.76	50.43	6.30	23.79	5.28	1.50	5.56	0.79	4.32	2.46	2.68	0.38
NST-15	9.69	21.11	2.63	9.95	2.67	0.85	2.69	0.44	2.65	1.28	0.99	0.12



	La	Ce	Pr	Nd	Sm	Eu	Gd	Tb	Dy	Er	Yb	Lu
<b>Karakorm complex</b>												
HST-43	46.99	93.42	11.25	39.9	7.71	2.34	5.96	0.72	3.57	1.75	1.33	0.18
HST-40	41.39	78.78	9.45	35.64	6.56	1.73	5.46	0.7	3.61	1.72	1.42	0.19
NST- 41	33.24	66.27	7.63	28.01	5.97	1.73	5.78	0.64	3.39	1.72	1.44	0.20
NST- 44	44.41	89.71	10.81	37.82	7.62	2.46	6.53	0.72	3.41	1.66	1.31	0.19
NST-31(A)	44.27	94.75	12.47	47.23	10.21	3.05	8.45	1.05	5.04	2.53	2.21	0.34
NST-31(B)	34.81	81.94	10.91	40.53	9.34	2.94	7.78	1.03	5.066	2.73	2.41	0.35
NST -28	41.06	83.54	9.97	34.61	7.24	2.98	6.27	0.62	2.84	1.50	1.26	0.18
NST- 29	32.63	68.99	9	34.56	6.98	1.94	6.09	0.75	3.64	1.87	1.69	0.25
NST -35	94.86	180.34	20.19	69.15	10.54	3.06	11.25	1.11	4.81	2.43	1.85	0.25
NST -42	30.49	62.23	7.64	28.90	6.42	2.04	5.60	0.71	3.55	1.77	1.50	0.22
NST -43	34.72	54.71	5.72	17.24	3.50	1.2	3.17	0.31	1.38	0.76	0.73	0.11
NST -45	33.03	58.83	6.52	20.76	3.88	1.55	3.40	0.28	1.15	0.49	0.34	0.05
NST- 40	65.73	120.84	13.10	41.31	8.50	2.85	7.42	0.74	3.55	1.68	1.28	0.16
<b>Shyok volcanics</b>												
HST-29	7.26	15.55	1.97	8.09	2.28	0.51	2.27	0.38	2.35	1.38	1.32	0.2
HST-22	7.38	16.93	2.46	11.19	3.31	1.13	3.86	0.66	4.13	2.44	2.4	0.34
HST-21	6.8	15.21	2.3	9.76	2.54	.62	2.32	.42	3.15	2.02	2.11	.19
HST-27	7.6	14.78	1.79	10.3	2.98	1.01	3.45	.57	2.85	1.87	1.45	.27
HST-32	3.72	6.63	0.89	3.87	1.18	0.41	1.08	0.18	1.1	0.7	0.73	0.12
<b>Tsoltak volcanics</b>												
NST- 64	25.94	49.57	5.60	17.59	3.52	1.05	3.50	0.41	2.11	1.18	1.24	0.19
NST- 67	25.82	47.98	5.40	17.84	3.91	1.24	4.26	0.58	3.43	1.99	1.96	0.31
NST- 68	34.61	72.17	7.72	25.99	5.24	1.35	5.10	0.63	3.59	2.29	2.65	0.42
NST- 69	1.36	2.93	0.42	1.74	0.56	0.28	0.67	0.12	0.80	0.48	0.50	0.08
NST- 71	18.51	37.20	4.60	16.15	3.97	1.36	4.05	0.55	2.89	1.56	1.42	0.22

APPENDIX 5

ISOTOPIC RATIOS ANALYZED BY TIMS, AT NATIONAL FACILITY FOR GEOCHRONOLOGY AND GEOSCIENCES, PONDICHERRY UNIVERSITY.

Sample	$^{143}\text{Nd}/^{144}\text{Nd}$	$^{147}\text{Sm}/^{144}\text{Nd}$	$(^{143}\text{Nd}/^{144}\text{Nd})_i$	$\epsilon_{\text{t Chur}}$ (t=110)	$\epsilon\text{Nd}_0$	$^{87}\text{Sr}/^{86}\text{Sr}$	$^{87}\text{Rb}/^{86}\text{Sr}$	$(^{87}\text{Sr}/^{86}\text{Sr})_i$	$\epsilon_{\text{t Sr}}$ (t=110)	$\epsilon\text{Sr}_0$
<b>Hundar</b>	<b>igneous suit</b>									
HST-17	0.512846	0.237011	0.512675	3.492504	4.05744404	0.704562	0.30554	0.704084	-4.0897	0.880057
HST-9	0.512572	0.139295	0.512471	-0.481729	-1.2874582	0.70746	0.561682	0.706581	31.3687	42.01561
HST-6	0.512548	0.207171	0.512398	-1.903150	-1.7556248	0.705073	0.068678	0.704965	8.42167	8.133428
HST-10	0.512687	0.188234	0.512551	1.074976	0.95584018	0.704921	0.163526	0.704665	4.15875	5.975869
HST-12	0.512669	0.17459	0.512543	0.915235	0.60471522	0.705745	0.453922	0.705035	9.41232	17.67211
<b>Shyok volcanics</b>										
HV-8	0.512505	0.13947	0.512404	-1.791503	-2.5944234	0.705619	0.5789	0.704714	4.84985	15.88361
HV-14	0.512792	0.14396	0.512688	3.745485	3.00406915	0.703989	0.071	0.703878	-7.01943	-7.25337
<b>Nubra</b>	<b>volcanics</b>									
HST-38	0.512804	0.189869	0.512667	3.334967	3.23815246	0.704889	0.184452	0.704600	3.24005	5.521647
<b>Karakorm complex</b>										
HST-40.r	0.512375	0.151962	0.512265	-4.5035321	-5.1303259	0.706499	0.043567	0.706430	29.2239	28.37473
HST-43	0.512352	0.151245	0.5122435	-4.942240	-5.5789856	0.706657	0.057834	0.706566	31.1504	30.61746
HR-4	0.512216	0.13402	0.512119	-7.354036	-8.2319297	0.70806	0.12404	0.707866	49.5995	50.53229
KP-7	0.512085	0.05597	0.5120441	-8.814156	-10.787339	0.710259	0.3243	0.709752	76.3745	81.74592
Kp-18	0.512243	0.13903	0.5121426	-6.89755	-7.7052423	0.711595	0.2427	0.711215	97.1527	100.7097
HREN-3	0.512295	0.16646	0.512175	-6.268092	-6.6908813	0.707991	0.12178	0.707800	48.67013	49.55287
<b>Ladakh pluton</b>										
Lp-2bf	0.512496	0.10106	0.512423	-1.427752	-2.7699858	0.705292	0.077496	0.705170	11.33513	11.24202
Lp-2cf	0.512602	0.1285	0.512509	0.255235	-0.7022499	0.705797	0.06557	0.7056945	18.76931	18.41022
Lp-15fm	0.512549	0.11681	0.512464	-0.61476	-1.7361179	0.706799	0.417544	0.706146	25.18334	32.63307
Lp-28f	0.512241	0.10302	0.512166	-6.430919	-7.7442562	0.71635	0.87931	0.714975	150.5312	168.2044
Lp-30f	0.512162	0.10022	0.512089	-7.93307	-9.2853046	0.71373	1.6051	0.711220	97.2274	131.0149
Lp-35m	0.512664	0.14586	0.512559	1.221227	0.50718051	0.70478	0.01533	0.704756	5.44591	3.97445
Lp-36m	0.512707	0.13803	0.512607	2.170208	1.34597903	0.704831	0.16041	0.704580	2.95018	4.698368
<b>Khardung volcanics</b>										
KST-4	0.512681	0.201244	0.512536	0.775218	0.83879853	0.706013	0.716663	0.704892	7.38609	21.47622